

The Performance of Locally Produced Supplementary Cementitious Materials When Incorporated In Concrete

by
Vital Jorge Alexandre

*Thesis presented in fulfilment of the requirements for the degree of
Master of Engineering (Research) in the Faculty of Engineering at
Stellenbosch University*



Supervisor: Prof. William Peter Boshoff

March 2016

Declaration

By submitting this thesis/dissertation electronically, I declare that the entirety of the work contained herein is my own, original work, that I am the sole author thereof (save to the extent explicitly otherwise stated), that reproduction and publication thereof by Stellenbosch University will not infringe any third party rights and that I have not previously in its entirety or in part submitted it for obtaining any qualification.

Signature:

Date:

Abstract

The production of cement has a strenuous impact on the environment. Nonetheless, it is required by the construction industry as a key parameter for socio-economic development. Supplementary cementitious materials (SCMs) are a group of materials that can be used to partially replace cement as a binder in concrete mixtures, two of which includes slag and fly ash (FA). These materials are obtained as waste products from iron smelting and coal combustion processes, respectively. These materials have the capability to generate hydration products similar to that of cement when used. The current study's main objective was to investigate the performance concrete containing slag and fly ash, produced in South Africa, as a means to reduce the dependency of cement as the only binder used in concrete.

The goal of the study was to establish to what degree each of the materials can replace the cement in a typical concrete mix and the impacts thereof. Experiments were conducted on concrete samples made from a series of mixes with a constant binder content and water-to-binder ratio. Cement was replaced on a mass basis, with limits defined by the typical construction replacements: slag at 25, 50 and 75 % and FA at 15, 25 and 35 %. The performance is based on: reactivity of the SCM, fresh state, mechanical properties and durability.

Setting time was found to be sensitive to the SCM quantity and reactivity, however it was accelerated by more reactive materials and low replacement level. In addition, a wider SCM-particle span increased the bleeding capacity and reduced the bleeding rate. FA was found to increase the plastic settlement of concrete more when compared to slag based concrete, with the maximum plastic settlement occurring at 25 % FA content. In addition, the unrestrained plastic shrinkage of all mixes was significantly greater than that of the reference, yet decreased with increased SCM content.

The compressive strength of SCM based concrete was lower than the reference at early ages and improved with curing age. At 91 days the control and a few SCM-based concretes had similar compressive strength of approximately 62 MPa. Moreover, the indirect tensile strength per unit compressive strength of the SCMs based concretes were higher than that of the control, signifying the improvement of the interfacial transition zone. The addition of SCMs also significantly improved the concrete microstructure. Additionally, the durability performance of the SCMs based concrete was better than or equivalent to that of the reference. The chloride resistance of slag-based concrete was four times lower than fly ash concrete or the control mix.

The knowledge from the current study shows that SCMs can be used, to a great extent, to replace cement in the construction industry. The early age properties may require attention, yet, in the end, the final product of SCM-based concrete is found to be superior to that of the control. Hence, the use of slag and fly ash, as a binder replacement, does provide a solution to reduce the environmental impact of cement production.

Opsomming

Die produksie van sement het 'n strawwe impak op die omgewing. Nietemin, is dit 'n belangrike parameter vir sosio-ekonomiese ontwikkeling. Aanvullende gesementeerde materiale (ASMs) is 'n groep materiale wat kan gebruik word om sement gedeeltelik te vervang as 'n binder vir betonmengsels. Twee van die materiale sluit in slagment en vliegas. Hierdie materiale word verkry as afvalprodukte uit die prosesse van yster-smelt en steenkool verbranding, onderskeidelik. Hierdie materiale het die vermoë om hidrasie produkte, soortgelyk aan dié van sement, te genereer wanneer dit gebruik word. Dus is die hoofdoel van die huidige studie om die verrigting van beton met slagment en vliegas, wat in Suid-Afrika vervaardig word, te ondersoek as 'n oplossing van die afhanklikheid van sement, as die enigste binder wat gebruik word in beton, te verminder.

Die doel van die studie is om vas te stel tot watter mate elk van die materiale die sement in 'n tipiese beton meng kan vervang asook die gesamende impak daarvan. Eksperimente is op beton monsters gedoen met 'n reeks van mengsels met 'n konstante binder inhoud en water-tot-binder verhouding. Sement is vervang op 'n massabasis, met grense gedefinieer deur die tipiese konstruksie vervangings: slagment op 25, 50 en 75% en vliegas op 15, 25 en 35%. Die verrigting is gebaseer op: reaktiwiteit van die ASM, plastiese-toestand, meganiese eienskappe en duursaamheid.

Die set-tyd is gevind om sensitief te wees vir die ASM hoeveelheid en reaktiwiteit, maar is versnel deur meer reaktiewe materiaal en teen lae-vervanging hoeveelhede. Daarbenewens is gevind dat 'n wyer SCM-deeltjie span die bloei-kapasiteit vermeerder en bloei-koers verminder. Vliegas is gevind om die plastiese nedersetting van beton meer te verhoog in vergelyking met slagment-gebaseerde beton, met die maksimum plastiese nedersetting by 25% vliegas inhoud. Die plastiese krimp van alle ASM-mengsels aansienlik hoër as dié van die verwysing, maar het nog afgeneem met verhoogde SCM inhoud.

Die druksterkte van SCM gebaseer beton was laer as die verwysing by vroeë ouderdomme en het verbeter met ouderdom. Op 91 dae was die druksterkte van die beheer en 'n paar ASM-gebaseerde beton soortgelyk teen ongeveer 62 MPa. Verder, was die indirekte treksterkte per eenheid druksterkte van die SCMS gebaseer beton was hoër as dié van die beheer, en dui aan op die verbetering van die grenslaagsone tussen die bry en aggregraat. Die byvoeging van SCMS verbeter ook die beton mikrostruktuur aansienlik. Daarbenewens is die duursaamheid van die ASMs-gebaseerde beton beter as, of gelykstaande aan dié van die verwysing. Die chloried weerstand van slag gebaseer beton was vier keer laer as die van vliegas-gebaseerde beton en die beheer.

Die kennis van die huidige studie toon dat ASMs gebruik kan word tot 'n groot mate om sement te vervang in die konstruksiebedryf. Die vroeë ouderdom eienskappe verg aanda, maar in die lang termyn is die finale produk van ASM-gebaseerde beton gevind om beter te wees as dié van die beheer. Dus, bied die gebruik van slagment en vliegas wel 'n oplossing teen die omgewingsimpak van sement produksie te verminder.

Acknowledgements

I would like to extend my thanks to the following people, who without them, the journey would have been more difficult. Their guidance, support and motivation has provided a great degree of encouragement to complete this study.

- Professor Billy Boshoff, for his mentorship, advice and guidance in conducting this study, and providing me with a great learning experience. Your patience and support is greatly appreciated.
- The staff at the University of Stellenbosch. I hope to make the most of all the advice and learning experiences I have gained during my years of study at the institute.
- The technical staff, for your assistance and companionship in the laboratories: Charlton Ramat, Peter Cupido, Luhan Jacobs and Johan van der Merwe.
- The secretarial staff for helping me with all the requests I had: Natalie Scheepers, Olivia van Wyk and Arthur Layman. Your assistance and friendliness has made the two years great.
- My family members, for their continual support, prayers and words of encouragement.
- My friends, with whom I shared an office with for two years. I will keep the memorable moments with me for a long time, as they made me attain my sanity in the two years. The motivation, advice and encouragement means a lot. Thank you: Nuraan Ebrahim, Oliver Lerch, Alex Bauer, Bernard le Roux, Vianney Ntibaziyaremye. I would also like to extend my thanks to my Marvin Ngwetjana, for his role in the two years of my study.

Finally, but not the least important, I would like to thank God, for His blessings have been abundant and full of glory.

I would also like to give my thanks to the suppliers of my material (in no specific order):

- PPC
- AfriSAM
- Ulula Ash
- Sephaku Ash
- Ash Resources.

Table of Contents

Declaration	i
Abstract.....	ii
Opsomming.....	iii
Acknowledgements	iv
Table of Contents	v
List of Figures	ix
List of Tables.....	xiii
List of Equations	xv
List of Symbols	xvi
Nomenclature	xviii
Chemical Notation.....	xx
Chapter 1 Introduction.....	1
1. 1. Problem Statement	2
1. 2. Objectives	2
1. 3. Methodology	2
1. 4. Report Layout	2
Chapter 2 Supplementary Cementitious Materials (SCMs).....	4
2. 1. Cement	4
2. 1. 1. Classification of Cement.....	4
2. 1. 2. Production Process.....	5
2. 1. 2. Characterisation: Chemical Properties.....	6
2. 1. 3. Characterisation: Physical Properties	7
2. 2. Types of SCMs	7
2. 2. 1. Classification of SCMs	7
2. 2. 2. A Note on LCA's.....	8
2. 2. 3. Production Process: Fly Ash.....	9
2. 2. 4. Production Process: Slag.....	9
2. 2. 5. Characterisation of Fly Ash: Chemical Composition	9
2. 2. 6. Characterisation of Slag: Chemical Composition.....	10
2. 2. 7. Characterisation of Fly Ash: Physical Properties	11
2. 2. 8. Characterisation of Slag: Physical Properties	11
2. 3. General Effects of the Addition of SCMs on the Binder System.....	12
2. 3. 1. The Physical Level.....	12
2. 3. 2. The Chemical Surface Level.....	13
2. 3. 3. The Chemical Level.....	13
2. 4. Reaction Kinetics	14
2. 4. 1. The Cement Hydration Reaction	14
2. 4. 2. The Pozzolanic Reaction.....	15
2. 4. 3. The Latent Hydraulic Reaction.....	16
2. 5. Quantifying Reactivity of SCMs.....	17
2. 5. 1. Direct Methods	17
2. 5. 2. Indirect Methods	19
2. 5. 3. Comparison of Test Methods.....	21
2. 6. Effect of SCMs on the Plastic Properties of Concrete	22
2. 6. 1. Setting Time.....	22
2. 6. 2. Workability	26
2. 6. 3. Bleeding	27
2. 6. 4. Plastic Shrinkage and Settlement.....	31

2. 7.	Effect of SCMs on the Microstructure of Concrete	36
2. 8.	Effect of SCMs on the Mechanical Properties of Concrete	39
2. 8. 1.	Compressive Strength	39
2. 8. 2.	Tensile and Flexural Strength	44
2. 8. 3.	Modulus of Elasticity	48
2. 9.	Effect of SCMs on the Drying Shrinkage of Concrete.....	50
2. 10.	Durability Properties of Concrete	51
2. 10. 1.	Transport Mechanisms in Concrete	52
2. 10. 2.	Causes of Concrete Deterioration	52
2. 10. 3.	Deterioration of Steel	54
2. 10. 4.	Effect of SCMs on the Deterioration of Concrete.....	56
2. 10. 5.	Durability Testing Methods in a South African Context	59
2. 11.	Concluding Summary	62
Chapter 3	Experimental Setup and Programme.....	64
3. 1.	Materials	64
3. 1. 1.	Water.....	64
3. 1. 2.	Binders	64
3. 1. 3.	Aggregates	65
3. 2.	Mixing Procedure.....	66
3. 2. 1.	Mortars.....	66
3. 2. 2.	Concrete	67
3. 3.	Curing Process.....	68
3. 4.	Reactivity	68
3. 4. 1.	ASTM Method.....	68
3. 4. 2.	BS-EN Standards	69
3. 5.	Workability	69
3. 6.	Setting Time.....	70
3. 7.	Bleeding	71
3. 8.	Plastic Shrinkage and Settlement.....	72
3. 9.	Mechanical Properties.....	74
3. 9. 1.	Compressive Strength	74
3. 9. 2.	Indirect Tensile Strength.....	76
3. 9. 3.	Flexural Strength.....	78
3. 9. 4.	Secant Modulus.....	79
3. 10.	Microstructure.....	81
3. 11.	Drying Shrinkage	82
3. 12.	Durability	83
3. 12. 1.	Sample Preparation	83
3. 12. 2.	Permeability	83
3. 12. 3.	Sorptivity.....	86
3. 12. 4.	Chloride Conductivity.....	88
3. 12. 5.	Durability Indices.....	90
3. 13.	Concluding Summary	91
Chapter 4	Results and Discussion Slag	92
4. 1.	Physical Properties	92
4. 2.	Chemical Properties	94
4. 3.	Reactivity	95
4. 4.	Workability	97
4. 5.	Setting Times	98
4. 6.	Bleeding	100
4. 6. 1.	Effect of Slag Type and Substitution on Bleeding Rate.....	101
4. 6. 2.	Effect of Slags on Bleeding Duration	102
4. 6. 3.	Effect of Slag on Bleeding Capacity.....	102
4. 6. 4.	Comparison between GGBS and GGCS on the Bleeding Phenomenon.....	103

4. 7.	Early Age Deformation.....	104
4. 7. 1.	Plastic Settlement.....	105
4. 7. 2.	Capillary Pressure Build-up.....	106
4. 7. 3.	Plastic Shrinkage.....	107
4. 7. 4.	Concluding Remarks.....	108
4. 8.	Microstructure.....	108
4. 9.	Compressive Strength.....	110
4. 9. 1.	Reference (0 % Cement Replacement).....	111
4. 9. 2.	The Effect of GGCS on Concrete Strength Development.....	111
4. 9. 3.	The Effect of GGBS on Concrete Strength Development.....	114
4. 9. 4.	The Relation between the SAI and Concrete Strength.....	116
4. 9. 5.	The Comparison between GGBS and GGCS with Regard to Strength Development.....	116
4. 9. 6.	Concluding Remarks.....	117
4. 10.	Indirect Tensile Strength.....	118
4. 10. 1.	The Effect of a Neat Concrete (0 % SCMs) on the Indirect Tensile Strength.....	118
4. 10. 2.	The Effect of GGCS on the Indirect Tensile Strength.....	119
4. 10. 3.	The Effect of GGBS on the Indirect Tensile Strength.....	120
4. 10. 4.	The Comparison of GGBS and GGCS on the Indirect Tensile Strength.....	120
4. 10. 5.	Concluding Remarks.....	121
4. 11.	Flexural Strength.....	121
4. 12.	Secant Modulus.....	121
4. 13.	Drying Shrinkage.....	122
4. 13. 1.	The Typical Drying Shrinkage of SCMs-free Concrete.....	123
4. 13. 2.	The Effect of GGCS on Drying Shrinkage.....	123
4. 13. 3.	The Effect of GGBS on Drying Shrinkage.....	125
4. 13. 4.	Comparing the Drying Shrinkage Performance of GGBS and GGCS.....	127
4. 13. 5.	Concluding Remarks.....	129
4. 14.	Durability.....	130
4. 14. 1.	The Permeability of Slag-Based Concrete.....	130
4. 14. 2.	The Sorptivity of Slag-Based Concrete.....	131
4. 14. 3.	The Chloride Conductivity of Slag-Based Concrete.....	132
4. 14. 4.	Durability Indices for South African Slags.....	133
4. 15.	Concluding Summary.....	133
Chapter 5	Results and Discussion Fly Ash.....	136
5. 1.	Physical Properties.....	136
5. 2.	Chemical Properties.....	139
5. 3.	Reactivity.....	140
5. 4.	Workability.....	141
5. 5.	Setting Times.....	142
5. 6.	Bleeding.....	143
5. 6. 1.	The Effect of Fly Ash Type on Bleeding.....	143
5. 6. 2.	The Effect of Fly Ash Substitution on Bleeding.....	144
5. 6. 3.	Concluding Remarks.....	145
5. 7.	Early Age Deformation.....	145
5. 7. 1.	Plastic Settlement.....	146
5. 7. 2.	Capillary Pressure Build-up.....	147
5. 7. 3.	Plastic Shrinkage.....	148
5. 7. 4.	Concluding Remarks.....	150
5. 8.	Microstructure.....	150
5. 9.	Compressive Strength.....	152
5. 9. 1.	The Effect of Increasing Fly Ash Content.....	154
5. 9. 2.	The Effect of Fly Ash Type.....	155
5. 9. 3.	Concluding Remarks.....	157
5. 10.	Indirect Tensile Strength.....	157
5. 11.	Flexural Strength.....	159

5. 12.	Secant Modulus.....	160
5. 13.	Drying Shrinkage	160
5. 14.	Durability	164
5. 14. 1.	The Permeability of Fly Ash Based Concrete.....	164
5. 14. 2.	The Sorptivity of Fly Ash Based Concrete	165
5. 14. 3.	The Chloride Resistance of Fly Ash Based Concrete	166
5. 14. 4.	Durability Indices for South African Fly Ash.....	166
5. 15.	Concluding Summary	167
Chapter 6	Discussion: A Comparison between Slag and Fly Ash.....	169
6. 1.	Reactivity	169
6. 2.	Fresh State Properties.....	170
6. 2. 1.	Workability	170
6. 2. 2.	Setting Time	171
6. 2. 3.	Bleeding	171
6. 3.	Early Age Deformation: Plastic Settlement and Shrinkage	172
6. 4.	Concrete Microstructure	174
6. 5.	Hardened State Properties of Concrete	174
6. 5. 1.	Compressive Strength	174
6. 5. 2.	Indirect Tensile Strength.....	176
6. 6.	Drying Shrinkage	176
6. 7.	Durability	176
6. 7. 1.	Permeability	176
6. 7. 2.	Sorptivity.....	177
6. 7. 3.	Chloride Conductivity.....	177
6. 7. 4.	Concluding Remarks.....	177
6. 8.	Concluding Summary	178
Chapter 7	Conclusion and Recommendations.....	179
7. 1.	Conclusions.....	179
7. 2.	Recommendations.....	181
7. 3.	Concluding Statement.....	181
References	182
Appendix A	Results: Slags.....	A-1
Appendix B	Results: Fly Ash.....	B-1

List of Figures

Figure 2-1. A schematic of the production process of cement.....	5
Figure 2-2. SEM image depicting the morphology of typical cement particles.	7
Figure 2-3. Classification of SCMs (Snellings et al., 2012).	8
Figure 2-4. The morphology of (a) a fly ash particle and (b) a granulated slag particle.	11
Figure 2-5. Explanation of the principle of achieving theoretical optimal packing density.	12
Figure 2-6. The two phenomena experienced by particles: (a) the wall effect and (b) the blocking effect (Moosberg-Bustnes et al., 2004).....	13
Figure 2-7. The strength gain contribution of the four main oxides present in Portland cement (Czernin, 1980).	15
Figure 2-8. The effect of SCMs on the compressive strength and calcium hydroxides concentrations (Lewis et al., 2003).	16
Figure 2-9. The Frattini curve used to demarcate the regions of pozzolanic and non-pozzolanic areas. .	19
Figure 2-10. The stages of concrete setting (Metha & Monteiro, 2006).	22
Figure 2-11. The influence of bleeding on a concrete element.....	28
Figure 2-12. The stages of bleeding.....	29
Figure 2-13. The formation of cracks due to plastic settlement.....	32
Figure 2-14. The capillary pressure build up between particles and the associated menisci forming.	33
Figure 2-15. The evolution of plastic shrinkage and capillary pressure.	34
Figure 2-16. The difference between porosity and permeability.	37
Figure 2-17. Diagrammatic representation of the ITZ.	38
Figure 2-18. The modulus of rupture setup to determine tensile strength of concrete by means of the three point bending test (left) the four point bending test (right).....	45
Figure 2-19. The stress distribution in elements for the modulus of rupture.	46
Figure 2-20. Indirect splitting test setup for a cylindrical and cube specimen.	46
Figure 2-21. The stress distribution in elements for the indirect tensile testing.	46
Figure 2-22. The different elastic modulus' that can be obtained from a loading cycle.	49
Figure 2-23. Explanation of drying shrinkage by using the capillary tension theory.	50
Figure 2-24. Durability factors typical of concrete deterioration (Ballim et al., 2009).	53
Figure 2-25. The onset cycle of concrete durability (Basheer & Barbhuiya, 2009).	54
Figure 2-26. Corrosion of steel.	56
Figure 3-1. Grading curves of the three different types of sand.	66
Figure 3-2. The mixing procedure for mortar specimens.	67
Figure 3-3. The occurrence of flocculation in mortars.	67
Figure 3-4. The equipment used to determine the slump of concrete.	70
Figure 3-5. The setup used to determine the setting time of concrete: (a) The Vicat apparatus, (b) the specimen mould, (c) an example of a specimen, (d) the needle used to determine initial set and (e) the needle for final set.....	71
Figure 3-6. The setup used to determine the bleeding of concrete.	72
Figure 3-7. Schematic for the setup to determine the vertical and horizontal displacements.....	73
Figure 3-8. Experimental setup for the recording of the plastic settlement and shrinkage.....	73
Figure 3-9. The anchors used to determine the horizontal displacement of the fresh concrete.	73
Figure 3-10. The wire lattice used in the recording of the vertical displacement of fresh concrete.	74
Figure 3-11. The setup (left) and pressure sensor (right) used to record the pressure build-up.	74
Figure 3-12. Compression testing setup of mortar specimens.	76
Figure 3-13. The setup to determine the compressive strength of concrete cube specimens.	76
Figure 3-14. Test setup for determining the tensile splitting capacity of concrete specimens.	77
Figure 3-15. Experimental setup of the four point bending test in determining the modulus of rupture..	78
Figure 3-16. Test setup to determine the elastic modulus of concrete samples.	80

Figure 3-17. Stress cycle imposed on concrete sample to determine the secant modulus of elasticity according to EN 12390-13:2013.....	81
Figure 3-18. Typically results of an X-ray CT-scan.....	82
Figure 3-19. The instruments used to determine the drying shrinkage of the concrete mixes. (a) All equipment used. (b) The electronic micrometer. (c) The spacer and reference. (d) The metal targets.....	82
Figure 3-20. Obtaining of core samples for durability testing.....	83
Figure 3-21. A schematic for determining the permeability of a concrete specimen.....	84
Figure 3-22. The OPI setup used in assessing the permeability of concrete specimens.....	86
Figure 3-23. Sealing of the vertical edges of a specimen using packing tape.....	86
Figure 3-24. The testing procedure of concrete specimens for the water sorptivity index.....	87
Figure 3-25. Vacuum facility for saturation procedure.....	88
Figure 3-26. A schematic of the chloride conductivity test.....	89
Figure 3-27. The test setup to determine the chloride conductivity of a concrete specimen.....	90
Figure 4-1. The PSD results (left) and the volume distribution (right) of the PC, GGBS and GGCS.....	92
Figure 4-2. SEM image of the cement particle distribution and morphology.....	93
Figure 4-3. SEM image of the particle distribution and morphology of the slag samples: GGCS (left) and GGBS (right).....	93
Figure 4-4. SAI for the slag samples.....	96
Figure 4-5. The workability of mixes containing different slag types.....	97
Figure 4-6. Setting times for the reference and slag.....	99
Figure 4-7. The bleeding of GGCS specimens at 0, 25 and 50 % cement replacement.....	100
Figure 4-8. The bleeding of GGBS specimens at 0, 25 and 50 % cement replacement.....	101
Figure 4-9. The bleeding of slag samples at 25 % cement replacement.....	103
Figure 4-10. The bleeding of slag samples at 50 % cement replacement.....	103
Figure 4-11. The particle distribution for the combination of slag and cement.....	104
Figure 4-12. Consolidation of the concrete containing different levels of slag, both GGBS and GGCS.....	105
Figure 4-13. Capillary pressure build up for concrete containing GGCS (left) and GGBS (right) at different replacement levels.....	106
Figure 4-14. Plastic shrinkage for concrete containing GGCS (left) and GGBS (right) at different replacement levels.....	107
Figure 4-15. Cumulative percentage of the pore diameters of the concrete microstructure incorporating GGCS (left) and GGBS (right).....	109
Figure 4-16. Differences between the pore volume for concrete containing no slag (left) and slag at 25 % cement replacement (right), with the frequency and cumulative percentage presented by the histogram and dashed lines, respectively.....	110
Figure 4-17. Strength development profile of GGCS at different partial cement percentages.....	112
Figure 4-18. The representation of the changes in the chemical compounds present with continual substitution with GGCS.....	113
Figure 4-19. Strength development profile of GGBS at different partial cement percentages.....	115
Figure 4-20. The representation of the changes in the chemical compounds present with continual substitution with GGBS.....	115
Figure 4-21. Strength development profile of GGBS and GGCS of 50 % cement replacement.....	117
Figure 4-22. Indirect tensile strength of concrete mixes incorporating GGCS and GGBS.....	118
Figure 4-23. The ratio of the indirect tensile strength and the compressive strength for the different slags used at different replacement percentages.....	119
Figure 4-24. The cumulative mass loss of GGCS specimens at 0, 25 and 50 % cement replacement.....	123
Figure 4-25. The drying shrinkage of GGCS specimens at 0, 25 and 50 % cement replacement.....	124
Figure 4-26. The plot of the mass loss vs shrinkage for concrete containing GGCS.....	124
Figure 4-27. The cumulative mass loss of GGBS specimens at 0, 25 and 50 % cement replacement.....	126
Figure 4-28. The drying shrinkage of GGBS specimens at 0, 25 and 50 % cement replacement.....	126
Figure 4-29. The plot of the mass loss vs shrinkage for concrete containing GGBS.....	127
Figure 4-30. The cumulative mass loss of slag samples at 50 % cements replacement.....	128
Figure 4-31. The drying shrinkage of slag samples at 50 % cement replacement.....	129
Figure 4-32. Mass loss vs shrinkage strain as a function of replacement level of 50 %.....	129
Figure 4-33. The relationship between porosity and sorptivity.....	131
Figure 5-1. The PSD results (left) and the volume distribution (right) of the cement and fly ashes.....	137

Figure 5-2. SEM image of the fly ash particle distribution and morphology.	138
Figure 5-3. SEM image of the defects found.	139
Figure 5-4. The SAI for the fly ash samples.	140
Figure 5-5. The workability of mixes containing different types of fly ash.	141
Figure 5-6. The setting times of fly ash based concretes.	142
Figure 5-7. The effect of fly ash samples on bleeding at 25 % cement replacement.	144
Figure 5-8. The bleeding of UA (left) and SA (right) specimens at 0, 15 and 25 % cement replacement.	145
Figure 5-9. Consolidation of the concrete containing different cement substitution with fly ash.	146
Figure 5-10. Capillary pressure build up for concrete containing UA (left) and SA (right) at different replacement levels.	147
Figure 5-11. Plastic shrinkage for concrete containing UA (left) and SA (right) at different replacement levels.	149
Figure 5-12. Plastic shrinkage for concrete containing DP (left) and PF (right) at different replacement levels.	149
Figure 5-13. Cumulative percentage of the pore diameters of the concrete microstructure incorporating 25 % fly ash.	151
Figure 5-14. Differences between the pore volume for concrete containing no fly ash (left) and 25 % cement replacement (right), with the frequency and cumulative percentage presented by the histogram and dashed curves, respectively.	151
Figure 5-15. The strength development of the UA concrete mixes.	153
Figure 5-16. The strength development of the SA concrete mixes.	153
Figure 5-17. The strength development of the DP concrete mixes.	154
Figure 5-18. The strength development of the PF concrete mixes.	154
Figure 5-19. The compressive strength at 15 % cement replacement.	156
Figure 5-20. The compressive strength at 35 % cement replacement.	156
Figure 5-21. Indirect tensile strength of concrete mixes incorporating UA and SA.	158
Figure 5-22. The ratio of the indirect tensile and the compressive strength.	159
Figure 5-23. The cumulative mass loss of the fly ash samples (25 %).	161
Figure 5-24. The drying shrinkage of fly ash concrete (25 %).	162
Figure 5-25. The cumulative mass loss vs drying shrinkage of the fly ash samples (25 %).	163
Figure 5-26. The effect on drying shrinkage with the increase of UA from 15 to 25 %.	164
Figure 6-1. The workability of the control and 25 % cement SCM-based concrete.	170
Figure 6-2. The bleeding information of the investigated SCMs.	171
Figure 6-3. The ultimate plastic settlement (left) of the SCM-based concrete and associated percentage difference (right).	172
Figure 6-4. The ultimate plastic shrinkage (per 300 mm) (left) of the SCM-based concrete and associated percentage difference (right).	173
Figure 6-5. The ultimate plastic shrinkage strain induced in the concrete.	173
Figure 6-6. The cumulative pore distribution of concrete containing 25 % fly ash or slag compared to the reference.	174
Figure 6-7. The compressive strength development of 25 % cement replacement with SCMs.	175
Figure A-1. Bleeding curves for GGCS at different replacement levels (40 °C).	A-2
Figure A-2. Bleeding curves for GGBS at different replacement levels (40 °C).	A-2
Figure A-3. Bleeding curves comparing GGBS and GGCS at 25 % cement replacement (40 °C).	A-3
Figure A-4. Bleeding curves comparing GGBS and GGCS at 50 % cement replacement (40 °C).	A-3
Figure A-5. The compressive strength development at 25 % cement replacement.	A-4
Figure A-6. The compressive strength development at 75 % cement replacement.	A-4
Figure A-7. The compressive strength development for the second batch of CCGS.	A-5
Figure A-8. The cumulative mass loss of slag samples at 25 % cements replacement.	A-8
Figure A-9. The drying shrinkage of slag samples at 25 % cement replacement.	A-9
Figure A-10. Mass loss vs shrinkage strain as a function of replacement level of 50 %.	A-9
Figure B-1. The bleeding of DP specimens at 0, and 25 % cement replacement.	B-2
Figure B-2. The bleeding of PF specimens at 0, and 25 % cement replacement.	B-2
Figure B-3. Bleeding curves for UA at different replacement levels (40 °C).	B-3
Figure B-4. Bleeding curves for SA at different replacement levels (40 °C).	B-3
Figure B-5. Bleeding curves for DP (40 °C).	B-4

Figure B-6. Bleeding curves for PF (40 °C).	B-4
Figure B-7. Capillary pressure build up for concrete containing DP (left) and PF (right) at different replacement levels.....	B-5
Figure B-8. The strength development of the fly ash concrete mixes at 25 % cement replacement.	B-6
Figure B-9. The cumulative mass loss of the fly ash samples (15 %).	B-9
Figure B-10. The drying shrinkage of the fly ash concrete (15 %).	B-9
Figure B-11. The cumulative mass loss vs drying shrinkage of the fly ash samples (15 %).....	B-9
Figure B-12. The cumulative mass loss of the SA based mixes.	B-10
Figure B-13. The drying shrinkage of the SA based mixes.	B-10
Figure B-14. The cumulative mass loss of the DP based mixes.	B-10
Figure B-15. The drying shrinkage of the DP based mixes	B-11
Figure B-16. The cumulative mass loss of the PF based mixes.....	B-11
Figure B-17. The drying shrinkage of the PF based mixes.....	B-11

List of Tables

Table 2.1. The notation used to describe the components of cement chemistry.....	6
Table 2.2. List of SCMs' chemical composition from selected literature.	11
Table 2.3. Requirements for fly ash samples according to the ASTM and EN Standards.	20
Table 2.4. Requirements for slag samples according to the ASTM and EN Standards.....	20
Table 2.5. Typical cement replacement levels and the intended use of the cement and concrete mixture.	41
Table 2.6. Typical optimum cement replacement levels as found in literature.	42
Table 2.7. Literature findings on the optimum cement substitution for tensile and flexural strength.	48
Table 2.8. Prediction models for the elastic modulus of concrete.	49
Table 2.9. Optimum SCMs replacement level in term of chloride resistance.	59
Table 2.10. Selected tests used to assess the durability of concrete.	60
Table 3.1. Material properties: The relative densities (RD) and Fineness Modulus (FM).	65
Table 3.2. Mix design of the mortars.....	66
Table 3.3. The concrete mix composition used in the study.....	68
Table 3.3. The chemical requirements of slag and fly ash according to the ASTM.	69
Table 3.4. Mortar mixes used to determine the use of SCMs in concrete.	69
Table 3.5. The chemical requirements as stated by the BS-EN Standards.	69
Table 3.7. Classification of the durability of concrete in term of durability performance (Alexander et al., 2010).	90
Table 3.8. Schedule of tests and mixes completed.	91
Table 4.1. The physical properties of the cement and slag.	93
Table 4.2. The chemical composition of the cementitious binders: cement and slags.	94
Table 4.3. The Bogue's composition of the PC.....	94
Table 4.4. Assessing the hydraulic activity of the slag based on the chemical composition.	95
Table 4.5. The flexural and compressive strength for the reference and slag samples at 7 and 28 days. .	96
Table 4.6. The bleeding rate, capacity and time for the slag based concrete.....	101
Table 4.7. The effect of slag substitution on the span of the particles.....	104
Table 4.8. Setting times and bleeding data for slag-based concrete at elevated temperatures.....	105
Table 4.9. Cumulative and frequency data for the pore diameters (mm) of concrete including slag.	109
Table 4.10. The strength (MPa) of the GGCS and GGBS at different ages and cement replacement percentages.	111
Table 4.11. The flexural strength of slag samples.	121
Table 4.12. Secant modulus for concrete containing different types of slag.	122
Table 4.13. The predicted elastic modulus for slag based concrete.....	122
Table 4.14. Permeability of slag based concrete.....	130
Table 4.15. Sorptivity and porosity of slag-based concrete.....	131
Table 4.16. Chloride conductivity of slag-based concrete.....	132
Table 4.17. The DI classification for the investigated slags.	133
Table 5.1. The physical properties of the cement and fly ash.....	137
Table 5.2. The chemical composition of the cementitious binders: cement and fly ashes.	139
Table 5.3. The SAI of fly ash samples.....	140
Table 5.4. The bleeding rate, capacity and time for the fly ash based concrete.	143
Table 5.5. Setting times and bleeding data for fly ash –based concrete at elevated temperatures.....	145
Table 5.6. The cumulative percentage of pore diameters for concrete with 25 % fly ash.	150
Table 5.7. The strength of the fly ashes as a percentage of the control at different ages and cement replacement percentages.	152

Table 5.8. The flexural strength of fly ash samples.	159
Table 5.9. Secant modulus for concrete containing different types of fly ash.	160
Table 5.10. Permeability of fly ash based concrete.	164
Table 5.11. Sorptivity and porosity of fly ash based concrete.	165
Table 5.12. Chloride conductivity of fly ash based concrete.	166
Table 5.13. The DI classification for the investigated fly ash.	166
Table 6.1. The SAI of the cementitious binders at 28 days.	169
Table 6.2. The slag and fly ash with the highest strength at specified ages.	175
Table A.1. The SAI data for slag at 7 days.	A-1
Table A.2. The SAI data for slag at 28 days.	A-1
Table A.3. The SAI data for the second batch of GGCS.	A-1
Table A.4. Summary of the Statistical data of the compressive strength development data for slag samples.	A-4
Table A.5. The compressive strength (MPa) data for the second batch of GGCS.	A-5
Table A.6. The indirect tensile strength data for slag samples at 0, 25 50 and 75 % cement replacement.	A-6
Table A.7. The flexural strength data for selected slag samples at 0, 25 and 50 % cement replacement.	A-7
Table A.8. The use of prediction models to determine the elastic modulus of concrete.	A-7
Table A.9. Strength of the concrete mixes used for the drying shrinkage.	A-8
Table A.10. OPI data for the PC samples.	A-10
Table A.11. OPI data for the GGCS and GGBS samples.	A-10
Table A.12. Sorptivity data for the PC samples.	A-10
Table A.13. Sorptivity data for the slag samples.	A-11
Table A.14. Chloride conductivity data for the PC samples.	A-11
Table A.15. Chloride conductivity data for the slag samples.	A-12
Table B.1. The SAI data for fly ash and the reference at 28 days.	B-1
Table B.2. The SAI data for fly ash and the reference at 90 days.	B-1
Table B.3. The strength (MPa) of the fly ashes at different ages and cement replacement percentages.	B-5
Table B.4. Summary of the statistical data of the compressive strength development data for fly ash samples.	B-6
Table B.5. The indirect tensile strength data for fly as samples at 15, 25 and 35 % cement replacement.	B-7
Table B.6. The flexural strength data for selected slag samples at 0, 25 and 50 % cement replacement.	B-8
Table B.7. The use of prediction models to determine the Secant modulus of concrete containing fly ash.	B-8
Table B.8. OPI data for the fly ash samples.	B-12
Table B.9. Sorptivity data for the fly ash samples.	B-13
Table B.10. Chloride conductivity data for the fly ash samples.	B-14

List of Equations

Equation 2.1	6
Equation 2.2	6
Equation 2.3	6
Equation 2.4	6
Equation 2.5	14
Equation 2.6	14
Equation 2.7	14
Equation 2.8	14
Equation 2.9	15
Equation 2.10	16
Equation 2.11	17
Equation 2.12	17
Equation 2.13	17
Equation 2.14	32
Equation 2.15	34
Equation 2.16	34
Equation 2.17	55
Equation 2.18	55
Equation 2.19	55
Equation 2.20	56
Equation 2.21	56
Equation 2.22	56
Equation 3.1	75
Equation 3.2	77
Equation 3.3	78
Equation 3.4	80
Equation 3.5	82
Equation 3.6	85
Equation 3.7	85
Equation 3.8	85
Equation 3.9	88
Equation 3.10	88
Equation 3.11	90

List of Symbols

<i>Symbol</i>	<i>Description</i>	<i>Unit/Value</i>
A	Area	m ²
d, d ₁ , d ₂	Cross Sectional Length/Width/Height/Thickness	m
d _n	Percentage Passing a Certain Value (n)	%
E	Elastic Modulus	GPa
ER	Evaporation Rate	kg/m ² /hr
F	Applied Force	N
F	Slope	
f _{cu} / f _{cyl}	Compressive strength (Cube/Cylinder)	MPa
g	Gravitational Acceleration	9.81 m/s ²
i	Electric Current	A
k	Coefficient of Permability	m/s
K	Efficiency Factor	
l, L	Length	m
M _{s0} , M _{sv}	Mass (Oven Dried, Saturated)	kg
P	Capillary Pressure	kPa
P	Point Load	N
P ₀ , P _t	Pressure (Initial, At time t)	kPa
R	Universal Gas Constant	8.313 Nm/Kmol
R ₁ , R ₂	Water Mensici Radius (Maximum, Minimum)	
RH	Relative Humidity	%
S	Sorptivity	mm/hr ^{0.5}
t	Time	s
T _A , T _c	Temperature (Ambient, Concrete)	°C
t _{set}	Initial Set	hr
V	Wind Speed	km/h
V	Voltage	V
V	Volume	l
w:b	Water-to-Binder Ratio	
w:c	Water-to-Cement Ratio	
W _{bl}	Bleed Water (Total)	kg/m ²
wt. %	Mass Percent	%
z	Slope of Regression Line	
ε	Strain	m/m

<i>Symbol</i>	<i>Description</i>	<i>Unit/Value</i>
θ	Absolute Temperature	K
ρ	Density	kg/m ³
σ	Surface Tension	MPa
σ	Chloride Conductivity	mS/cm
σ_a, σ_p	Stress (Upper, Preload)	MPa
σ_c, σ_T	Strength (Compressive, Tensile)	MPa
ω	Molecular Mass of Oxygen Gas	32 g/mol

Nomenclature

ACI	American Concrete Institute
AI	Activity Index
ASTM	American Society for Testing and Materials
BDT	Bulk Diffusion Test
BS EN	British Standards European Norm
C ₂ S	Dicalcium Silicate
C ₃ S	Tricalcium Silicate
C ₄ AF	Tetracalcium Aluminoferrite
CCT	Chloride Conductivity Test
CEB-FIP	
CEN	European Committee for Standardisation
CH	Calcium Hydroxide
CoV	Coefficient of Variation
C-S-H	Calcium Silicate Hydrates
CPT	Cambureau Permeability Test
CT	Computed Tomography
ER	Evaporation Rate
FM	Fineness Modulus
GGAS	Ground Granulated Arc-furnace Slag
GGBS	Ground Granulated Blast-furnace Slag
GGAS	Ground Granulated Corex Slag
GHG	Greenhouse Gases
IR	Insoluble Residue
ITZ	Interfacial Transition Zone
LCA	Life Cycle Assessment(s)
LOI	Loss on Ignition
LVDT	Linear Variation Displacement Transducer
OPI	Oxygen Permeability Index
OPT	Oxygen Permeability Test
PC	Portland Cement
PSD	Particle Size Distribution
RCPT	Rapid Chloride Conductivity Test
RD	Relative Density
RH	Relative Humidity
SAI	Strength Activity Index
SCC	Self-Compacting Concrete
SCMs	Supplementary Cementitious Materials
SEM	Scanning Electron Microscopy
St.D	Standard Deviation
TGA	Thermo-Gravimetric Analysis

TPT	Torrent Permeability Test
WST	Water Sorptivity Test
XRD	X-Ray Diffraction
XRF	X-Ray Fluorescence

Chemical Notation

Aluminium Oxide	Al_2O_3
Aluminium Sulphate	$\text{Al}_2(\text{SO}_4)_3$
Calcium Bicarbonate	$\text{Ca}(\text{HCO}_3)_2$
Calcium Carbonate	CaCO_3
Calcium Chloroaluminate	$\text{C}_3\text{A}\cdot\text{CaCl}_2\cdot 10\text{H}_2\text{O}$
Calcium Hydroxide	$\text{Ca}(\text{OH})_2$
Calcium Oxide	CaO
Calcium Sulphate	CaSO_4
Carbon Dioxide	CO_2
Carbon Dioxide Equivalent	CO_{2e}
Carbonic Acid	H_2CO_3
Chromium (II) Oxide	Cr_2O_3
Dicalcium silicate	$2\text{CaO}\cdot\text{SiO}_2$
Ferric Hydroxide	$4\text{Fe}(\text{OH})_3$
Ferrous Hydroxide	$\text{Fe}(\text{OH})_2$
Friedel's Salt	$\text{C}_3\text{A}\cdot\text{CaCl}_2\cdot 10\text{H}_2\text{O}$
Gamma Iron Oxide	$\gamma\text{-FeOOH}$
Gypsum	$\text{CaSO}_4\cdot 2\text{H}_2\text{O}$
Iron (II) Oxide	Fe_2O_3
Lithium Borate	$\text{Li}_2\text{B}_4\text{O}_7$
Lithium Iodide	LiI
Lithium Metaborate	LiBO_2
Magnesium Oxide	MgO
Manganese Oxide	MnO
Phosphorus Pentoxide	P_2O_5
Potassium Oxide	K_2O
Rust (Hydrated Ferric Oxide)	$\text{Fe}_2\text{O}_3\cdot\text{H}_2\text{O}$
Silica Oxide	SiO_2
Sodium Chloride	NaCl
Sodium Hydroxide	NaOH
Sodium Oxide	Na_2O
Sodium Silicate	Na_2SiO_3
Sulphur Trioxide	SO_3
Tetracalcium alumino-ferrite	$4\text{CaO}\cdot\text{Al}_2\text{O}_3\cdot\text{Fe}_2\text{O}_3$
Titanium Oxide	TiO_2
Tricalcium aluminate	$3\text{CaO}\cdot\text{Al}_2\text{O}_3$
Tricalcium silicate	$3\text{CaO}\cdot\text{SiO}_2$
Water	H_2O

Chapter 1

Introduction

Concrete is stated to be the most widely consumed product by humans (Flower & Sanjayan, 2007; Zhang et al., 2013). The use of concrete as a building material is observed in the benefits of its use: cheaper relative to steel, durable (if properly designed and maintained), as well as being able to be cast into varying shapes and sizes. However, the production of cement is considered to be an energy-intensive process and linked to the release of anthropogenic carbon dioxide (CO₂) as well as pollutants such as dust (Shi et al., 2012; Uwasu et al., 2014; Yang et al., 2014). In addition, a relationship can be observed between the production of cement and the growth of the world population as well as the development associated with the mentioned growth. Flower and Sanjayan (2007) reports that 1 tonne of concrete was produced per person per annum on average in 2007.

The CO₂ emissions caused by the production of cement accounts for 7 % of the global CO₂ emissions (Uwasu et al., 2014) and in 2006, 1.8 Giga-tonnes of CO₂ was released by the cement industry (Gao et al., 2015). The release of CO₂ is generally linked to the negative impacts imposed on the environment, as CO₂ is said to be a leading contributor to the global warming phenomenon. The reduction of greenhouse gases (GHG), such as carbon dioxide, has been a priority in terms of global agendas. Due to the threat imposed by the release of GHGs, various initiatives have been proposed to reduce the amount of CO₂ being produced and released into the atmosphere. Physical or direct measures include the change to lower carbon content fuel types, addition of chemical adsorption processes, efficient grinding and the use of supplementary cementitious materials (SCMs) (Yang et al., 2014).

SCMs are classified as materials that under certain conditions, exhibit similar behaviour to that of cement during the hydration process. An array of SCMs exists, capable for use in concrete. These materials can be natural occurring or artificially produced. The use of SCMs is also not limited to the sole purpose of reducing carbon dioxide emissions. However, it can reduce the carbon footprint of clinker production. For example, two commercially available SCMs, namely, blast furnace slag and fly ash, can reduce the CO₂ emissions associated with concrete production by 22 % and 13 %, respectively (Flower & Sanjayan, 2007). Additionally, the use of these materials in concrete can ensure that concrete that is more economical is produced as well as being of a higher level of sustainability. Additionally, the use of SCMs in concrete can also produce an improvement in concrete microstructure, durability and mechanical performance (Zhang et al., 2013).

1. 1. Problem Statement

The production of cement causes a subsequent strain on the environment and natural resources. Hence, the question arises on how the impact of cement dependency can be reduced. More specifically, how does the performance of SCM-based concrete compare to that of a SCM-free concrete, and how does it relate to the possible reduction of cement dependency.

1. 2. Objectives

The objective of this study is to investigate the performance of concrete that can be achieved when SCMs are used in the concrete mix design process. The investigation seeks to establish how or to what degree the level of sustainability is achieved when incorporating the mentioned materials.

Moreover, the research aims to better understand the behaviour of slag and fly ash in a typical concrete mixture. The material properties of the various cementitious samples will be assessed to recognise any possible differences that may affect the performance once incorporated in concrete. The performance of SCM-based concrete will be measured by comparing the experimental results to a reference, containing no SCMs, in terms of the fresh and hardened state properties, and also concrete durability. A better insight into the material behaviour could grant better clarity on further research prospects as well as in establishing how the material can be used to the best efficiency and optimum level.

1. 3. Methodology

The methodology used included physical experiments when replacing cement content with a certain percentage of slag or fly ash, with reference to industry, and evaluating the results obtained. The different slag and fly ash produced in South Africa were investigated when used in a concrete mixture. The influences of the SCMs were investigated on two states of concrete: the fresh/plastic state and hardened state. The fresh state properties investigated included setting times, workability and bleeding. The deformation in the fresh state was also measured and tests included the plastic setting, plastic shrinkage and capillary pressure. The hardened state properties were assessed using both mortars and concrete specimens. The tests conducted included compressive, tensile strength (via indirect tensile testing and flexure), elastic modulus, and drying shrinkage. Additionally, durability aspects are also assessed when these materials are used. The South African durability tests are used to determine the durability efficiency and includes the chloride conductivity, oxygen permeability and water sorptivity tests. Additional tests are also used to assess material properties such as particle size distribution via laser diffraction, morphology via scanning electron microscopy and chemical composition via XRF.

1. 4. Report Layout

The report is sub divided into seven chapters. The chapter to follow, Chapter 2, is a literature study based on the use of SCMs in concrete. The literature focuses primarily on the effect of slag and fly ash

when incorporated in a conventional concrete mixture. These findings include effects on plastic and hardened states.

Chapter 3 provides the methodology used to gain the required data and information. This chapter focuses on the test method used as well as the parameters employed. Equally as important, any changes or deviations from standard method are addressed within this section.

Chapters 4 and 5 focus on the results obtained, the former focussing on the results pertaining to the use of slag and the latter on the use of fly ash. The results are also discussed in these mentioned chapters.

Chapter 6 is given to establish an overall comparison between the materials used in the investigation. This chapter seeks to compare the use of slag and fly ash, as well as establishing a comparative basis between the two said materials.

Chapter 7 gives the final conclusions that can be drawn from the study undertaken and also provides possible recommendations based on the findings as well as the potential of new research topics.

Chapter 2

Supplementary Cementitious Materials (SCMs)

The production of cement is seen as environmentally unfriendly (Meyer, 2009). The reason lies in the fact that the process of manufacturing cement is energy intensive and a contributor to environmental issues such as the release of carbon dioxide. However, the production of cement is essential for socio-economic development. Construction and development is continuous and, depending on the project, requires concrete as a building material. A solution to limit and/or reduce the negative impacts of the production of cement, hence creating a more sustainable concrete mixture, is found by using supplementary cementitious materials (SCMs). This chapter explains the impact(s) of SCMs when incorporated in concrete mixtures.

2. 1. Cement

2. 1. 1. Classification of Cement

Cementing materials are used as a way of connecting or unifying materials in a solid mass or unit. However, a description like this encompasses a large amount of materials; cement being one these materials. Cement forms part of a range of, typically, lime rich materials that react with moisture to form compounds attributed to the cementing nature. Notably, not all cements are the same, as the chemical composition can vary resulting in cements with different behaviour.

Cementitious materials can be subdivided into two different categories. Firstly, there exist the hydraulic limes which can furthermore be subdivided into two classes: pozzolanic limes and burnt hydraulic limes. The difference between these two exists in the hydration process undergone when these materials come into contact with moisture. Moreover, the products that may form can potentially also be different as a result (see *Cement Chemistry and Physics for Civil Engineers* (Czernin, 1980)).

The second category of cementitious materials is the Portland Cements (PC), which can also be subdivided into a range of sub classes. For example, under this class exists White Portland Cement, Grey Portland Cement and Rapid Hardening cement, to name a few. The PC class has received the greatest attention in recent times due to its continual use in the construction industry. The mentioned class of cement is also the focus of this report and section in particular. The production process and characterisation of it is focused on in the next section.

2. 1. 2. Production Process

Cement is produced by the inter-grinding of clinker and additives. Clinker is generated by feeding two main categories of raw materials into a kiln, namely, calcareous materials, such as limestone, and argillaceous materials, such as clay and shale (Kosmatka et al., 2003). Inside the kiln, the raw materials undergoes a change in physical and chemical properties, leading to the formation of clinker, which is ground to form cement.

The kiln can subsequently be divided into four zones: (1) decomposition, (2) transition, (3) sintering and (4) cooling (Ishak & Hashim, 2014) and is shown in Figure 2-1. The first zone, the decomposition zone, is linked to the calcination of lime. During the decomposition phase, the limestone (or dolomite) is reduced to slaked lime (Ca(OH)_2) and carbon dioxide. It is this part of the process that generates the majority of the GHG associated with clinker production. Moreover, the carbon dioxide does not take part in the formation of clinker and is a generated waste product. The slaked lime on the other hand, is an essential component in the second phase of the kiln.

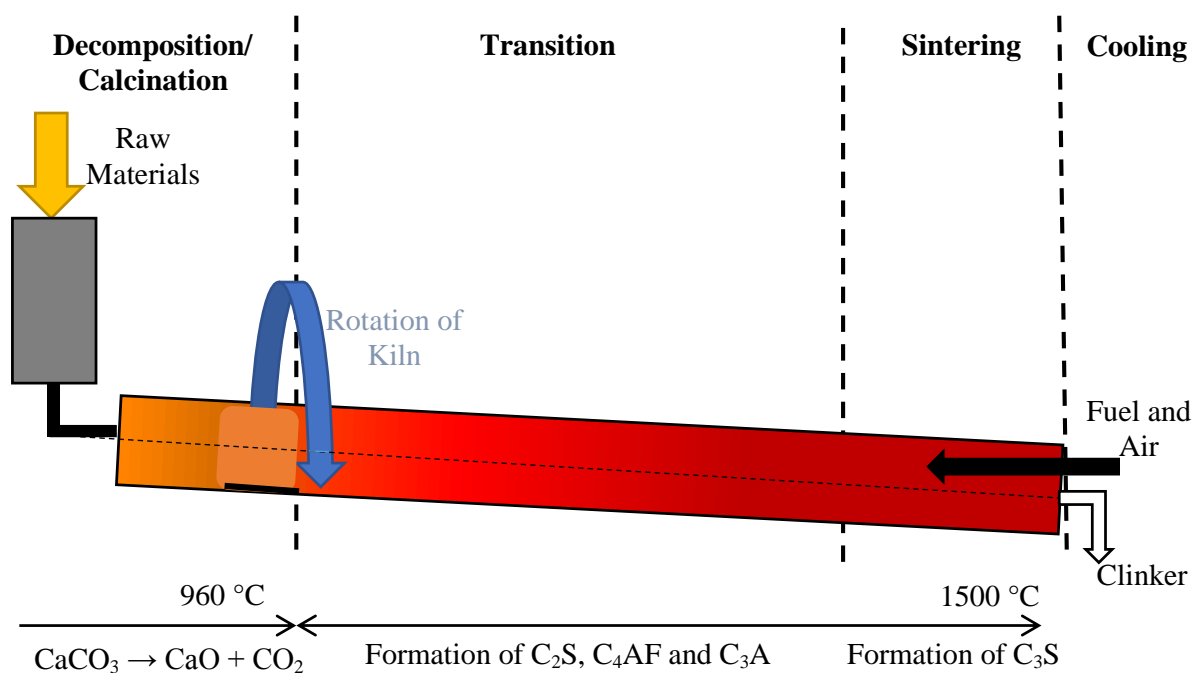


Figure 2-1. A schematic of the production process of cement.

In the transition zone, the material undergoes a phase transformation. Figure 2-1 displays the transition zone where the main constituents of clinker are formed, namely, alite (C_3S), belite (C_2S), and calcium aluminoferrite (C_4AF). Firstly, the slaked lime combines with the reactive silica to produce belite and with an increase in temperature, the belite and free lime combine to form alite (Kosmatka et al., 2003). In the sintering zone, more belite is transformed into alite by reacting with slaked lime. Moreover, typical descriptions of the change in the state and composition can be found elsewhere for better understanding (Kosmatka et al., 2003; Domone & Illston, 2010; Ishak & Hashim, 2014).

At the end of the kiln, the clinker is expelled and the cooling process is instigated. The final product is in the form of chunks of solids known as clinker. Hereafter, the material is ground to the required fineness and additional additives are introduced. One such addition is gypsum which is necessary to prevent the flash setting phenomena during the hydration process. This phenomenon is explained in the sections to follow.

2. 1. 2. Characterisation: Chemical Properties

The reactivity of cement is a function of its chemical composition. The highest weight percentage of cement is calcium oxide and silica, 60 – 67 % and 17 – 25 %, respectively (Domone & Illston, 2010). Cement consists of a complex matrix of four main compounds formed in the kiln (Domone & Illston, 2010). The compounds are: tricalcium silicate, dicalcium silicate, tricalcium aluminate and tetracalcium aluminoferrite (Zhang et al., 2013). The approximate quantities of each of the four main oxides can be quantified by the use of Bogue's equation (Neville & Brooks, 2010):

$$C_3S = 4.07(C) - 7.60(S) - 6.72(A) - 1.43(F) - 2.85(S') \quad \text{Equation 2.1}$$

$$C_2S = 2.87(S) - 0.75(C_3S) \quad \text{Equation 2.2}$$

$$C_3A = 2.65(A) - 1.69(F) \quad \text{Equation 2.3}$$

$$C_4AF = 3.04(F) \quad \text{Equation 2.4}$$

The abbreviations are as defined in Table 2.1. The denotation in parenthesis indicates the mass percentage of each component present in the cement. Kosmatka et al. (2003), has however stated that the use of Bogue's equations are not as accurate and developed methods, including X-ray diffraction, should be used to quantify the amount of oxides present. Each of the four oxides present play a role in the hydration reactions of cement. The role of each of the mentioned oxides is discussed in the sections to follow.

Table 2.1. The notation used to describe the components of cement chemistry.

Name	Formula	Abbreviation*
Calcium oxide	CaO	C
Silica	SiO ₂	S
Aluminium oxide	Al ₂ O ₃	A
Iron (II) oxide	Fe ₂ O ₃	F
Water	H ₂ O	H
Calcium hydroxide	Ca(OH) ₂	CH
Sulphur trioxide	SO ₃	S'
Tricalcium silicate	3CaO·SiO ₂	C ₃ S
Dicalcium silicate	2CaO·SiO ₂	C ₂ S
Tricalcium aluminate	3CaO·Al ₂ O ₃	C ₃ A
Tetracalcium aluminoferrite	4CaO·Al ₂ O ₃ ·Fe ₂ O ₃	C ₄ AF

*Note: The abbreviation used for the name of the compounds is a form of chemical shorthand and should not be confused as the representation of chemical elements.

Additionally, clinker is blended with gypsum (CaSO₄·2H₂O) to cater for flash setting. Flash setting is a phenomenon occurring when cement and water react and almost instantaneously turn into a solid material. This is discussed in the section regarding the hydration process, namely Section 2.4.

Moreover, additional impurities also exist within cement, such as magnesium oxide (MgO) and alkalis in the form of sodium and potassium oxides, Na₂O and K₂O respectively

2. 1. 3. Characterisation: Physical Properties

The physical properties of cement are also an influencing factor in cement reactivity. Cement consists of individual angular particles (Figure 2-2) which can be smaller than 45 µm (Kosmatka et al., 2003), but the majority range lies between 2 – 80 µm (Domone & Illston, 2010). Domone and Illston (2010) further state that the average particle size can be stated to be a function of the grinding process and the requirement of the cement.

Moreover, the reactivity of cement is influenced by the fineness: the finer the cement, the more reactive it can be. The increased reactivity is based on the increased surface area available or exposed for the hydration process to occur. The Blaine fineness of cement is used as a typical physical measure of its fineness. The Blaine test (air permeability test for specific surface area) is based on the principle of resistance to air flow through a partially compacted cement sample (Lea & Hewlett, 1998). Typically, cement has a Blaine fineness ranging between 300 – 500 m²/kg (Domone & Illston, 2010).

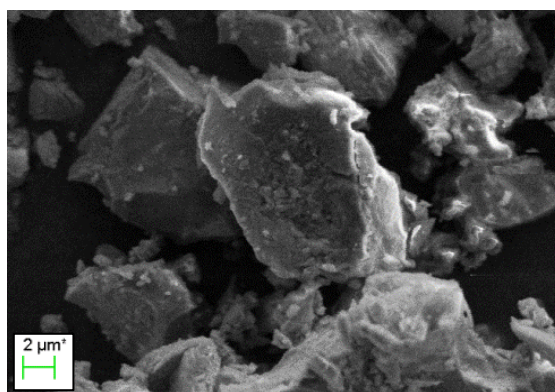


Figure 2-2. SEM image depicting the morphology of typical cement particles.

2. 2. Types of SCMs

2. 2. 1. Classification of SCMs

SCMs can be divided into two types of materials, defined by the behaviour of the material, namely, hydraulic binders and pozzolanic binders. Hydraulic binders form cementitious products, and therefore set when submerged in water (Snellings et al., 2012). On the other hand, the ASTM C125 defines a pozzolan as ‘a siliceous or siliceous and aluminous material that itself possess little or no cementitious value but will, in finely divided form and in the presence of water, chemically react with calcium hydroxide at ordinary temperatures to form compounds possessing cementitious properties.’

Possibly, SCMs can be classified based on: (i) origin, (ii) chemical and mineralogical composition and (iii) typical particle properties (Snellings et al., 2012). The first mentioned, namely basing the classification on the origin, provides a good way of creating a classification system (Snellings et al., 2012). It is to be noted that the term ‘origin’ does not refer to the geological location of the material, but

rather the way it is obtained or how it occurs. Therefore, the material can be divided into two broad classes: natural and artificial materials (Snellings et al., 2012).

Natural occurring SCMs can be further divided into two classes: volcanic material and sedimentary material (Figure 2-3). Volcanic material, such as ash, tuffs, zeolites and pumice, can exhibit pozzolanic properties if the cooling of the molten material is at a fast enough rate. The cooling rate is required to be relatively fast in order to ensure that the silica is in its reactive form. Sedimentary materials, which includes diatomaceous earth, clay and shale, are deposits of high-silica rocks (Snellings et al., 2012).

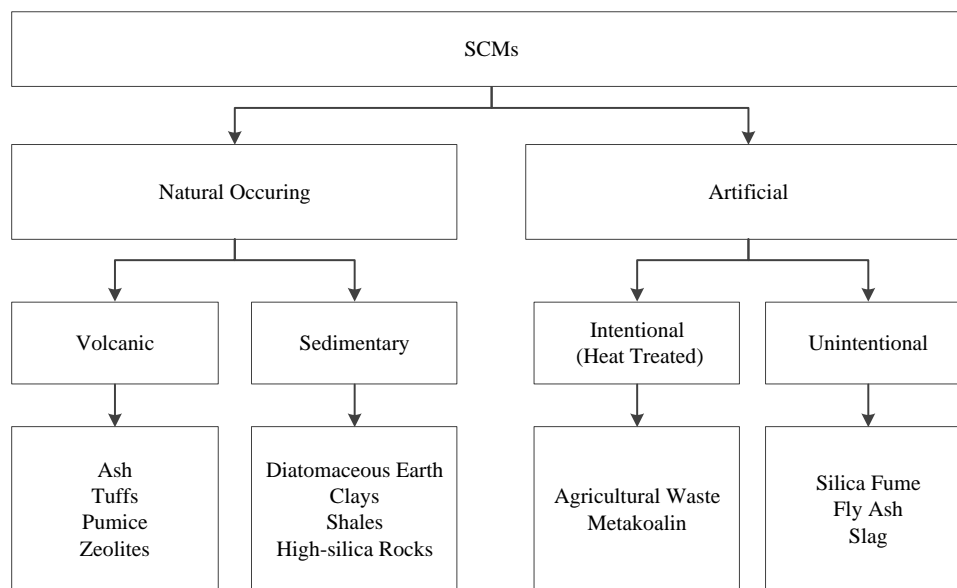


Figure 2-3. Classification of SCMs (Snellings et al., 2012).

Artificial SCMs can also be subdivided into two sub-classes, namely, those that are intentionally produced and those which are from unintentional production (in other words, waste materials). The intentionally modified materials are typically thermally treated to enhance the reactivity of the material (Snellings et al., 2012). Examples of materials within this category include the treatment of agricultural waste, such as baggashe ash, or the activation of metakaolin. The unintentional production of SCMs are typically from industrial production processes. Three of the most common products include silica fume (from the production of ferrosilicon alloys), fly ash (from the combustion of coal) and slag (from the production of iron). The latter two mentioned materials are focused on in the remainder of the literature review.

2. 2. 2. A Note on LCA's

The use of SCMs in the production of concrete provides a means of reducing the carbon footprint of the cement industry. However, the extent to which these materials have been assessed, in terms of the carbon dioxide reduction, has been criticised. Juenger and Siddique (2015) have listed in their review the necessity to address the importance of stating the allocation of SCMs when incorporated in a Life Cycle Assessment (LCA). For instance, if the waste material is considered as to be “avoided waste”, no allocation is made for the production of the product; this in turn considers the product to effectively

produce no carbon dioxide in its production. Hence, the idea is fostered that the total carbon dioxide released for concrete using this material is effectively reduced. In fact, the production of SCMs are also linked to a certain degree of carbon release; the difference being that the extent of carbon being released is reduced as well as using materials that would otherwise have generated additional problems, such as disposal issues. Therefore, the general use of these products still have value, as material is recycled and with the efficient production, the global cement usage can be decreased.

2. 2. 3. Production Process: Fly Ash

Fly ash is generated as a by-product of the combustion of coal. Kosmatka et al. (2003) describes the formation process by stating that the mineral impurities, which for example include clay and shale, fuse together during the ignition of the coal. The exhaust gases in turn carry off these suspended materials. Hereafter, the materials cool and solidify into spherical particles known as fly ash (Kosmatka et al., 2003). The collected materials can undergo one of two processes: a dry process or a wet process. For the dry process, the gases are collected by electrical or mechanical precipitators and rapidly cooled to produce the amorphous structure. The wet process is considered an older method and the quality is inferior compared with that of the dry process (Xu, 1996).

2. 2. 4. Production Process: Slag

Slag is derived as a by-product from the production of iron. Iron ores contain oxides of silica, iron and aluminium. Inside a blast furnace, the iron oxide is reduced to a metallic iron. This is aided by the use of a fluxing agent, typically a dolomitic or limestone material. The calcium oxide in the flux reacts with impurities such as the oxides of silica and aluminium. The molten material forms a layer on top of the metallic iron, known as slag. The slag is tapped from the blast furnace and quenched with water to rapidly cool the material and create the material with an amorphous glassy structure (Alexander et al., 2003; Domone & Illston, 2010).

Moreover, in South Africa, a second, more environmentally friendly, method of slag production is also used, namely the Corex process. With this process, the coke ovens and blast furnace are replaced with a direct reduction shaft and a melter-gasifier. This change produces slag of a different chemical composition and hydraulic activity compared to the slag produced by the blastfurnace process, although not a pronounced difference (Alexander et al., 2003).

2. 2. 5. Characterisation of Fly Ash: Chemical Composition

The chemical nature of SCMs play a vital role in the reactivity of the SCMs, and inadvertently the possible use of the material as a binder. The silica found in SCMs is also in a glassy, amorphous state, making it more reactive within the optimum conditions. The alumina present can also be in its reactive form and therefore form part of the hydration reactions.

The composition of fly ash is dependent on the type and quality of coal that is combusted and the process that is used (Xu, 1996; Lea & Hewlett, 1998). The main constituents of fly ash consists of

silica, alumina and the oxides of calcium and iron (Lohtia & Joshi, 1995). These materials originate from the presence of inorganics (contained in the coal) that are disintegrated during the combustion process.

ASTM C-618 (2010) defines two types of fly ashes depending on the type of coal combusted (Xu, 1996; Shi et al., 2012). Two types of fly ash are thus identified, specifically, Class F and Class C. The Class F fly ash is obtained when anthracite or bituminous coal is combusted, while Class C is obtained by the combustion of sub-bituminous coal or lignite coal (Xu, 1996). The combustion of the different coal types also influences the calcium content. Anthracite and bituminous coal produce low calcium fly ash and the latter two (sub-bituminous and lignite coal) produce high-calcium fly ashes (Xu, 1996).

The different calcium contents also have an impact on the oxides formed during the combustion process. These mentioned differences in the oxides that are present provides a means of classifying the ashes based on the sum of three key oxides, viz. silica, alumina and iron oxide. If the sum of the mentioned oxides exceeds 70 wt. % the ash is classified as a Class F. Furthermore, if the sum of the three oxides is 50 wt. %, the ash is classified as Class C.

Additionally, fly ashes can be distinguished based on the lime content. A fly ash sample is considered to be a high-lime content if there is more than 10 wt. % of free lime present. The differences in lime content affect the oxides present: the alumina and silica content is similar, yet the iron oxide content is lower for the high-lime fly ashes (Xu, 1996). In addition, the higher constituents of calcium also affect the degree of the self-cementing capacity of the fly ash and are addressed in the sections to follow.

2. 2. 6. Characterisation of Slag: Chemical Composition

The composition of slag is also a function of the raw materials used and the type of blast furnace used (Lewis et al., 2003). The rapid cooling process of the molten slag creates amorphous glass particles consisting of silica, alumina and iron oxides (Lewis et al., 2003) in addition to the oxides of calcium and magnesium (Talling & Krivenko, 1996).

The chemical composition of slag consists mostly of calcium oxide, silica alumina and magnesia; notably, these are also the major components found in typical Portland Cement (Talling & Krivenko, 1996). In addition, the glass content of the slag aids in the material being a potential latent hydraulic binder, with a glass content of at least 66 %, yet preferably exceeding 90 %. Moreover, it is preferable that the sum of the oxides of calcium, magnesium and silicon exceeds two thirds of the total compounds on a mass basis (Talling & Krivenko, 1996). Table 2.2 gives the chemical composition range of selected literature.

Table 2.2. List of SCMs' chemical composition from selected literature.

Material	Chemical Composition (%)						
	CaO	SiO ₂	Al ₂ O ₃	Fe ₂ O ₃	MgO	*	
Portland Cement	55 - 66	20 - 24	0 - 8	-	0 - 5	[1]	
	60 - 67	17 - 25	3 - 8	0.5 - 6	0.1 - 4	[3]	
	63 - 69	19 - 24	4 - 7	1 - 6	0.5 - 3.6	[2]	
Slag	GGBS	30 - 50	28 - 40	8 - 24	-	1 - 18	[1]
		34 - 45	30 - 37	9 - 7	0.2 - 2	4 - 13	[3]
		32 - 37	34 - 40	11 - 16	0.3 - 0.6	13 - 10	[2]
	GGCS	34.17	37.8	34.17	0.65	11.14	[4]
Fly Ash	Class F	1.5 - 6	44 - 58	20 - 38	4 - 18	0.5 - 2	[3]
	Class C	8 - 40	27 - 52	9 - 25	4 - 9	2 - 8	[3]
		South African	4 - 7	48 - 55	28 - 34	2 - 4	1 - 2

* Reference: [1] Talling and Krivenko (1996); [2] Grieve (2009); [3] Domone and Illston (2010); [4] Otieno et al. (2014).

2. 2. 7. Characterisation of Fly Ash: Physical Properties

The physical properties of fly ash and slag differ considerably with regard to morphology and therefore affect the impact these materials have in concrete. Fly ash consists mainly of particles that are spherical in shape (Figure 2-4 a). The spherical shape has been noted to enhance the workability of concrete and the water demand and is discussed in the subsequent sections. The particle size ranges of SCMs are also in a similar, if not smaller, range as cement particles. Fly ash ranges between 1 – 80 μm (Domone & Illston, 2010). The true ranges of the materials can however change, depending on the production process. In addition, the relative densities of SCMs tend to be lower than that of cement. Typically, cement has a relative density of 3.14, whereas fly ash a typical relative density of 2.3.

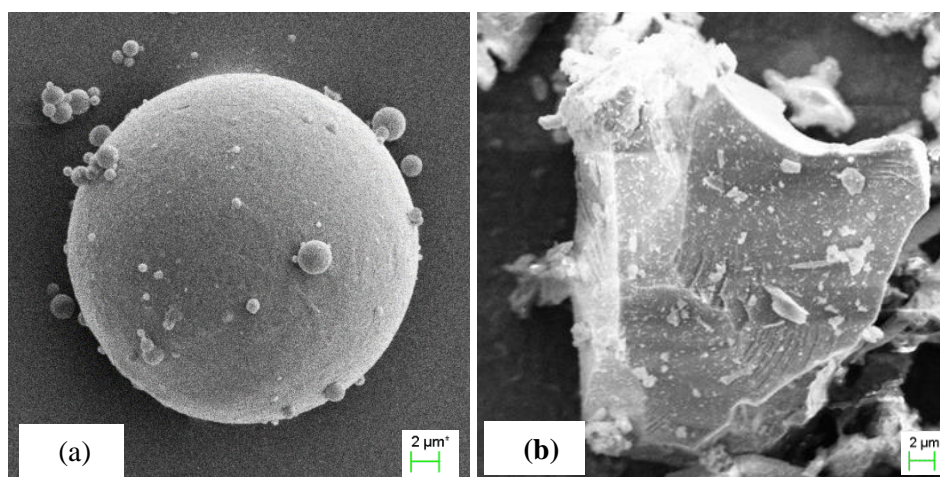


Figure 2-4. The morphology of (a) a fly ash particle and (b) a granulated slag particle.

2. 2. 8. Characterisation of Slag: Physical Properties

In contrast, slag particles are noted to be similar in shape as cement particles i.e. angular (Figure 2-4 b), as opposed to fly ash particles. The angular particles are a result of the rapid cooling and grinding process. Slag particles lie in the range of 3 – 100 μm (Domone & Illston, 2010). The relative density of slag is also lower than that of cement, however, higher compared with the relative density of fly ash. The average relative density of slag is approximately 2.9.

2. 3. General Effects of the Addition of SCMs on the Binder System

The addition of SCMs in a concrete mixture affects the system of the binder in total. The effects of the use of SCMs are noted in three different ways. Firstly, the addition of SCMs impact concrete on a physical level. Secondly, the addition affects the concrete mixture on a surface chemical level. This effect is associated with the surface area and also the filler effect. And thirdly, a chemical level, where the added material takes part in the reactions (Moosberg-Bustnes et al., 2004).

2. 3. 1. The Physical Level

The physical effect of SCMs on a system is commonly referred to as the filler effect. This phenomenon is related to the particle packing efficiency of a system. As mentioned in the preceding sections, the particles of SCMs are generally on the same micro-scale as cement particles. However, in some instances the particles can even be smaller in comparison with the cement. Therefore, the smaller particle sizes have a beneficial role in enhancing the overall packing density of a concrete mix and also enhance the nucleation and growth of C-S-H growth during the hydration process (Juenger & Siddique, 2015).

Larger particles fill a volume of space, yet a series of voids form between these particles. Thus, the full volume is not occupied by the said larger particles; voids are found between the particles and give rise to the concepts of porosity. If another set of particles, smaller than the first set of particles, are added, these smaller particles will tend to and potentially fill the gaps between the larger particles. Therefore, the overall result is a decrease in the ratio of voids i.e. a less porous system. The process can thus theoretically continue until a system is reached where all the voids are filled with particles i.e. the volume of voids decrease to zero and full particle packing is achieved. Figure 2-5 shows the concept of achieving perfect particle packing. This idea forms the basis for the filler effect. However, this assumes an ideal system, which is not plausible in practice, mainly because of the difference in particle sizes and shapes.

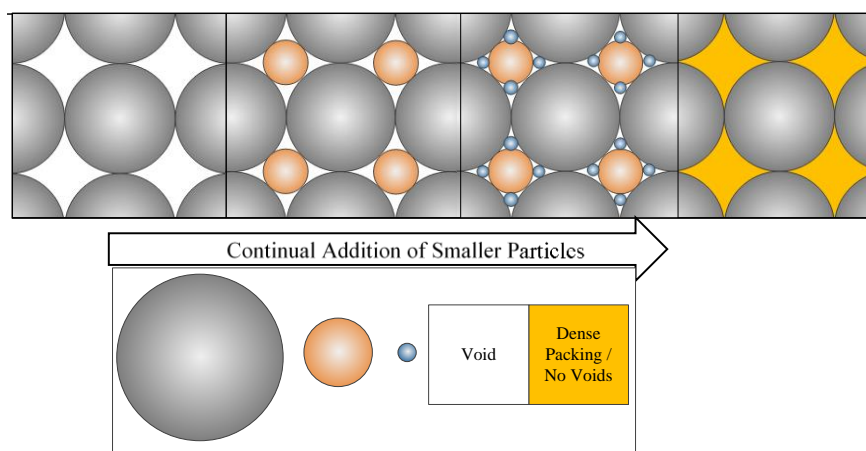


Figure 2-5. Explanation of the principle of achieving theoretical optimal packing density.

Moreover, two additional phenomena inhibit the achievement of perfect particle packing, namely, the wall effect (Figure 2-6 a) and the blocking effect (Figure 2-6 b) (Moosberg-Bustnes et al., 2004). In a cementitious paste system, water forms a key component and adsorbs to the particles' surface. Therefore, the region between the paste cement particles and products are not in close proximity to the aggregate; also known as the interfacial transition zone (ITZ). This creates a weak spot in a concrete structure and is discussed in the sections to follow (Section 2.7). However, adding finer material optimally reduces the size of the ITZ. The blocking effect results from the occurrence of two aggregates situated so close to each other that it reduces the probability of cementing particles getting in between the mentioned particles. The paste generated between aggregates are therefore considered to be of a lower density (Moosberg-Bustnes et al., 2004).

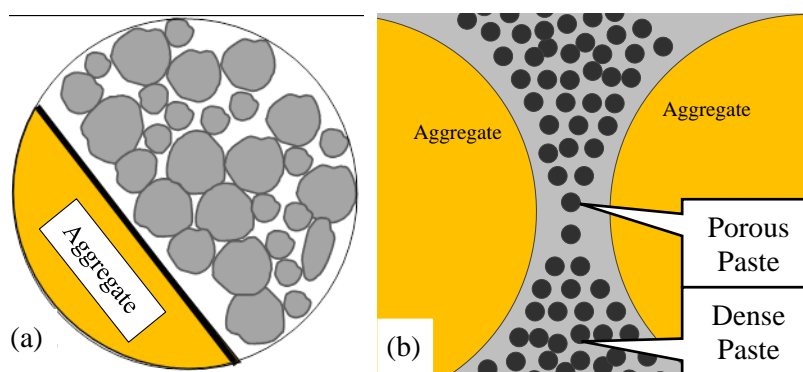


Figure 2-6. The two phenomena experienced by particles: (a) the wall effect and (b) the blocking effect (Moosberg-Bustnes et al., 2004).

2.3.2. The Chemical Surface Level

The chemical surface effect is also related to the filler effect and acts as one of the mechanisms contributing to the latter mentioned (Lothenbach et al., 2011). The finer particles added act as a nucleation site for hydration products formed (Moosberg-Bustnes et al., 2004; Lothenbach et al., 2011; Juenger & Siddique, 2015). The smaller particles fill the gaps and decrease the overall number and volume of voids. Therefore, inadvertently the bridging distance between hydration products formed during the hydration process is decreased. More on this is discussed in the section on hydration kinetics, i.e. Section 2.4.

2.3.3. The Chemical Level

In the finely divided form, SCMs can also react with available compounds to form hydration products. Therefore, the addition of certain SCMs aid in terms of producing calcium silicate hydrates, the compound attributed to giving concrete its relatively high strength. The reactions undergone by SCMs are discussed in the Section 2.4.

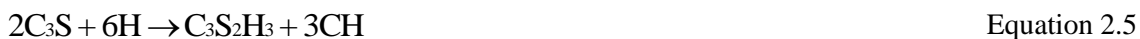
2. 4. Reaction Kinetics

The hydration of cementitious materials is an exothermic reaction that produces compounds, such as calcium-silica-hydrates, that contribute to the binding nature and strength of cementitious material. There are factors that contribute to the reactions, such as the type of material (and inadvertently the compounds presents), fineness, the particle distribution and the environmental conditions required for the process to occur. However, it is firstly required to understand the difference between the reaction of cement particles and SCMs.

2. 4. 1. The Cement Hydration Reaction

Concrete undergoes a transformation from a semi-plastic material to a rigid compound due to the chemical reactions occurring; this is known as the hydration of cement. The solidification and strength gain of a cementitious compound occurs as the result of the four main compounds reacting with the moisture introduced, thereby creating a paste with desirable properties.

The hydration reaction of cement and water is a strong exothermic reaction. Using the abbreviations listed in Table 2.1, the hydration reaction of cement can be described as (Grieve, 2009):



where, $C_3S_2H_3$ is the calcium silicate hydrate gel (C-S-H). C-S-H gel which is typically smaller, and has needle and plate like structures. It is also the C-S-H that gives a hydraulic cement paste its strength. CH tends to be larger in size compared with C-S-H crystals and do not contribute to the strength development of hydraulic cement pastes. The calcium hydroxide does however create a high alkaline environment (pH >12) that is required by the products which are formed and therefore acts as a “traditional ‘activator’ to increase hydraulic activity of vitreous phases” (Zhang et al., 2013).

As mentioned before, it is the C-S-H product that contributes to the strength of the cement paste. The alite (C_3S) and belite (C_2S) are the main reactants that produce the C-S-H crystals. In addition, these two oxides also make up the majority weight percentage of Portland cement. By comparing the reaction of these two materials, it is observed that alite reacts at a faster rate compared to the belite, as is shown in Figure 2-7. The alite is attributed to the early age strength gain and setting time (Bullard et al., 2011). The belite on the other hand, is mostly linked to the long term strength gain (Kosmatka et al., 2003).

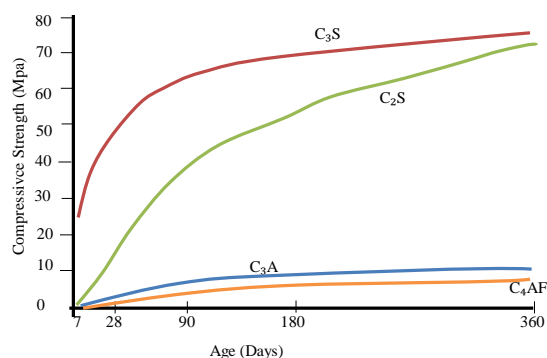


Figure 2-7. The strength gain contribution of the four main oxides present in Portland cement (Czernin, 1980).

The C₃A and C₄AF produce a relatively small contribution to the strength gain as seen in Figure 2-7. In addition, C₃A tends to react rapidly with moisture and can cause a flash set in cement pastes. Flash set occurs when the transition from a molten state to a solid state occurs rapidly and abruptly. In order to prevent such an event, gypsum is added to the ground clinker. The gypsum reacts with the C₃A and causes a delay in the reaction between moisture and C₃A. The quantity of gypsum added is therefore a function of the amount of C₃A present.

2. 4. 2. The Pozzolanic Reaction

SCMs are capable of taking part in a hydration reaction under given circumstances mainly due to the presence of the reactive component, i.e. the silica and alumina. When cement is hydrated, calcium hydroxide (CH) is produced (as seen in Equation 2.5). CH does not provide any significant strength in hydraulic pastes (Czernin, 1980). However, CH creates an environment with a relatively high alkalinity in a cementitious paste and also acts as a reactant in the pozzolanic reaction (Snellings et al., 2012). The pozzolanic reaction is given by:



The reactive silica present in the SCMs reacts with the CH and a product similar to C-S-H gel is produced. This secondary reaction has a positive influence on the long-term strength capacity of the cement matrix, as the CH does not contribute to any significant strength.

The hydraulic activity of pozzolans also tends to be at a slower rate compared to that of cement hydration. This reduced reaction rate is typically the reason for the reduced early age performance of concrete and mortars containing SCMs (see Figure 2-8). Two interdependent reasons can be described for the reduced performance: (i) the dilution of cementing particles and therefore (ii) the reduction in required reactants. With the partial replacement of cement with SCMs, the initial amount of products formed (C-S-H and CH) is initially reduced, therefore, the time required to reach the same pH as well as concentration of products is prolonged for a sample containing SCMs. Moreover, the delay in reaching the required conditions inhibits the initial performance of the SCMs.

Figure 2-8 shows the described phenomena. As seen, the initial hydration, described in terms of strength development, of the SCM based sample (A) is less compared to that of the reference (B). The

reason for the differences is most likely because of the lower hydration products available as the initial reactants are less. Yet, as the hydration of cement increases, and more CH is produced, the SCM constituents in the respective concrete starts reacting as well (demarcated by the decrease in CH concentration) and the hydration is enhanced.

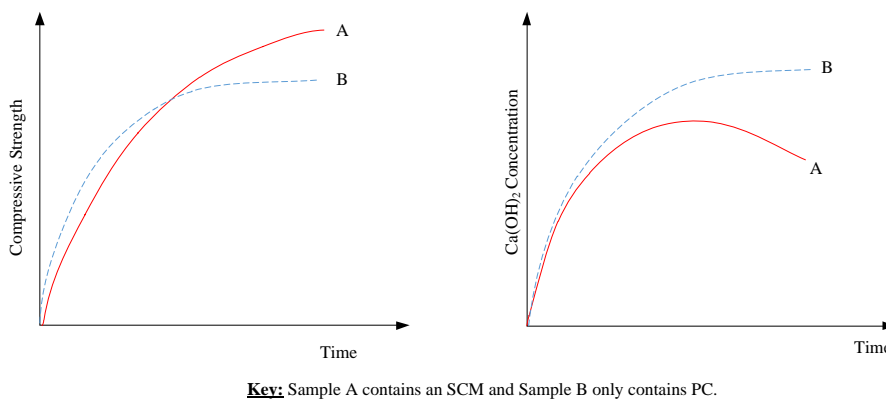


Figure 2-8. The effect of SCMs on the compressive strength and calcium hydroxides concentrations (Lewis et al., 2003).

2. 4. 3. The Latent Hydraulic Reaction

SCMs can also possess self-cementing properties to a certain extent, for instance slag. In the presence of moisture, slag can react to create the same hydrated phases as in the case when Portland cement hydrates (Kurdowski, 2014). However, the reaction of slag with water is too slow for it to be regarded as an independent hydraulic binder (Czernin, 1980). Yet, in the presence of activators, the slag reaction with moisture can be increased as the dormant activation energy is released (Czernin, 1980; Kurdowski, 2014).

Czernin (1980) states that upon contact with water, slag reacts rapidly and a layer of silica-alumina gel is formed around the slag; this layer of gel acts as a barrier between the water and the slag particles inhibiting additional reactions to occur as it has a relatively low permeability (Kurdowski, 2014). However, Czernin (1980) further states that in the presence of a strong alkali, typical of cement pastes, the silica-alumina gel has a coarser texture, as the alumina becomes more soluble in a solution of a relatively high pH (Kurdowski, 2014), with a relatively higher permeability. The increased permeability therefore does not inhibit the contact between granulated slag particles and moisture.

Kurdowski (2014) mentions three activators that can be implemented to allow the ‘activation’ of slag. The first type of activator can be a basic compound, which include Ca(OH)_2 , NaOH and Na_2SiO_3 . Secondly, low acidic materials, such as CaSO_4 and $\text{Al}_2(\text{SO}_4)_3$, are also potential activators. Lastly, physical conditions, such as higher temperature and pressure are reported to enhance the reaction of slag as a binder. Additionally, ground granulated slag can also undergo hydration without an activator, possibly due to the hydrolysis of calcium sulphide, described by Kurdowski (2014) as:



However, by inspecting the reaction given by Equation 2.10, it is observed that $\text{Ca}(\text{OH})_2$ is a product from the reaction of calcium sulphide and water. Therefore, taking into account the earlier mentioned statement that the $\text{Ca}(\text{OH})_2$ acts as a basic activator, it can be concluded that the granulated slag is still ‘activated’ in a sense by the CH.

The reactions of slag-based concrete are complex and not yet fully understood, however, Grieve (2009) gives a simplification of the reaction as follows:



where the granulated slag is represented by $(\text{C} + \text{S})$ and a and b denotes constants for stoichiometric equilibrium. CA products refer to the calcium aluminates. Granulated slag reacts with the moisture and produces C-S-H and silica (Equation 2.11). The silica produced can in turn react with CH, typically from the reaction of cement hydration or the hydrolysis of calcium sulphide, thereby creating C-S-H.

2. 5. Quantifying Reactivity of SCMs

The use of SCMs as a potential replacement of cement in concrete requires testing, and various methods have been developed to assess the potential of a given SCM. These tests can be divided into two main categories, namely, direct and indirect methods (Pourkhorshidi, 2013). Each of these test methods have benefits and downfalls which should be considered when choosing a method of assessing a said material for use in the concrete binder system.

2. 5. 1. Direct Methods

Direct methods make use of analytical means to determine the presence of calcium hydroxide (CH) and its subsequent reduction in abundance with time (Donatello et al., 2010). This classification is based on the notion that a potential SCM will react with the available CH in a system, as discussed in the previous section, thereby diminishing the CH content. This depends on the reactivity of the material. Typical direct methods include X-ray diffraction (XRF), thermo-gravimetric analysis (TGA), Frattini test and the saturated lime test (Donatello et al., 2010; Pourkhorshidi, 2013).

- Thermo-gravimetric Analysis (TGA)

Thermo-gravimetric analysis is a means of measuring the lime binding capacity of a test sample based on thermal decomposition of crystalline calcium hydroxide (Pourkhorshidi, 2013). At a temperature range between 400 – 500 °C, the crystalline CH decomposes into water and calcium oxide:



Furthermore, the mass loss over time, as a result of water evaporating at the higher temperatures, is recorded. The lower the water loss is, the more suitable the SCM is, and vice versa (Pourkhorshidi, 2013). If a SCM consumes the available CH in a system, the overall concentration of the CH decreases indicating that a less crystalline CH is available for degradation, hence a higher level of pozzolanic activity.

An area of concern of using this test method lies in the sample preparation. The samples are dried prior to testing in order to get rid of any evaporable water. However, it should be noted that the evaporable water is a function of the degree of hydration. This in turn would suggest that the basis for mass loss calculation is not constant and may result in variations (Juenger & Siddique, 2015). Solutions to the problem have been suggested, such as not drying the sample prior to testing, thus accounting for evaporable water loss (Taylor-Lange et al., 2015). Additionally, a possible factor that may influence the results is evident in the fact that other mineralogical components may also decompose at the mentioned temperature range (Juenger & Siddique, 2015).

- Mineralogical Analysis

One method of detecting the mineral components of a sample is via X-ray diffraction. This method identifies the amount of crystalline minerals and from this established the amount of non-crystalline silica (Pourkhorshidi, 2013; Juenger & Siddique, 2015). Pourkhorshidi (2013) suggests a good correlation between XRD results and the insoluble residue (IR). Furthermore, it is suggested that a sample with less than 15 % amorphous minerals would display poor pozzolanic performance (Kosmatka et al., 2003). One of the drawbacks of this test however is the difficulty in differentiating between the different amorphous phases present in a sample (Juenger & Siddique, 2015).

- Frattini Test and BS EN 196-5:2011 Standard

The Frattini test, adopted for use by the BS EN 196-5 (2011), assesses pozzolanic activity based on the concentration of calcium ions (Ca^{++}) that are present in an aqueous solution and that has been in contact with a hydrated blend of cement for a fixed period of time. A unique, predefined curve has been created to establish a region between a pozzolanic and non-pozzolanic areas (Figure 2-9) (Donatello et al., 2010; Pourkhorshidi, 2013).

Any result obtained that is lying below the curve (“Curve of Zero Pozzolanic Activity” in Figure 2-9) is attributed to the removal of calcium ions, thus potentially being a SCM. The curve of zero activity represents the lime solubility curve and represents only the creation of calcium ions by the cement. A potential drawback with the discussed test method is the sensitivity to solution preparation. Therefore, the filtration should be done with great care as to not introduce any solids that may act as a buffer and alter the readings. In addition, the initial ion concentration is not known, which could be influenced by the difference in reaction of cements.

- Saturated Lime Test

The saturated lime test is similar in concept to the Frattini test. The saturated lime test is also deemed to be simpler and provides a quantitative result (Donatello et al., 2010). The saturated lime test differs from the Frattini test in which sample preparation; for the lime saturation test, the SCM is mixed with a saturated lime solution instead of a water-cement mixture. This in turn means that the total amount of calcium ions present is known at the start of the test. The test method then measures, by means of

titration, the amount of residual dissolved calcium, which can be presented as a percentage of the initial calcium concentration (Pourkhorshidi, 2013).

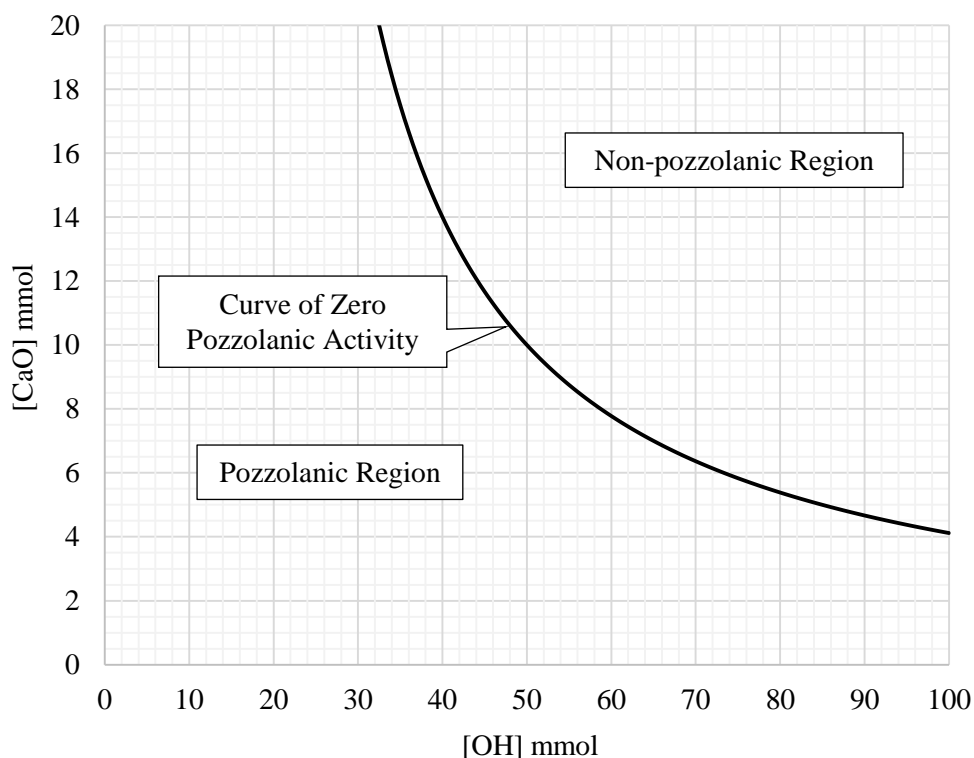


Figure 2-9. The Frattini curve used to demarcate the regions of pozzolanic and non-pozzolanic areas.

2.5.2. Indirect Methods

The indirect methods “measure a physical property of a test sample that indicates the extent of pozzolanic activity” (Donatello et al., 2010). Some of the parameters are measured in combination with cement, such as the strength activity index (Pourkhorshidi, 2013) while other tests include electrical conductivity and heat evolution by heat calorimetry (Donatello et al., 2010).

- Strength Activity Index (SAI)

The strength activity index is used as a prescribed method by the ASTM Standards C618 (2010) and ASTM Standards C989 (2013), as well as by the BS EN 450-1(2012) and BS EN 15167-1 (2006) . For the test, two mixes are created. Firstly, a reference mortar, of a standard water-to-binder and binder-sand ratio, is cast containing only Portland cement and no SCMs. A second set of specimens is also cast, with a portion of the binder replaced with the test SCM. The specimens are cured and tested after selected curing periods by means of a compression tests. The results are measured as the ratio between strengths of the SCM based mix to the reference and needs to be above a certain minimum percentage, as shown in Table 2.3 and Table 2.4, to be fit for use in concrete.

Table 2.3. Requirements for fly ash samples according to the ASTM and EN Standards.

Standard	Binder (g)	Cement Substitution (%)	Binder : Sand w:b		SAI Requirement (%)		
					7	28	90
ASTM C311	500	20	1:2.75	varies	> 75	> 75	-
BS EN 450-1	450	25	1:3	0.50	-	> 75	> 85

Table 2.4. Requirements for slag samples according to the ASTM and EN Standards.

Standard	Binder (g)	Cement Substitution (%)	Binder : Sand w:b		SAI Requirement (%)		
					7	28	Grade
ASTM C989	500	50	1:2.75	varies	...	> 75	80
					> 75	> 95	100
					> 95	> 115	120
BS EN 15167-1	450	50	1:3	0.50	> 75	> 75	-

From Table 2.3 and 2.4, it is apparent that the EN and ASTM standards have a few notable differences in assessing the SAI of SCMs. Firstly, the mix constituents of the two standards differ, however, this is just due to the mortar samples having different dimensions. The ASTM mortar cubes are 50 x 50 x 50 mm specimens in contrast to the EN prisms having dimensions of 40 x 40 x 160 mm.

Secondly, the water binder ratio for the standards also differs. For the EN standard, both specimens, the control and the sample containing SCMs, have a fixed water-to-binder ratio of 0.5. The equal water-to-binder ratio makes it easier to compare the two mixes to each other. However, The ASTM Standards have a varying approach in the sample preparation and therefore the difference in water-to-binder ratio is noted. For ground granulated slag mixes, the water for the reference mix and the test mix depends on the achievement of a certain flow (ASTM Standards C989, 2013). Additionally, mixes containing fly ash are compared to a reference, which has a set water-to-binder ratio of 0.485. However, the test sample's water content is again also controlled by a flow requirement (ASTM Standards C618, 2010). The final outcome could therefore result in a reference and a test mix having two different water-binder ratios. Hence, the differences in water-to-binder ratios can result in a specimen having a lower water-binder ratio compared to the reference and inadvertently it could show favourable results and vice-versa. Pourkhorshidi (2013) has also highlighted this criteria and suggested that a constant water-binder ratio should be used in order to be able to compare the result. The fineness of SCMs can cause an increase in the water requirement and therefore result in a higher water-to-binder ratio, hereby, potentially decreasing the strength. The addition of cement is done on a mass basis, which ultimately results in a difference in the volume fraction of the water-filled space, which is due to the differences in the relative densities (Pourkhorshidi et al., 2010). However, basing the results on the water requirement has a practical relevance: a SCM could exhibit good reactivity, if the basis of comparison is a constant water-to-binder ratio, but could not be of a significant use in a concrete mix if it has a high water demand to achieve a certain level of workability.

Thirdly, for the fly ash requirements, there is a difference in the cement substitution percentage. The ASTM C618 (2010) allows for a 20 % replacement of cement with fly ash, whereas, the BS EN 450-1

(2012) allows for a 25 % replacement. In addition, to cater for this, the two standards also allow for testing at different ages: 7 and 28 days for the ASTM C618 (2010) and 28 and 90 days for the BS EN 450-1 (2012). The delayed testing ages of the BS EN 450-1 (2012) ensures that the additional fly ash can have time to potentially react.

2. 5. 3. Comparison of Test Methods

Each of the previous mentioned test methods are individually sufficient. However, the question remains as to how these tests compare relative to each other, as well as their capability to identify the reactivity as efficiently and accurately as possible. In other words, the applicability of the mentioned tests, as well as the relevant applicability is a topic of debate. The previous section set out to explain how the relevant tests are conducted. Yet, as all these mentioned tests differ in principle, it is debatable on how these tests compare relative to each other to identify the reactivity of a material in question.

Donatello et al. (2010) conducted an investigation to compare the saturated lime, Frattini and SAI tests. The researchers tested sand, fly ash, metakaolin and sludge ash to replace the cement (and compared them to the control). The authors found that a significant correlation exists between the Frattini test and the SAI; with a $R^2 = 0.86$ for the tests completed. Furthermore, it was stated that the Frattini test could potentially be a representation of the pore solution that exists within the SAI specimens. Moreover, no correlation was established between the saturated lime test results and the SAI results; this again may be due to the fact that the saturated lime test represents a different system compared with that of the pore solution. Additionally, the lack of a solid phase forming may also be an underlying reason for the observed differences (Donatello et al., 2010).

Pourkhorshidi et al. (2010) investigated the applicability of the ASTM Standard C618 (2010) in conjunction with additional methods such as IR and SEM-images. The condition of summing the oxides had shown to overestimate the pozzolanic activity of some of the samples investigated. The sample that would have shown to perform the best under the chemical requirement, a tuff used in the mentioned research, actually showed no activity when subjected to the EN 196-5 (2011) test method. Also, the pozzolan that would classify as having the least pozzolanic activity, according to the summation of oxides, showed to outperform the before mentioned tuff according to the Frattini test (Pourkhorshidi, Najimi, et al., 2010). This again shows the need to use different methods in conjunction with one another to establish the validity of a given result.

Testing SCMs tend to focus on the performance of the material in a paste or mortar system. However, this neglects the performance of the SCM when used in a concrete system. This matter is essential and should be incorporated in the specifications set out for SCMs. Arguably, determining the water requirement can be seen as a method of evaluating the possible detrimental or favourable outcomes. However, this is not sufficient as some mechanical and durability aspects are not catered for using the mentioned criterion. Moreover, the plastic state properties are often neglected as well. Researchers have however found that the EN specifications displays a good compatibility between the prescribed

methods and performance of the pozzolans once used in concrete, hence highlighting the use of the EN Standard test methods (Pourkhorshidi, Najimi, et al., 2010; Pourkhorshidi, Hillemeier, et al., 2010).

2. 6. Effect of SCMs on the Plastic Properties of Concrete

The early age properties of concrete play a prominent role in the performance of concrete structures. The behaviour of the concrete within this period influences the overall long-term factors such as creep, shrinkage and durability. Therefore, even though the period at which concrete is in a plastic state is significantly less compared to the time of its structural use, the knowledge attained during this time is of great significance.

2. 6. 1. Setting Time

In terms of concrete technology, setting time is used to phrase the transformation of cementitious sample from a plastic to a rigid state (Neville, 2011). Setting times of concrete therefore marks a change in the physical-chemical characteristics of a cementitious paste and is measured by means of penetration resistance (Mehta & Monteiro, 2006). Therefore, the time over which concrete can be moulded and handled is limited to the time of reaching initial set. Initial set is regarded as the time after which concrete can no longer be handled or vibrated without causing significant damage to the internal structure. Final set is the time at which the concrete has lost all significant plasticity and is therefore considered a rigid or solid material and the onset at which concrete gains significant strength with time (Figure 2-10).

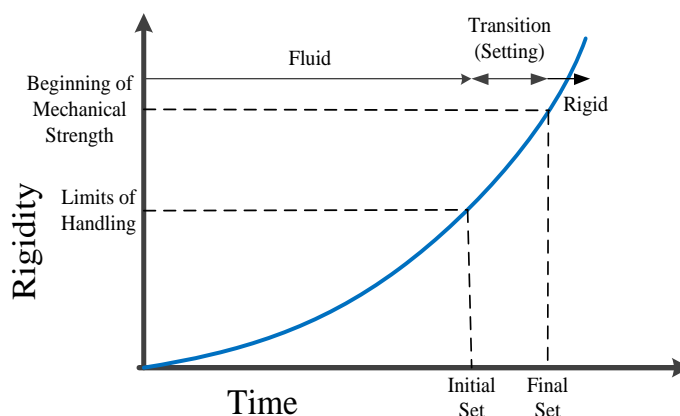


Figure 2-10. The stages of concrete setting (Metha & Monteiro, 2006).

The time taken to achieve initial set is set as a function of the amount of hydration products that form after bringing the components together; setting is mainly a function of the amount of C_3A and C_3S present in the concrete (Metha & Monteiro, 2006). Hence, setting is “controlled by the formation of a network of partially hydrated cement particles connected by hydration products that can resist a shear force” (Bentz et al., 1999). The shear resistance is measured by means of penetrations tests. As mentioned in Section 2.4, two phenomena can occur as setting concrete undergoes hydration, namely flash set and false set.

Flash set occurs because of C_3A rapidly reacting with moisture in a short span of time and releasing a large amount of energy, therefore preventing the placing and working of concrete. However, the flash set of concrete can be mitigated by the addition of gypsum. The gypsum reacts with the C_3A by encapsulating it. This retards the instantaneous reaction, thereby allowing the concrete to be in a plastic state for enough time to be handled and placed. False set in contrast occurs with negligible heat loss and can, with continual mixing, retain its original state of workability.

The setting time in turn is affected by (Kosmatka et al, 2003):

- water content,
- cement content and type,
- water-to-binder ratio,
- fineness,
- and temperature.

The first three listed parameters are somewhat inter related to the definition of setting time described earlier i.e. the generation of hydration products and therefore to the degree of hydration. Also, the setting time is directly related to the increase of water and the water-to-binder ratio (Bentz et al., 1999). The increase in setting time is explained by the dilution of cementing particles: as the water content or the water-to-binder ratio increases, the average distance between cementing particles increases, thereby increasing the required distance needed to achieve an inter-particle bond. In contrast, if the amount of cement increases, the inter-particle distance decreases. Moreover, there is also an overall increase in the amount of hydration products formed per unit time.

The fineness of cement accelerates the setting time of pastes if it (fineness) is increased. Firstly, the increased fineness has a surface chemical effect namely, that each particle acts as a nucleation site for hydration product as well as generating its own hydration products at the same time. Hence, the increase in total surface area can increase the contact between the cement particles and water i.e. more hydration products can form, as the increase in surface area is a known method of catalysing a chemical reaction. Bentz et al. (1999) conducted tests on the setting time of pastes with different fineness and water-to-binder ratios. The fineness, in terms of PSD, was selected to be at 5 and 30 μm and water-to-binder ratios to be 0.246, 0.3 and 0.5. At a water-to-binder ratio of 0.246 the time of set increased from 0.58 to 0.90 hours for a change in fineness of 5 to 30 μm . The time of set, for a water-to-binder ratio of 0.5, was 1.44 and 3.36 hours, for the same fineness of 5 and 30 μm , respectively. The latter mention result signifies the effect of increasing the w:b ratio. In their findings, Bentz et al. (1999) also mentions that even though an increase in fineness accelerates the setting of pastes, note should be taken that more hydration is required as a result of the increased inter-particle bridging. In addition, the acceleration of achieving set for finer cements can also be related to the increase in C_3A content with finer cements (Zhang et al., 2011), as C_3A contributes to the setting of cementitious pastes.

The hydration of cementitious pastes is an exothermic reaction. Therefore, at elevated temperatures, the setting of concrete will be achieved within a shorter period compared to one at a lower temperature (Kosmatka et al., 2003). Metha and Monteiro (2006) noted a retardation of 4 and 7 hours for initial and final set, respectively, when the ambient temperature was decreased from 23 °C to 10 °C.

The partial replacement of cement with SCMs is generally associated with causing the retardation of concrete setting. There is an advantage to the delayed setting time: there is more time to handle and place the concrete. However, in terms of the construction process, a delay in the setting time results in the delay of finishing operations and therefore the project completion. The reason for the retardation results from (i) the slower hydration of SCMs compared with cement (Beushausen et al., 2012) and (ii) the dilution of the cement particles.

As aforementioned, the hydration of SCMs is slower compared to that of cement itself, owing to the lower reactivity and self-cementing capacity (Alexander et al., 2003; Beushausen et al., 2012). Slag can react with moisture, yet the reaction is slow and impeded by the formation of a layer of low permeability, but in the presence of a catalyst, such as an activator, can increase the rate of reaction. The activator is generally in the form of the CH produced by the hydration of cement. However, if the concentration of CH is low, the catalyst effect is reduced: concentration affects the chemical reactions. This brings to mind the second effect that impedes hydration, viz. dilution of cement.

Dilution, resulting from the addition of SCMs by the partial replacement of cement, results in a decrease in hydration products, which is expected due to the reduction in initial reactants available. For example, take a scenario where a system containing 100 % PC, takes an arbitrary amount of x hours to achieve a sufficient degree of hydration to set. It stands to reason that a system with less cement, say for example only 80 % of PC, would theoretically take longer to achieve a similar degree of hydration as the 100 % PC system; it would only achieve setting at a period greater than the said x hours. Two reasons can be used to describe the delayed effect. Firstly, as mentioned, there are less products that can be formed and therefore the pH of the systems are not achieved at a similar rate to activate the SCMs. Therefore, the addition of the SCMs only has a filler function. Secondly, the cementing particles are also dispersed, hereby increasing the amount of inter-particle bridging required to achieve a certain degree of hydration.

An additional factor that also affects setting times with regard to a system containing SCMs is whether the material is chemically active or inert (a microfiller). Microfillers have a retarding effect on the setting time (Khan et al., 2014). Microfillers increase the packing density and cause an increase in the amount of fines, which increase the total surface area. The outcome therefore is a greater volume of hydration products required to establish an inter-particle bond (Bentz et al., 1999). Chemically active SCMs on the other hand can potentially reduce the setting time (Khan et al., 2014). The reason for the reduction of setting time is as a result of the SCMs contributing to the amount of hydration products formed per unit time. However, this therefore depends on the reactivity of the SCM used.

The addition of slag (Alexander et al., 2003; Beushausen et al., 2012; Siddique & Khan, 2011; Khan et al., 2014) and fly ash (Siddique, 2008; Bentz et al., 2011) results in the increase of setting times. The result is due to the aforementioned dilution effect. Moreover, slag and fly ash also reacts slower compared to cement, hereby causing the retardation of mixes setting.

With regard to the amount of cement replaced by slag, Prusinski (2006) reports that delays in setting time will occur at replacement levels exceeding 25 %; this is at an ambient temperature of 21°C. It is suggested that not all cement particles do hydrate at the early ages. Therefore, 75 % cement is still sufficient to achieve the same degree of hydration. In addition, the filler and surface-chemical effect at the low replacement level can be regarded as sufficient to promote the hydration rate. Prusinski (2006) also showed the trend of setting time decreasing with an increase in temperature, despite the replacement level; as at 33 °C, the setting times for a mix containing 0, 30 and 50 % cement replacement showed similar setting times of 5.8, 5.9 and 6 hours, respectively. Therefore, the effect of temperature plays a prominent role in the setting time of concrete containing slag (Khan et al., 2014).

In addition, composition is also a factor affecting the setting time. For example, the work by Beushausen et al. (2012) investigated three South African slags namely, GGCS, GGBS and GGAS. The GGCS and GGBS had similar setting times and the setting time did increase with cement replacement. The GGAS in contrast had longer setting times and the retardation increased with increasing cement replacement; at 50 % replacement, both GGCS and GGBS had an initial set of approximately 3.6 hours, whereas the GGAS had an initial setting time of 3.9 hours and the control achieved initial set at 3 hours. This suggests that the type of slag, or more aptly the chemical composition of the material, may influence the setting time.

The composition of fly ash also affects the setting time of concrete mixes. Class F fly ash specimens, especially those with low calcium content and higher amounts of carbon/LOI tend to exhibit an effect of causing the retardation of concrete setting time when compared with the reference (Siddique, 2008). It should be mentioned that, as previously discussed, Class F fly ash is not as reactive as Class C fly ash; this again suggests that there is a possible influence of the level of activity on setting times. However, fineness of cement has a greater influence on setting time when compared with fly ash substitution (von Berg & Kukko, 2004; Siddique, 2008), mainly due to the fly ash particles acting as a nucleation site as the fineness increases. Moreover, von Berg and Kukko (2004) and Siddique (2008) both conclude that cement fineness, water content and ambient temperatures have a greater influence on setting time than the fly ash itself.

In summation, the addition of SCMs, such as fly ash and slag, in concrete tend to retard the setting times. Moreover, the concrete containing SCMs are also more sensitive to cold weather conditions as it takes longer to set. This therefore can lead to potentially delaying the finishing of construction projects and an adequate measures may be required to counter the delay (Prusinski, 2006). Hence, the factors

affecting setting time of concrete containing SCMs are linked to the reactivity/composition, fineness, ambient temperature and replacement level.

2. 6. 2. Workability

Workability is a key factor in the construction industry as it gives an indication of the ease with which concrete can be handled and placed. The concrete should be able to attain homogeneity while having substantially good flow. Three types of tests exist to measure workability of the concrete and depend on the nature of the concrete. The most common test is the slump test, which measure consistency of concrete i.e. ease of flow. The Vebe test in turn is used for concrete of low consistency. The other tests worth mentioning include the compaction factor test (measuring the degree of compaction achieved when concrete is subjected to a standard amount of work) and the Tattersal test.

The factors that have an impact on concrete tend to be interdependent, as the change in one parameter could cause a change in the other. The main factors affecting the workability include:

- mixture composition,
- material characteristics,
- ambient temperature and
- entrained air.

For example, in terms of mix composition, a higher water content could increase the slump, i.e. the workability; given that the paste does not lose consistency, therefore requiring a redesign. In addition, the amount of fines and aggregates can increase or decrease the workability and ties in with the effect of material properties. Finer material increases cohesion of concrete mixes and increases the water demand due to the increased surface area. Moreover, smoother, rounder aggregates also reduce water content and improve workability as opposed to irregular particles. This relates to the surface area of the former being lower compared with the latter. Also, smoother and rounder particles reduce the inter-particle contact point which reduces the amount of friction between particles, referred to as a ball-bearing effect.

The addition of slag and fly ash have good outcomes when used in concrete as the overall amount of water required can be reduced (ACI, 1986; ACI, 2003; Alexander et al., 2003; Oner et al., 2005; Oner & Akyuz, 2007; Berndt, 2009; Beushausen et al., 2012). The water reduction and/or increase in workability of concrete incorporating fly ash is more pronounced compared to concrete containing slag.

The different effects on workability are mostly due to the differences in the morphology of slag and fly ash. As mentioned in the previous sections, fly ash particles are typically spherical in shape (Figure 2-4 a), whereas cement particles are irregular and angular (Figure 2-2). Therefore, the total surface area of the fly ash particles is less compared with that of a cementing particle, i.e. the volume of water required to cover a fly ash particle is lower compared with that for a cement particle. Slag particles in contrast have a similar morphology (Figure 2-4 b) to that of cement particles, i.e. angular. However, it is

reported that slag absorbs slightly less water, despite the fineness, (ACI, 2003; Beushausen et al., 2012) due to the smoother surface with smooth and dense slip planes (ACI, 2003; Siddique, 2008; Khan et al., 2014). The reduced water absorption is also a result of the mentioned layer that forms initially. The final outcome still points to both these materials having a lubricating effect on concrete. The lubrication phenomenon can also be described as a result of the differences in density of slag, fly ash and cement (2.9, 2.3 and 3.14, respectively). The partial replacement of cement is done on a mass basis, therefore the volume of paste increases with the percentage substitution. Therefore, a concrete mix with a higher paste content has a better dispersion of particles, higher fluidity and improved cohesion (ACI, 2003; Alexander et al., 2003; Lin et al., 2011). The increased cohesion is typical of the slag and fly ash being finer compared to the cement that is being replaced.

Moreover, the type, and therefore the composition, of the material can also affect the workability. For example, fly ash samples with high carbon contents and high LOI, does not reduce the water requirement as significantly as recorded in most literature (Xu, 1996; Siddique, 2008). The phenomenon can be explained by the fact that the unburnt material has a higher porosity and no smooth, glassy or spherical shape. Therefore, the total surface area increases, and results in an increase in water absorption. Slag is no exception, as the type of slag also affects the workability of concrete (Siddique, 2008). GGBS is more renowned in terms of global use in concrete and is recorded to decrease the water requirement by approximately 3 % to achieve similar workability as a reference (Khan et al., 2014). Alexander et al. (2009) states that, in a South African context, this equates to 5 – 10 l/m³ water reduction for GGBS, yet for GGCS the water required remains approximately the same. Beushausen et al. (2012) also noted that at different replacement levels for different slag types (GGBS, GGCS and GGAS), no noteworthy changes in slump were observed, hereby stating that slump is independent of slag type.

In summation, fly ash and slag does enhance workability. The increase in workability is as a result of the particle morphology, replacement level and the differences in densities. Despite both SCMs displaying positive results in terms of workability, literature shows that the use of fly ash has a greater impact on workability compared with slag.

2. 6. 3. Bleeding

Bleeding is regarded as a form of segregation where water in fresh concrete moves to the surface via the capillary network present. The movement of water to the top is due to the differences in relative densities; most of the constituents, if not all, in conventional concrete are heavier compared to water. Hence, the heavier particles tend to sink and displace the water to the surface (Wainwright & Rey, 2000). Moreover, bleed water can only be visible if the rate of bleed water accumulating at the surface is higher than the water evaporating from the surface i.e. a nett collection of water at the surface.

Bleeding has a positive aspect as it can act as a curing mechanism for concrete elements; this is given that the evaporation rate is less than the bleeding rate. Moreover, bleeding can also affect the water-to-

binder ratio of an element in both a positive and negative way. Firstly, as seen in Figure 2-11, the lower parts of an element will have a lower water-to-binder ratio, hence resulting in structurally stronger sections. However, near the top a higher water-to-binder ratio is present resulting in a weaker concrete zone (Wainwright & Rey, 2000). Hence, the change of water-to-binder ratio across the height of the specimen complicates the material behaviour. Additionally, the pathways through which the water escapes generates a potential problem in terms of durability aspect and ponding can create anaesthetic surface finishes (Yim et al., 2015). Additionally, in cases of excessive bleeding, plastic settlement cracking may also develop (Wainwright & Ait-Aider, 1995). Internal bleeding occurs as a result of water accumulating as pockets below aggregates and rebar. The collection of water at these points introduce problems as localised weak spots develop. Moreover, the bond between the rebar and the cementitious material is also weakened at these locales and furthermore creates an environment for which corrosion can initiate (Wainwright & Ait-Aider, 1995; Yim et al., 2015).

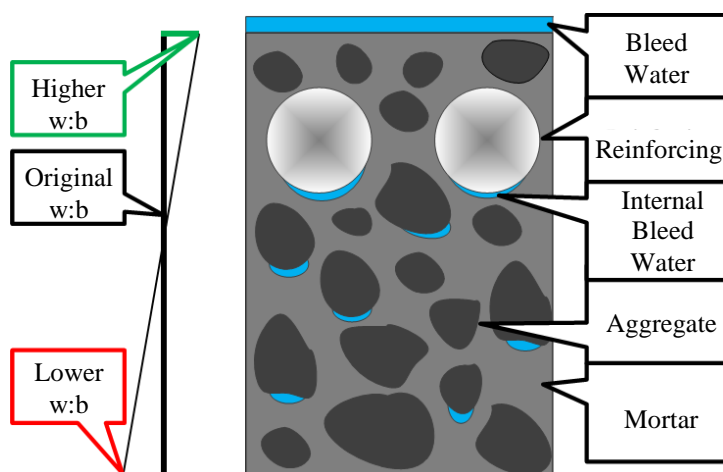


Figure 2-11. The influence of bleeding on a concrete element.

The phenomena of bleeding occurs in three stage stages: (i) constant bleed, (ii) reduced bleeding and (iii) cessation (Lin et al., 2011; Wainwright & Rey, 2000); the stages are shown in Figure 2-12. Stage 1 represents the early stage of bleeding after placing and compaction and has a near linear slope. Stage 2 is identified by a constant change in slope. Less bleed water escapes due to the closing of capillaries as a result of hydration and/or blocking with transported sediments (Wainwright & Rey, 2000). The third stage is regarded as the point at which no bleed water escapes to the surface anymore.

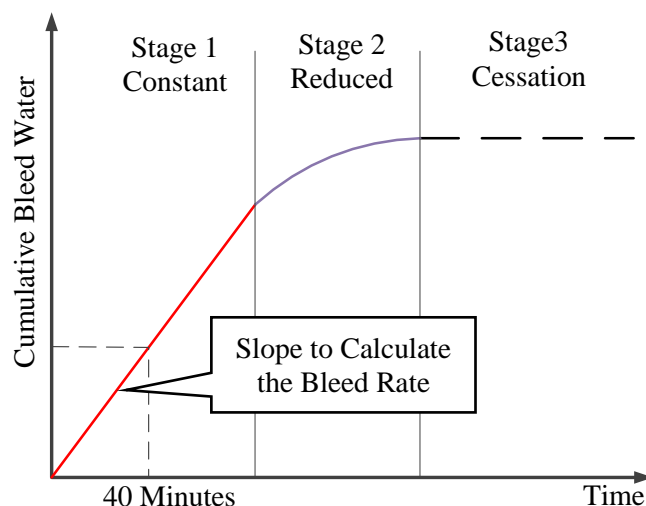


Figure 2-12. The stages of bleeding.

From Figure 2-12 two terms can be described commonly found in literature, namely bleeding rate and bleeding capacity. The bleeding rate ($\text{ml}/\text{cm}^2/\text{s}$) is determined as the amount of bleed water (in ml/cm^2) collected within the first 40 minutes of acquiring bleeding data. The bleed water can therefore typically be obtained from Stage 1. The capacity is obtained from Stage 3 and is the total bleed water collected as an expression of initial volume of concrete.

The bleeding of concrete is affected by factors such as (Almusallam et al., 1998; ACI, 2003; Neville, 2011):

- cement content: leaner mixes bleed more,
- cement fines: finer cement reduces bleeding, possibly due to hydration,
- fines: particles less than $150\ \mu\text{m}$ reduce bleeding possibly by blocking pores and increasing the surface area,
- water-to-binder ratio: bleeding increases with the increase of the w:b as the average particle distance increases and particle-to-particle friction is reduced (Olorunsogo, 1998);
- ratio of solids-to-liquids: the higher the ratio, the less bleeding that occurs as the total surface area increases,
- specimen thickness,
- and the addition of admixtures.

The incorporation of SCMs, such as fly ash and slag, also affect the bleeding of concrete. However, the influence of SCMs on the bleeding of concrete depends on the basis on which the mix is evaluated. Typically, concrete specifications are based on the 28 day compressive strength. If this criterion is used as the basis for the measurement, then there is no significant difference in the bleeding capacity between a mix containing SCMs and a reference (Wainwright & Ait-Aider, 1995). This is because in order to achieve the same strength, an increase in cementitious paste and/or lower water-to-binder ratio is required for a mix incorporating SCMs to achieve the same level of hydration. This in turn creates a

richer mix which is associated with better bleeding characteristics, i.e. less bleeding (Neville, 2011; Almusallam et al., 1998).

The inclusion of fly ash is reported to lower the bleed capacity of concrete (ACI, 1986; Siddique, 2008; Lin et al., 2011; Khan et al., 2014). The decrease in bleed water is attributed to the earlier discussed lubricating effect causing a reduction in the water requirement (Siddique, 2008). Moreover, the addition of fly ash also increases the solid to liquid ratio of a concrete mixture (Siddique, 2008), hence creating a more viscous mixture (Lin et al., 2011). Due to the fineness of fly ash, there is a subsequent increase in the total surface area of the solids and therefore requires a greater amount of water to ensure full surface saturation of all particles. However, these observations are based on the workability being the control of experiments. Moreover, as discussed in the preceding section, the use of fly ash reduces the amount of water required to achieve a slump similar to the reference. Therefore, it can be concluded that the amount of water used per mix is not effectively comparable, but evaluating the data on the basis of similar workability has advantages in terms of practicality.

In addition, Class C fly ash has been reported to yield less bleed water compared with Class F fly ash (Khan et al., 2014). As aforementioned, Class C fly ash is considered slightly more reactive which suggests that Class C fly ash may hydrate at early stages of hydration; thereby reducing the period the concrete remains plastic. In addition, the effect of the fineness and reduced water demand can explain the differences in bleeding observed between the two classes of fly ash.

The fineness of slag, and the subsequent increase in surface area, can also reduce the bleeding capacity of concrete mixes (ACI, 2003; Alexander et al., 2003; Wainwright & Ait-Aider, 1995). This can be related to an increase in viscosity that is noted when slag is included in concrete mix (Lin et al., 2011). In addition, the previous mentioned ability of slag to absorb water better compared with cement adds in providing an explanation to the reduced bleeding (Alexander et al., 2003).

A study done by Yim et al. (2015) attributed the reduced bleeding to the decrease of the water-to-powder ratio when slag is included; again, this relates to an increase in total surface area. Moreover, the mentioned study also used SEM images of particles of slag and cement, and found less flocculation of GGBS particles and displayed a lower packing density compared with the control and speculates this to be a reason for the reduced bleeding. This is in agreement with an earlier study by Olorunsosgo (1998) who investigated the effect of PSD on bleeding. A narrower particle range is indicative of less dense packing; this creates more voids and reduces the amount of bleeding. Moreover, Wainwright & Ait-Aider (1995) reported a similar finding in their respective study. However, it should be noted that all these mentioned investigations were done on a basis of equivalent workability and therefore the volumetric percentages are different for the mixes.

The bleeding capacity of a concrete mixture also increases with the increase in cement substitution with slag (Wainwright & Rey, 2000; Wainwright & Ait-Aider, 1995). The increase in bleeding with an increase in slag substitution can be related to the retardation effect. As the amount of slag increases, the

amount of hydration products are reduced and the concrete can be stated to be more porous and in a plastic state for a longer period. However, Wainwright & Rey (2000) found substitute rates exceeding 85 % had no more influence on the bleeding of concrete; neither did the origin of the slag have an effect.

To summarise, the effect of SCMs on concrete systems are dependent on the basis of evaluation: workability versus same volumetric composition. The former has the advantage of representing the construction needs and the latter yields information on the effect of the material and replacement, making it possible to compare two materials. Nonetheless, the overall parameters noted to affect the bleeding were found to be dependent on the type of material, fineness and retardation effect.

2. 6. 4. Plastic Shrinkage and Settlement

Concrete is a porous material at early ages and undergoes a volumetric change with the progressive loss of water. However, the volumetric change is not limited to mass loss via evaporation. For example, when water and cementitious material are made to come in contact, there is a subsequent chemical reaction and the hydration products tend to occupy a smaller space compared to the reactants. This is known as chemical shrinkage. Moreover, the mentioned water loss continues progressively and is typical associated with drying shrinkage. Yet, at early ages when concrete behaves as fluid material, moisture is also lost. Hence, a distinction between the transgression between early ages volumetric changes and later age is a bit difficult, even more so as hydration is continuous. Therefore, the shrinkage of concrete is dependent on an array of parameters. For the current discussion, attention is placed on the early age deformation of concrete, i.e. while the concrete is still in a plastic state. More specifically, the focus is on the volumetric changes associated with vertical and horizontal displacement, referred to as plastic settlement and shrinkage, in that order.

- Plastic Settlement

Plastic settlement is explained by the occurrence of particles moving downward as a result of gravity. If the settlement of concrete is obstructed, vertical cracks may form due to the tensile strain being created (Domone & Illston, 2010). Cracking can however not form if there is no means of restraint (Boshoff, 2012). This can occur at locations where reinforcing is present and is illustrated by Figure 2-13. In addition, changes in section geometry also cause an onset of settlement cracking (Figure 2-13).

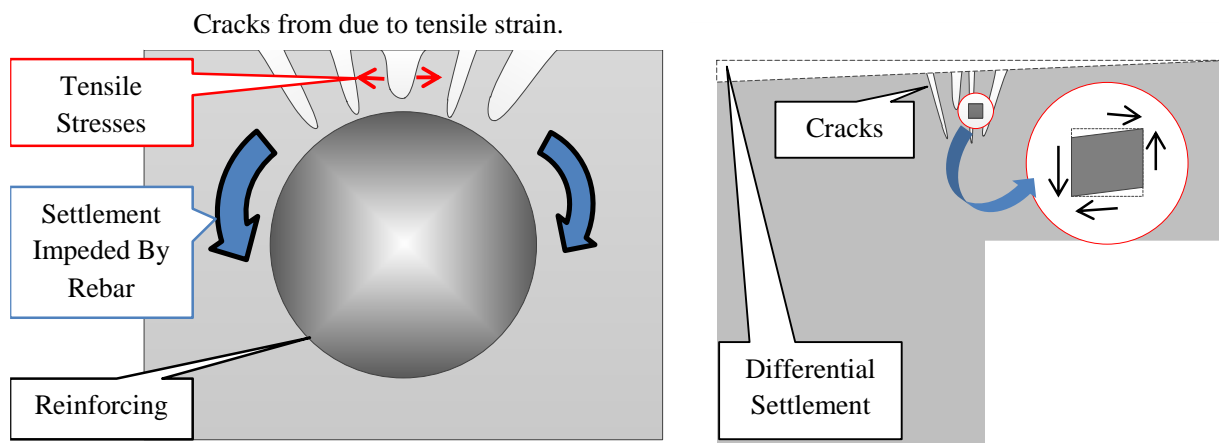


Figure 2-13. The formation of cracks due to plastic settlement.

- Plastic Shrinkage

Plastic shrinkage is a phenomenon of concrete undergoing a volumetric change that is associated with the gradual loss of water in the early ages of hydration. As discussed earlier, water percolates to the top of the concrete section via bleeding. The accumulated water is ultimately removed by evaporation, thereby causing the drying of the exposed face. Hence, water is drawn from the capillaries, resulting in capillary pressure build up, which is a phenomenon leading to the plastic shrinkage. Hence, plastic shrinkage is a result of another phenomenon known as capillary pressure.

Capillary pressure is caused by the water evaporation creating menisci between two particles and increases as the water evaporation proceeds. In addition, the fluid pressure is less on the convex side of the menisci and causes a net negative pressure in the pore water pressure. Consequently, contraction forces develop between the particles; this leads to the decrease in the particle distance, which leads to the reduction in paste volume as material moves closer together. In other words, plastic shrinkage occurs due to the particles being drawn closer to each other by suction. Typically, the pressure (P) can be related to the Gauss-Laplace equation:

$$P = -\sigma \left(\frac{1}{R_1 + R_2} \right) \quad \text{Equation 2.14}$$

where,

P is the capillary pressure,

σ is the surface tension,

R_1 is the maximum radius of the water menisci and

R_2 is the minimum radius of the water menisci.

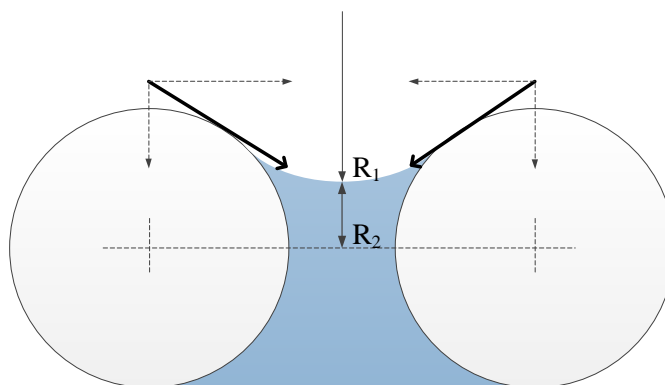


Figure 2-14. The capillary pressure build up between particles and the associated menisci forming.

Equation 2.14 states that the mentioned capillary pressure is inversely proportional to the main radii of water surface, in addition to the surface tension of the liquid. Hence, finer pores will result in a larger capillary pressure build up.

Reports by Combrink and Boshoff (2012) and Boshoff (2012) state that the capillary pressure is affected by the following interdependent factors:

- i. Rate of water loss – a faster rate of water loss causes a steeper pressure build up,
- ii. Evaporation – the higher the evaporation is, the more water evaporates which leads to faster capillary build up,
- iii. Bleeding – slower bleeding causes a higher pressure build up in concrete capillaries,
- iv. Material composition – this is affected by size, distribution,
- v. Hydration rate and setting time
- vi. The use of admixtures.

However, in the event of the evaporation rate exceeding the bleeding rate, drying shrinkage occurs at the surface while the concrete is still in a state of plasticity; this creates a state of tension in the top surface of the concrete and leads to the onset of plastic shrinkage cracking (Domone & Illston, 2010).

Plastic shrinkage cracking is a phenomenon that occurs commonly with hot-weather concreting, yet not limited to the condition of hot weather. The conditions that may increase the rate of plastic shrinkage cracking include, but are not limited to, high concrete temperatures, low humidity and high wind speed. As mentioned, plastic shrinkage occurs as a result of tensile forces building up and exceeding the concrete tensile capacity, which is at its lowest at early ages (Holt & Leivo, 2004).

The ACI Committee 302 (1997) report however states that the risk of cracking is increased when the evaporation rate exceeds a value of 1 kg/m^2 . In the case of pozzolans, this value is potentially half of the latter, i.e. 0.5 kg/m^2 . This is an area of concern for structural elements with large exposed areas, such as slabs and bridge decks. The rate of shrinkage is linear to the evaporation rate (Darquennes et al., 2011; Holt & Leivo, 2004). Evaporation is affected by environmental factors which include: ambient temperature, humidity and wind speed (Combrinck & Boshoff, 2012). In addition, the properties of the

concrete also affect the evaporation, such as: concrete temperature, paste volume and bleeding characteristics (Juenger & Siddique, 2015). By incorporating these factors, Uno (1998) has developed a means of estimating the evaporation rate of concrete using the ACI nomographs:

$$ER = 5 \left\{ (T_C + 18)^{2.5} - \frac{RH}{100} (T_A + 18)^{2.5} \right\} \times (V + 4) \times 10^{-6} \quad \text{Equation 2.15}$$

where ,

ER is the evaporation rate (kg/m²/h),

T_C and T_A is the temperature of the concrete and the ambient environment, respectively (°C),

RH is the relative humidity (%),

V is the wind speed (km/h)

In order to signify the relation between evaporation and plastic shrinkage cracking, Boshoff and Combrinck (2013) proposed a model to quantify the effect of evaporation, amongst other factors such as bleeding, fibres and setting time, on the severity of plastic shrinkage cracking, which is:

$$\text{Plastic Shrinkage Cracking Severity} = ER \cdot t_{\text{set}} - W_{\text{bl}} \quad \text{Equation 2.16}$$

where,

ER is the evaporation rate (kg/m²/h),

t_{set} is the initial set (hours) and

W_{bl} is the total bleed water (kg/m²).

Before advancing to the influence of SCMs on plastic shrinkage, it is worthwhile to explain the evolution of plastic shrinkage. Three stages are present in the process depending on the state the concrete is in and can be seen in the Figure 2-15 as defined by Darquennes et al. (2011). The model of the previous mentioned author is used for the explanation.

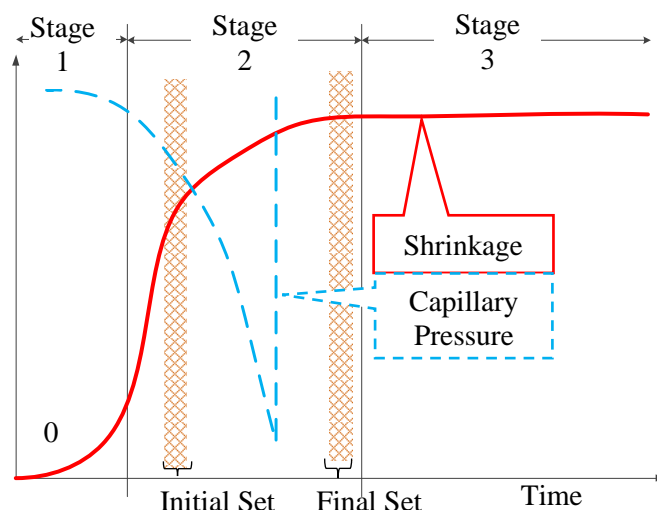


Figure 2-15. The evolution of plastic shrinkage and capillary pressure.

Stage 1: The concrete is in a semi-fluid state and is typical of the consolidation process. The material influences on the evaporation is limited at this stage. In addition, the plastic shrinkage is low as there is no, or very low, pressure development at this stage.

Stage 2: The hydration process proceeds and the hydration products form a skeletal structure full of pores and capillaries. The continuous process of hydration extracts water from capillary pores and water is also lost to the environment. This leads to the pore refinement and the pressure difference between the atmosphere and the capillaries increase. This in turns leads to the build-up of negative capillary pressure due to the previous mentioned fact that capillary pressure is inversely proportional to the pore size. The increasing pressure therefore leads to the contraction at an accelerated rate; this is noted by the steep increase in the curve presenting the plastic shrinkage. After initial set, there is a subsequent decrease in the shrinkage due to the increase in hydration products; hence, the material reaches Stage 3.

Stage 3: After final set, the kinetics of hydration diminishes and the concrete's plastic shrinkage starts trending towards a plateau due to the increased rigidity.

Taking the general trend into account, the question of how SCMs affects the plastic deformation arises. The fineness of the SCMs could potentially be a contributing factor to increase the plastic shrinkage and inadvertently, a leading contributor to plastic shrinkage cracking (Almusallam et al., 1998). In addition, the addition of SCMs generally results in a richer mix containing a higher paste content. The higher paste content is also said to increase the capillary pressure that builds up, hence leading to a potentially higher level or probability of shrinkage occurring (Almusallam et al., 1998).

Besides an increase in the paste quantity, the incorporation of SCMs also improves the consistency and contribute to a more viscous paste. This results in reduction in pores as stated earlier as well as reduces the bleeding capacity, thus increasing the susceptibility of concrete containing SCMs to higher shrinkage levels and increased risk of cracking at early ages. A study by Lin et al. (2011) found that the incorporation of slag increased the crack area. This is likely due to the reduced bleeding capacity of concrete containing slag. Moreover, the increased viscosity may have a positive effect on the settlement of fresh concrete (Alexander et al., 2003), yet due to the associated reduction in bleeding and increased setting time, the concrete may be prone to plastic shrinkage cracking.

Darquennes et al. (2011) performed a study on plastic shrinkage of concrete containing 50 and 75 % slag and 50 % fly ash. Their findings reported that:

- Slag based concrete had a similar evolution of shrinkage as the reference, yet with an offset,
- No trend was apparent in slag substitution, as the shrinkage decrease with 50 % slag, yet increase at 75 % cement replacement,
- 75 % cement substitution with slag resulted in a shrinkage of three time larger than at 50 % replacement,
- 50 % slag produced the lowest shrinkage value recorded,
- 50 % fly ash had no early on deformation and had a similar deformation as the reference (300 μm), and
- Optimised mixes resulted in higher recorded shrinkage values.

The results of the mentioned study provide some useful trends. The offset produced by the incorporation of slag is likely due to the delay in setting time. Moreover, larger pores were reported with the inclusion of slag and therefore increased permeability is assumed as capillary pressure increases with the increase in porosity. This is suggested to be the reason for the increase in shrinkage from 50 to 70 % increase in slag content. Moreover, the slower degree of hydration results in an increased porosity, adding to the effect of capillary pressure increase. In addition, the paste quantity increases, which is associated with higher capillary pressure build-up. The optimised concrete mixes have a higher shrinkage degree due to the increase in paste as well as lower water-to-binder ratios. In addition, the accelerated hydration with the mentioned mixes also reduce the pore size and as a result increase the capillary pressure.

In conclusion, the effect of SCMs on the plastic shrinkage is likely to have an adverse effect. Similarly, the susceptibility of concrete containing SCMs to plastic shrinkage cracking requires a degree of precautionary measures as the risk can be comparatively higher.

2. 7. Effect of SCMs on the Microstructure of Concrete

The microstructure of concrete is a vital factor with regard to the durability aspect of concrete and more so, an influencing factor to ensure that the concrete can effectively withstand the environment, loading and age effects. During the mixing procedure, water causes the separation of cementing particles, and with time, the gap filled with water is reduced; water is used in the hydration reaction and replaced with hydration products. However, not all gaps are closed and pores are generated within the cementitious paste.

Two systems can be used to classify pores, both of which are based on the relative sizes of pores. Firstly, in terms of concrete technology, two sets of pores are identified: gel pores and capillary pores. Gel pores are less than 0.01 μm and is associated with the porous C-S-H gel formed. Capillary pores in turn exists due to the aforementioned scenario of water separating cement particles and being consumed and replaced due to hydration. Capillary pores are larger than gel pores and lie within a range of 0.01 – 10 μm . The second classification, generally for porous systems, defines three pore size ranges: (i) micro- (less than 0.0025 μm), (ii) meso- (0.0025 - 0.05 μm) and macro pores (0.05 - 10 μm) (Aldea et al., 2000).

The pores present in concrete have different effects on the behaviour of the concrete. For example, the strength of concrete is affected by the total pores, yet the shape and size also have an influence (Aldea et al., 2000). In terms of durability, the volume, shape, size, distribution, tortuosity and connectivity have an impact, mostly the pores between 0.12 and 0.16 μm i.e. capillary or macro pores (Aldea et al., 2000). Also, meso pores (0.001 – 0.025 μm) affect the drying shrinkage (Dellinghausen et al., 2012).

Two terms to mention before progressing are porosity and permeability. Porosity refers to the percentage voids in a system. Permeability refers to the ease with which a fluid can move through a

system. Figure 2-16 displays the difference between porosity and permeability, clearly indicating that a material can have different degrees of permeability and porosity.

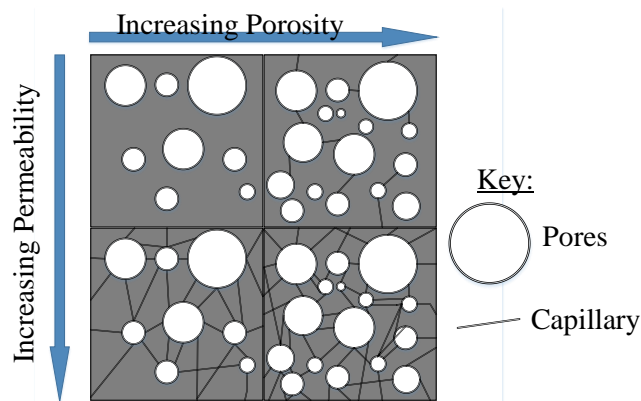


Figure 2-16. The difference between porosity and permeability.

The permeability of concrete is affected by cement type and quantity, water content, aggregate grading, consolidation and curing used (ACI, 1986). More so, the inclusion of SCMs in concrete exhibit favourable results. Pore refinement is a typical association made with concrete made from slag and fly ash (ACI, 1986; Siddique, 2008; Bouikni et al., 2009; Otieno et al., 2014; Juenger & Siddique, 2015; Aldea et al., 2000). Firstly, the densification, increase in viscosity and better dispersion of pastes containing slag and fly ash result in the refinement of the micro structure. A refined pore structure is typically associated with a decreased porosity as large permeable pores are less and there is an increase in smaller, discrete pores (Bouikni et al., 2009).

Secondly, closely associated with the first factor is the filling effect of SCMs (Zhang & Zhang, 2014). As mentioned before, SCMs are smaller compared to cement particle and enhance the packing density of a cementitious paste. Therefore, as the packing is increased, less air voids is generated and the continuity between capillaries is reduced as a result of pathways becoming blocked. This leads to the decrease in the median pore size.

Thirdly, and possibly the most significant, is the hydration that also causes the enhancement of the microstructure and is commonly reported in literature. Firstly, the secondary hydration reactions convert soluble calcium hydroxide into C-S-H (ACI, 1986). The formation of more hydration products therefore also aid in the blocking mechanism, hence reducing pore connectivity, hereby decreasing the overall permeability. Also, slag takes part in a process of chloride binding, which forms a denser product commonly referred to as Friedel's salts (Siddique, 2008), which is discussed in the section focusing on durability, namely Section 2.10.

The replacement level of cement also shows favourable results. Otieno et al. (2014) found an increasing decrease of porosity with continual cement substitution with slag. The findings can be described to the pore refinement. Bouikni et al. (2009) also reported a similar trend when slag replacement was increased from 50 to 65 %. Siddique (2008) reports that a mix containing up to 50 % slag had pores of 10 – 50 μm , whereas the OPC mixture had a higher percentage of capillary pores ranging between 0.05

– 60 μm . Moreover, he (Siddique, 2008) reports that a 70 % slag addition has a greatest impact on microstructure.

The inclusion of fly ash also provides an improvement in the microstructure, however, at early ages the porosity is slightly increased (Boa & Topu, 2012). The higher porosity occurs due to the lower reactivity of fly ash at early ages. However, the porosity does decrease with time. Ramezani-pour and Malhotra (1995) also reported the porosity of fly ash based concrete to be lower than the reference.

The effect of curing is an important factor in terms of ensuring an improved microstructure (Siddique, 2008), especially due to the susceptibility of SCM based concrete to poor curing regimes. The curing temperature influences the pores, as higher curing temperatures are reported to increase the amount coarse pores (Aldea et al., 2000). The explanation is that the pore distribution is affected by the curing temperature; higher temperatures increasing the meso pores (Aldea et al., 2000). In addition, at higher temperatures, free water leaves with greater ease. Bouikni et al. (2009) also found that drying has a major influence on porosity, for as the temperature increases so does the evaporation of free water and therefore hampering the secondary reaction.

An additional aspect of concrete microstructure is the interfacial transition zone (ITZ). The ITZ is the zone between the aggregates and the paste and affects the strength and permeability of concrete. The ITZ has a different microstructure to that of the entire structure; associated with a higher water-to-binder ratio and less paste due to the wall effect. The effect of internal bleeding aggravates the impact on the ITZ. The RILEM Technical committee 159-ETC (Bentur & Alexander, 2000) however emphasised that the wall effect and particle size distribution plays a greater role compared to the water-to-binder ratio and the cement content. Moreover, the ITZ has a higher porosity due to the increased water-to-binder ratio and wall effect.

For conventional concrete, the typical size range of the ITZ is between 10 – 50 μm (Domone & Illston, 2010) and is reduced by the inclusion of finer materials (Bentur & Alexander, 2000). Therefore, it can be expected that the inclusion of slag and fly ash can reduce the ITZ by increasing the particle packing (filler effect) and enhancing the surface chemical effect. Hence, the ITZ can potentially become narrower by mere inclusion of finer materials.

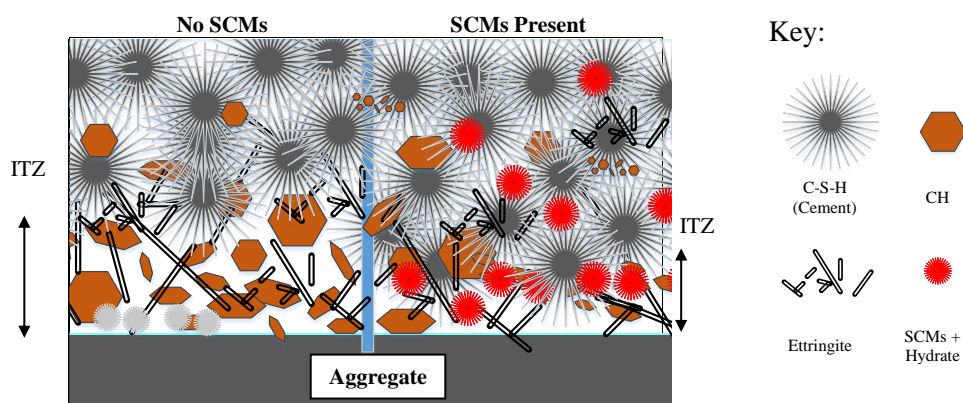


Figure 2-17. Diagrammatic representation of the ITZ (Hooten, 2000).

The ITZ has higher levels of calcium hydroxide and sulphoaluminate hydrates due to sufficient space available for these products to form, hereby increasing the porosity at this area. However, in the presence of SCMs the calcium hydroxide can be utilised to form secondary hydration products, increasing the paste density in this area. Therefore, with aging the SCMs fill the porous areas by replacing the weaker calcium hydroxide with a more dense, stronger C-S-H gel (Hooton, 2000) which is illustrated by Figure 2-17.

2. 8. Effect of SCMs on the Mechanical Properties of Concrete

2. 8. 1. Compressive Strength

The compressive strength of concrete is the primary factor that makes it such a valuable construction commodity. For example, advances in the study of concrete materials have yielded the development of high strength concrete, which can have strengths that exceed 100 MPa. This has contributed to the continual growth of the construction industry. Achieving these high strengths depend on various factors and the general parameters influencing the compressive strength of concrete include water-to-binder ratio, cement content, cement type, cement fineness, mixture composition and the addition of SCMs.

The use of SCMs in a concrete mix affect the strength development, in addition to the strength, of concrete by three known phenomena: (i) filler effect, (ii) dilution and (iii) the reactivity of SCMs. The three mentioned mechanisms mostly have a greater impact on the early age strength development. Equally as important, replacement level, fineness and type of SCM also have an impact on the concrete strength and the rate at which the strength is gained. These factors are interdependent to some extent, as for example, replacement levels enhance the dilution, which in turn reduce hydration products.

As aforementioned, the filler effect relates to the decrease of voids present in a concrete mix. The presence of voids causes an overall decrease in concrete strength. Hence, reducing the total amount of voids can reduce the negative impact of voids on concrete strength. In addition, fly ash and slag tend to have smaller particle size ranges compared to the cement that is replaced. Therefore, the addition of SCMs can cause an increase in the packing capacity and effectively lower the volume of voids.

The addition of SCMs can be achieved in two ways: substitution of the aggregates or substitution of the cement. If SCMs replace the aggregates instead of the cement, an increase in early age strength is observed (Papadakis et al., 2002; Oner et al., 2005; Oner & Akyuz, 2007). However, on the basis of replacing aggregates, the effective water-to-binder ratio is not the same as that of the control, and effectively, a lower water-to-binder ratio is achieved. As the compressive strength of concrete is inversely proportional to the water-to-binder ratio, it stands to reason that the strength would increase. In addition, the finer particles create nucleation sites (surface chemical effect) thereby enhancing the hydration process of the cement.

In contrast, when SCMs replace cement, a reduction in strength development occurs, more noticeable at early ages (Siddique, 2008; Juenger & Siddique, 2015). This is related to the effect of dilution and the slower pozzolanic reaction, as well as the requirement of an activator. In terms of the dilution effect, if

cement is replaced with a SCM of relatively lower reactivity, the total amount of hydration products that can form is reduced and as a result, it affects the pozzolanic reaction at the early ages. The pozzolanic reaction is affected by the presence of an alkaline environment and with a reduction in cement, and inadvertently a reduction in hydration products associated with its hydration, namely calcium hydroxide, the rate at which the required alkaline environment is achieved is decelerated, therefore, hindering the pozzolanic reaction.

Despite the possible adverse effects at early ages, the strength of concrete containing SCMs can potentially be equal to or even exceed the strength of reference mixtures (Oner et al., 2005; Siddique, 2008; Alexander et al., 2003). For instance, Papadakis et al. (2002) investigated fly ash from three sources and a slag and found that the compressive strength of these mixes incorporating these SCMs exceeded the control's strength at 91 days of testing. Even more so, the slag had a compressive strength similar to the control's strength. The increase in strength at later ages is attributed to the pozzolanic reaction. The hydration of cement creates C-S-H and $\text{Ca}(\text{OH})_2$ (refer to Equation 2.5). The C-S-H contributes to the strength, whereas the $\text{Ca}(\text{OH})_2$ provides an alkaline environment and is also weaker and more soluble (Oner & Akyuz, 2007). The pozzolanic reaction however utilises the $\text{Ca}(\text{OH})_2$ as a reactant and produces C-S-H (Equation 2.9), thus replacing the *weaker* $\text{Ca}(\text{OH})_2$ with C-S-H, which adds to the strength gain. Moreover, the continual replacement of $\text{Ca}(\text{OH})_2$ refines the concrete pores and enhances particle packing. Therefore, concrete containing SCMs are sensitive to curing (Ramezani-pour & Malhotra, 1995) due to the moisture required to facilitate the pozzolanic reaction. This is due to SCMs being able to densify pastes and also to retain water better for later hydration (Aponte et al., 2012).

The type of SCM incorporated also affects the strength gain and can be related to the reactivity, morphological and physical properties. Berndt (2009) found that slag does not decrease the strength as much as fly ash does. At 50 % substitution, fly ash resulted in a strength reduction of 16 MPa, whereas slag only resulted in a reduction of 3.8 MPa. At 7 days, and at 28 days the slag containing mix reported an increase of strength (6 MPa) and the fly ash based concrete reported a near 50 % reduction in strength. Moreover, even the samples containing 70 % slag showed a reduction less than that of the 50% fly ash mixture. However, it should be mentioned that the fly ash concrete mixture is regarded as a high volume fly ash mixture and the lower results is typical of such mixes. In addition, slag exhibits self-cementing properties, meaning that C-S-H is produced by the slag's activation as well as the accompanying pozzolanic activity.

The differences in the type of slag also affects the strength gain and rate. Otieno et al. (2014) investigated GGCS, GGAS and GGBS at two water-to-binder ratios (0.4 and 0.6) and three replacement rates (20, 35 and 50 %) and reported that at 28 days the GGCS performed the best, followed by the GGAS and GGBS. The GGCS reported strengths exceeding the control at all replacements and water-to-binder ratios, which is corroborated by previous investigations (Alexander et al., 2003; Beushausen

et al., 2012). The better performance of GGCS is linked to the lower mass percentage of manganese, higher calcium oxide and aluminium oxide content, lower silica and greater fineness; therefore, it can be stated that the GGCS exhibits a higher hydraulic reactivity in comparison to the other two slags.

The impact of slag on concrete strength at early ages suggests that the addition reduces the strength as aforementioned. The general consensus is that significant strength gain is only after 7 days, regardless of the slag source and reactivity (Alexander et al., 2003; Oner & Akyuz, 2007; Siddique, 2008; Beushausen et al., 2012) and can again be related to the slower pozzolanic reaction and dilution of cement. The ACI Report R233 (2003) also states that all slag grades (Grade 80, 100 and 120) result in lower early age strengths and show significant strength characteristics at 28 days or more.

The difference in the type of fly ash also result in deviations of behaviour, as it is reported that high calcium fly ash results in *stronger* concrete (Oner et al., 2005). High lime fly ashes show higher strengths at early ages, yet display a slower strength gain pattern, similar to that of the control which reduces with time (ACI, 1986; Siddique, 2008; Aponte et al., 2012). Low calcium fly ashes exhibit lower early age strength when it replaces cement, but higher 91 day strengths (Oner et al., 2005).

The replacement level of cement with SCMs depend to a great degree on the intended use of the concrete, as shown in Table 2.5. Some of the implementations are not as dependent on high strength and use other benefits of SCMs, such as reduced heat of hydration (although the concrete should still be designed to be of sufficient strength). Therefore, the importance of concrete strength cannot be ignored, nor the effect that the cement substitution has on the result.

Table 2.5. Typical cement replacement levels and the intended use of the cement and concrete mixture.

Replacement	Use	Reference
Fly Ash		
0 – 35 %	Cement production Blended cement General construction and civil work Mass concrete	Siddique (2008)
> 35 %	Structural fills Sub-base and base courses HVFA concrete	Siddique (2008)
Slag		
0 – 35 %	Cement production Blended cement General construction and civil work	Alexander et al. (2003)
35 – 55 %	Structural, durability and building work	Alexander et al. (2003)
55 – 70 %	Long-term strength Mass concrete Sulphate resistance	Alexander et al. (2003)

It can be noted that as the percentage replacement increases, the strength of the concrete decreases compared to the reference. However, it is suggested that there is an optimum replacement level that reduces the impact of the continual strength reduction. The term *optimum* refers to the difference in strength between a SCM-based mix and the reference and is therefore age dependent; typically at 28

days as this is the age on which most structural designs are based on. Therefore, as the amount of SCMs in the system increases (i.e. increasing substitution), the strength development increases and strength difference becomes less. However, after a certain degree of cement replacement, an increase in SCM percentage would cause a decrease in strength gaining rate and an increase in the strength difference.

The optimum replacement can be discussed as the achievement of an optimum particle packing state. As the finer SCMs are added to a system, the surface area increases and so does the particle packing. Therefore, nucleation increases as well as the overall decrease in voids. However, if too much fines are added, the particle packing is disturbed and the packing density decreases again.

The dilution can also affect the binder system such that the additional SCMs only act as microfillers and not hydrate, thereby not contributing to the strength development. For example, Oner et al. (2004) found that with continual substitution, fly ash is underutilised and merely has the role of a microfiller in concrete.

Table 2.6 provides typical optimum replacement levels for both slag and fly ash concrete systems. Slags show an optimum replacement between 50 and 60 %. For fly ash, the optimum is observed to be lower, at 25 %. The difference in optimum levels can be described as a result of the difference in reactivity. In addition, slag also exhibit latent hydraulic activity as was discussed in Section 2.4.

Table 2.6. Typical optimum cement replacement levels as found in literature.

Material	Percentage (%)	Replacement		
		Aggregate	Cement	Reference
Slag:	GGBS		50	Aldea et al. (2000)
	GGBS		65	ACI (2003)
	GGBS		55 – 59	Oner and Akyuz (2006)
	GGBS		40 - 60	Siddique (2008)
	GGCS		50	Alexander et al. (2009)
	GGBS		50	Berndt (2009)
	GGBS, GGCS & GGAS		50	Otieno et al. (2014)
Fly Ash	40			Oner et al. (2004)
Fly Ash			25	Bentz et al. (2011)

The strength of concrete is also dependent on the fineness of the cementitious material, as noted earlier finer materials can improve particle packing via the filler effect. The importance of fineness had been discovered in search of increasing early age strength and to ensure construction is done at a faster pace (Bentz et al., 2011). Therefore, researchers (Zhang & Napier-Munn, 1995; Bentz et al., 1999; Chindaprasirt et al., 2004; Celik, 2009; Zhang et al., 2011; Bentz et al., 2011) have investigated the effect of cement fineness on strength development over many years, especially since technology has improved to produce cements of greater fineness.

Cement particles have been divided into three categories, in terms of particle sizes, to assess the effects on strength development, namely, finer ($< 8 \mu\text{m}$), middle ($8 - 24 \mu\text{m}$) and coarser ($> 24 \mu\text{m}$) particle sizes (Zhang et al., 2011). Each of these particle classes have shown to affect the strength of concrete at

different ages. The finer fraction has shown to increase the strength of concrete at earlier ages (Zhang & Napier-Munn, 1995; Celik, 2009; Zhang et al., 2011; Bentz et al., 2011) and is associated with the chemical and surface chemical effects. Moreover, the chemical composition of different size fractions also undergo changes (Celik, 2009; Zhang et al., 2011). For example, Zhang et al. (2011) found that as the mean particle size decreased, so did the chemical composition of each particle range. The SiO_2 decreased from 21.60 % for the original cement to 19.20 % for a particle range with a mean particle size of 3.98 μm . Similar trends were observed for the Al_2O_3 and CaO , whilst the opposite occurred for the quantity of MgO and LOI . This means that more of the reactive constituents are available to partake in the reaction process.

The coarser particles showed better performance in terms of strength at later ages (Celik, 2009; Zhang et al., 2011). This can be as a result of the particles not reaching full hydration. In addition, with time, water may penetrate the outer gel and react with the un-hydrated inner portion of the cement particles. These coarser particles therefore only behave as a “filler” in the initial stages of compressive strength.

The middle fraction of cement particles have shown to perform relatively better when used (Zhang et al., 2011). It was found that acceptable early age strength is still achieved while leaving enough cement particles to hydrate at late ages and contribute to the later age strength. Zhang et al. (2011) have suggested that the coarser and finer particle ranges can be replaced with SCMs, with negligible performance loss.

However, it must be acknowledged that the investigation of the effect of particle sizes by Zhang et al. (2011) has been done by controlling the workability of the mixes. The method of assessing the particle effect by using workability is good in giving an indication of the probability of applying such a technique in practice, as in general, the production of concrete is dictated by the workability and required strength. However, the results of Zhang et al. (2011) are not as eligible for comparison due to the differences in water-to-binder ratios. This is due to the fact that, in a theoretical sense, a mix with a lower water-to-binder ratio could potentially have a higher strength. Furthermore, the details of the mix constituents are not available to assess the influence of the different water-to-binder ratios. Celik (2009) has however stated that the notion of fineness increasing strength may not be correct, as the researcher's work was done based on a constant water-to-binder ratio. Moreover, Celik (2009) attributes the variation in results to the possibilities of poor compaction and the presence of weak zones resulting from the presence of un-hydrated cement particles.

Chindaprasirt et al. (2004) conducted a study on the effect of fly ash fineness on mortar strengths with a constant replacement of 40 %. The specimens consisted of an original fly ash, two graded samples and three single size range samples. The graded samples performed better compared to the reference and the single range samples; a wider particle range promoting the particle packing best explains this observation. The study also found that the fly ash sample with finer material required less water, due to better particle dispersion (Siddique, 2008) and a reduction in the water-to-binder ratio. Despite the

lower water-to-binder ratio additional, explanations of the better strength performance could be attributed to the finer particles being more reactive as well as the partial filler effect and increased packing density (Chindaprasirt et al., 2004). Furthermore, the finer particles are also said to have undergone complete combustion as well as being spherical and smoother to a greater extent compared to the coarser particles (Chindaprasirt et al., 2004). In addition, Bentz et al. suggested that a coarse fly ash is best suited to be used with a fine cement, most likely as the finer particles of the cement can mitigate the reduction in early age strength.

The particle size distribution of slag also affects activity and thereby the strength development of concrete containing it (ACI, 2003). It was found that particles less than 3 μm increases the early age strength development, likely due to the filler and surface chemical effect. In addition, particles between 3 and 20 μm are beneficial for long-term strength (Siddique, 2008).

To summarise, it can be stated that the addition of SCMs in concrete affects the strength development and depends on the constituent being replaced. If aggregate are replaced, the outcome is generally a faster and higher strength development. This is explained by the physical and surface chemical effects. Moreover, the secondary hydration reactions also aid to the strength development, as well as the fact that the water-to-binder ratio is effectively reduced. However, on the basis of cement replacement, the early age strength tends to be adversely affected at early ages. This is dependent on the replacement level and reactivity of the SCM used, however, with time the strength gain reaches, if not surpasses the strength of the control. This leads one to conclude that the effect of diminishing strength becomes less pronounced with time.

2. 8. 2. Tensile and Flexural Strength

The performance of concrete has been mostly related to strength based performance. However, with the increase in research on concrete, it has been seen that a performance based on durability would be largely beneficial. The tensile strength of concrete has an influence on the cracking mechanism that is related to durability. In addition, the presence of cracks result in unpleasant aesthetics of structural elements.

The tensile capacity of concrete is used to assess the shear that can be resisted by unreinforced sections. Additionally, the tensile capacity is also used in assessing the potential of resisting shrinkage and temperature stresses. Therefore, mitigating cracking potential can improve the design prediction and minimise failure as a result of under- or overestimating the tensile capacity (Oluokun, 1991). The testing of the tensile strength of concrete is done using three methods, namely, the direct tensile test, the beam/modulus of rupture test and the split cylinder test (Arioglu et al., 2006). Each of the three test methods have potential drawbacks and benefits when considered.

For example, the direct tensile test is thought to underestimate the tensile strength (Oluokun, 1991) due to concrete being a brittle material and as a result indicating that minor stress redistribution occurs.

Furthermore, it is difficult to ensure that a truly axial load is applied during specimen testing (Oluokun, 1991). Hence, the test method is regarded as sensitive to eccentricities in the applied loading (Li & Li, 2015).

The modulus of rupture test can be done by means of a three point bending tests or a four point bending test (Figure 2-18). The principle is based on inducing a bending moment in a specimen by applying a load using roller supports and calculating the flexural strength. The four point bending test gains favourable attention due to two factors. Firstly, as long as the crack forms in a region between the two upper supports, the maximum load to induce this crack is recorded and can be seen by studying the typical moment diagram of a beam loaded as such (Figure 2-18). Secondly, in the region between the two upper supports, no shear is developed and it can be concluded that the region is in a state of uniaxial load. The three point bending test, in contrast, requires preparation to ensure that the crack is forced to occur at the centre of the beam, i.e. to record the maximum force at failure, and can be done by notching the beam prior to testing. If the crack occurs at any other location, the true flexural strength is not obtained as the maximum is limited to the centre point of the beam.

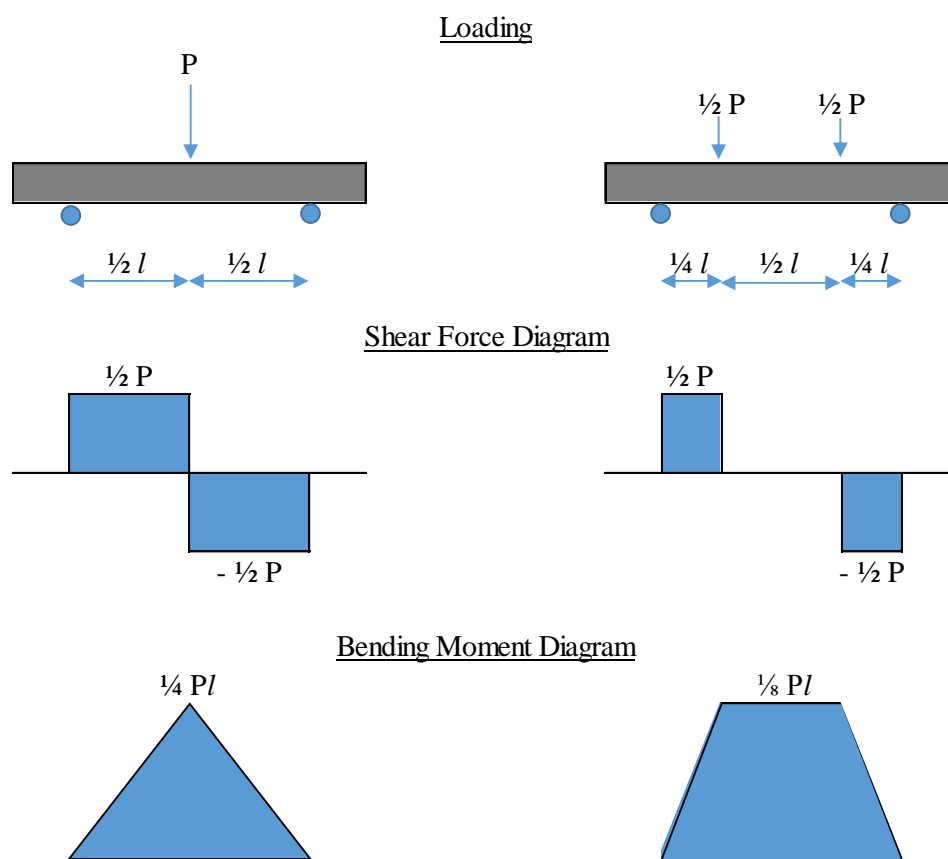


Figure 2-18. The modulus of rupture setup to determine tensile strength of concrete by means of the three point bending test (left) the four point bending test (right).

In addition, the use of a beam test to record the maximum load of tensile failure does not account for the development of minute and hairline cracks (Oluokun, 1991). Moreover, due to the fact of the stress-

strain curve not being truly linear for the section in tension, the beam test often over estimates the tensile strength of concrete, as shown in Figure 2-19 (Oluokun, 1991; Oluokun et al., 1991).

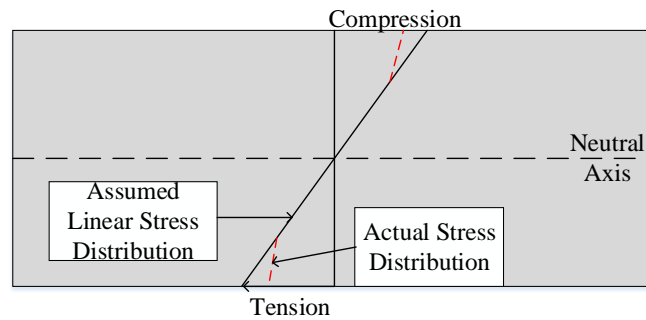


Figure 2-19. The stress distribution in elements for the modulus of rupture.

The splitting test (Figure 2-20) is performed on a cylinder or cube by applying a load across two diametrically opposed lines on the specimen. This test method has been favoured due to its ease of use and the fact that the stress distribution is reasonably uniform, as seen in Figure 2-21 (Oluokun, 1991; Oluokun et al., 1991). In addition, it is stated that the splitting tensile strength provides a lower coefficient of variation, adding to the favourability of the test method (Arioglu et al., 2006).

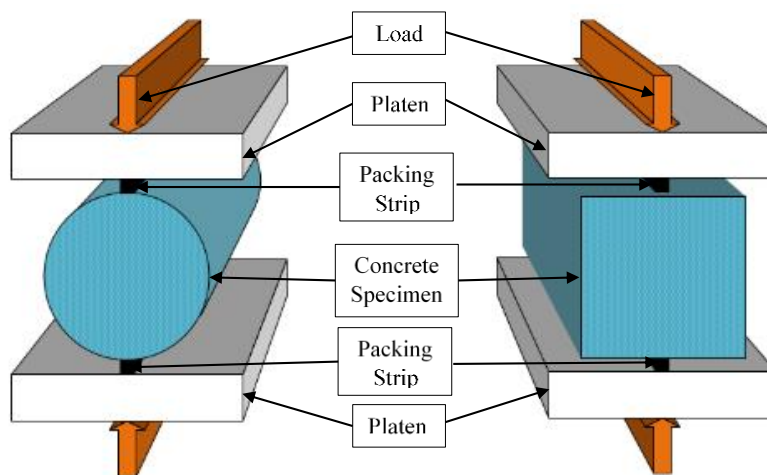


Figure 2-20. Indirect splitting test setup for a cylindrical and cube specimen.

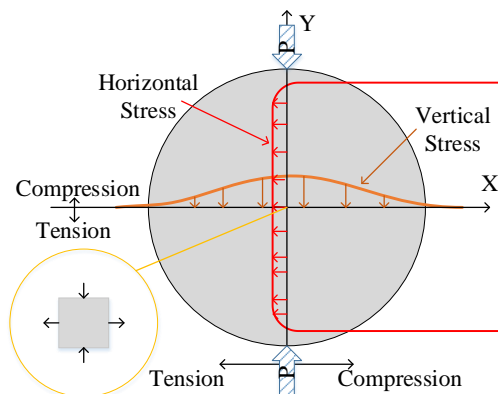


Figure 2-21. The stress distribution in elements for the indirect tensile testing.

Researchers (Oluokun et al., 1991; Arioglu et al., 2006) have agreed that the tensile strength of a concrete specimen is dependent on the age of testing and the time of curing. These researchers have performed regression analyses on existing data in order to evaluate the power models that are available for assessing the said relationship existing between compressive strength and tensile strength. The data collected included results where the water-binder ratio, cementitious/binder quantity, age and temperature of curing differed. The final conclusion reproduced an agreement that the tensile strength can be defined as a function of the concrete compressive strength.

However, as noted from the previous section (Section 2.8.1), based on the compressive strength, it was shown that the compressive strength is a function of the replacement level of SCM and age of testing. Therefore, as the overall compressive strength of a mixture decreases, it is expected that the tensile strength would also decrease. When concrete is designed on the basis of equal strength, mixtures containing SCMs display improved and greater capacities than the mixtures containing no SCMs (ACI, 2003). The improved paste density and the reduction in the interfacial transition zone (ITZ) (Berndt, 2009) are underlying reasons for the improved resistance. There is general agreement in literature that the addition of SCMs improve the ITZ and thereby the tensile capacity of concrete (Berndt, 2009; Arivalagan, 2014)

Substituting the cement with SCMs produce variable results, depending on the material used, temperature and level of substitution. Siddique (2008) reported on findings in literature of the effect of slag replacement at elevated temperatures (more than 42 °C) on the flexural strength and reported that greater flexural strengths were reported for up to 40 % cement substitution. The improved results are due to the increased hydraulic activity of slag at elevated temperature in conjunction with the microfiller effect, hence, resulting in paste densification and a reduced ITZ.

Khatib and Hibbert (2005) reported an optimum slag use of 60 % resulted in flexural strengths exceeding that of the reference. Moreover, at 40 and 80 % replacement levels, a decrease in flexural strengths was noted and was even lower compared to the reference. Berndt (2009) found that concrete containing slag percentages of 50 and 70 % to yield greater tensile strength than the reference. Table 2.7 gives a list of optimum levels of SCMs in terms of tensile and flexural strength. Nazari and Riahi (2011) discovered that the tensile strength increased with an increasing amount of slag. This trend was observed up to a replacement of 45 % of cement with slag for a SCC mixture. The fact that the optimum was achieved at 45 % replacement was also linked to the latent hydraulic activity of slag (Nazari & Riahi, 2011). As an increase in slag content beyond 45 % could potentially inadvertently reduce the amount of C-S-H present. Moreover, the increasing trend observed by Nazari and Riahi (2011) contrasts the findings of Li and Li (2015), whom found a decreasing trend in compressive strength and tensile strength with an increasing cement replacement with slag. It is suggested that due to the variation in the chemical composition of the respective slags as well as the difference in type of mixes that were designed; the former mentioned researchers designed a paste and the latter a SCC. The two research groups also used two different methods of testing the tensile strength, namely, a splitting

test (Nazari & Riahi, 2011) and a direct axial test (Li & Li, 2015). It is mentioned that the direct splitting test results are approximately 5 – 12 % greater than the direct tensile strength.

Table 2.7. Literature findings on the optimum cement substitution for tensile and flexural strength.

Material	Replacement (%)	Reference
Slag	50	Aldea et al. (2000)
	50 & 70	Berndt (2009)
	45	Nazari and Riahi (2011)
	25	Arivalagan (2014)
Fly Ash	50 *	Siddique and Khan (2011)
	15 & 25	Jalal et al. (2013)

Note (*): Aggregate replaced.

Li et al. (2011) conducted an investigation into the relationship between pore structure and cement paste and used two different water-to-binder ratios, namely 0.30 and 0.35. In addition, they used silica fume (5 and 10 %), ground granulated blast furnace slag (25 and 50 %) and fly ash (15 and 30 %), at two replacement levels (mass basis) per water-to-binder ratio. The findings of Li et al. (2011) included a good linear correlation between the compressive strength and tensile strength of the pastes. As expected, the tensile strength did decrease with an increase in SCM replacement. For example, the increase in slag content from 25 % to 50 % reported a drop in tensile strength of 2.8 MPa to 2.6 MPa for a water-to-binder ratio of 0.30 and 2.6 MPa to 2.2 MPa for a paste with a water-to-binder ratio of 0.35. The increase in water-to-binder ratio and the effect of pozzolanic reactivity are the causes for the decrease of tensile strength. The mixes containing slag did show higher results in terms of both the compressive and tensile strength. The better performance, relative to the fly ash and silica fume is explained by the relatively higher reactivity of slag.

Jalal et al. (2013) investigated the effect that fly ash replacement (5, 10 and 15 % on a mass basis) had on the tensile strength of concrete. Their overall findings were corroborated with the results of previous mentioned researchers (Li et al., 2011; Li & Li, 2015) i.e. that the tensile strength of concrete generally showed a decline in tensile strength as the replacement level increased, yet the effect diminished with increasing ages of testing. However, at 90 days after casting Jalal et al. (2013) reported that the tensile strength was 3.9 MPa for the 0, 15 and 25 % cement replacements which is indicative that the tensile strength is dependent on the age of testing as well as the compressive strength.

Finally, it is observed the use of SCMs result in an overall decrease in the ITZ of concrete. Even more so, the refinement of the ITZ also leads to an improved tensile strength capacity for similar strengths as those of a mixture containing no SCMs. In addition, there is also a reported optimum replacement level, in terms of tensile strength: on average, it is 50 % for slag and 15-25 for fly ash based concretes.

2. 8. 3. Modulus of Elasticity

The modulus of elasticity is the relationship between the stress of a material and the elastic strain associated with the said stress. The elastic modulus is typically calculated at 30 % of the compressive

capacity of the concrete, yet different types of modulus of elasticity can be determined from a stress-strain diagram and are shown in Figure 2-22.

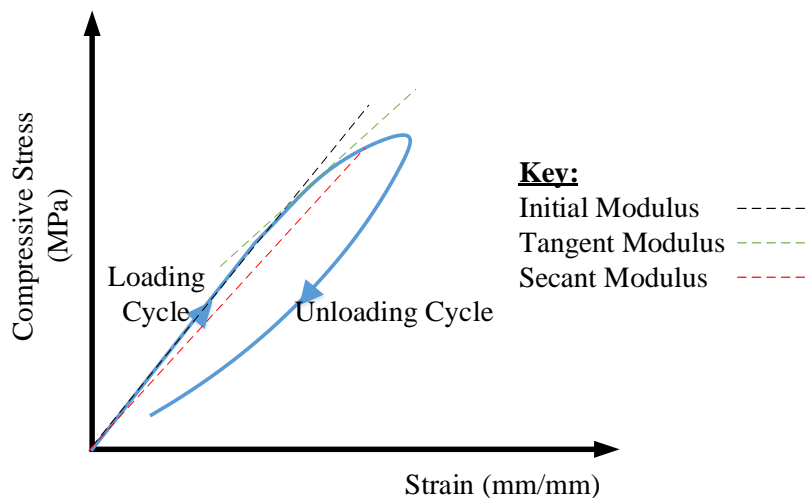


Figure 2-22. The different elastic modulus' that can be obtained from a loading cycle.

In addition, the elastic modulus is affected by moisture conditions, aggregates (volume and the aggregate elastic modulus) and the mix composition. From the last mentioned fact, it is evident that the SCMs will have an effect on the modulus of elasticity. Moreover, Table 2.8 provides a few prediction models used to determine the elastic modulus of conventional concrete. However, the models do not explicitly cater for composition, but rather strength of concrete specimens. Therefore, investigating the influence of SCMs on elastic modulus is valuable in the sense that the elastic modulus could potentially be over or under estimated by the given models.

Table 2.8. Prediction models for the elastic modulus of concrete.

Model	Elastic Modulus (GPa)	Limitation
	$9.1f_{cu}^{1/3}$	$\rho = 2300 \text{ kg/m}^3$
	$1.7\rho^2 f_{cu}^{0.33} 10^{-6}$	$1400 < \rho < 2300 \text{ kg/m}^3$
ACI 318 (2008)	$4.70f_{cyl}^{0.5}$	$\rho = 2500 \text{ kg/m}^3$
ACI 318 (2008)	$43\rho^{1.5} f_{cyl}^{0.33} 10^{-6}$	$1500 < \rho < 2300 \text{ kg/m}^3$
CEB-FIP (1993)	$10(f_{cyl} + 8)^{1/3}$	
BS EN 1992 (2004)	$22\left(\frac{f_{cu} + 8}{10}\right)^{0.3}$	28 Days
BS EN 1992: (2004)	$\left(\frac{f_{cu,t}}{f_{28}}\right)^{0.3} \times E_{28}$	Ages other than 28 days

Where: f_{cu} = cube strength, f_{cyl} = cylinder strength, E_{28} = Elastic Modulus and ρ = density

In general, the addition of fly ash causes a slight reduction in elasticity (ACI, 1986; Swamy, 1990; Khan et al., 2014; Berndt, 2009). A higher elasticity modulus can be expected on the basis of fly ash replacing the aggregates as there is an increase in the quantity of paste (Siddique, 2008). The same pattern is found for slag based concrete mixes (ACI, 2003; Berndt, 2009; Swamy, 1990). Berndt (2009) found a similar elastic modulus for 0 and 50 % slag replacement and a slight reduction was noted for

mixes with 70 % slag. Curing seemed to have the most notable effect on the elasticity of concrete. This is most likely related to the susceptibility of SCM-based concrete to poor curing which adversely affects the pozzolanic hydration process (Boa & Topu, 2012; Swamy, 1990). Despite the effect of curing, the elastic modulus of SCM-based concrete is similar to the compressive strength and that of the control.

2. 9. Effect of SCMs on the Drying Shrinkage of Concrete

The loss of water from concrete is not only associated with a mass loss, but also with a volumetric decrease. Hence, the term drying shrinkage is explained as the shrinkage associated with the loss of internal water via evaporation. Drying shrinkage can lead to the deterioration of concrete if hindered by restraints, both internal and external, as well as induce tensile stresses. As mentioned, the tensile capacity of concrete is relatively low compared to the compressive strength and is therefore susceptible to tensile cracking. The shrinkage of concrete is dependent on factors that include: paste volume, cement type and content, type and volume of aggregate and curing and environmental conditions (ACI, 1986), as well as specimen shape and size (Eguchi & Teranishi, 2005).

The drying shrinkage phenomenon is best explained by using the capillary tension theory (see Figure 2-23). Firstly, the difference in relative humidity between concrete elements and the environment causes the consequent onset of moisture loss from elements. The water in the large capillaries is removed via the evaporation process (1 on Figure 2-23) without any volumetric changes; there is an impact on the internal humidity as a gradient is created to maintain hygral equilibrium. Therefore, to achieve the mentioned equilibrium, adsorbed water is extracted from the gel pores (2), and as a result, the C-S-H is reduced in volume (3). Subsequently, the capillary tension increases due to the curvature setup by the menisci causing a compression balance of the C-S-H (4). Moreover, the removal of adsorbed water or the disjoining pressure is also thought to be the cause of the reduction in volume (Brooks, 2003).

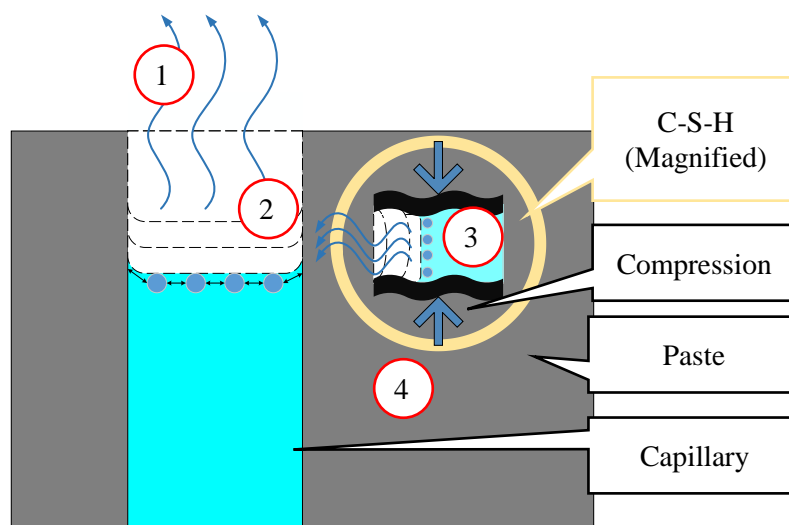


Figure 2-23. Explanation of drying shrinkage by using the capillary tension theory.

The effect of slag and fly ash on the drying shrinkage of concrete has resulted in some conflicting results. Siddique (2008) provides a summary of investigations based on cement substitution with fly ash. He summarises that the addition of fly ash causes a slight, yet negligible, decrease in drying shrinkage, especially up to 20 % replacement. However, the drying shrinkage of concrete can potentially increase in the case of the workability not remaining constant. The increase in paste volume and free water are possible reasons for the expected increase in shrinkage. Arguably, greater amount of free water available does not relate to a greater degree of drying shrinkage (Bissonnette et al., 1999). Therefore, the increase in paste volume provides a better explanation of the drying shrinkage.

As mentioned, the influence of slag on drying shrinkage has yielded interesting results as different investigations report contradicting results (ACI, 2003). Firstly, similar results as that of the reference can be expected. For example, Alexander et al. (2006) state that the incorporation of GGCS should have no influence on the drying shrinkage; although, it may lower it by 10 – 15 % and no effect is expected for a water-to-binder ratio exceeding 0.6. Other researchs also state that the addition of slag could reduce the drying shrinkage, yet only by a minimal amount (Prusinski, 2006; Siddique & Khan, 2011; Yuan et al., 2015). Dellinghausen et al. (2012) found that the magnitude of the drying shrinkage decreases with the incorporation of slag. Moreover, the effect of different water-to-binder ratios was also found to be negligible as similar results were obtained. However, correcting the mixes, and therefore taking into account the true paste volume, an increase of up to 3 % in drying shrinkage was reported.

In conclusion, the effect of SCMs, specifically slag and fly ash, are reported to have varying effects on the drying shrinkage of concrete. This highlights an area of required research to better understand the possible effect these SCMs may have in the concrete system.

2. 10. Durability Properties of Concrete

Concrete is a useful and most used man-made construction material (Shi et al., 2012) and the compatibility of concrete when used in conjunction with steel has contributed to its (concrete) growing success. However, deterioration remains an issue. This is true for concrete itself as well as the steel embedded in the concrete. Structural steel is prone to the process of oxidation, during which iron oxide (rust) is formed. The oxidation process, which is discussed in the following sections, causes the premature demise of structural elements. In addition, aesthetics also become an issue of concern. Concrete encases the embedded steel and in doing so provides a barrier thus, preventing deleterious substances from coming into direct contact with the embedded structural steel. However, as discussed in the Section 2.7, concrete paste has a series of pores that act as possible gateways of reaching the embedded steel. The next section discusses the methods by which aggressive substances can penetrate through concrete which leads to the reduced performance of structural elements.

2. 10. 1. Transport Mechanisms in Concrete

In the presence of aggressive substances, concrete undergoes a process of reduced performance. The harmful substances may be in the form of ions, gases or liquids. The interaction with the concrete and pore solutions therefore differs based on the type of substance the concrete is exposed to. The movement of substances in concrete depends on the penetrability of the concrete i.e. the ease at which substances can move through the concrete. Moreover, the movement of these substances within concrete is driven by different factors. Typically, these factors can occur individually or in conjunction with each other (Basheer et al., 2001).

The factors affecting the movement of harmful materials in concrete are driven by differentials and these differentials can be due to pressure (air and water), humidity, temperature or concentration (Basheer et al., 2001). Based on the driving mechanisms and the type of material, the processes of transportation through concrete is divided into three distinguishable categories, namely, (i) diffusion, (ii) absorption and (iii) permeation.

- Diffusion

The diffusion process is described as the movement of particles, from one region to another, as a result of a concentration gradient. Typically, diffusion occurs under partial or fully saturated conditions. Therefore, the process of diffusion can be described as an internal transport mechanism in concrete. Typically, ions of chloride and oxygen penetrate concrete by mean of diffusion. The impact of the aforementioned substances are described in the sections to follow.

- Absorption

Absorption is a process of liquid transportation due to the effect of capillary tension. The degree of absorption is dependent on the geometry of the pores through which it travels, as well as the degree of saturation (Basheer et al., 2001; Ballim et al., 2009). The effect of absorption in concrete is typically more significant at the surface level and becomes less significant with increasing depth of the concrete (Ballim et al., 2009).

- Permeability

Permeability is used to describe the level of ease with which a fluid will pass through a porous medium due to an applied pressure.

2. 10. 2. Causes of Concrete Deterioration

The deterioration of concrete typically leads to issues of decreased performance, structural failure and is aesthetically a hindrance; moreover, these deterioration processes typically occur in tandem. More so, the environment, which the concrete is placed as well as the concrete system itself, has an impact on the type of deterioration (Figure 2-24).

As shown in Figure 2-24, the concrete system can be divided into two classes or categories that affect it: intrinsic and extrinsic. The intrinsic factors are mainly associated with the constituents of the mix

and the design process; alluding to the fact that the durability of concrete can be catered for at the design stage. Additionally, it should be noticed that all the intrinsic factors are dependent on each other. For example, the change in binder content ultimately leads to a change in the other constituents such as the aggregates. Moreover, the extrinsic factors are affected by quality control on site. As expected, an increase in the level of quality control can lead to a concrete system with a better performance.

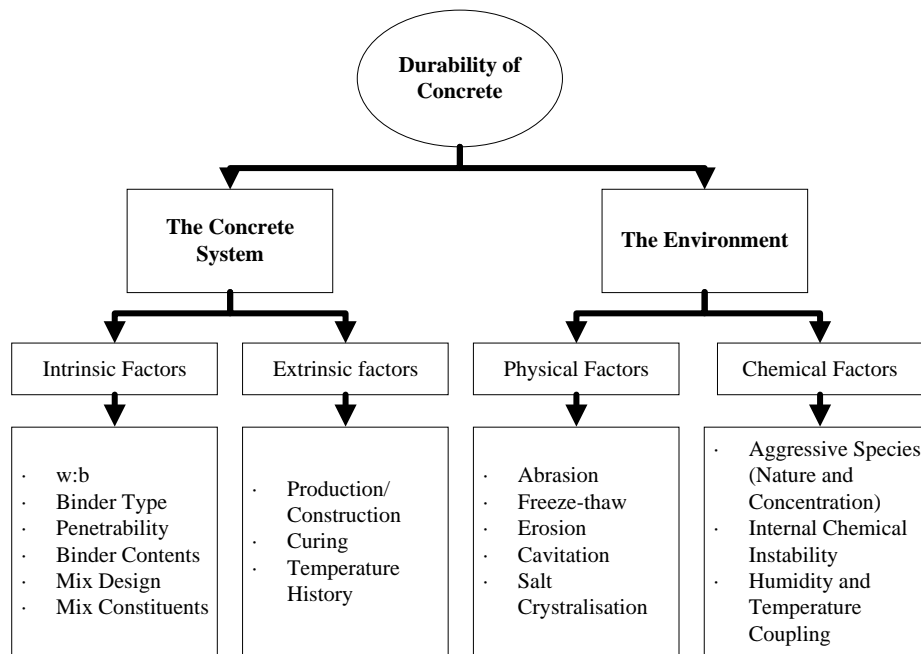


Figure 2-24. Durability factors typical of concrete deterioration (Ballim et al., 2009).

The role of the environment also brings in a new level of durability considerations for a concrete system. Physical factors often occur as a result of weathering phenomena or associated elements. The effect of abrasion, for example, leads to the wearing down of the physical concrete matrix. The continual processes therefore exposes the internal matrix (as well as any shallow reinforcing) and increases the total surface area of degeneration. The damage could thus increase at an exponential rate.

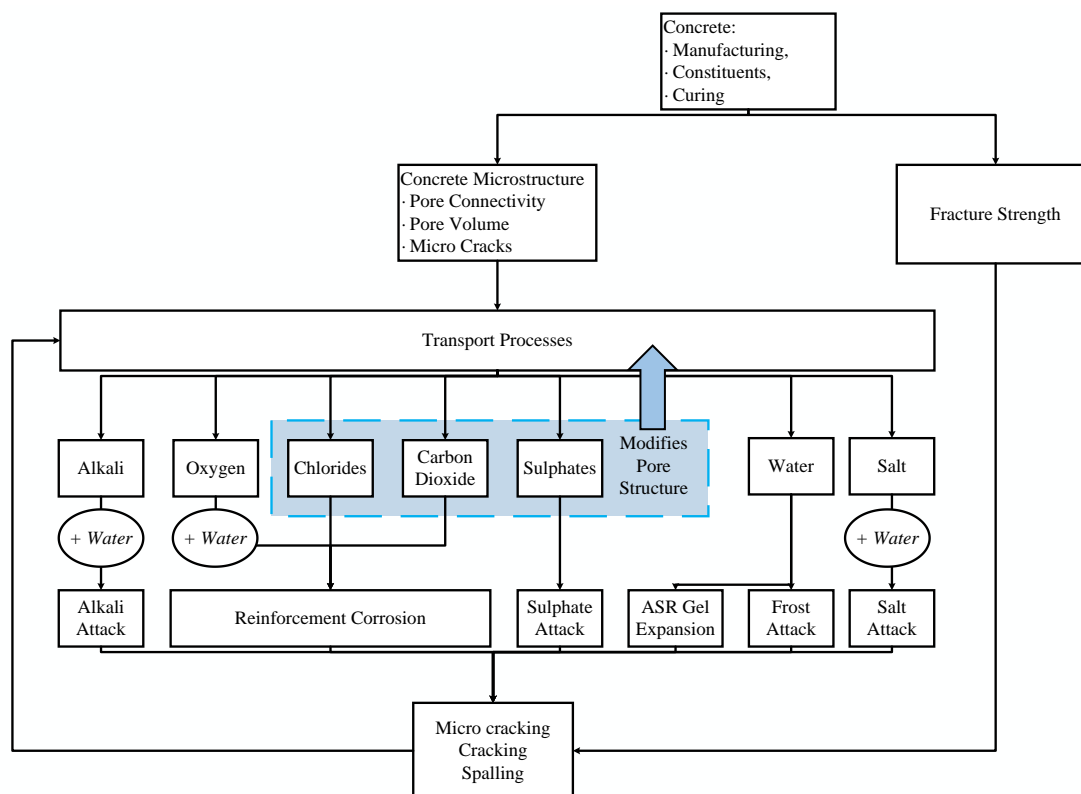


Figure 2-25. The onset cycle of concrete durability (Basheer & Barbhuiya, 2009).

Figure 2-25 displays the cycle of concrete deterioration. The two main influences being the microstructure and fracture strength. The fracture strength is associated with the formation of cracks, as concrete has a low tensile threshold compared with its compressive capacity. Micro cracks, as a result of low tensile strength capacity, increases the concrete's permeability and in doing so, increases the subjectivity of the concrete to aggressive species. The deterioration mechanism of these substances can be found in elsewhere with good explanations of the processes (Basheer et al., 2001; Bijen, 2003; Ballim et al., 2009; Soutsos, 2010). Moreover, each process tends to alter the microstructure, which typically leads to an increase in the permeability. For example, carbonation converts calcium hydroxide into soluble calcium carbonate that is removed from the system, thereby increasing the porosity. Additionally, some processes involve the generation of expansive products which causes localised internal tensile stresses, which induce micro cracking. For example, the process of rust generates oxides that are 3 - 6 times greater in volume than the original reactant (Bijen, 2003). However, as seen in the previous section, the use of SCMs improve the pore structure of concrete and has been used in concrete to improve the durability with good results. The next section delves into how the use of SCMs improve the durability of concrete as found in literature.

2. 10. 3. Deterioration of Steel

When steel is used in conjunction with concrete for structural elements, concrete provides compressive resistance and steel provides tensile resistance. The concrete also protects the steel by acting as a physical barrier between the environment and steel. Due to the high pH of concrete ($\text{pH} > 12$), an

additional mechanism of passivation also creates a protective layer around the concrete (Ballim et al., 2009; Soutsos, 2010).

The passivation of steel occurs where a passive layer of gamma iron oxide (γ -FeOOH) forms around steel. The oxide layer formed prevents the movement of iron ions (Bijen, 2003) and is approximately 1 nanometer thick (Bijen, 2003; Soutsos, 2010). The layer formed is dense, complicated by the surface of the steel and is dynamic i.e. constantly forming and breaking down (Soutsos, 2010). However, the layer will only be present if the correct conditions are present, namely, (i) a relatively high pH ($\text{pH} > 10.5$) and (ii) the absence of aggressive electrolytes (Bijen, 2003; Ballim et al., 2009; Soutsos, 2010). The breakdown of this layer is typically due to two mechanisms: carbonation and chloride ingress.

- Carbonation

Carbon dioxide present in the atmosphere can combine with water to form a weak acid, namely carbonic acid, as shown by the reaction (Bijen, 2003; Ballim et al., 2009; Soutsos, 2010):



A similar process occurs within concrete as carbon dioxide diffuses into the concrete and reacts with the pore solution, forming the carbonic acid. The carbonic acid in turn reacts with calcium hydroxide in the concrete to form insoluble calcium carbonate (Bijen, 2003; Ballim et al., 2009; Soutsos, 2010):



The insoluble calcium carbonate reacts with carbon dioxide and water to generate soluble calcium carbonate, calcium bicarbonate, which is easily removed by water:



The overall porosity of the concrete therefore increases as calcium hydroxide is broken down into a soluble form (Basheer et al., 2001). In addition, the carbon dioxide also reacts with the C-S-H gel and decomposes it into calcium carbonate and a porous amorphous silica gel (Basheer et al., 2001; Bijen, 2003; Soutsos, 2010), thereby increasing the amount of reactants and porosity. This process in turn has a second effect of reducing the pH of the pore solution to a value below 10.5. As aforementioned, this pH value is essential for the presence of the passive layer to form on steel. As the process of carbonation occurs and continues, the overall pH of the pore solution drops and causes the depassivation of the steel. The depassivation of steel and the increased porosity subjects the concrete to the ingress of deleterious substances to enter with ease, for example, the chloride ions that typically act as a catalyst for corrosion.

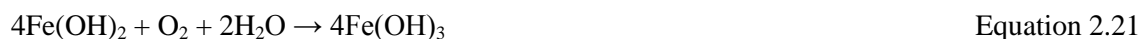
- Chloride Ingress

There is an interaction between chlorides and concrete that relates to the phenomenon of chloride binding. The chlorides can be bound chemically to form calcium chloroaluminate (Fridel's salts) or be adsorbed physically to the system (Basheer & Barbhuiya, 2010), yet it is set free by the process of

carbonation. However, chlorides are likely to interact with the steel to initiate the corrosion process, therefore acting as a counter mechanism to the protective passive layer.



The corrosion process involves the development of a cathode and an anode, and requires moisture and oxygen to start the initiation process. Oxygen is required for the reactions to occur and water acts as a transport medium. Firstly, iron dissolves into soluble iron ions and electrons at the anode. Hereafter, the cations react with hydroxide ions to form a ferric hydroxide:



The electrons move to a cathodic region and reacting with water and oxygen to form hydroxide ions. These hydroxide ions move along the electronic current and react with the ferrous ions. Hereafter, the formed ferric hydroxide reacts with moisture and oxygen to generate ferric hydroxide (Equation 2.21) and then rust (Equation 2.22):

The corrosion process is divided into two types, viz. non-expansive and expansive oxide formation. Non-expansive oxides occurs in saturated conditions where the iron remains in solution form. This is known as black rust or anaerobic corrosion. Expansive corrosion results from the rust occupying a larger volume compared to the rebar itself; these products can be up to 6 times larger in volume (Bijen, 2003). This generates expansive products that can cause spalling of concrete and delamination. The process of corrosion is shown in Figure 2-26.

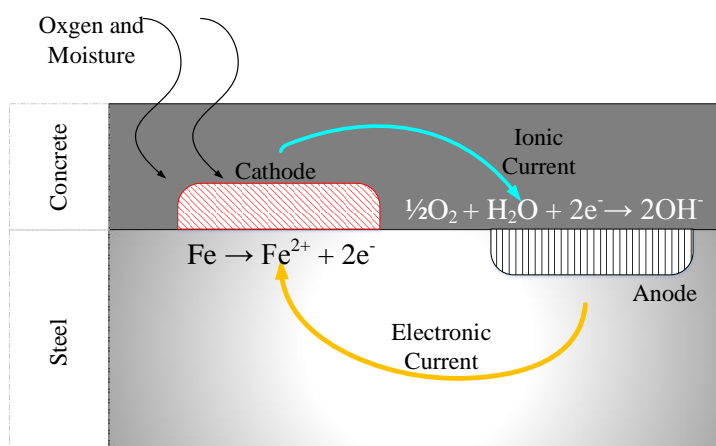


Figure 2-26. Corrosion of steel.

2. 10. 4. Effect of SCMs on the Deterioration of Concrete

The durability of concrete is associated with the permeability and transport mechanisms of aggressive substances. Hence, reducing the permeability and inhibiting the transport mechanisms can potentially prolong the durable life span of concrete and this can be achieved by incorporating SCMs into concrete mixes. Researchers have investigated the effect of concrete containing slag and fly ash in the mix design and have reported favourable results in terms of durability performance (Papadakis et al., 2002;

Glasser et al., 2008; Ramezaniapour et al., 2011; Aponte et al., 2012; Boa & Topu, 2012; Dellinghausen et al., 2012; Otieno et al., 2014; Zhang & Zhang, 2014).

The first method by which the durability of concrete incorporating SCMs is improved is as a result of pore refinement of the concrete as discussed in Sections ???. In addition, the incorporation of SCMs tend to produce a better pore distribution and shapes (Shi et al., 2012) and reduces the amount of critical pores (Zhang & Zhang, 2014). With an increase in pore refinement, the overall permeability of the concrete decreases, reducing the amount of deleterious substances that can enter into the concrete system. However, with the use of SCMs, the total porosity is the dominating factor in comparison to the distribution (Zhang & Zhang, 2014).

- Permeability

Dellinghausen et al. (2012) states that the oxygen permeability decreases with the decrease in water-to-binder ratio. This is due to the formation of a more dense hydraulic paste as well as the increase in cementing particle hydration. Hence, the reduction in free water causes a reduction in capillary pore pathways and a reduction in porosity. For example, the coefficients of permeability were 24.2 -, 9.0 - and $1 \times 10^{-16} \text{ m}^2$ for water-to-binder ratios of 0.55, 0.42 and 0.30, respectively. However, the addition of slag caused a decrease in permeability. For example, at 50 % replacement the coefficients were 13.0 - , 10.6 - and $6 \times 10^{-16} \text{ m}^2$ for water-to-binder ratios of 0.55, 0.42 and 0.30, respectively. However, the researchers found, by comparing the permeability to strength, that a higher strength concrete does not designate for a more permeable concrete.

The increased substitution of fly ash or slag also affects the permeability. Siddique (2008) summarises the work of various authors and makes two statements on the effect of fly ash on concrete permeability. Firstly, the increase in fly ash content decreases the permeability of the concrete and Class F fly ash is more effective than Class C. Secondly, the permeability of Class F mixtures are reported to be equal to or superior to those of mixtures containing slag. Moreover, increasing the amount of fly ash does reduce the permeability. Thomas & Matthews (1992) reported that cement substitutions of 15, 30 and 50 % fly ash, yielded in permeability reductions of 50, 60 and 80 %, respectively. However, Dhir et al. (1997) reported that the increase in fly ash content resulted in concrete caused an increase in permeability at substitutions above 50 %; below 50 %, a reduction in permeability was recorded. Moreover, with time, the permeability did decrease (Dhir et al., 1997).

- Chloride Resistance

Additionally, the addition of SCMs in concrete is linked to increasing the chloride resistance of concrete. Conductivity is suggested to be a function of the pore solution, chemical composition and pore structure (Ramezaniapour et al., 2011). Again, the function of SCMs to improve the pore structure is highlighted and backed by researchers (Aponte et al., 2012; Boa & Topu, 2012; Shi et al., 2012; Otieno et al., 2014). Therefore, the first reason for increased chloride resistance is pore

refinement. The smaller SCM particles aid in blocking pathways and form additional hydration products, which leads to the second mechanism.

Secondly, with the formation of more C-S-H, pastes containing SCMs can also increase the chloride binding capacity of a mixture. Chloride binding is a phenomenon whereby chloride ions are incorporated in the chemical structure of hydration products. The first means of achieving this is by the adsorption of chloride ions in the C-S-H gel (Luping & Nilsson, 1993) and is stated to be a reason for the reduced chloride conductivity of the results obtained by Leng et al. (2000).

Thirdly, and also closely related to the second reason, is the formation of Friedel's salts ($C_3A \cdot CaCl_2 \cdot 10H_2O$). In a cementitious paste chloride ions react with aluminate phases to form Friedel's salt via a mechanism of dissolution/precipitation and ionic exchange (Glasser et al., 2008). The explanation of the theories on the chloride binding and formation of Friedel's salts can be found elsewhere (Glasser et al., 2008). Studies involving investigations of the chloride binding capacity of concrete, research typically yields that mixes containing fly ash and slag perform better compared with plain concrete (Arya et al., 1990; Arya & Xu, 1995; Dhir et al., 1996; Dhir et al., 1997; Leng et al., 2000; Luo et al., 2003). In addition, the effect of slag in terms of binding has also been reported to not only exceed that of a reference concrete mixture, but also to show better results compared to fly ash mixes (Arya & Xu, 1995). In their study, Arya et al. (1990), used 15 and 35 % fly ash and 70 % slag replacement and reported increased capacities of 38, 57 and 85 %, respectively. Therefore, slag exhibits better chloride binding capabilities compared to fly ash.

The increase in cement substitution therefore increases the chloride binding capacity. For example, Dhir et al. (1996) found that when two-thirds of cement was replaced with slag, the binding capacity increased by a factor of 5 relative to the reference. This is due to the nature of slag having better chloride binding capabilities compared to Portland cement.

Fourthly, the conductivity can also be affected by the percentage replacement and reported by researchers that it decreases with increasing replacement of cement with SCMs (Aponte et al., 2012; Boa & Topu, 2012; Zhang & Zhang, 2014). To serve as an example, an investigation of South African blast furnace slag conducted by Otieno et al. (2014) found that at a constant water-to-binder ratio, the chloride conductivity reduced from 0.99 mS/cm (reference mixture) to 0.41, 0.30 and 0.27 mS/cm for the respective cement replacements of 20, 35 and 50 %.

By considering this, it comes to reason that a theoretical optimum replacement level should exist for durability. For example, Alexander et al. (2003) concluded that substituting cement with 50 % Corex slag yielded optimum results in terms of chloride resistivity. Moreover, below 25 % replacement, no appreciable reduction in chloride conductivity was reported compared to the reference (Alexander et al., 2003). A similar result was reported by Ramezani-pour and Malhotra (1995) that found that the reference and 25 % replacement with a blast furnace slag produced very high values for charge passing through samples (>1500 Coulombs). The loss in reduction potential may be as a result of not as many

secondary reaction products being formed, but most likely is a result of the reduced chloride binding capacity. Table 2.9 provides a list of studies that established a potential optimum replacement level in terms of chloride resistance. It can be seen from the table that the range for slag is between 45 and 60 % replacement. For fly ash, the replacement levels range between 35 and 40 % replacement of cement.

Table 2.9. Optimum SCMs replacement level in term of chloride resistance.

SCMs	Replacement (%)	Authors
GGBS (Chloride and Strength)	50	Aldea et al. (2000)
GGBS (Chloride only)	75	Aldea et al. (2000)
GGCS	50	Alexander et al. (2003)
GGBS (SCC)	60	Shi et al. (2012)
GGBS	50	Shi et al. (2012)
GGCS, GGBS & GGAS	45-60	Otieno et al. (2014)
Fly Ash	33	Dhir and Jones (1997)
	33	Leng et al. (2000)
	40	Ampadu et al (1999)
	40	Shi et al. (2012)
	35-40	Boa and Tocu (2012)

From the aforementioned section, an obvious conclusion is drawn to the idea that the type of SCMs used can also affect the durability of concrete (Leng et al., 2000). This may be as a result of the differences in chemical composition. A study by Otieno et al. (2014), of three different slag types (GGBS, GGCS and GGAS), found that in all instances, the GGCS displayed better results compared to the GGAS and GGBS. At a constant water-to-binder ratio, the reference had a chloride conductivity of 0.99 mS/cm, whilst at 50 % replacement the values dropped to 0.17, 0.27 and 0.38 for GGCS, GGAS and GGBS, respectively and a similar trend was observed for other replacement levels and w:b ratios (Otieno et al., 2014). Upon further investigation, it was found that the GGAS had a lower glass content (93 % compared to the other two slags which had contents exceeding 98 %) and a higher manganese content (6.93 % whereas the other two slags had levels below 1 %) (Otieno et al., 2014). The difference in these components were thought to be the reason for the reduced performance of GGAS. Moreover, the investigation concluded that the composition would therefore also affect the chloride binding capacity. Another study on the use of steel slag as a potential SCM was investigated and found that the permeability, at all ages, were reported to be higher than the reference concrete, further supporting the hypothesis that of chloride conductivity resistance being a function of the type of material used (Wang et al., 2013).

2. 10. 5. Durability Testing Methods in a South African Context

In South Africa three methods have been developed to assess the durability properties of concrete, namely, the chloride conductivity, oxygen permeability and the water sorptivity tests. The data typically found by these results, known as durability indices (DI), have been related to service life prediction models. A study undertaken by RILEM (Kropp, 1999) compared the developed methods to those established before and found a near linear relationship between the test results, despite the differences in test philosophies. An exception was however found in the results of the water sorptivity test which

could not be explained (Beushausen & Alexander, 2008). Table 2.10. provides a brief comparison of the different tests used to assess concrete durability and provided as a means to evaluate the use of the South African durability indices in a design context.

Table 2.10. Selected tests used to assess the durability of concrete.

Test	Sample	Precondition	Mechanism	Factors
Permeability				
OPT	Cores: 70 mm diameter 30 mm thick	Dried sample 50 °C for 7 days	<ul style="list-style-type: none"> • Varying pressure gradient. • Oxygen decay across a sample. • Unidirectional pressure flow. 	<ul style="list-style-type: none"> • Area • Thickness • Pressure difference • Open porosity • Gas viscosity
CPT	Cores 150 mm diameter 50 mm thick	Dried sample A: 20 °C for 28 days or B: 105 °C for 7 days	<ul style="list-style-type: none"> • Constant pressure gradient. • Absolute pressure difference. 	<ul style="list-style-type: none"> • Area • Thickness • Pressure difference • Open porosity • Gas viscosity
TPT	On site	None	<ul style="list-style-type: none"> • Pressure Gradient. 	<ul style="list-style-type: none"> • Saturation conditions
Chloride Conductivity				
CCT	Cores 70 mm diameter 30 mm thick	Dried sample 50 °C for 7 days. Saturated (5 M NaCl solution)	<ul style="list-style-type: none"> • A current is applied until 10 V is measured across the specimen. 	<ul style="list-style-type: none"> • Thickness • Saturation • Area • Voltage
RCPT	Cores 102 mm diameter 51 mm thick	Saturated (water)	<ul style="list-style-type: none"> • Sample is subjected to two solutions. • Applied current of 60 V for 6 hours. • Record the current profile. 	<ul style="list-style-type: none"> • Thickness • Saturation • Area • Voltage
BDT		Saturated (lime) Submerge in water for 35 days	<ul style="list-style-type: none"> • Chloride profiling by grinding 0.5 mm and determining the amount of chloride. 	<ul style="list-style-type: none"> • Thickness of ground sections
Water Sorptivity				
WST	Cores 70 mm diameter 30 mm thick	Dried sample 50 °C for 7 days	<ul style="list-style-type: none"> • Unidirectional penetration of water. • Mass change over time. 	<ul style="list-style-type: none"> • Area • Thickness
RILEM TC 116- PCD 1999	Cores 102 mm diameter 51 mm thick	Dried sample A: 20 °C for 28 days or B: 105 °C for 7 days	<ul style="list-style-type: none"> • Unidirectional penetration of water. • Mass change over time. 	<ul style="list-style-type: none"> • Area • Thickness

Where: OPT = Oxygen Permeability Test; CPT = Cembureau Permeability Test (Kropp, 1999); TPT = Torrent Permeability Test (Torrent, 1992); CCT = Chloride Conductivity Test; RCPT = Rapid Chloride Permeability Test (ASTM Standards C1202, 2013); BDT = Bulk Diffusion Test (NT BUILD 433, 1995); WST = Water Sorptivity Test.

The use of the South African durability indices have potential to be implemented as a standardised test, despite each test having certain drawbacks and benefits. For example, all the test results are sensitive in terms of sample preparation and limited to lab implementation.

If concrete samples are not properly conditioned the OPT could give a false reading due to potential pathways being blocked, therefore reducing the gas flow. The same argument holds for the Cembureau Permeability Test (CPT). These tests are also limited to the lab and require the samples to be core drilled from on-site elements. The TPT in contrast is better suited for on-site application, however, the sample conditions are in turn hampered by the on-site conditions; the conditions however give a realistic interpretation of the 'true' site conditions.

A concern exists with regard to the drying of samples as there is a possibility of affecting the microstructure (Ballim et al., 2009). However, the lower temperature, compared to the CPT, is believed to have a minimal effect. On the issue of sample preparation in terms of drying, the OPT shows good correlation to the general microstructure of concrete, discerning different water-to-binder ratios, compaction and internal bleeding (Stanish et al., 2006). The OPT has also proven to yield near similar results compared to other test methods (Beushausen & Alexander, 2008).

The chloride conductivity test is also subjected to the influences of sample preparation. Firstly, poor saturation in concrete samples lead to issues concerned with the hampering of ion migration; chloride ions travels better in solution and therefore would be hampered by areas of poor saturation. In addition, the effect of drying samples, as mentioned previously, could affect the microstructure. Compared to the RCPT and BDT, the CCT incorporates the same solution and concentration in all aspects: environment and saturation. This has the advantage of only investigating the ions migrating and not the effect of diffusion. In addition, the application of a voltage across the specimens is also less and for a shorter duration. This eliminates the possibility of the samples being heated up and therefore causing a possible alteration to the microstructure. The setup is also sensitive as poor sealing could hamper the results, as ions would not travel through the specimen but rather around it. The reproducibility and repeatability of the test is good, but can do with improvement (Stanish et al., 2006) and seems to be as good as other international; tests such as the RCPT and BDT (Beushausen & Alexander, 2008).

The WST is also affected by sample preparation in the same manner as the OPT and CCT. The reproducibility and repeatability is deemed acceptable, yet sensitive to sample preparation (Stanish et al., 2006). Another factor that does affect the WST is the poor sealing of the specimen.

To conclude, the South African durability tests are seen to be good indicators for the durability of concrete mixture. The results obtained are deemed satisfactory and comparable to international standards. Hence, the continual investigation and improvement of the tests could benefit the scientific knowledge gained by understanding concrete better. The implication of the tests as standards could also aid in the design of more durable structures as well as incorporating a specification approach to concrete design.

2. 11. Concluding Summary

The impact of the production of cement on the environment has been seen to have issues of concern, yet the use of cement is linked to both economic and social growth and development. The literature review focussed on the use of SCMs, mostly in terms of slag and fly ash, in concrete and the associated behaviour. This clearly indicates that the use of SCMs in concrete is most beneficial in terms of the end outcomes.

In terms of the fresh state properties, the workability of SCM-based concrete is affected in a favourable sense. The addition of SCMs to concrete can make the concrete more workable, hence leading to the possible reduction in water content. This would in turn lead to a reduction in the total binder required if the water-to-binder ratio is kept constant. On the other hand, if only the water is reduced, a stronger concrete can be created. However, the addition of SCMs tend to increase the concrete setting time. The higher cement replacement, the greater the effect on setting time. The retardation is as a result of the dilution and lower reactivity of the SCMs. This retardation can therefore hamper the construction process by causing delays. In terms of early age properties, the use of SCMs are often reported to show poorer performance. This is due to the susceptibility to evaporation, and as a result, increased plastic shrinkage that can potentially be mitigated with improved mix design philosophies.

The addition of SCMs do lead to concrete with better pore structures. The pore refinement is as a result of enhanced particle packing and the pozzolanic hydration products. The pozzolanic reaction utilises the CH from cement hydration. The CH typically only generates an alkaline environment and is associated with weaker structural properties. Hence, replacing it with C-S-H is beneficial as the microstructure is refined and the strength can be increased. Moreover, the addition of SCMs in concrete shows to improve the ITZ.

The early age compressive strength of SCM-based concrete is lower than a 100 % PC concrete mixture due to the dilution and lower reactivity. Some materials, such as GGCS, have shown to exceed the strength of the control (Alexander et al., 2003). However, the concrete containing SCMs are typically greater to or equal compressive strength to that of the reference at later ages. There is also an apparent optimum cement replacement level, which depending on the material, is approximately 50 % for slag based concrete and 35 % for fly ash based concrete. Equally as important, factors such as fineness, curing, material type and composition, and age of testing also affect the compressive strength. The tensile strength of SCMs based concrete is also improved. This is most likely due to the improvement of the ITZ.

The durability performance of concrete containing SCMs generally exceeds that of the control. This is due to pore refinement and the generation of additional hydration products, which can inhibit the movement of deleterious substances.

Chapter 2: Supplementary Cementitious Materials (SCMs)

Finally, the use of SCMs have some pitfalls, yet the lucrative properties, in terms of performance and economics, cannot be ignored. Hence, studying the effects of using SCMs provides valuable knowledge in the way of greening the concrete industry and increasing its sustainability for future use.

Chapter 3

Experimental Setup and Programme

Due to the negative impact associated with the production of cement, multiple studies have been implemented to study possible ways of reducing the impact. Nonetheless, concrete is still a needed commodity in terms of both the construction industry and for economic development and is not likely to be replaced in the near future. Therefore, favourable attention has been given to investigating methods of reducing the negative impacts associated with the consumption of concrete. The use of supplementary cementitious materials (SCMs) provides a solution to alleviate the associated environmental problems. The objective of this study is to investigate the performance of concrete when SCMs are incorporated; more aptly, the performance of fly ash and slag produced in South Africa. The three areas of the investigation include the plastic state, mechanical and durability properties. The test methods are discussed in this chapter.

3. 1. Materials

Concrete is a composite material that varies depending on the specification required and with continual research, additional materials have been incorporated in concrete mixes to develop a range of properties suited for different requirements. These added materials include fibres, admixtures, and various aggregates and, in some cases, even the absence of fine aggregates. Examples include self-compacting concrete (SCC) used to cast structures with dense reinforcing and complex geometries, high-performance concrete (HPC) for high-rise buildings and fibre reinforce concrete (FRC). Supplementary cementitious materials (SCMs) also fit under these additional materials added. For the purpose of this study only the basic constituents were used, i.e. aggregates (fine and coarse), binders (cement, fly ash and slag) and water.

3. 1. 1. Water

Water is added to facilitate the hydration process and provide the necessary means to induce workability. The amount of water varies depending on the material constituents and the intended use of the final concrete. For the concrete mixing process, ordinary municipal tap water was used.

3. 1. 2. Binders

The binders used in this study consisted of a Portland cement (CEM I 52.5 N), four different fly ash samples and three different slag samples. Both the physical and chemical characteristics of the binders

were determined and includes: (i) the particle size distribution (PSD), (ii) visualisation of the morphology via scanning electron microscopy (SEM), and (iii) the chemical composition via X-ray fluorescence (XRF).

The particle size distribution was determined by laser diffraction using a particle size analyser, namely Saturn DigiSizer® 5200 V1.10. The powder samples are diluted in isopropanol for sample preparation, mainly as the binders do not dissolve to the required degree in water and would start to hydrate, hence affecting the results. All tests are conducted at a refractive index (RI) of 1.38 for the binders.

A visual study undertaken to observe the morphological properties of the samples, which is performed using a Leo® 1430VP Scanning Electron Microscope. Samples are prepared by lightly dusting samples onto a piece of double sided carbon tape attached to a metal stub. Hereafter, the samples are gold coated for to ensure that the sample have conductive properties. Images are then taken using the SEM microscope under the following beam conditions: 7 kV and a spot size not exceeding 230 with the magnifications varying to establish a good quality image.

The chemical composition of the materials was determined on a PANalytical® Axios Wavelength Dispersive spectrometer. A glass disk is prepared by using 0.7 g of the sample being investigated with high purity trace element and Rare Earth Element-free flux ($\text{LiBO}_2 = 32.83\%$, $\text{Li}_2\text{B}_4\text{O}_7 = 66.67\%$, $\text{LiI} = 0.50\%$). Hereafter, major elements are analysed on the fused disk using a 2.4 kW Rhodium tube.

3. 1. 3. Aggregates

3. 1. 3. 1. Course Aggregate

The course aggregates typically make up the majority volumetric matrix of a concrete. For the purpose of the study a 13 mm Greywacke stone was used. The relative density given in Table 3.1 and was determined in accordance with SANS 5844 (2006).

3. 1. 3. 2. Finer Aggregate

Three batches of sand were used in the investigation. A CEN reference sand in addition to two natural sand batches locally referred to as Malmesbury sand. Figure 3-1 displays the grading of each of the sands used. The grading was done in accordance with SABS SM 829 (2002). The CEN sand was reserved for used in the mixing of mortar specimens. The batches of Malmesbury sand were used for concrete mixes. Additionally, the FM and RD of all sands are given in Table 3.1.

Table 3.1. Material properties: The relative densities (RD) and Fineness Modulus (FM).

	Water	Cement	Fly Ash	Slag	Stone Greywacke (13 mm)	Sand CEN	Batch 1 (M1)	Batch 2 (M2)
RD	1	3.14	2.3	2.9	2.72	-	2.62	2.61
FM	-	-	-	-	-	2.54	2.21	2.13

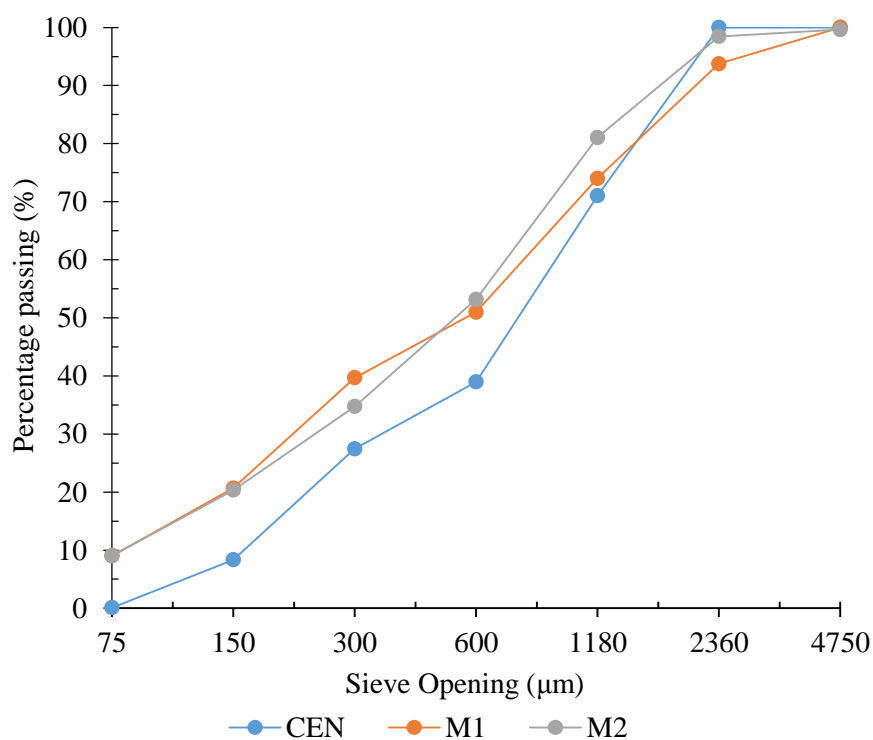


Figure 3-1. Grading curves of the three different types of sand.

From Figure 3-1 it is noticed that the particles sizes present are all less than 2.36 mm and all sands have a relatively good grading. The CEN Sand has no particles finer than 0.075 mm, whereas the two batches of Malmesbury sand both have approximately 10 % particles that are finer than 0.075 mm.

3. 2. Mixing Procedure

A different mixing protocol was adopted for the mortar and concrete mixes. The sequence of adding material and mixing times were kept relatively constant for all mixes. The differences in preparing the mixtures are discussed in the following section.

3. 2. 1. Mortars

Mortar specimens were used as part of the investigation to evaluate the activity index of the binders. The mixes used to assess the strength activity consisted of a predefined water-to-binder ratio of 0.5 and a sand-binder ratio of 2.5; furthermore, the mix designs are given in Table 3.2 and the mixing procedure is depicted in Figure 3-2. Both the mix design and procedure is adopted according to the EN 196-1 (2005a).

Table 3.2. Mix design of the mortars.

	Reference	Slag Based	Fly Ash Based
Water (g)	225	225	225
Sand (g)	1350	1350	1350
Cement (g)	450	225	337.5
Slag (g)	0	225	0
Fly Ash (g)	0	0	112.5

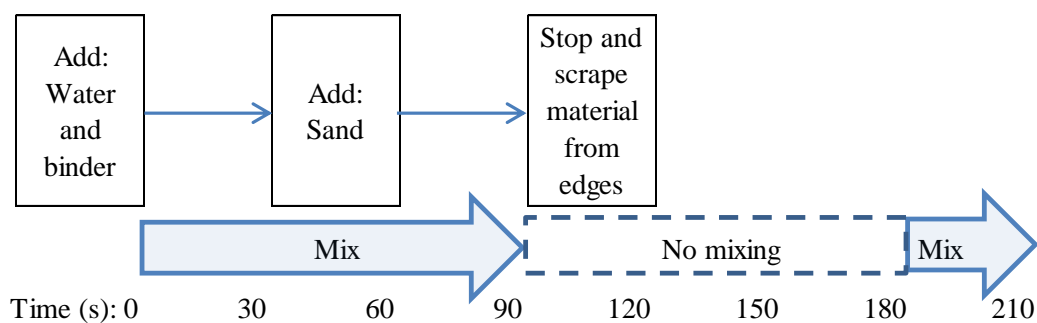


Figure 3-2. The mixing procedure for mortar specimens.

The mixing procedure did however lead up to a problem of conglomeration of the binders in the mortar specimens. An example of this is shown in Figure 3-3. The occurrence of this agglomeration affected the tested results of the compressive and flexural strengths. To circumvent this, the paste mixes were mixed for an additional 20 seconds. This modification mitigated the occurrence of binder agglomeration.



Figure 3-3. The occurrence of conglomeration in mortars.

3. 2. 2. Concrete

Concrete mixes were done using the C&CI method (Addis & Goodman, 2009) and work was based on selecting the material quantities of a mixture by considering material properties. The sand grading and stone size determine the amount of water. The binder was calculated based on this amount of water and the water-to-binder ratio. The amount of stone is calculated from its compacted bulk density, the fineness modulus of the sand and an efficiency factor, K. The sand is then calculated to make up a 1000 l mixture. Through a process of trial-and-error the quantities are altered. The main difference in mixes are that the cement is replaced, on a basis of mass substitution, with a SCM of interest. Therefore, the total binder, in addition to the amount of water and aggregates used per mix remains unchanged. The mixes were conducted in the following manner:

- Step 1 Washing of the pan and drying it with a paper towel. This is done at the start of every mix to represent the condition of a recently washed mixer and to ensure that this condition is applied to all mixes.

- Step 2 Adding the dry constituents in the order of sand, binder and followed by the coarse aggregates.
- Step 3 Allowing the dry materials to mix for a period of 15 seconds.
- Step 4 Adding the water to the dry materials and allowing it to mix for 4 minutes.
- Step 5 Measuring the workability of the mixture by means of a slump test.

Table 3.3. provides the mix composition used in the experimental programme. Mix 1 is used for concrete samples used in the compressive and tensile tests. Mix 2 is used for concrete specimens used in the remaining tests. The only difference between the mixes is the amount and type of sand used. This occurs due to the difference in densities. Ultimately, the theoretical yields also differ, with the yield of Mix 1 and Mix 2 being 2388 and 2385 kg/m³, respectively.

Table 3.3. The concrete mix composition used in the study.

		Control	Fly Ash			Slag			
Mix 1 (kg/m ³)	% Cement Replacement	0	15	25	35	25	50	75	
	Binder	Cement	420	357	315	273	315	210	105
		SCM	0	63	105	147	105	210	315
	Water	210							
	Coarse Aggregate	13 mm Greywacke	1050						
Fine Aggregate	Malmesbury (M1)	708							
Mix 2 (kg/m ³)	% Cement Replacement	0	15	25	35	25	50	75	
	Binder	Cement	420	357	315	273	315	210	105
		SCM	0	63	105	147	105	210	315
	Water	210							
	Coarse Aggregate	13 mm Greywacke	1050						
Fine Aggregate	Malmesbury (M2)	708							

3.3. Curing Process

All samples were de-moulded ± 24 hours after casting. After which, the specimen were placed in curing tanks filled with water at a temperature of 25 °C. The specimens remained in the curing tanks until the day of testing.

3.4. Reactivity

The reactivity of the mixes were assessed on the chemical requirements set out by the BS EN 450-1 (2012) and BS EN 15167-1 (2006), in addition to the ASTM Standard C618 and C989. The EN standards were however used in assessing of the strength activity indices.

3.4.1. ASTM Method

The chemical requirements of the ASTM standard was used to assess the applicability of the samples for use in concrete. These requirements are listed in Table 3.4. The data used to assess the chemical composition was obtained from the XRF analysis.

Table 3.4. The chemical requirements of slag and fly ash according to the ASTM.

ASTM	Requirement			
	Fly Ash	N	F	C
C618	$\text{SiO}_2 + \text{Al}_2\text{O}_3 + \text{Fe}_2\text{O}_3$	$\geq 70\%$	$\geq 70\%$	$\geq 50\%$
	SO_3	$\leq 4\%$	$\leq 5\%$	$\leq 5\%$
	Moisture Content	$\leq 3\%$	$\leq 3\%$	$\leq 3\%$
	LOI	$\leq 10\%$	$\leq 6\%$	$\leq 6\%$
	Slag			
C989	S	$\leq 2.5\%$		

3. 4. 2. BS-EN Standards

The BS-EN standards were used to determine the conformity of the test samples based on the physical parameters. Mortar specimens were cast and tested at specified ages to assess the use of the SCMs in concrete. Details of the generic mixes are shown in Table 3.5. The SAI is calculated as the percentage ratio of the mixture containing the SCMs to the reference mixture.

Table 3.5. Mortar mixes used to determine the use of SCMs in concrete.

	Water (g)	CEN		Cement (g)	SCMs (g)	SAI (%)		
		Sand (g)	Replacement (%)			7 (days)	28 (days)	91 (days)
Reference	225	1350	0	450	0	-	-	-
Fly Ash	225	1350	30	315	135	75	-	85
Slag	225	1350	50	225	225	75	75	-

Moreover, the BS-EN Standards also provide chemical requirements that the SCMs samples need to conform to in order to be accepted for use in concrete and Table 3.6 provides the requirements. It should be mentioned that this does not state that the material is hydraulic active, but that it can potentially exhibit the behaviour of a SCM.

Table 3.6. The chemical requirements as stated by the BS-EN Standards.

BS-EN	Requirement			
	Fly Ash	N	F	C
450-1:2012	$\text{SiO}_2 + \text{Al}_2\text{O}_3 + \text{Fe}_2\text{O}_3$	$\geq 70\%$	$\geq 70\%$	$\geq 50\%$
	SO_3	$\leq 4\%$	$\leq 5\%$	$\leq 5\%$
	Moisture Content	$\leq 3\%$	$\leq 3\%$	$\leq 3\%$
	LOI	$\leq 10\%$	$\leq 6\%$	$\leq 6\%$
	Slag			
15167-1:2006	$\text{CaO} + \text{MgO} + \text{SiO}_2$	$\geq 66 \frac{2}{3}\%$		
	$(\text{CaO} + \text{MgO}) / \text{SiO}_2$	$\geq 1\%$		
	MgO	$\leq 18\%$		
	LOI	$\leq 3\%$		

3. 5. Workability

The workability of the concrete was measured by means of a slump tests as specified by BS EN 12350-2 (2009a). The slump cone (Figure 3-4) and base plate is firstly checked to be clean and damp. Hereafter the concrete sample is added into the cone in three layers with each layer filled to represent approximately one third of the volume. After each layer is added, the tamping rod is used and the

concrete is compacted manually with 25 strokes. After the addition and tamping of the third and final layer, the excess material is removed using the tamping rod and all material is removed from the base plate as well. The demoulding process entails the upward lifting of the cone within a time slot of 5 - 10 seconds after the final compaction. This is done to ensure that a true slump is obtained and not influenced by the rate of demoulding. A fast rate of demoulding could result in a slump that is higher than the true slump. In contrast, with a demoulding rate that is too slow, a smaller slump could be potentially reached. After the demoulding process, the cone is inverted and used as a reference to measure the slump. This measurement would be from the top of the inverted cone to the highest point of the concrete. In addition, the sample should also be visually assessed to determine whether segregation is evident.

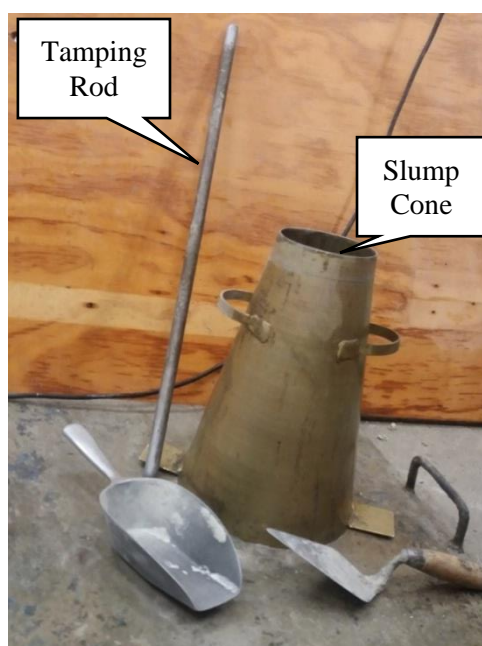


Figure 3-4. The equipment used to determine the slump of concrete.

3. 6. Setting Time

The EN 196-3 (2005b) provides a descriptive means of determining the setting time of pastes. For the research project, the setting time of concrete mixtures was completed using the same procedure as was developed for pastes. It is acknowledged that the test is intended for paste specimens; however, useful data can be obtained by isolating the mortar of a concrete mixture and determining the setting times.

The setting times (both initial and final) were conducted using a Vicat apparatus and the needles used for the setting time are depicted in Figure 3-5. When the water is added to the dry constituents, the time is recorded and this is referred to as zero time. The setting time is measured from this point as hydration is initiated. After the concrete had been mixed as described previously, mortar was obtained by sieving the concrete through a sieve with an aperture size of 4.75 mm. This is done to ensure that no stones are included in the sample and can therefore affect the results obtained by giving a false reading on the Vicat apparatus.

The initial time is recorded as the time at testing that the 1.1 mm diameter needle (Figure 3-5 d) measures a distance of 6 ± 3 mm from the base plate of the specimen. When initial set is reached, the specimen is twisted, using a shearing circular motion, and inverted. The shearing movement is done to create a smooth surface on which the final setting time can be determined. Final set is recorded as the time at which the outer ring of the setting needle (Figure 3-5 d) does not make a visible imprint on the specimen surface. Readings for both setting times were recorded at 10 minute intervals after significant resistance is observed.

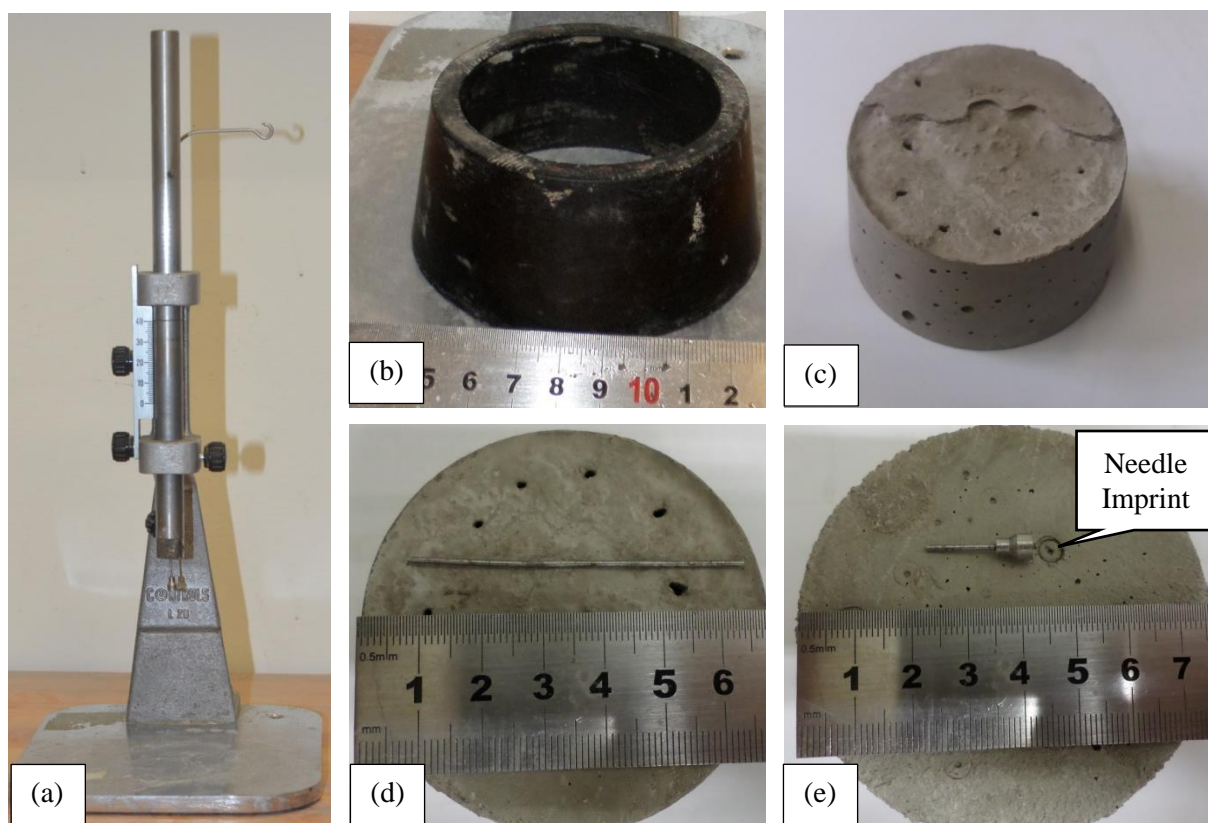


Figure 3-5. The setup used to determine the setting time of concrete: (a) The Vicat apparatus, (b) the specimen mould, (c) an example of a specimen, (d) the needle used to determine initial set and (e) the needle for final set.

3. 7. Bleeding

The test method used to determine the bleeding of the concrete specimens was done in accordance with ASTM Standards C232/C232M-09 (2010). The setup is shown in Figure 3-6. Two cylindrical moulds, made of PVC (Figure 3-6), were used with a diameter of 120 mm and height of 120 mm whereas ASTM C232/C232M-09 (2010) specifies dimensions of 250 mm and 285 mm diameter and internal height, respectively. As stated, the amount of bleed water that rises to the surface is a function of the specimen height/depth; therefore, to be able to use the bleed data in conjunction with the other test results, such as plastic settlement and shrinkage, the specimens were limited to a height of 100 mm of concrete. Once the concrete has been cast in the moulds, the initial mass is taken and the specimens are covered with a plate to minimise the amount of water that could potentially be lost due to evaporation.

In addition, the bleeding was done under two different climatic conditions. Two samples were subjected to conditions of 40 °C and humidity of 10 % and an additional two samples were placed in a climate controlled room at 23 °C and 60 % RH. The temperature was the main factor as the samples were sealed, thereby reducing the influence of the humidity.

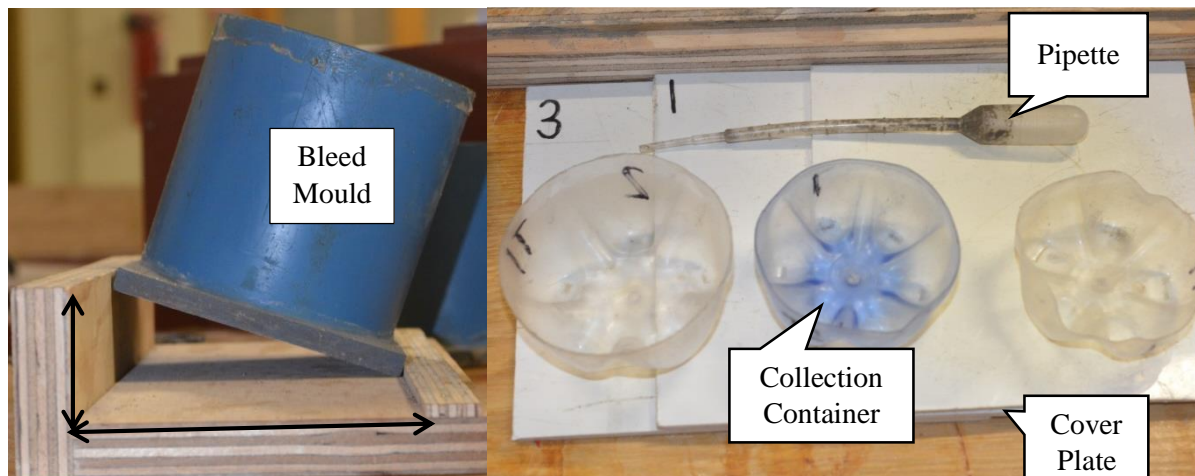


Figure 3-6. The setup used to determine the bleeding of concrete.

After casting, readings are taken at 10 minute intervals for the first 40 minutes. After which, reading are taken at 30 minute intervals until no physical bleed water accumulates at the surface at all. The general procedure includes weighing and recording the mass of the moulds and concrete at each time interval. Hereafter, the specimens are placed on a wooden pedestal, Figure 3-6, for two minutes to ensure that all water collects at a specific area and to facilitate easier collection of the water. The bleed water is extracted by means of a pipette and placed in a plastic container where after the respective masses are recorded. The mass of the container in which the bleed water is collected does however not yield the net mass of bleed water extracted, as some solid particles are also extracted in the process. To cater for the additional solids, the bleed water is transferred to a second plastic container. Care is taken to ensure that the majority of the solids remain in the first container and the mass is determined. The bleed water is hereafter calculated by taking into account the amount of solids present as well as evaporation and is plotted against the time of extraction.

3. 8. Plastic Shrinkage and Settlement

The plastic shrinkage and settlement of the concrete specimens were determined at levels of high evaporation i.e. more than 1 kg/m²/h. The climatic conditions, as mentioned before, were simulated in a climate control chamber, which was developed by (Combrinck, 2012). The climate chamber is designed to accommodate temperatures up to 50 °C, wind speeds of up to 70 km/h and a minimum relative humidity of 10 %. The full development of the climate chamber can be found in the document by Combrinck (2012). To achieve a high evaporation rate, the climatic conditions were set at 40 °C, 10 % RH and wind speeds of 22 km/h. With the use of the mentioned climatic conditions and Equation 2.15, the evaporation rate was determined to be 1.07 kg/m²/h.

Three samples were cast in 300 x 300 x 100 mm plastic moulds, see Figure 3-7 and Figure 3-8. The moulds have two anchors (Figure 3-9), placed on opposite ends, which are cast within the concrete. These anchors are free to move and therefore displace with the concrete as shrinkage takes place. On the external face of the anchors, a spring loaded LVDT is positioned to record the displacement. The shrinkage of the specimen is therefore equal to the sum of the recorded displacement of the two LVDTs. The recording is automated and a reading is taken at 1 second intervals. With this mentioned setup and geometry, it can be assumed that the shrinkage on the faces adjacent to the sides containing markers should be relatively equal.

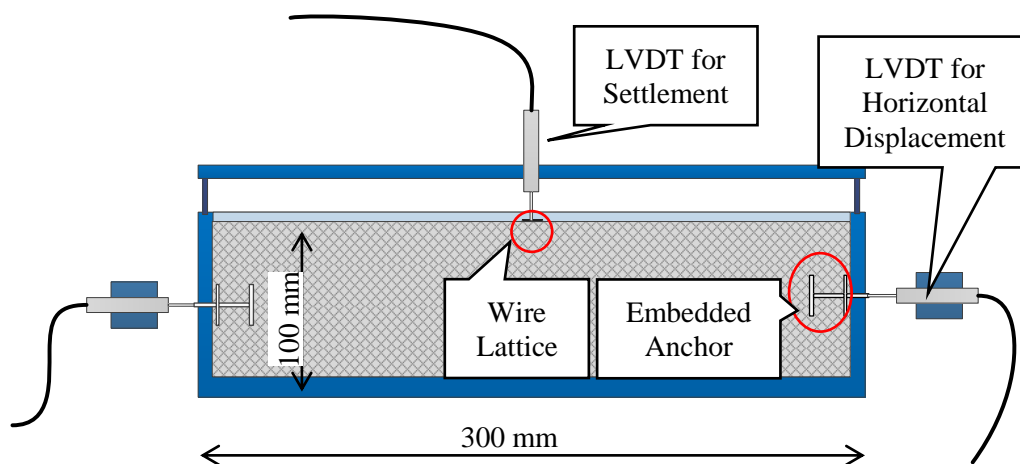


Figure 3-7. Schematic for the setup to determine the vertical and horizontal displacements.

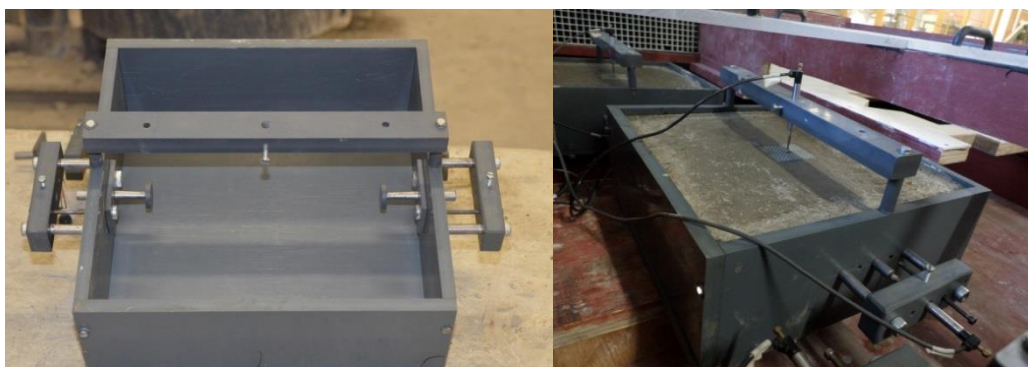


Figure 3-8. Experimental setup for the recording of the plastic settlement and shrinkage.

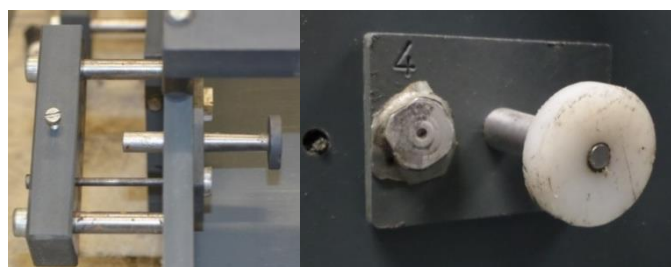


Figure 3-9. The anchors used to determine the horizontal displacement of the fresh concrete.

The anchors are lubricated with a light layer of grease. This is done to ensure that the effect of friction on the recording.

In addition, the vertical displacement (referred to as settlement) is also recorded for each specimen. In order to record the settlement, a 45 x 50 mm wide metallic wire lattice (see Figure 3-10) is attached to the tip of a LVDT. The lattice provides a means of determining the displacement without the tip of the LVDT penetrating the concrete in its plastic state. Therefore, it also aids the LVDT in staying afloat above the concrete surface.

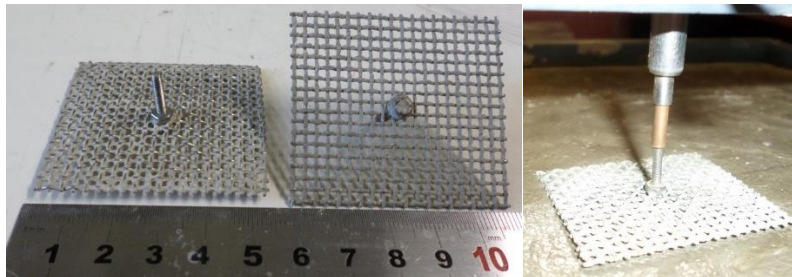


Figure 3-10. The wire lattice used in the recording of the vertical displacement of fresh concrete.

Capillary pressure of the concrete samples were also investigated. A test setup, similarly as those performed by Slowik et al. (2008). A 300 x 300 x 100 mm mould was used with a small aperture at a height of 35 mm was used to cast the concrete in. The aperture is used to insert a small metal tube filled with distilled water. The end of the tube is blocked with a piece of porous sponge; this is to prevent the blockage of the hollow tube with concrete particles, thus affecting the results obtained. The other end of the tube is connect to a small electronic pressure sensor and acts as transducer to record the pressure as it builds up within the concrete; this is shown in Figure 3-11. The pressure build-up is recorded against time until the air breaks through. At this point there is a loss of contact between the water and the sensor, signifying the air entry into the system. Note should be taken that because of this, the capillary pressure is seen as a local failure.

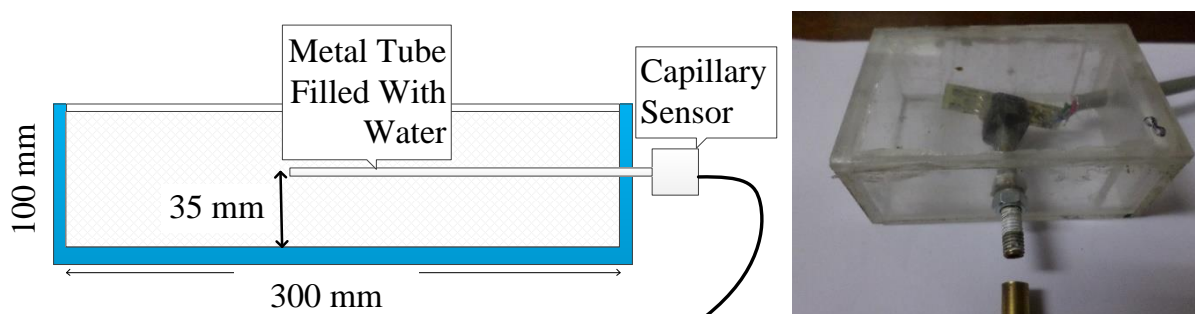


Figure 3-11. The setup (left) and pressure sensor (right) used to record the pressure build-up.

3. 9. Mechanical Properties

3. 9. 1. Compressive Strength

The compressive strength of the concrete were determined for both mortars and concrete cubes as well as cylinders. The mortars were used to assess the Activity Index of the SCMs and the concrete cubes were used to develop a model of strength development with time.

The compressive strength of concrete is dependent on both intrinsic and extrinsic factors. The intrinsic factors include: the aggregates used, the aggregate-paste interface, the hardened cement paste, the porosity of the specimen and the microstructure (Perrie, 2009). The extrinsic factors include: the direction of loading relative to the casting direction, size of the specimen, the moisture content, loading rate and the testing machine (Perrie, 2009). The specimens are loaded at a specified rate until failure; at the point the maximum force is recorded. The maximum force applied that causes failure is used to calculate the compressive strength of the specimen, i.e.:

$$\sigma_c = \frac{F}{A} \quad \text{Equation 3.1}$$

where,

σ_c is the compressive strength of the specimen in (MPa),

F is the force at failure (kN),

A is the surface area over which the force is applied (mm^2).

- Mortar Bars

Mortar specimens were cast in 40 x 40 x 160 mm steel moulds; each mould has the capacity to cast three specimens. The mix compositions are given in Table 3.2 and three different mixes were cast. A minimum of six mortars were cast for each slag and fly ash investigated to ensure that at least three specimens could be tested for at the a specified age. For the reference an additional three bars were cast due to the difference in testing ages for fly ash and slag based mortars. The mortar specimens were first broken into two pieces by means of a three point flexure test. The two resultant specimens were then tested under compression using a Zwick Z250 (Figure 3-12). The setup shows the platens used to allowed the transfer of the load as well as the steel 40 x40 x12 mm steel plates that ensure that the load is applied over an area of 40 x 40 mm. The specimens are then subjected to a compressive load, at a loading rate of 2400 N/s and perpendicular to the direction of casting, until failure occurs.

- Concrete Cubes

The concrete cubes had dimensions of 100 x 100 x 100 mm. The concrete mixes are given in Table 3.3 and gives the mass of each constituent per cubic meter of concrete. A water-to-binder ratio of 0.5 was selected for the mixes. All components of the mix remained constant; only the mass of the cement varied due to the replacement with a respective SCM. The fly ash samples were substituted at levels of 15, 25 and 35 wt. % on a mass basis. The amount of slag was replaced at levels of 25, 50 and 75 wt. %.

A total of 20 specimens were casted for testing. This would result in 4 cubes being tested on 3, 7, 28, 56 and 91 days. The choice of selecting 4 cubes over 3 cubes was selected as a precautionary measure in the event that a cube may get damaged during the de-moulding process. In addition, the additional cube catered for the event that a result is statistically not valid.

The mass and dimensions of the concrete cubes were taken prior to testing. The recordings were done under surface saturated conditions. The test was done in accordance with BS EN 12390-3 (2002). The specimens were tested in a Contest (Figure 3-13) compression-testing machine, at a loading rate of 180 kN/min until failure is reached. The loading is applied in a direction perpendicular to the casting direction. The strength of the sample is calculated as per Equation 3.1.

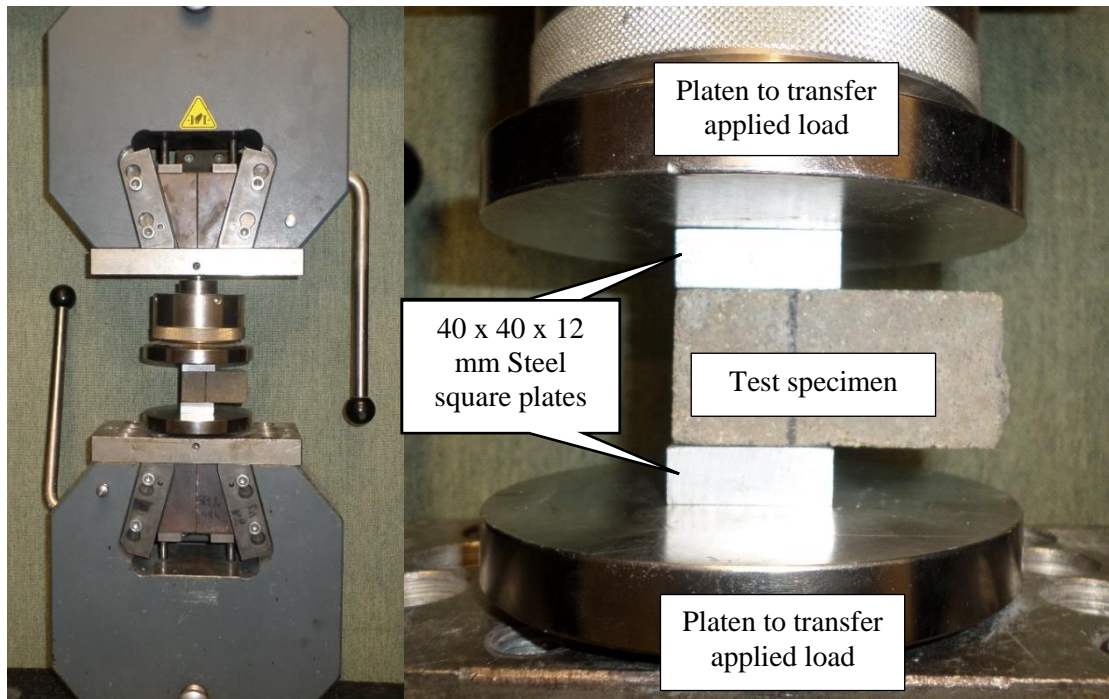


Figure 3-12. Compression testing setup of mortar specimens.



Figure 3-13. The setup to determine the compressive strength of concrete cube specimens.

3. 9. 2. Indirect Tensile Strength

The indirect tensile strength of the concrete specimens was tested at 7, 28 and 56 days after casting. Four cube specimens, 100 x 100 x 100 mm, were cast for each day of testing. The same mixing composition (

Table 3.3. provides the mix composition used in the experimental programme. Mix 1 is used for concrete samples used in the compressive and tensile tests. Mix 2 is used for concrete specimens used in the remaining tests. The only difference between the mixes is the amount and type of sand used. This occurs due to the difference in densities. Ultimately, the theoretical yields also differ, with the yield of Mix 1 and Mix 2 being 2388 and 2385 kg/m³, respectively.

Table 3.3) was used as for the compressive concrete specimens, in order to be able to establish the correlation that exists between the tensile strength and compressive capacity of a given concrete mix.

The test setup for determining the tensile strength capacity of concrete specimens is shown in Figure 3-14. The test procedure is done according to the specifications of the BS EN 12390-6 (2003). For the test, a concrete cube is subjected to a compressive load, along two diametrically opposed lines. The load is chosen to be applied perpendicular to the casting direction, hereby ensuring that the line load is applied on a flat surface until failure. In addition, a strip of packing board is used to transmit the load between the jig and the specimen to ensure that the load is spread evenly over the designated lines of the specimen and to reduce stress concentrations that may occur at the extremities (Domone & Illston, 2010).



Figure 3-14. Test setup for determining the tensile splitting capacity of concrete specimens.

Equation 3.2 is used to determine the tensile capacity of the concrete specimens using the maximum load applied to cause failure.

$$\sigma_T = \frac{2F}{\pi Ld}$$

Equation 3.2

where,

σ_T is the tensile strength of the specimen in (MPa),

F is the force at failure (N),

L is the line of contact between the packing board and the specimen (mm),

d is the designated cross-sectional length (mm).

3.9.3. Flexural Strength

The flexural strength of selected concrete mixes were also determined as it also provides a means of determining the tensile capacity of concrete specimens. For the named method, a concrete beam is subjected to loading by either applying a single point load or two point loads.

Figure 3-15 shows the setup used in the study to determine the flexural strength of the concrete mixes. Sets consisting of three beams (each having dimensions of 100 x 100 x 500 mm) per mix were cast and tested, according to BS EN 12390-5 (2009b), at 28 days after casting. The setup has two roller supports at the bottom spaced at 100 mm from the edges, with a 300 mm centre-to-centre spacing in between. The upper supports are used to apply the load, at a rate of 1700 N/s with 100 mm spacing between the upper loading rollers. The specimens are loaded perpendicular to the direction of casting.

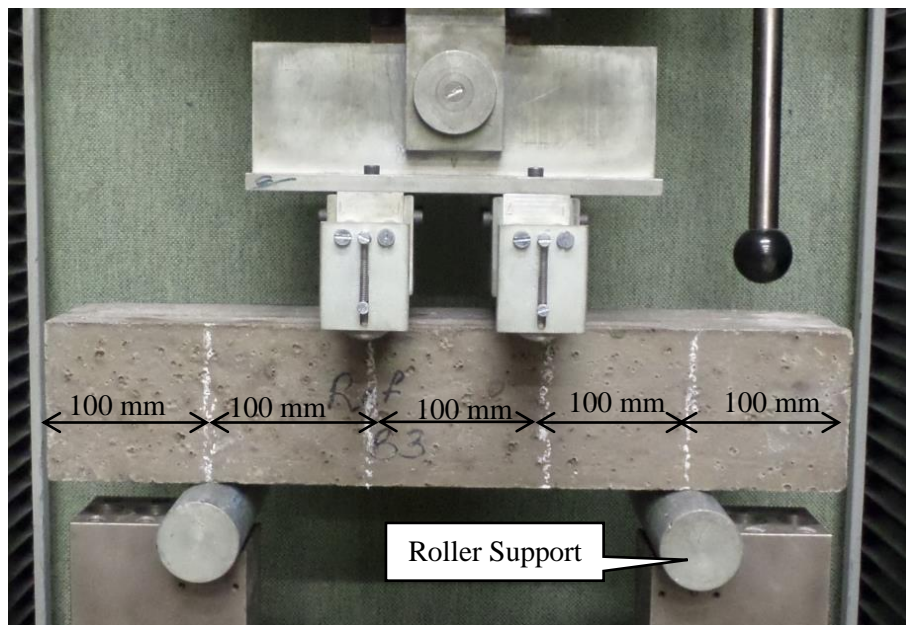


Figure 3-15. Experimental setup of the four point bending test in determining the modulus of rupture.

The specimens are loaded perpendicular to the casting face until failure occurs. This happens when a crack is formed in the region situated between the two upper supports that apply the load; the result for any crack forming in a region between the upper support and the edge of the beam is disregarded. The maximum load (P) at failure is recorded and the flexural strength is calculated by using Equation 3.3.

$$\sigma_F = \frac{Pl}{d_1 d_2}$$

Equation 3.3

where,

σ_F is the flexural strength of the specimen in (MPa),

P is the force at failure (N),

l is the distance between the two lower supports and should be equal to $3d_1$ (mm),

d_1 is the width of the beam (mm),

d_2 is the height of the beam (mm).

3.9.4. Secant Modulus

The elastic modulus of concrete gives an indication on the stiffness of the concrete and the data in turn can be used for correlation with the effect of dryings shrinkage and creep. The elastic modulus is determined according to BS EN 12390-13 (2013). The principle of the test is to load a specimen under compression, to a limited load that does not exceed the capacity of the sample and recording the associated strain. A plot is generated and the slope of the stress strain curve is calculated to be the elastic modulus of the specimen.

Three cylindrical specimens were cast per mix, with specimen dimensions of 100 mm diameter and a height of 200 mm (aspect ratio = 2). The cylindrical specimens are favoured over cube specimens due to the slenderness of the specimen. In addition, four cubes are cast to determine the strength of the concrete samples and the limited loading required to ensure that the code specifications are not exceeded. The compressive strength obtained from the cube crushing is multiplied by a factor of 0.8 to take into account that cylindrical specimens will yield at a lower compressive strength compared to cylindrical specimens. The reduction in compressive strength is a result of the difference in aspect ratios, 2 versus 1 for cylinders and cubes, respectively.

For sample preparation, the specimens are ground flat by removing approximately 1 mm of the cast end to ensure a flush surface is available for the test when the load is applied. Moreover, two circumferences are drawn across the specimen to mark the position of the frame (Figure 3-16) and ensure that the reference gauge length of 70 mm is obtained. Three load varying displacement transducers (LVDTs) are placed, at equidistant intervals of 120° , around the test specimen (Figure 3-16). Three LVDTs are used to ensure a reliable average can be calculated and be a good representative of the deformation occurring.

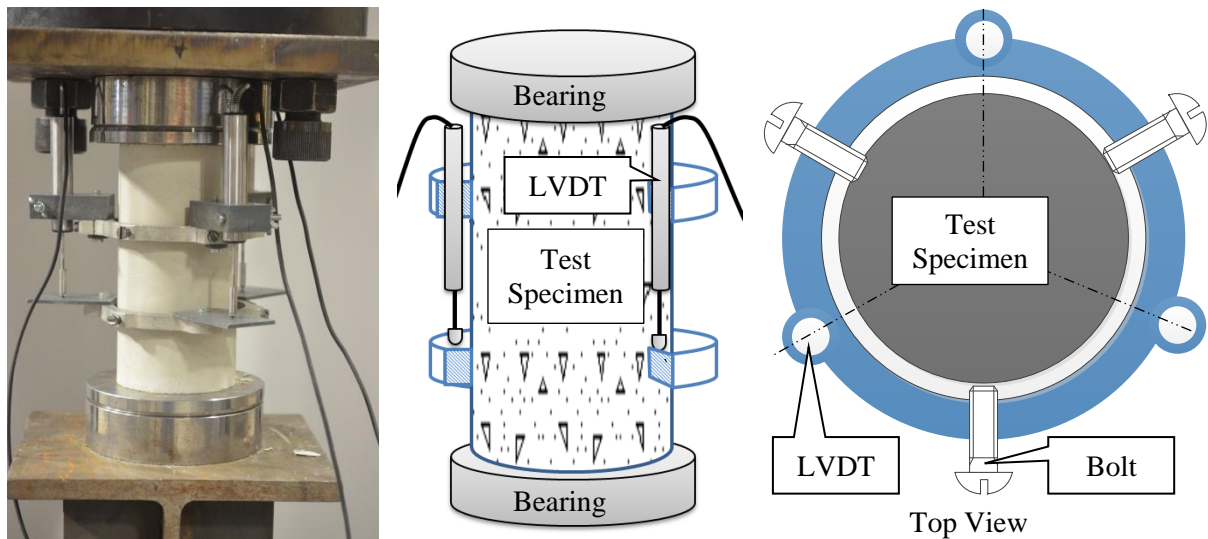


Figure 3-16. Test setup to determine the elastic modulus of concrete samples.

Once in place, a preload, equivalent to 0.5 MPa, is applied to the sample using an Instron materials testing machine, which has a capacity of 2 MN, and is maintained for a period less than 20 seconds. Hereafter, three loading cycles are applied, as shown in Figure 3-17, while ensuring that a minimum stress is still maintained. The preload (σ_p) is set to be equal to the lesser of 0.5 MPa and σ_b , where σ_b is in the range of 10 – 15 % of the maximum compressive strength. The maximum stress applied is equal to a third of the compressive stress i.e. σ_a in Figure 3-17 and is maintained at a maximum of 20 seconds. The loading rate for all samples is kept at an equivalent of 0.6 MPa. The loading cycle is graphically shown by Figure 3-17.

The elastic modulus of the specimen is then calculated as follows:

$$E = \frac{\Delta\sigma}{\Delta\varepsilon_s} = \frac{\sigma_a^m - \sigma_p^m}{\varepsilon_{a,3} - \varepsilon_{p,2}} \quad \text{Equation 3.4}$$

where,

σ_p is the stress on the specimen when the preload is applied (MPa),

σ_a is the stress on the specimen when the upper load is applied (MPa),

$\varepsilon_{a,3}$ is the strain recorded at the upper stress level on the third loading cycle (mm/mm) and

$\varepsilon_{p,2}$ is the strain recorded at the preload level the second loading cycle (mm/mm).

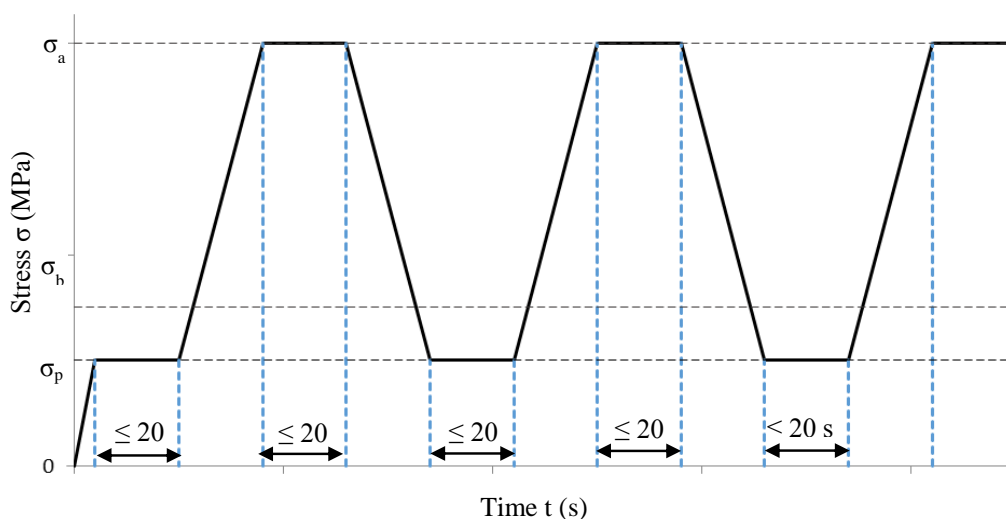


Figure 3-17. Stress cycle imposed on concrete sample to determine the secant modulus of elasticity according to EN 12390-13:2013.

3. 10. Microstructure

The microstructure of concrete is typically measured by means of Mercury Intrusion Porosimetry (MIP). However, work done by du Plessis et al. (2014) have found that the data achieved from simple and fast X-ray computed tomography scans can be more economical and less time consuming. Therefore, X-ray CT scans were used to evaluate the microstructure of concrete for this study. The CT scans were performed using a General Electric Phoenix V|Tome|X L240 scanner.

Initially, cylinders (100 mm diameter and 200 mm height) were cast for the tests. However, due to the samples being too large to obtain relative data, cores of 70 mm diameter and 100 mm heights, were drilled from standard 100 x 100 x 100 mm cubes. Cylinders are chosen over cubes due to the optimal geometry. The effect of beam hardening is minimized due to the own axis rotation of the cylindrical specimens and the resulting equal X-ray penetration (du Plessis et al., 2014).

Scans were taken under the following conditions: resolution of 80 μm , 160 kV, 220 μA at 500 ms per image for 2400 images. A 0.5 mm copper and 0.5 mm filter was used to minimize the beam hardening. Data is reconstructed using Datos-reconstruction software. The analysis was done using VGStudioMax 2.2 commercial 3D analysis software package, using the defect module. Figure 3-18 displays a typical output of the voids present in a sample, as well as the colour coding.

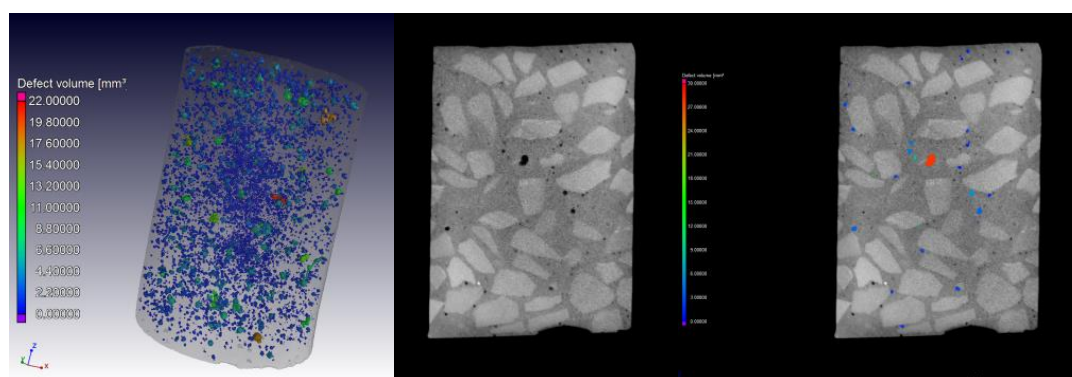


Figure 3-18. Typically results of an X-ray CT-scan.

3. 11. Drying Shrinkage

When concrete is exposed to the atmosphere, water escapes the concrete and a change in volume is experienced. The volumetric change causes a corresponding development in strain which in turn is correlated to the development of stresses. Therefore, in the extreme event of significant strain development the concrete can undergo a series of cracking, especially in cases where the concrete elements are constrained, which is related to bad aesthetics and may lead to issues concerning with the durability of the structural element.

The drying shrinkage of the concrete mixes was determined using three beams per mix; with the beam dimensions of 100 x 100 x 500 mm. The procedure as stipulated by BS ISO 1920-8 (2009c) was followed to investigate the drying shrinkage. 24 Hours after casting, the beams were de-moulded and cured in water for a period of 7 days, after which, the beams were removed and two metal *targets* (Figure 3-19 d) are glued to the smooth surfaces at a known gauge length of 100 mm. In addition, the mass of the beam and the length are also measured. The length measured between the gauges is done using a digital micrometer (Figure 3-19 b). Measurements were done at 3, 7, 14, 28, 56, 91 and 133 days after wet curing. The beams were subjected to standard laboratory conditions of 23 °C and RH of 60 % during the execution of the experiment.



Figure 3-19. The instruments used to determine the drying shrinkage of the concrete mixes. (a) All equipment used. (b) The electronic micrometer. (c) The spacer and reference. (d) The metal targets.

The strain is calculated as:

$$\varepsilon = \frac{L_o - L_t}{L_{\text{gauge}}} \quad \text{Equation 3.5}$$

where,

ε is the strain at the time of interest (mm/mm),

L_o is the length recorded at the start of the experiment (mm),

L_t is the length recorded at the time of interest (mm),

L_{gauge} is the length recorded between the datum studs i.e. 100 mm.

3. 12. Durability

The durability of concrete is typically associated with the ingress of deleterious substances. The South African durability tests were used in this study to assess the influence of SCMs when used in a concrete mixture, in accordance with the Durability Index Testing Manual (Alexander et al., 2009). The permeability was determined by means of the OPI (Oxygen permeability test), the water absorption via the sorptivity test and diffusion via the chloride conductivity test.

3. 12. 1. Sample Preparation

For the durability test specimens are cast into standard 100 x 100 x 100 mm cubes. After which, the samples are cured for 21 days and then prepared as specified by Concrete Durability Index Testing Part 1 (Alexander et al., 2009). Cylindrical cores are drilled from four cubes, per mix, perpendicular to the casting direction (Figure 3-20). The cored samples are then cut using an appropriate tool, i.e. a diamond tipped, water cooled blade. The first 5 mm from each side of the core is discarded and outer portion of the core is marked to represent the test face of the specimen. After which, a 30 mm (± 2 mm) is cut from each side of the core specimen, with the mid-section being discarded. The removal of the outer 5 mm is to ensure that the homogenous concrete sample is obtained as during casting the outer edges of the concrete cubes consists mainly of a paste as an effect of the wall effect (Figure 2-6 a). The adjacent 30 mm from each section is also chosen as to represent the first portion of the concrete where materials may enter and migrate through i.e. the covercrete. The 30 mm section can also represent the protective layer of cover to the rebar. After the samples are cut, they are placed in an oven, set at 50 °C, for 7 days. This is to ensure that the samples are free of moisture, throughout, before commencing the testing.

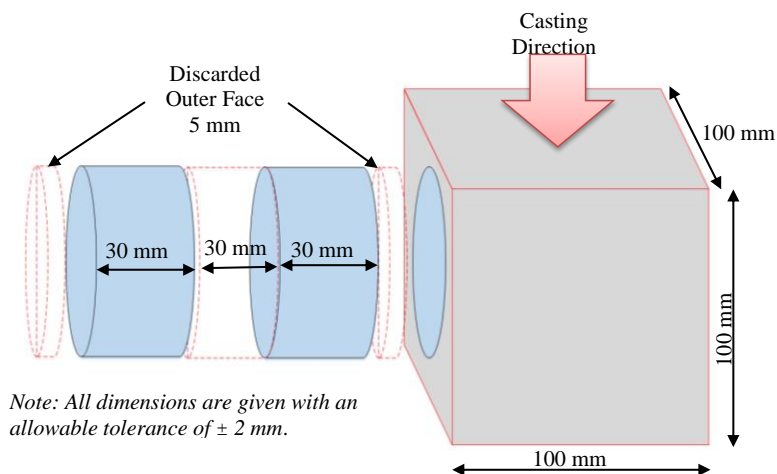


Figure 3-20. Obtaining of core samples for durability testing.

3. 12. 2. Permeability

Permeation is defined as the overall potential movement of moisture, ions and gases through a medium when subjected to a pressure head (Basheer & Barbhuiya, 2010). The ease of permeation is described as the permeability of a given medium. The oxygen permeability test uses the principle of permeation to assess the permeation property of concrete.

During the test procedure, the rate of oxygen decay through a concrete core sample is measured as a falling head permeameter is established. A specimen is loaded in an airtight vessel and the pressure loss of the vessel is recorded with time. The pressure loss is as a result of the oxygen gas contained, diffusing through the concrete specimen and dispersing out of a perforated plate. A schematic representation is shown in Figure 3-21. Hereafter, the flow of the gas through the concrete sample is modelled using Darcy's Law. A Darcy's coefficient of the sample's permeability is calculated and in turn converted into an index, the OPI, by calculating the negative log of the coefficient.

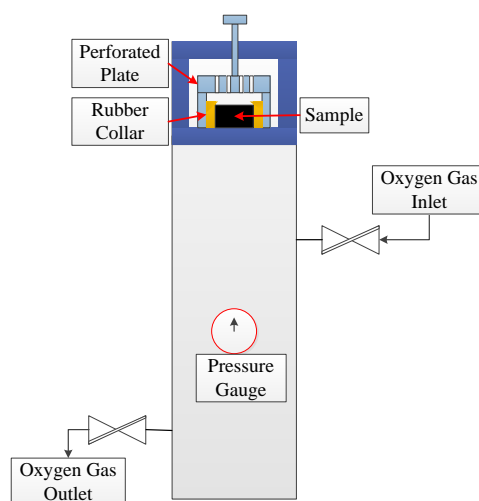


Figure 3-21. A schematic for determining the permeability of a concrete specimen.

The 4 cored concrete specimens, per mix, are removed from the oven 2 to 4 hours prior to commencing the test. The specimens are placed in a desiccator with silica gel to ensure the specimens absorb no moisture. The dimensions (thickness and diameter) are recorded as well as the oven dried mass. Hereafter, the specimens are loaded into a rubber collar (Figure 3-22); ensuring that the test face is exposed toward the inner part of the vessel and the inner face subjected to the perforated plate. This is done to ensure the simulation of gasses permeating through the concrete i.e. form the outer face inward.

Once the specimen have been loaded, the inlet and outlets are opened to purge the chambers of any gases. The purging process continues for 5 seconds where after the outlet is closed and pressure is allowed to build up to approximately 120 kPa. The following step requires relieving pressure in the chamber until a pressure reading of approximately 105 kPa (± 5 kPa) is achieved. Hereafter, the pressure differential of the chamber is digitally recorded. However, only the data recorded from the first 6 hours since the test commences or when the pressure drops below 50 kPa, is used in the analysis; depending on which condition occurs first.

With the collected data, a line of best fit via linear regression of the natural log of the original pressure (P_0) over the pressure at a given instance in time (P_t), is plotted against time (t). This is done by forcing the regression through the origin of the Cartesian plane. The slope (z) of the regression line is determined by:

$$z = \frac{\sum \ln\left(\frac{P_0}{P_t}\right)^2}{\sum \ln\left(\frac{P_0}{P_t}\right)t} \quad \text{Equation 3.6}$$

where,

z is the slope of linear regression through the point (0, 0),

P_0 is the initial pressure recording at the start of the test (kPa),

P_t is the pressure recording at a given time (kPa) and

t is the time recorded from the start of the test (s).

The value obtained for the slope is in turn used in Equation 3.7 to determine the coefficient of the permeability (k), namely:

$$k = \frac{\omega V g d z}{R A \theta} \quad \text{Equation 3.7}$$

where,

k is the coefficient of permeability (m/s),

ω is the molecular mass of oxygen gas i.e. 32 g/mol,

V is the volume of oxygen under pressure in the oxygen chamber (l),

g is the gravitational acceleration constant i.e. 9.81 m/s²,

d is the average specimen thickness (mm),

z is the slope of linear regression (See Equation 3.7),

R is the universal gas constant i.e. 8.313 Nm/K mol,

A is the specimen cross sectional area (m²) and

θ is the absolute temperature (K).

The oxygen permeability index (OPI) is hereafter calculated as the negative log of the average permeability constants i.e.

$$\text{OPI} = \log_{10} \frac{1}{n} \left(\sum_1^n k \right) \quad \text{Equation 3.8}$$

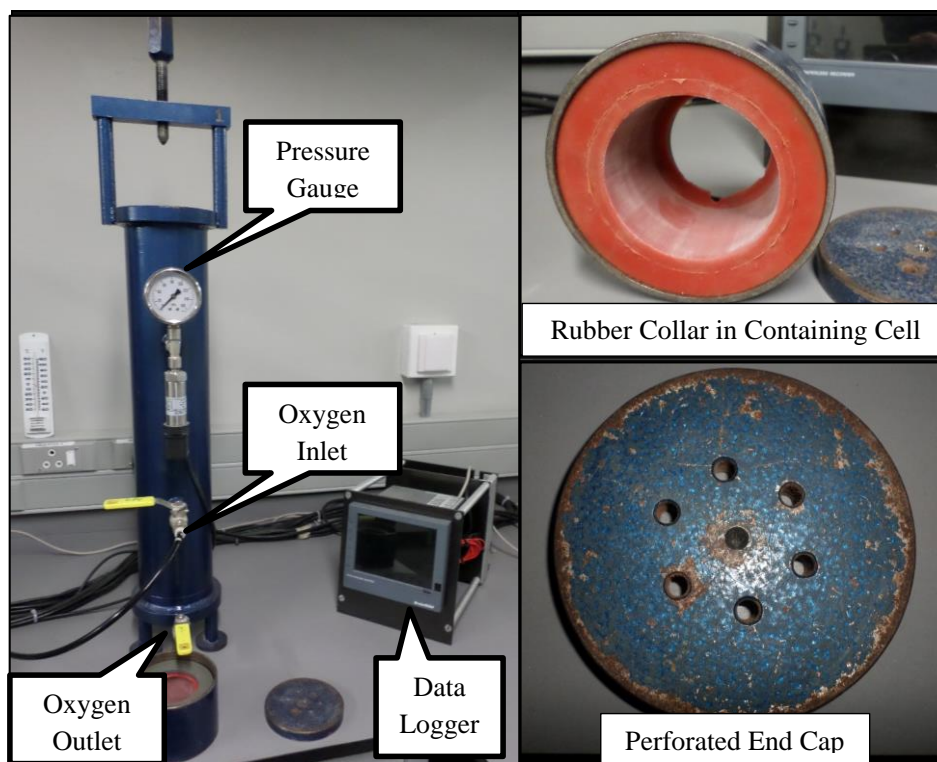


Figure 3-22. The OPI setup used in assessing the permeability of concrete specimens.

3. 12. 3. Sorptivity

Absorption occurs as a process of water being drawn up by a substance by capillary action. Therefore, the process is affected by the saturation level of concrete. In addition, the pore geometry also affects the level of adsorption that takes place. Narrower pores tend to suck up more water as a result of capillary action.

The sorptivity of the concrete specimens can be tested by using the samples used in the OPI determination. After the completion of the OPI testing, the samples are removed and the vertical edges are sealed using packing tape (Figure 3-23). This process is done in order to ensure that no liquid enters the specimen around the edges; the solution should only penetrate the specimens on the flat cross sectional area of the test face i.e. unidirectional flow. Here after, the mass of the specimen is recorded as the dry mass (M_{s0}).



Figure 3-23. Sealing of the vertical edges of a specimen using packing tape.

A layer consisting of ten pieces of paper towels are stacked on a plastic tray and a saturated solution of calcium hydroxide is added to the tray (Figure 3-24). The saturated solution of calcium hydroxide is prepared by mixing 5 g of $\text{Ca}(\text{OH})_2$ per one litre of tap water to give a 0.0674 M solution. The layer of paper towels is hereafter smoothed out to remove any trapped water bubbles.

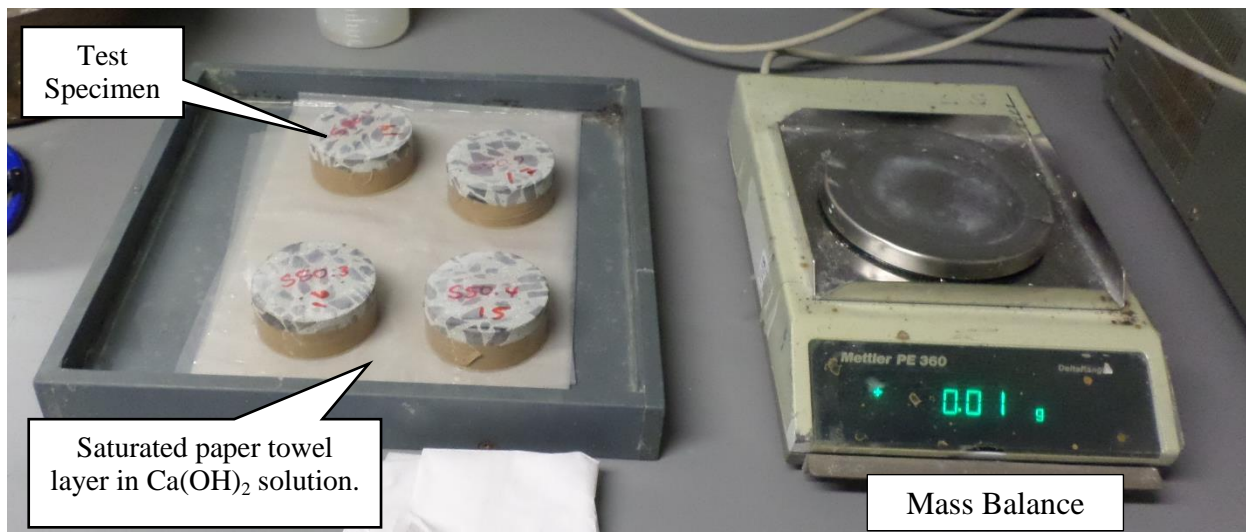


Figure 3-24. The testing procedure of concrete specimens for the water sorptivity index.

The test specimens are placed on the saturated paper towels and a stop watch is started. The specimens are then removed at intervals of 3, 5, 7, 9, 12, 16, 20 and 25 minutes. At each time of removal, the specimen is patted dry, ensuring surface saturation is maintained, and the mass recorded and the specimen is replaced back onto the tray. Care has to be taken to ensure that no water is spilled or dropped onto the other specimen faces exposed to the atmosphere. Once the last reading is completed, the specimens are placed in a vacuum chamber (Figure 3-25), that is maintained at a pressure of -80 kPa once all specimens are sealed in. After a period of three hours the tank is isolated and $\text{Ca}(\text{OH})_2$ saturated solution is allowed to enter the chamber, ensuring that all specimens are covered. The vacuum pressure of -80 kPa is re-established and the specimens are allowed to soak under the mentioned pressure for an additional hour. This process of vacuum saturation is undertaken to ensure that all voids and pores in the specimens are filled with the $\text{Ca}(\text{OH})_2$ saturated solution. After an hour, air is allowed to enter the system and the specimens are soaked for an additional 18 hours before recording the saturated mass (M_{sv}).

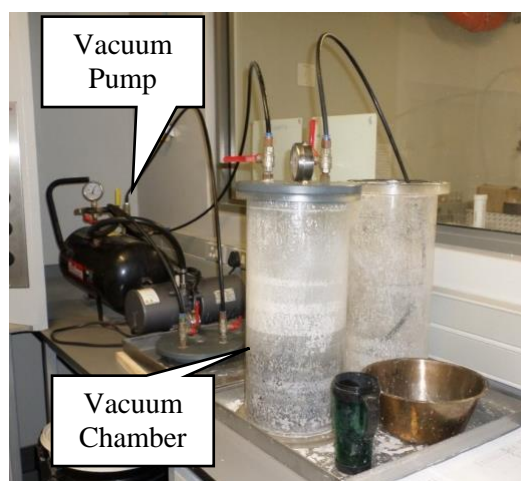


Figure 3-25. Vacuum facility for saturation procedure.

Once all recording are done the porosity of the specimen can be determined. The porosity is calculated as the mass difference (of the dry and saturated specimens) as a percentage of the equivalent volume of water solution:

$$n = \frac{M_{sv} - M_{s0}}{Adp_w} \times 100 \quad \text{Equation 3.9}$$

where,

n is the porosity (%),

M_{sv} is the saturated mass (g),

M_{s0} is the oven dried mass (g),

A is the average cross sectional area (mm^2),

d is the average specimen thickness (mm) and

p_w is the density of water i.e. 0.001 g/mm^3 .

Using the data recorded, a plot of mass gain against the square root of time is generated. This plot is used to obtain the slope (F) via a linear regression analysis. Once the slope is obtained, the sorptivity is calculated as:

$$S = \frac{Fd}{M_{sv} - M_{s0}} \quad \text{Equation 3.10}$$

where,

S is the sorptivity ($\text{mm/hr}^{0.5}$),

F is the slope of the mass gain plotted against the square root of time ($\text{g/hr}^{0.5}$),

d is the average specimen thickness (mm)

M_{sv} is the saturated mass (g) and

M_{s0} is the oven dried mass (g).

3. 12. 4. Chloride Conductivity

The diffusion property of concrete specimens is assessed using the chloride conductivity test. Diffusion is the process of materials moving from a region of a high to a low concentration, thus the process of diffusion can be lengthy. Also, it is affected by saturation levels and temperature. The chloride conductivity test measure the resistance of concrete by assessing the migration of chloride ions through the specimen.

For the chloride conductivity test, specimens are tested under saturated conditions and exposed to a salt solution on both sides; one cell contains a cathode and one an anode (see Figure 3-26). When the power supply is switched on, a potential is generated and anions (of chloride) start moving from the cathode cell to the anode cell. The potential difference is measured and the resistance of the concrete sample is tested.

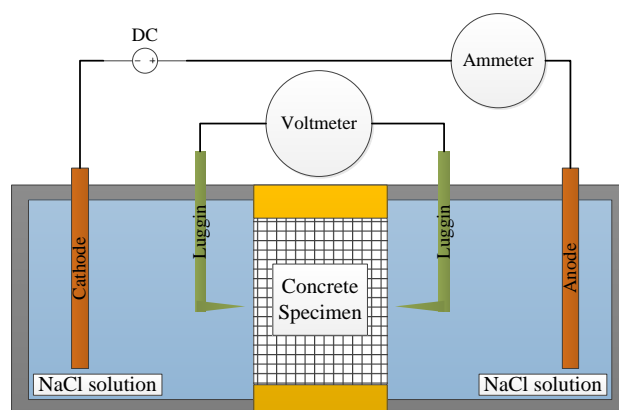


Figure 3-26. A schematic of the chloride conductivity test.

The specimens are vacuum saturated, in a similar process to the one mentioned in the previous section, after being oven dried for seven days. The same setup (Figure 3-25) is also used to achieve saturation. The only difference is that 5 M sodium chloride solution is used. The sodium solution is made by dissolving 2.93 kg of NaCl in 10 litres of water and stirring occasionally to ensure full dissolution.

After the saturation process, the specimens are inserted into a conductivity cell (Figure 3-27) where an electric current is applied. Firstly, both the anode and cathode cells are filled with the NaCl solution (5 M). Hereafter, the luggins, which are used to measure the potential difference across the specimen, are filled with the solution as well. Any air that is trapped in the system is removed from the system at this point by gently tapping the cell. After the air is removed, the electrical connections are attached and the cell is placed in a horizontal position.

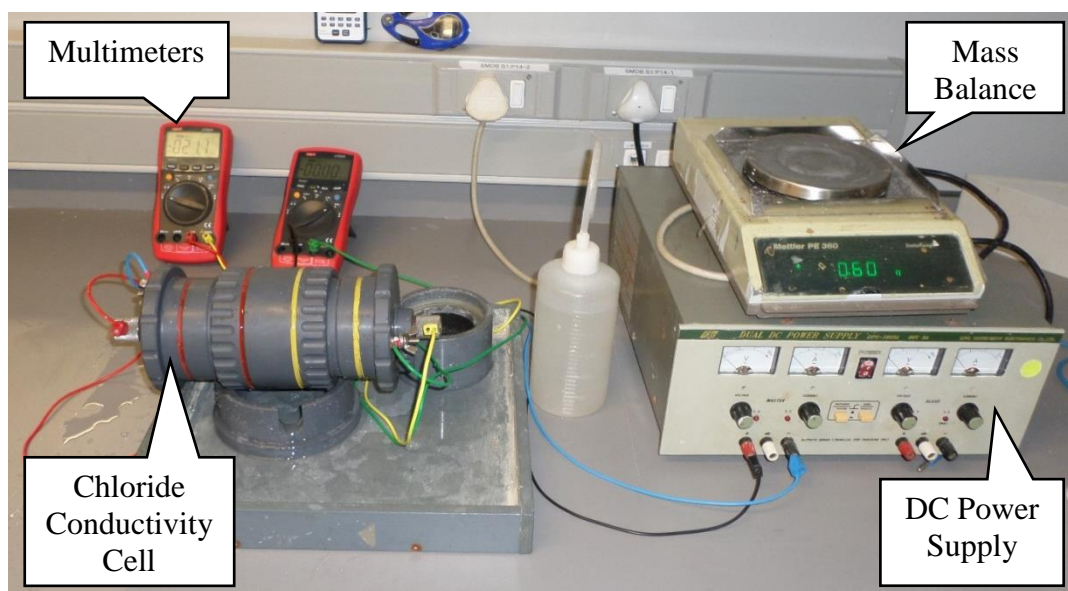


Figure 3-27. The test setup to determine the chloride conductivity of a concrete specimen.

A power supply is switched on and the voltage across the specimen is monitored and adjusted until a potential difference of approximately 10 V is applied across the specimen. Once the required voltage is obtained, the recorded voltage and associated current is recorded. The chloride resistance is determined, using as follows:

$$\sigma = \frac{id}{VA} \quad \text{Equation 3.11}$$

where,

σ is the chloride conductivity (mS/cm),

i is the electric current (mA),

d is the average specimen thickness (cm),

V is the voltage measure across the specimen (V) and

A is the average cross sectional area (cm²).

3. 12. 5. Durability Indices

The durability values obtained from testing using the aforementioned methods will be used in conjunction with Table 3.7 to evaluate the performance of the concrete.

Table 3.7. Classification of the durability of concrete in term of durability performance (Alexander et al., 2010).

Durability Class	OPI (Log Scale)	Sorptivity (mm/h ^{0.5})	Conductivity (mS/cm)
Excellent	> 10.0	< 6	< 0.75
Good	9.5 – 10.0	6 – 10	0.75 – 1.50
Poor	9.0 – 9.5	10 – 15	1.50 – 2.50
Very Poor	< 9.0	> 15	> 2.50

3. 13. Concluding Summary

This chapter discussed the various tests used to investigate and achieve the goals of the current research. The tests include investigations of fresh and hardened concrete incorporating SCMs. Table 3.8 provides a summation of the tests done with the standards/methods followed to complete the tests. The next chapters are set out to explain the results obtained from the current investigation.

Table 3.8. Schedule of tests and mixes completed.

Test	Standard/Reference	PC			Slag GGCS			GGBS			Fly Ash UA			SA			DP			PF		
		0	25	50	75	25	50	75	15	25	35	15	25	35	15	25	35	15	25	35		
SAI	BS EN 450-2:2012	X										X			X			X			X	
	BS EN 15167-1:2006	X		X			X															
Workability	BS EN 12350-2:2009	X	X	X	X	X	X	X	X	X	X	X	X	X	X	X	X	X	X	X	X	
Setting Time	BS EN 196-3:2005	X	X	X		X	X		X	X		X			X	X			X	X		
Bleeding	ASTM C232-09	X	X	X		X	X		X	X		X	X		X	X			X	X		
Plastic Settlement		X	X	X		X	X		X	X		X	X		X	X			X	X		
Plastic Shrinkage		X	X	X		X	X		X	X		X	X	X	X	X			X	X		
Capillary Pressure	Slowik <i>et al.</i> (2008)	X	X	X		X	X		X	X		X			X				X			
Compressive	BS EN 12350-3:2002	X	X	X	X	X	X	X	X	X	X	X	X	X	X	X	X	X	X	X	X	
Indirect Tensile Strength	BS EN 12350-6:2003	X	X	X	X	X	X	X	X	X	X	X	X	X								
Flexural Strength	BS EN 12350-5:2009	X		X		X			X			X							X			
Secant Modulus	BS EN 12350-	X		X		X			X			X							X	X		
Drying Shrinkage	BS ISO 1920-8:2009	X	X	X		X	X		X	X		X	X		X	X			X	X		
Permeability	Durability Testing	X	X	X		X	X		X	X		X	X		X	X			X	X		
Sorptivity	Manual: Alexander <i>et al.</i> (2009)	X	X	X		X	X		X	X		X	X									
Chloride Resistance	<i>al.</i> (2009)	X	X	X		X	X		X	X		X	X		X	X			X	X		

Chapter 4

Results and Discussion

Slag

South Africa has two types of slag available for use in concrete: Ground Granulated Blastfurnace Slag (GGBS) and Ground Granulated Corex Slag (GGCS). The GGCS originates from the Saldanah Steel Plant in the Western Cape, whereas the GGBS is obtained from the Vanderbijlpark, Gauteng. The difference, although minimal in terms of composition, exists as a result of the derivation process and affect the impact these slags have in a concrete system. For the given study, these two materials were investigated to establish the performance of the two materials when used in concrete. The performance of these two types of slag are discussed in this chapter.

4. 1. Physical Properties

The morphological characteristics, fineness and particle size distribution was recorded and presented in Table 4.1. The particle size distributions of the slag and cement samples fall in a similar size range and the graphical representation produce a near-overlap for particle diameters below 10 μm (Figure 4-1). Moreover, Figure 4-1 displays the volume frequency percent plotted against the particle diameter on a log scale and corroborates the data presented in Table 4.1. In addition, Figure 4-1 shows that all three materials display a lognormal distribution with a negative skewness.

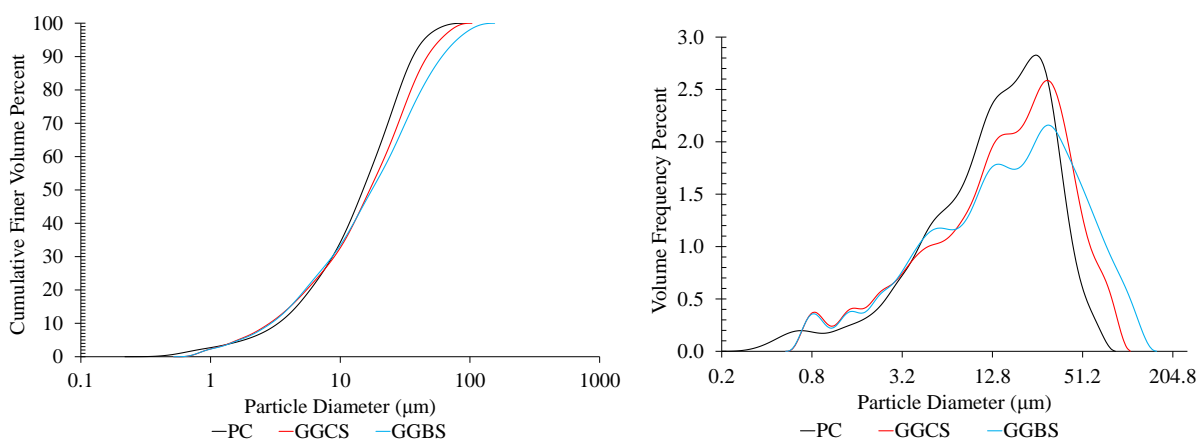


Figure 4-1. The PSD results (left) and the volume distribution (right) of the PC, GGCS and GGBS.

The cement has a maximum particle size of 87 μm . This is also the smallest maximum particle size relative to the two slags. The smaller maximum particle is suggested to be as a result of the cement type

(CEM I 52.5 N) as the cement strength is a function of particle size. The ground granulated blast furnace slag (GGBS), recorded bigger particle sizes compared to those of the ground granulated Corex slag (GGCS) and the cement, for instance, the maximum size recorded for the GGBS was 146 μm compared to the 97 and 87 μm for the GGCS and cement, respectively. As a result of the larger particles, the GGBS also yields a wider span of 3.3 compared to that of the GGCS (2.6) and PC (2.2).

Table 4.1. The physical properties of the cement and slag.

Material	Particle Sizes				Span $(\frac{d_{90} - d_{10}}{d_{50}})$
	Maximum μm	Median (d_{50}) μm	90% (d_{90}) μm	10% (d_{10}) μm	
PC	87	14.5	35.1	3.2	2.2
GGCS	97	16.8	46.6	2.8	2.6
GGBS	146	17.5	60.8	2.9	3.3

Figures 4-2 and 4-3 gives a display of the particle range for the cement, GGCS and GGBS, respectively. As can be seen, all of the materials display similar morphological characteristics as described in literature. The cement and slag particles both exhibit angular characteristics. The effect of the particle morphology will later be discussed on how it may have an impact on the results observed.

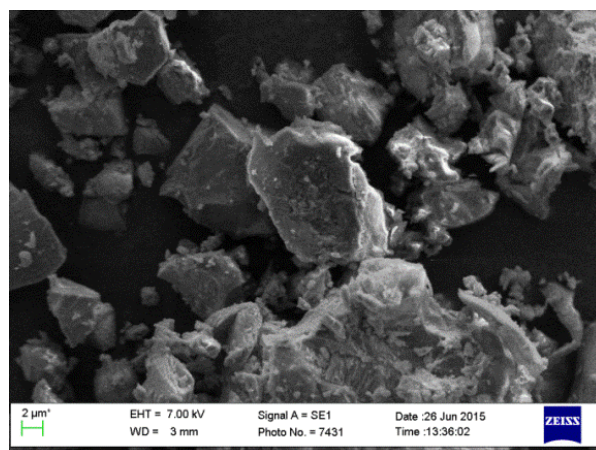


Figure 4-2. SEM image of the cement particle distribution and morphology.

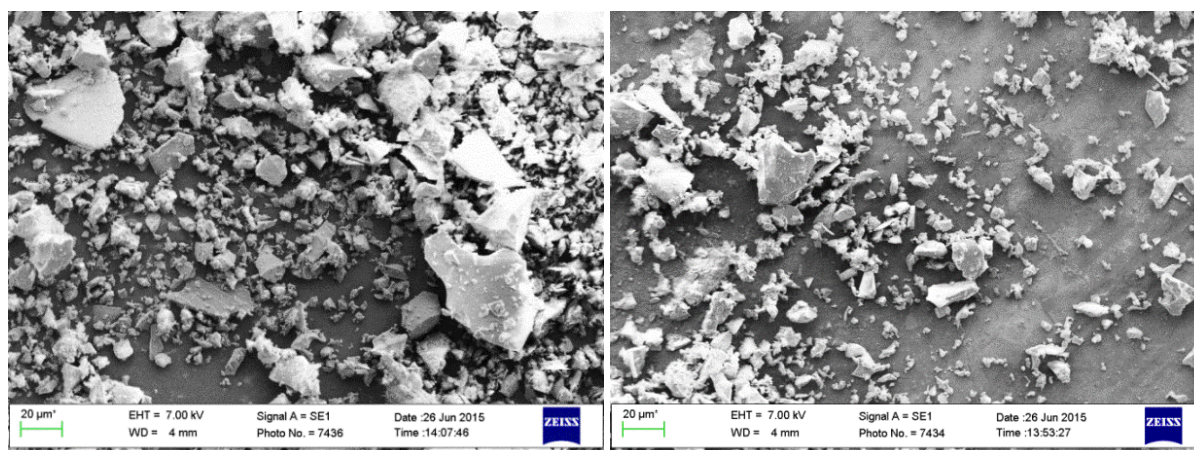


Figure 4-3. SEM image of the particle distribution and morphology of the slag samples: GGCS (left) and GGBS (right).

4. 2. Chemical Properties

The chemical properties of the slag and cement are given in Table 4.2. By comparing the data given in Table 4.2 with Table 2.2, it is clear that both the slags and cement fall within typical ranges compared to those found in literature. The slag has a similar composition to that of the PC, yet at different percentages. For example, both slag and cement contain Al_2O_3 , CaO and SiO_2 , however, slag contains higher percentages of Al_2O_3 (14.08 and 13.72 % for GGCS and GGBS, respectively, while the PC has 4.98 %) and lower percentages of CaO compared with PC (37.49 and 33.43 % for GGCS and GGBS, respectively, while the PC has 59.90 %). The slag also shows similar percentage compositions when compared to each other.

Moreover, BS EN 15167-1 (2006) has a requirement that the sum of CaO , MgO and SiO_2 should exceed two thirds of the mass composition of the slag. Both the GGCS and GGBS comply to the prerequisite with GGCS and GGBS having a sum of these compounds equal to 81.25 % and 79.52 %, respectively.

The data given obtained from the chemical composition will in turn be used to describe the possible effects that it may have on the properties of concrete. In addition, the data obtained from the Table 4.2 can also be used to assess the Bogue's composition of the cement by using Equation 2.1 – 2.4 and is given in Table 4.3. The data presented here is to be used in the following sections to describe the effects of the composition on parameters investigated.

Table 4.2. The chemical composition of the cementitious binders: cement and slags.

Composition (%)	PC	GGCS	GGBS
SiO_2	21.37	31.73	37.18
CaO	59.90	37.49	33.43
Fe_2O_3	3.07	1.09	0.50
Al_2O_3	4.98	14.08	13.72
MgO	2.58	12.02	8.91
K_2O	0.24	0.64	1.15
MnO	0.46	0.03	0.99
Cr_2O_3	0.01	bdl*	bdl*
Na_2O	0.14	0.21	0.26
P_2O_5	0.07	0.02	0.01
TiO_2	0.43	0.52	0.67
L.O.I.	3.02	0.21	N/A
Sum Of Conc.	96.27	98.04	96.05
$\text{CaO} + \text{MgO} + \text{SiO}_2$ **		81.25	79.52

* bdl = below detection limit

** EN 15167-1 (2006) requires the sum to exceed two thirds of the mass.

Table 4.3. The Bogue's composition of the PC.

Composition:	C_3S	C_2S	C_3A	C_4AF
(%)	42.7	29.3	7.99	9.35

4. 3. Reactivity

The reactivity of slag is dependent on the fineness, glass content, chemical composition, mineralogical composition and the type of activation (Pal et al., 2003). Based on the chemical composition of the slags, certain ratios have been developed and investigated to try and better formulate a means of assessing the level of reactivity of slags.

Firstly, the reactivity of slag tends to increase with the amount of CaO, MgO and Al₂O₃ present, whereas SiO₂ tends to decrease the activity (Alexander et al., 2003; Pal et al., 2003). Hence, using the data obtained in Table 4.2 it is noted that GGCS has higher mass percentages of CaO, MgO and Al₂O₃ compared to the GGBS; therefore it can be stated that the reactivity of GGCS is expected to be higher compared to that of GGBS. In addition, the percentage of SiO₂ of GGCS is lower than that of the GGBS, 31.73 % and 37.18 % respectively, further adding to the likelihood of GGCS exhibiting higher levels of reactivity. Hence, it can be stated that the GGCS will have a higher level of reactivity compared to the GGBS; the higher level of reactivity of GGCS in comparison to GGBS have also been found by other researchers (Alexander et al., 2003; Otieno et al., 2014).

Researchers have investigated different ratios in order to determine the hydraulic activity of slag based on the ratios of certain chemical compositions. Table 4.4 provides a list of ratios as established in literature in corroboration with the data of Table 4.2 to assess the hydraulic activity. GGCS shows to be more reactive compared to GGBS when used in concrete (Beushausen et al., 2012) and this is shown in Table 4.4 when comparing all the ratios. It is noted that the difference for all reactivity criteria, the GGCS exceeds that of the GGBS. In addition, the EN 15167-1 (2006) requires that the ratio of (CaO + MgO):SiO₂ to exceed 1; for the case, both GGCS and GGBS conform to the requirement with values of 1.56 and 1.14, respectively.

Table 4.4. Assessing the hydraulic activity of the slag based on the chemical composition.

Formula	Preference	GGCS	GGBS	Authors (*)
CaO/SiO ₂	> 1.0	1.18	0.90	(2)
(CaO + MgO)/ SiO ₂	> 1.0	1.56	1.14	(2), (3)
(CaO + MgO)/(SiO ₂ + Al ₂ O ₃)	> 1.0	1.08	0.83	(1), (2)
(CaO + 0.56 Al ₂ O ₃ + 1.4 MgO)/ SiO ₂	> 2.0	1.96	1.44	(2)
(CaO + Al ₂ O ₃ + MgO)/ SiO ₂	> 3.0	2.00	1.51	(1), (2), (4)
(CaO + 1/3 Al ₂ O ₃ + MgO)/(SiO ₂ + 2/3 Al ₂ O ₃)		1.32	1.01	(1)
Al ₂ O ₃ / SiO ₂		0.44	0.37	(1)
For MgO < 10 %:				
(CaO + Al ₂ O ₃ + MgO)/(SiO ₂ + TiO ₂)		-	1.48	(1)
For MgO > 10 %:				
(CaO + Al ₂ O ₃ + 10)/(SiO ₂ + TiO ₂ + MgO - 10)		1.80	-	(1)

*(1) Talling & Krivenko, 1997; (2) Pal et al., 2003; (3) Neville, 2011; (4) Otieno et al., 2014

The reactivity of the slag samples were also assessed by means of the strength activity index (SAI) and are graphically depicted in Figure 4-4. The dashed line in Figure 4-4 represents the requirement set by EN 151767-1 (2006) stating that the minimum required for a slag sample to be accepted i.e. 45 % and 70 % at 7 and 28 days, respectively. From Figure 4-4 it is clear that the GGCS has passed the criteria at

both ages, whereas the GGBS has failed the requirement, albeit with 0.2 % and 0.6 % at respective ages of 7 and 28 days. Despite not having the required SAI at the ages of testing, the difference between the result and the requirement are not substantial to disregard the GGBS as not being a suitable SCM.

Table 4.5. The flexural and compressive strength for the reference and slag samples at 7 and 28 days.

Age (days)	7			28		
	Flexural Strength (MPa)	Compressive Strength (MPa)	SAI (%)	Flexural Strength (MPa)	Compressive Strength (MPa)	SAI (%)
Reference	3.7	34.5	-	4.9	52.0	-
GGCS	3.9	27.5	79.5	4.6	48.3	92.9
GGBS	2.6	15.5	44.8	4.1	36.1	69.4
EN 15167-1:2006 Requirement:			45.0			70.0

Moreover, Figure 4-4 can be used to compare the reactivity of the two slags to each other at the respective ages. The GGCS shows to be more reactive at both ages of 7 and 28 day compared to the GGBS. The SAI for GGCS and GGBS were 79.5 % and 44.8 % at 7 days, respectively, and equates to a difference of 34.7 %. In addition, at 28 days the SAI was 92.9 % and 69.4 % for GGCS and GGBS, respectively; at this age the difference was 23.5 %. The results are substantiated by literature that has yielded the results of GGCS performing better, in terms of reactivity, compared to GGBS (Beushausen et al., 2012). The difference in production process is a likely reason for the observed differences. As a result, the relatively better performance of the GGCS compared to the GGCS can be because of the difference in chemical composition. Firstly, as mentioned, the GGCS had a higher mass per cent of compounds that increase activity, namely CaO, MgO and Al₂O₃ and secondly a lower mass per cent of SiO₂, which has an adverse effect on the hydraulic activity of slag.

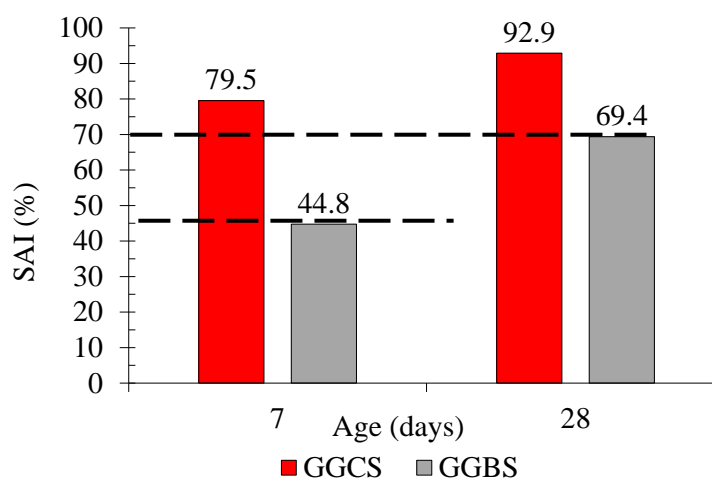


Figure 4-4. SAI for the slag samples.

In terms of the strength development with age, the activity of the GGBS shows a greater increase with a percentage increase of 24.6 % from 7 to 28 days than the GGCS (13.4 %). However, despite the substantial increase, the GGBS still had a lower SAI compared to the GGCS. This is furthermore indicative of the reactivity of GGBS being slower compared to that of GGCS, as well as likely being activated at a later age. To conclude, the GGCS show higher levels of reactivity as found in the

literature that also investigated GGCS and also compared the results with GGBS samples (Alexander et al., 2003; Beushausen et al., 2012).

4. 4. Workability

The workability of the slag mixes are given in Figure 4-5. Firstly, as expected the workability of both slag-based concrete mixes were higher compared to the reference. Therefore, the addition of slag lead to an overall increase in workability with increasing addition.

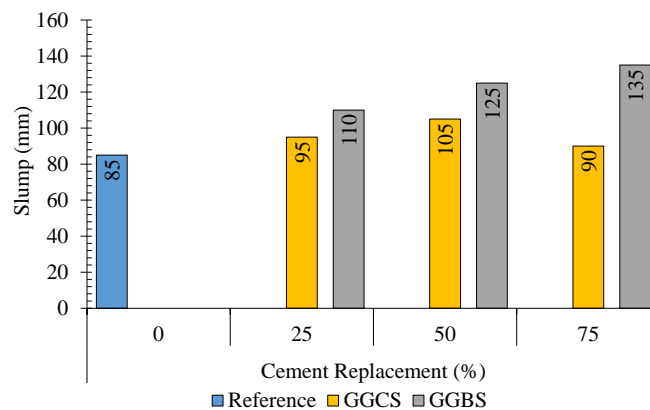


Figure 4-5. The workability of mixes containing different slag types.

The trend of slag increasing the workability has been noted in literature (Alexander et al., 2003; Beushausen et al., 2012). The reason for the increased workability is explained by the following:

- Slag particles absorb less water (Czernin, 1980; Alexander et al., 2003), therefore, more water is available for inter-particle lubrication. The reduced water absorption is due to slag reacting rapidly with water and a layer of impermeable hydration products forming around the particles. Therefore, initially, less water is used for hydration.
- The addition of slag causes an increase in paste consistency and volume and a decrease in viscosity (Park et al., 2005). These factors therefore lead to the overall decrease in inter-particle frictional forces. Hence, with the reduction in particle friction, particles can slide or move past one another with relative ease.
- The LOI of the PC (3.02 %) is also higher compared to that of the GGBS (a LOI less than 0 % was recorded) and for GGCS (0.21 %). The particles that have not combusted fully absorb more water and by increasing the slag content causes an effective reduction in these particles when 100 % PC is used.

In terms of slag type, the GGBS had higher slump values compared to the GGCS samples. The SEM images of the particles does show that the particles have similar angular morphology. It is suggested that the fineness has an impact on the trend in increasing workability. The increase in slag can result in a shift of the system from a PC-dominated matrix to one where the slag component is the main factor. Therefore, as the slag increases, despite having a lower water binding capacity at the start, the total

surface increase sufficiently to cause a decrease in workability. Similarly, the work by Park et al. (2005) shows an initial decrease in yield stress and increase with increase in slag content, this can be used to describe the effect of increasing GGCS on the concrete system. The yield stress increases with added substitution, therefore increasing the inter-particle frictional forces, thereby decreasing the workability. However, the yield stress is still lower compared to the reference. Nevertheless, the slag sample still improve workability and is beneficial from a construction point of view.

As a concluding statement, the use of South African slags do exhibit the pattern of increasing the workability of concrete, as found in this study. Moreover, the increase in slag content also improved the workability; the GGBS however, did produce higher slump values.

4. 5. Setting Times

The setting times of both the GGCS and GGBS is illustrated by Figure 4-6. Firstly, an apparent effect of slag type on the setting times seems to exist: the GGCS had an accelerating effect and the GGBS had a retarding effect on the setting time. For both replacement levels, the GGCS displayed initial setting time less than that of the reference i.e. 671, 522 and 613 minutes at 0, 25 and 50 wt. % of cement replacement. The reduction in setting time is suggested to be due to two of the three discussed effects SCMs have on a concrete system (Section 2.3.): chemical surface and chemical effects.

The smaller particles of both the GGBS and GGCS act as nucleation sites for cement hydration products, yet as seen from the physical properties of the slag particles (Figure 4-1), the GGCS has a smaller range. Hence, the nucleation phenomenon is increased in a certain extent. Secondly, since the reactivity of GGCS is higher compared to that of GGBS, the chemical effect of GGCS is likely occurring at an earlier age compared to the GGBS. Moreover, CH is reported to slightly retard hydration of a PC system (Ramachandran et al., 2002); however, the effect of the slag, especially the GGCS, using the CH as a reactant, is not a substantial reason for the acceleration of the initial setting time. However, the likelihood of this mechanism having an effect cannot be ignored.

At all replacement levels, the GGCS showed lower setting times compared to the GGBS. For example, at 25 % cement replacement, GGCS resulted in an acceleration of 2.48 hours and GGBS caused a retardation of 0.47 hours to achieve initial set. This means that the working time for a concrete containing GGCS is reduced which could be a potential problem for construction purposes. However, this accelerated setting time is beneficial in terms of formwork removal. The opposite of both mentioned facts are thus valid for GGBS.

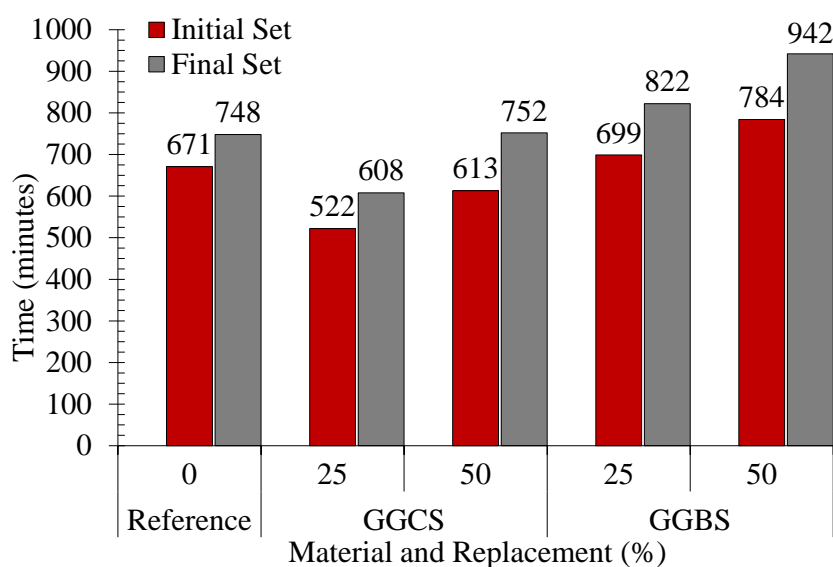


Figure 4-6. Setting times for the reference and slag.

A secondary trend, commonly found in literature pertaining to slag, is the increasing retardation effect with increasing substitution of cement. The trend was observed in both slags: the continual replacement of cement with slag is associated with an increase in retardation. Even though, the addition of GGCS did accelerate the setting time, increasing the percentage of GGCS caused the acceleration effect to diminish. At 25 and 50 % replacement with GGCS the time by which the initial hydration is reduced is 149 and 58 minutes, for initial set, respectively. For final set, the 25 % replacement causes an acceleration period of 140 minutes, whereas at 50 % the final set is retarded by 4 minutes. GGBS caused a retardation effect for both the initial and final set times: the retardation times equate to 28 and 113 minutes for initial set at 25 % and 50 % cement replacement, respectively, and final set retardation of 74 and 194 minutes.

The relative retardation associated with the continual increase is suggested to be due to the dilution of hydration products and it is also related to the reactivity of the slag compared with the cement. As discussed, slag reacts with water to form an impermeable layer, inhibiting the continuous reaction to form hydration products and thus requires an activator to *dissolve* the layer formed, i.e. calcium hydroxide as an activator (Kurdowski, 2014). The rate of breaching the permeable layer is therefore tied to the amount of CH present. However, the dilution of cement relates to a reduction in the products formed per unit time. The reduction in C-S-H relates to a prolonged time to achieve a continuous network, whereas the reduction in CH produced per unit time delays the potential reactivity of slag.

When looking at the time between the final and initial set, a gradual increase is seen at different replacement levels as well as for different materials. The increase in the duration of reaching the final setting time can be as a result of the potential of slag reducing the rate of heat release. A future investigation into the heat peaks that are achieved and the time of reaching such peaks could yield more information into the effect of the different slag types.

In summation, the type of slag as well as the amount of slag used to replace the cement impacted the setting time of the concrete mixtures in this study. The two slags, GGCS and GGBS, had different effects based on the type. The GGCS had an accelerating effect on setting times, likely as a result of the increased reactivity. Moreover, both slags had an increasing retardation effect with the increasing cement substitution: this trend is related to the increasing dilution of hydration products with the increasing substitution.

4.6. Bleeding

The experimental results of the slag-based concrete of the current study displayed the three stages present during the occurrence of the bleeding phenomenon. Figure 4-7 to 4-10 display the results, and provide a visualisation of the mentioned trend, when either GGCS or GGBS are incorporated at different replacement levels, respectively. These figures show the effect of slag type on the overall bleeding characteristics, as well as highlighting the difference that each respective slag has on bleeding with a subsequent increase in its relative quantities. Furthermore, the mentioned figures are to be used in conjunction with Table 4.6, which provides a tabulated account of the bleeding characteristics, namely: bleeding rate, capacity and duration. Bleeding rate is calculated as the amount of bleed water evaporated during the first 40 minutes. Bleeding capacity is the percentage of the final cumulative bleed water as a function of the total sample mass and bleed duration is the time until stage three of bleeding is achieved (Figure 2-12).

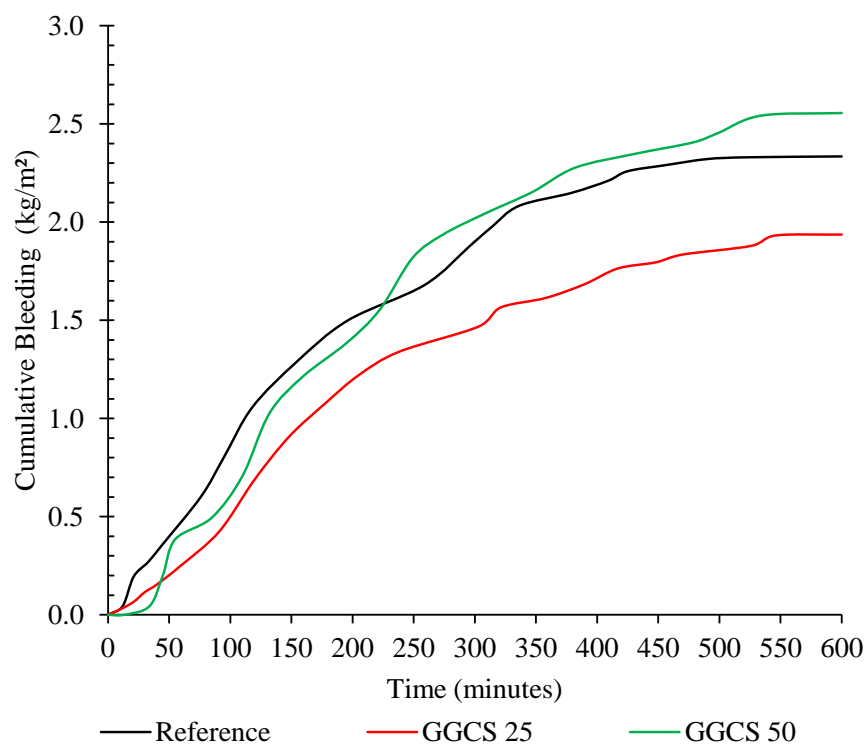


Figure 4-7. The bleeding of GGCS specimens at 0, 25 and 50 % cement replacement.

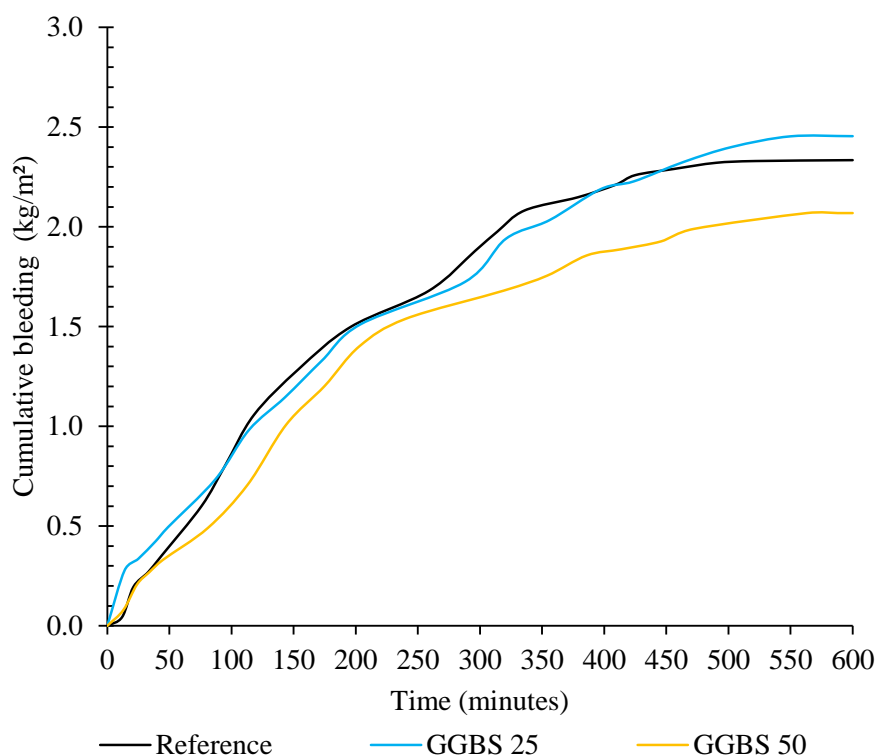


Figure 4-8. The bleeding of GGBS specimens at 0, 25 and 50 % cement replacement.

Table 4.6. The bleeding rate, capacity and time for the slag based concrete.

Material	SCM (%)	Bleeding Rate (g/m ² /s)	Bleeding Rate (kg/m ² /hr)	Bleeding Capacity (%)	Bleed Duration (minutes)
PC	0	0.134	0.482	2.33	450
GGBS	25	0.181	0.653	2.45	550
	50	0.123	0.476	2.07	575
GGCS	25	0.064	0.232	1.93	500
	50	0.142	0.513	2.42	475

4. 6. 1. Effect of Slag Type and Substitution on Bleeding Rate

The effect of the type of slag on the bleeding rate is essential to assess the time at which plastic shrinkage cracking may occur. As a higher bleeding rate could potentially prolong the time until curing is essential. Although curing of concrete is still advised, especially for SCMs based concrete. If water is transported to the surface at a faster rate than it is removed, a layer can form that provides protection against plastic shrinkage cracking until required measures are implemented. From the current study, the increase in substitution with GGBS causes an overall increase in the bleeding rate, as seen in Figure 4.8. At 25 %, the capacity exceeds that of the reference and at 50 % replacement being lower than the reference. The GGCS in turn caused the bleeding rates to increase from a value lower than the reference (the gradient is approximately half of the reference) to a value exceeding that of the reference's bleeding rate. However, when the cement substitution with GGCS increased to 50 %, the bleeding rate was also noted to increase to double of the 25 % replacement's rate. From the mentioned data, it is reasonable to state that curing implementation for GGBS-based concrete is required sooner than for GGCS-based concrete; albeit essential to all concrete mixtures.

The differences in respective bleeding rates are suggested to be due to the volumetric increase in paste, as Almusallam et al. (1998) reported that leaner mixes bleed less. Hence, due to the replacement of cement being done on a mass basis, for the current study, there was a subsequent increase in the volumetric percentage of paste. This, in conjunction with the higher levels of workability, is indicative of more water being available for displacement when the initial effect of settlement occurs, hereby increasing the rate of water migrating upward.

4. 6. 2. Effect of Slags on Bleeding Duration

Slag-based concrete is observed to bleed for longer periods as opposed to those containing none. The current study yielded similar results, as it can be seen from Table 4.6 that the reference did exhibit similar bleeding rates and capacities as the slag-based concrete, yet the reference had a shorter bleeding duration. The bleeding process stopped at approximately 450 minutes, which is less than the initial set (671 minutes), indicative that the bleeding ceased more likely as a result of a mechanical restraint as opposed to the hydration process. The mechanical restraint occurs as particles settle and reach the maximum displacement. Hence, less water is likely to migrate upward if the heavier particles cease to settle. Similarly, the slag-based concretes also achieved the cessation-stage before initial set occurred.

Nonetheless, the effect of hydration is still an influencing factor on the bleeding duration. This is due to water chemically binding and as a result, the hydration products block pores and reducing the plasticity of the concrete.

In addition, increasing the slag, regardless of the type, caused a subsequent increase in bleeding duration relative to the reference. This is due to the slag-based samples remaining in a plastic state for a longer duration, as a result of the enhancement of the dilution effect. The GGCS-based concrete did exhibit a decrease in bleed duration when the slag content increased from 25 to 50 %. This is likely a result of the finer particles being transported by the bleed water and thereby blocking bleedwater pathways.

4. 6. 3. Effect of Slag on Bleeding Capacity

Wainwright and Ait-Aider (1995) and Wainwright and Rey (2000) found that the bleeding capacity of slag-based concrete increases with an increase in cement substitution due to the retardation effect. However, the results from the current study are both contradictory and in agreement with their findings. For example, an increase in GGBS from 0 to 25 % has a near identical, albeit higher by 0.12 %, bleeding capacity compared with that of the reference. However, the increase of GGBS from 0 to 50 % caused a reduction in bleed capacity equal to 0.26 %. In contrast, the increase of GGCS in concrete had an opposite effect as that of the GGBS when the substitution increased from 0 to 50 %. At 25 % replacement, the bleeding characteristics of the concrete improved as the capacity was reduced by 0.4 %. However, at 50 % replacement the capacity increased by 0.9 %. The results of the capacity do however follow a similar trend as that of the bleeding rate.

4. 6. 4. Comparison between GGBS and GGCS on the Bleeding Phenomenon

As discussed, it is apparent that the addition of slag has a varying effect based on the type of the material. This is in contradiction to the work by Wainwright and Ait-Aider (1995) and Wainwright and Rey (2000). When comparing the two slags on a substitution bases, it is noted that the addition of 25 % GGBS displays a similar bleed profile as the reference; the same percentage substitution with GGCS shows a similar trend, yet at a reduced capacity (see Figure 4-9). With the increase in cement substitution, the GGCS show to have a bleeding profile that is the same as that of the reference, whereas the GGBS mixtures improves in terms of bleeding capacity.

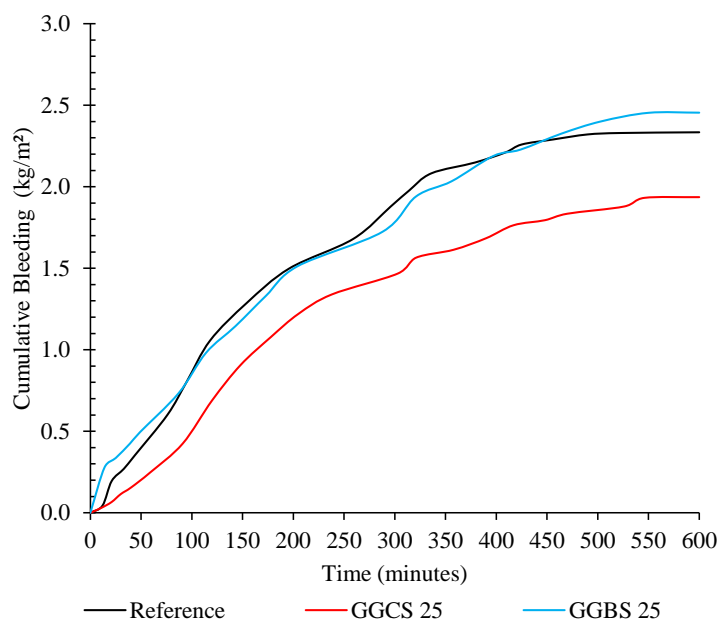


Figure 4-9. The bleeding of slag samples at 25 % cement replacement.

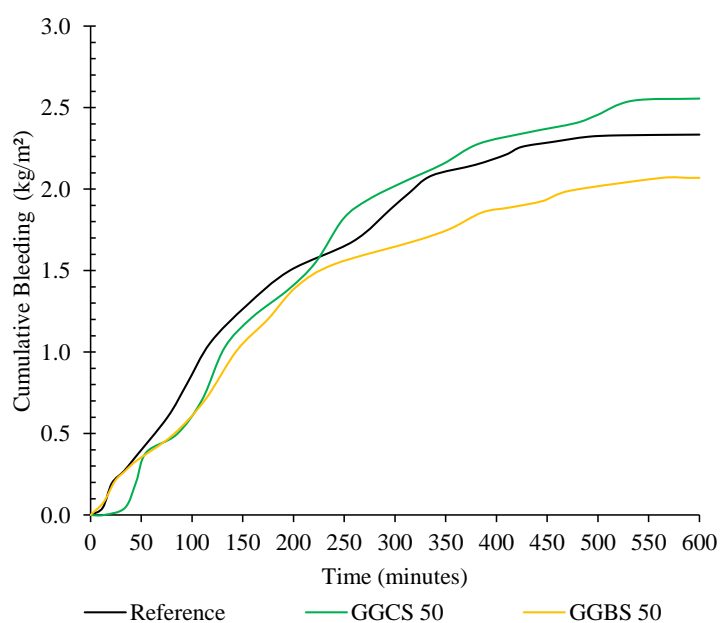


Figure 4-10. The bleeding of slag samples at 50 % cement replacement.

Interestingly, the bleed capacity of the GGBS at 25 % replacement and GGCS at 50 % show similar bleed capacities. The particle packing of the mix affects the bleed capacity. Hence, when the span ratios

are compared (Table 4.7), it is noted that the ratio in these two blends show a similar value. This implies the possibility that the fines of these two mixes may possibly achieve a similar packing density and therefore exhibit similar bleed capacity values. Moreover, if the volume frequency percent is proportioned on the PC:Slag ratio, similar plots are obtained as shown in Figure 4-11. The conclusion is that for different slag types, the GGCS shows improved bleeding characteristics at lower substitution and GGBS performs better (higher bleeding rates and capacities) at higher substitutions.

Table 4.7. The effect of slag substitution on the span of the particles.

	PC	GGBS	GGCS		
% SCM	0	25	50	25	50
Span	2.20	2.40	2.75	2.30	2.40

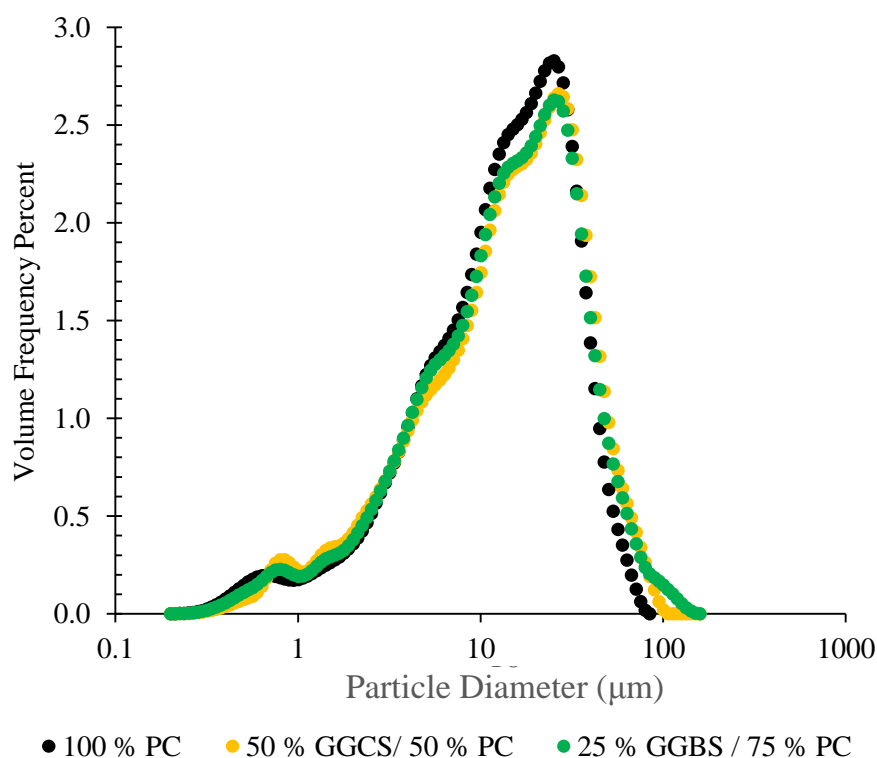


Figure 4-11. The particle distribution for the combination of slag and cement.

4. 7. Early Age Deformation

Plastic shrinkage and settlement poses as a problem in terms of restrained concrete. Early age cracking could lead to future durability issues. The results of plastic shrinkage and settlement are given and is discussed in this section. The section first describes the effect of settlement and then follows the discussion of shrinkage. The capillary pressure is also given in an attempt to explain the observed data. In addition, Table 4.8 provides the setting times and bleeding characteristics of the concrete mixes and the graphical representation of the data can be found in Appendix A.

At an elevated temperature of 40 °C, the trend of including GGCS reduces the setting time and is similar to the trend observed and discussed in the previous sections. The inclusion of GGBS at 40 °C

did however cause a slight retardation in setting times. The setting times are accelerated, in comparison to 23 °C, due to the increased reactivity under higher temperatures.

Table 4.8. Setting times and bleeding data for slag-based concrete at elevated temperatures.

	Slag (%)	Setting Times		Bleeding Characteristics		
		Initial (Minutes)	Final (Minutes)	Rate (g/m ² /s)	Duration (Minutes)	Capacity (%)
Reference	0	373	463	0.12	390	2.30
GGCS	25	357	420	0.12	450	2.44
	50	318	409	0.15	400	2.82
GGBS	25	395	438	0.18	467	2.72
	50	434	524	0.10	446	2.36

The bleeding data shows that the rate of bleeding is fairly similar to that of the results done at 23 °C, with 25 % GGBS-based concrete having the fastest rate and 50 % the lowest rate, 0.18 and 0.10 g/m²/s, in that order. In addition, the bleeding capacity and duration does show an increase compared to the reference. This may be as a result of the higher temperature promoting the hydration process, yet due to dilution present in SCM-based mixes, the degree of hydration is not achieved to the same level. Moreover, porosity at the elevated temperatures may also be higher as a result of the enhanced hydration.

4. 7. 1. Plastic Settlement

Figure 4-12 shows the consolidation process of the concrete mixes after placing. As can be noted, the settlement rate for low levels of substitution has an initial rate similar to that of the reference. At 50 % cement substitution, the initial rate of settlement is relatively higher. The increased viscosity and fluidity may be underlying reasons for these initial differences that are observed. The more viscous material has a better particle dispersion and therefore slows down the particle movement.

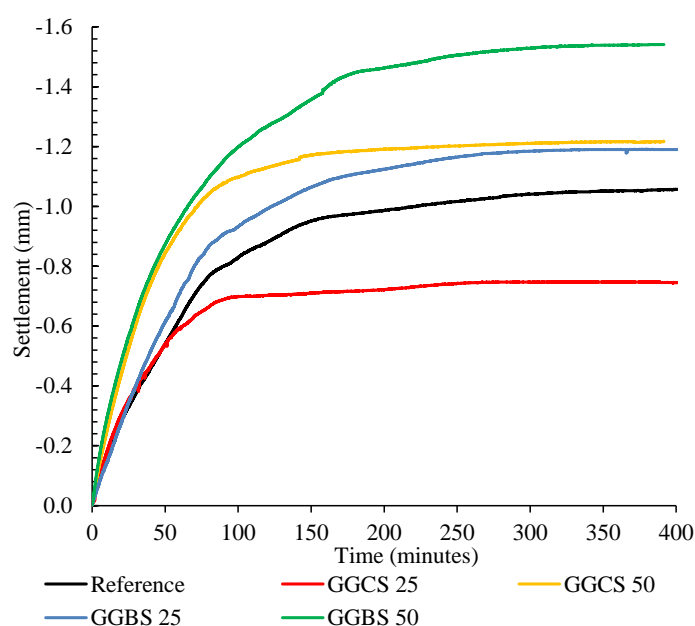


Figure 4-12. Consolidation of the concrete containing different levels of slag, both GGCS and GGBS.

From Figure 4-12 it can be concluded that an increase in slag content from 25 to 50 % results in a corresponding increase in settlement. It is suggested that the increase in paste and workability cause the material to settle more with the presence of more free water in the paste. In addition, the GGCS based concrete does display lower displacement compared to the GGBS sample; hence, the performance of GGCS is relatively better and corroborates with the statement made by Alexander et al. (2003): GGCS can potentially result in lower settlement because of the increased viscosity.

4. 7. 2. Capillary Pressure Build-up

The capillary pressure build up for both slag types were less compared to the reference and a decrease was observed with increase in cement replacement (Figure 4-13). The slopes of the capillary increase is observed to be more gradual compared to the reference mixture. The steeper capillary pressure build-up of the reference can be explained by investigating the bleeding characteristics. The reference mixture has a lower bleeding rate, capacity and duration in comparison to the slag-based concrete mixes. As aforementioned, a lower bleeding capacity is typically associated with higher capillary pressures. The less steep slopes of the capillary pressure curves of mixes containing slag is suggested to be a result of the higher bleed characteristics. Moreover, it is noticed that the 50 % GGBS displays a near similar trend to that of the reference in terms of both pressure build-up and bleeding characteristics; a similar trend as observed by Darquennes et al. (2011).

In addition, it is noted that the vertical settlement also affects the capillary pressure in an inverse manner. As the vertical displacement increases, there is a subsequent decrease in the capillary pressure. Referring to Figure 2-14, it is noted that for the capillary pressure, there are two force components; one of the components is a vertical force resulting from the gravitational effects. Therefore, if the vertical force increases, the radii of the menisci increase as liquid moves up and results in a decrease in capillary pressure.

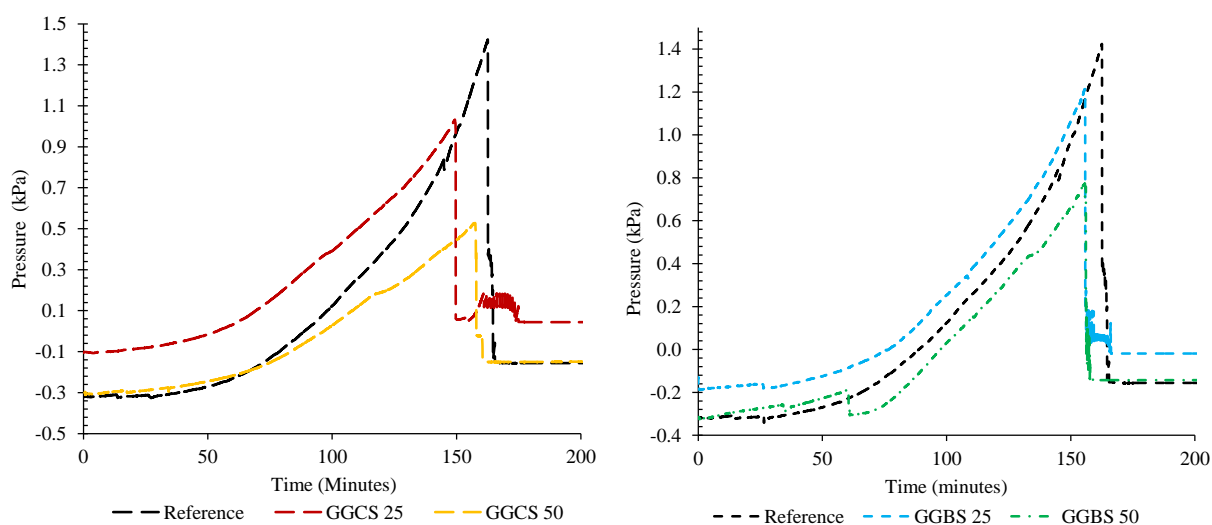


Figure 4-13. Capillary pressure build up for concrete containing GGCS (left) and GGBS (right) at different replacement levels.

In addition, due to the dilution effect, the amount of hydration products in the reference mixture is also higher than that of the slag-based concrete mixtures. As a result of the increase or higher amount of hydration products, the pores of the reference may also start narrowing. This inevitably aids in the pressure build-up. Moreover, the slag based concrete may have a higher degree of pores, yet larger due to the delayed hydration (Darquennes et al., 2011). This mechanism can therefore be suggested to be the reason for the higher pressure build up present in the reference mixture.

4. 7. 3. Plastic Shrinkage

Figure 4-14 displays the shrinkage of the two different types of slag-based mixtures. In terms of shrinkage, the mixtures containing the 25 % slag had the highest degree of shrinkage at nearly 4333 and 5333 $\mu\text{m}/\text{m}$ for GGCS and GGBS, correspondingly. The increase in slag resulted in a corresponding decrease in shrinkage values observed: shrinkages were 4000 and 2000 $\mu\text{m}/\text{m}$ for GGBS and GGCS, respectively. The first stage of shrinkage lasted approximately the same period, i.e. 50 minutes, and had similar, low magnitude and order shrinkage values. It is only noted that the 25 % GGCS concrete mix had a relatively higher strain at this early stage. In addition, Stage 2 of the shrinkage was maintained between 150 and 200 minutes. Hence, from the latter mentioned and the data of Table 4.8, it is noted that the end of Stage 2 is reached before initial set, as opposed to what was stated by Darquennes et al. (2011). The difference is likely as a result of the differences in environmental conditions, such as the temperature of testing.

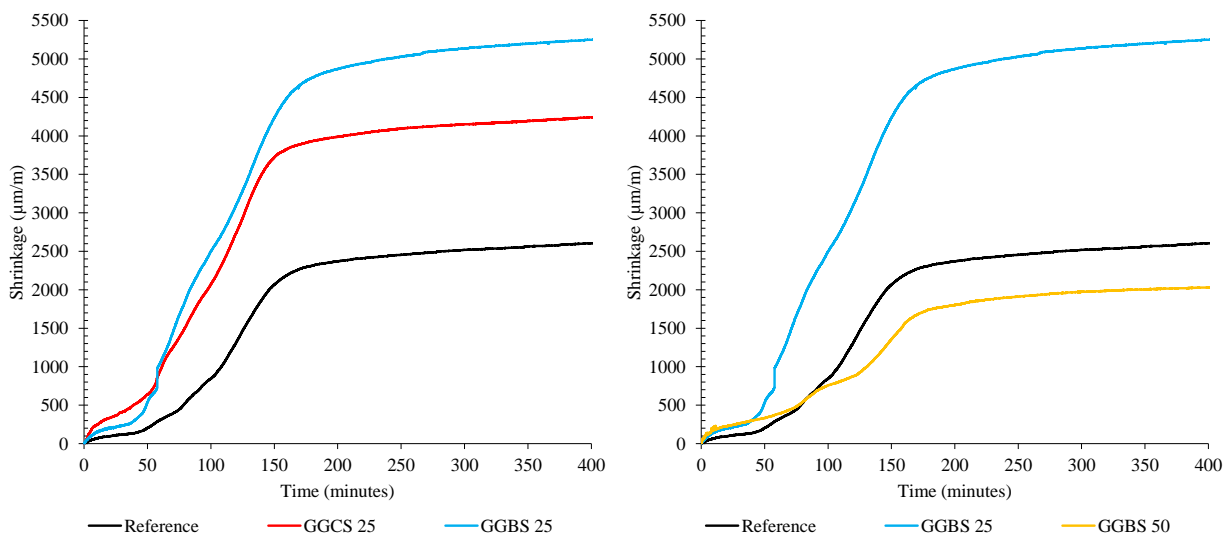


Figure 4-14. Plastic shrinkage for concrete containing GGCS (left) and GGBS (right) at different replacement levels.

The data of the shrinkage of the 50 % GGBS is lower than the reference and a similar result was attained by Darquennes et al. (2011) in study investigating GGBS. The 50 % replacement of that study also produced shrinkage values less than the reference. In addition, the capacity of the 50 % GGBS was higher than that of the reference (marginally by 0.06 %) and had a longer bleeding duration as well as

setting time. Even more so, the capillary pressure build-up of the 50 % GGBS sample was lower than that of the reference and had a longer build up.

A lower capillary pressure drop however does not relate to a lower shrinkage (Kronlöf et al., 1995). This corroborates the results between the reference and the 25 % GGBS and GGCS samples. Both of these two mixtures had a relatively lower pressure drop (Figure 4-13), yet, significantly higher shrinkage values (Figure 4-14), even for the 50 % GGCS, which exhibited the lowest pressure drop. Equally as important, the bleeding capacity of the mixes were also higher than that of the reference. This could be explained using the hydration mechanism proposed (Kronlöf et al., 1995; Darquennes et al., 2011).

Arguably, the reference generates more hydration products and can be said to achieve a level of rigidity relatively sooner compared to the SCMs based concrete. Therefore, as the material becomes more rigid, it is capable of withstanding higher pressures before succumbing to the shrinkage capacity. Hence, the material does not deform as much under the imposed pressure. This explains why the 25 % GGBS has a higher shrinkage. The argument can also be used to explain the increase in shrinkage with GGCS, even though these mixes set earlier than the reference. The second stage of the shrinkage completes approximately 2 hours prior to initial set. Therefore, the effect of reduced setting time could be delayed as the hydration of the GGCS, albeit having a higher level of reactivity than the GGBS, has not formed sufficient amounts of hydration products to generate the required level of stiffness to reduce the impact of the imposed strain.

4. 7. 4. Concluding Remarks

The mechanisms of plastic shrinkage and settlement is not yet fully understood and the information on the impact of SCMs is rather limited. The basic assumption is that due to the fineness, the shrinkage is expected to increase. Yet, the current study found that the 50 % GGBS concrete sample had the lowest shrinkage, even less than that of the reference. Therefore, the need to investigate the mechanism when SCMs are incorporated requires more attention to try and better explain the shrinkage results. The study also found that a lower pressure drop does not always relate to a higher shrinkage value as noted by Krönlof et al. (1995).

4. 8. Microstructure

The use of slag improves the microstructure of concrete paste due to the generation of smaller, more discrete pores (Bouikni et al., 2009). The result is mainly due to the secondary pozzolanic reaction creating more voluminous phases which result in less porous structures and higher strength (Jin et al., 2015). The current study investigated the porosity, by means of X-ray CT Scans, and found the results to be in agreement with the hypothesis of slag improving the microstructure.

The results are represented in Figure 4-15, and compares the differences in the pore size distribution with the inclusion of slag in concrete. As can be seen in the figure, the inclusion of slag causes a progression of the cumulative percentage curve to the left, as well as increasing the span of the curve. This relates to a general refinement of the pores. Table 4.9 provides the relevant cumulative pore diameters, i.e. the 90th, median and 10th percentile. As seen, in all instances, the pore diameter of the slag-based concrete is less than that of the reference.

Table 4.9. Cumulative and frequency data for the pore diameters (mm) of concrete including slag.

Cumulative %	Reference	GGCS		GGBS	
	0	25	50	25	50
10	2.1	0.87	0.93	0.99	0.87
50	3.2	2.01	2.11	2.26	2.03
90	6.7	4.04	4.80	4.59	4.50

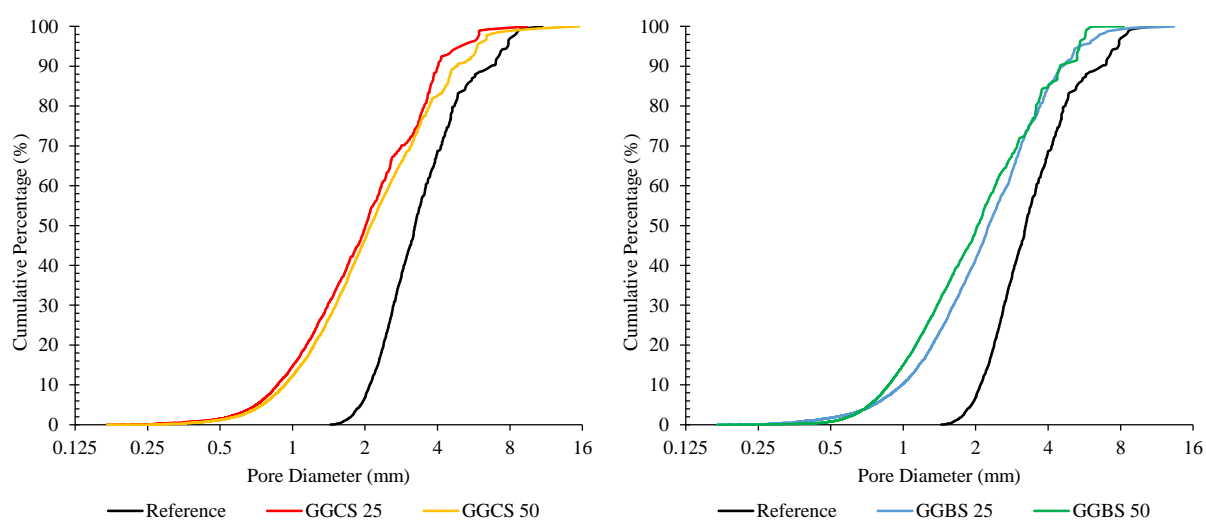


Figure 4-15. Cumulative percentage of the pore diameters of the concrete microstructure incorporating GGCS (left) and GGBS (right).

Figure 4-16 displays the cumulative volume distribution (dashed line) and the relative pore volumes counts per sample. The reference (no slag) has a relatively large range of pore volume, with the most significant quantity between 1 and 2 mm³; the small pores account for approximately 35 % of the cumulative percentage. Therefore, the remaining 65 % (approximately) accounts for pore volumes exceeding 2 mm³. In contrast, the addition of slag refines the pore diameter and volumes significantly. This is seen in Figure 4-16 with more than 95 % of the cumulative pores being less than 1.5 mm³.

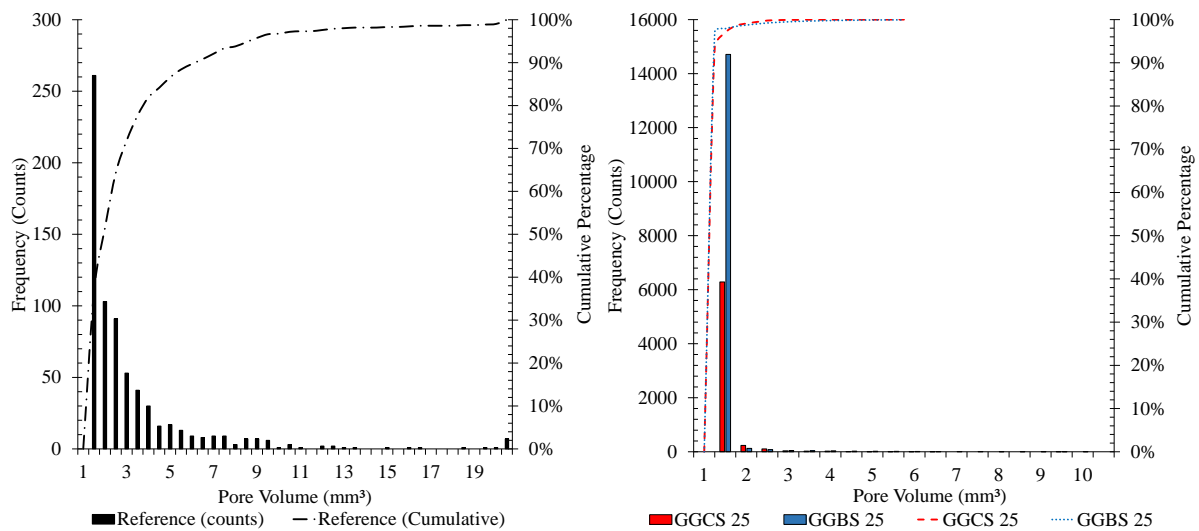


Figure 4-16. Differences between the pore volume for concrete containing no slag (left) and slag at 25 % cement replacement (right), with the frequency and cumulative percentage presented by the histogram and dashed lines, respectively.

The impact of adding slag shows to be significant in terms of improving the concrete microstructure. This has been shown to be a general trend amongst researchers investigating the effect of slag on concrete microstructure (Siddique, 2008; Bouikni et al., 2009; Otieno et al., 2014). The improved microstructure results are as a result of increased paste content, inclusion of fine material and the latent, as well as, pozzolanic reaction occurring in the paste.

The increase in fines, and subsequent increase in fines, result in an enhanced particle packing. Therefore, as the packing is enhanced, the volume of voids are reduced. Also, the finer particles aid in creating nucleation sites for hydration products, hence, increasing the densification of the paste. The pozzolanic reaction reduces the amount of larger CH present by replacing it with a more dense C-S-H gel. The more dense paste structure was also found by Hooton (2000). Moreover, the inclusion of slag increases the overall content of MgO present in the concrete mixture. In a study based on alkali-activated slag, Jin et al. (2015) investigated the impact of MgO in concrete. Their findings were that the increase in MgO caused an increase in the hydrotalcite-like phases and C-S-H. The former is mentioned to be more voluminous than the latter, hence decreasing the porosity. This can be used to explain the increase in pore refinement found in the study when slag is incorporated. The increased pore refinement is beneficial in terms of the reduced transportation of deleterious substances within concrete.

To conclude, the study found that the inclusion of slag increased the level of pore refinement, as well as decreasing the relative pore sizes. The underlying reasons for the improved microstructure is related to the filling capability and reduced porosity of the finer materials and pozzolanic reactivity, respectively.

4. 9. Compressive Strength

The use of SCMs in concrete are typically associated with the reduction in early age strength development as a result of dilution, yet an increase in the later age strength as a result of the latent

hydraulic activity and/or pozzolanic reaction. The current study also established a similar trend. The data collected for the strength development of slag based concrete is given in Table 4.10 and visually depicted by Figure 4-17 and Figure 4-19. The former figure indicating the trends associated with the replacement of cement with GGCS and the latter with GGBS.

4. 9. 1. Reference (0 % Cement Replacement)

The reference strength profile shows typically a pattern that is associated with concrete strength development. At an early age of 3 days, the reference mixture achieved a strength of 23.1 MPa which increases to 42.0 MPa at 7 days. This is approximately equivalent to a strength gain of 19 MPa. In addition, as expected, the strength gain at later ages (56 and 91 days) is not as substantial as the majority of the hydration has occurred. The relatively high early age strength can be related to the fineness of the cement used as well as the strength classification. Moreover, upon investigating the particle size distribution, 26.8 % of the particles are less than 8 μm ; particles below this range are associated with early age hydration (Zhang & Napier-Munn, 1995). It is also estimated that 35.7 % of the particles exceed 20 μm , which is associated with later age strength development. The Bogue's composition of the PC also indicates a relatively higher percentage of C_3S (42.7 %) which is associated with early age strength development and explains the relatively high strength of 42 MPa at 7 days.

Table 4.10. The strength (MPa) of the GGCS and GGBS at different ages and cement replacement percentages.

	Cement Replacement (%)	Compressive Strength (MPa)				
		Age (Days)				
		3	7	28	56	91
Reference	0	23.1	42.0	55.2	60.9	62.7
GGCS	25	17.9	36.9	49.3	55.1	57.3
	50	11.5	32.8	42.5	51.7	48.8
	75	10.9	30.8	39.9	46.3	45.6
GGBS	25	21.1	31.1	48.1	49.8	63.0
	50	12.2	20.5	41.5	45.7	50.1
	75	7.0	17.3	32.8	38.9	42.7

4. 9. 2. The Effect of GGCS on Concrete Strength Development

The addition of GGCS is generally reported to improve concrete strength, even at early ages of hydration (Alexander et al., 2003; Beushausen et al., 2012). This is suggested to occur as a result of the differences in iron smelting processes; the process of iron production via the Corex production process yields a slag with a higher reactivity. The study at hand did find that the GGCS exhibits higher reactivity compared with GGBS, which is in agreement with the work of Alexander et al. (2003) and Beushausen et al. (2012). In addition, at 50 % cement substitution the optimum strength development is achieved (Alexander et al., 2003). However, the current study found the results not to corroborate with literature in terms of the strength development. The concrete strength did follow the typical strength development profile, yet the average strengths were reported to be less than the reference at all ages and

decreasing with percentage replacement (see Figure 4-17) and the statistically data is given in Appendix A (Table A.4).

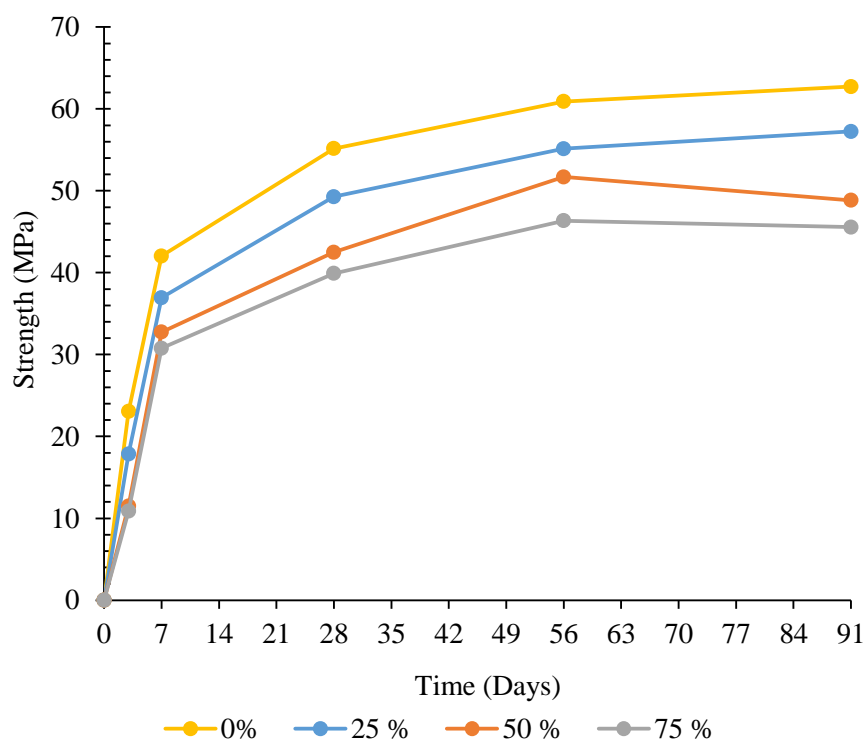


Figure 4-17. Strength development profile of GGCS at different partial cement percentages.

As mentioned, chemical composition of slag has an influence on the reactivity of the material and therefore a direct influence on the strength development. Further investigation of the slag sample used yielded that the composition of the slag used in this study is similar to that of previous investigations (Alexander et al., 2003; Otieno et al., 2014). The chemical composition of the slag used is good in terms of compounds that increase the reactivity of slag: MgO , CaO and Al_2O_3 . Also, the relative amount of silica (SiO_2) is low, which is associated with decreasing slag reactivity. The data presented in Table 4.2 is used to set up Figure 4-18 that demonstrates how the concentrations present are altered when GGCS replaces cement at substitutions from 0 to 100 %. The 0 % replacement represents a binder of only PC and the 100 % a binder consisting of only GGCS. However, this graph is only valid on two assumptions: (i) there is no error in sampling and (ii) that as a result of the previous mentioned, the material composition remains constant.

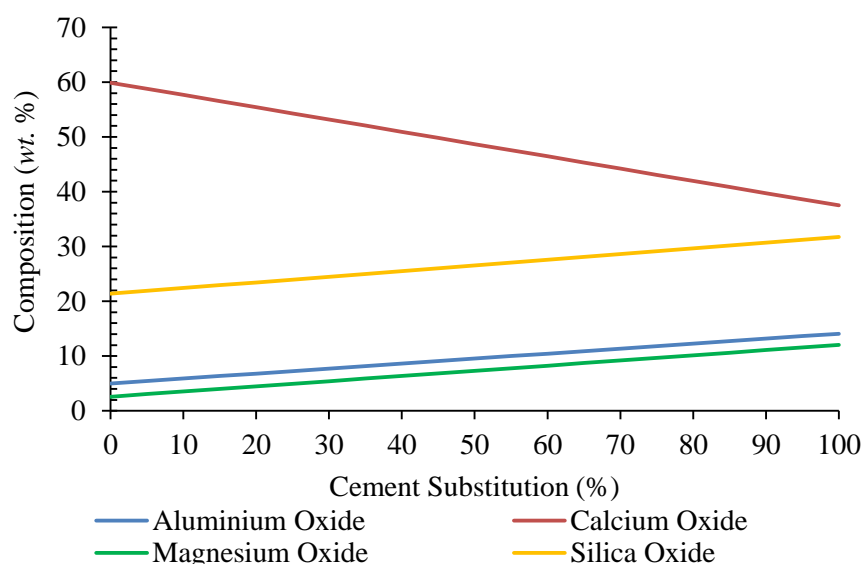


Figure 4-18. The representation of the changes in the chemical compounds present with continual substitution with GGCS.

As seen, the trend displays an increase in two reactivity-enhancing constituents, namely MgO and Al₂O₃ at gradients of 9.4 and 9.1 % respectively. In addition, the SiO₂, which decreases reactivity, increases with a similar gradient of 10.4 %. The effect on the CaO is almost twofold (gradient of 22.4 %); however, the CaO is decreasing which is not favourable in terms of slag reactivity. This trend in the components affecting the reactivity of slag can be suggested as the cause for the reduction in strength with increasing cement substitution. Due to the dilution effect, there is arguably a reduction and or delay in the establishment of a substantially higher alkaline environment. The environment should however only have an impact on the early ages, therefore explaining the decrease in early age strengths (less than 7 days).

In terms of the substitution levels, it is apparent that the early age difference in strength is not as significant at early ages; the differences are less than 10 MPa. This is suggested to be a result of the dilution of hydration products. Moreover, GGCS is suggested to react slower compared to the usual reported norm (Alexander et al., 2003; Beushausen et al., 2012). Even though the GGCS based mixes do not achieve or exceed the reference mix for the given replacements and ages, it is suggested that the given data can be used to establish a prediction model and estimate the expected time period at which the hydration of slag based materials may achieve, or even exceed that of the reference mix. It can be seen from Figure 4-17 that the strength difference amongst the mixes are gradually decreasing with the reported ages. However, there is an inexplicable decrease in strength for the 50 % GGCS based mix between the ages of 56 and 91 days. The reduced strength is not a true representative of the mix, and a prediction value of approximately 57 MPa is estimated to be the true strength for the given mix by visual inspection. The reduction in strength is most possibly as a result of poor sampling, and/or poor compaction. The standard deviation and coefficient of variation of testing at 56 days also proved to be

the highest in the 50 % GGCS series, in addition to the entire compressive strength investigation, at 4.24 MPa and 8.20 %, respectively.

As stated, the results obtained from the study (when considering GGCS) is not in agreement with typical studies using GGCS. Alexander et al. (2003) and the Beushausen et al. (2012) found that the use of GGCS to increase concrete strength, even surpassing that of the reference. The complete reason behind the reduced performance is not fully understood, yet it is suspected to be as a result of a *bad* batch being used to conduct the study or a possible interference in the slag-cement system that hinders the slag hydration. In addition, the test was repeated with a *new* batch of slag and a new reference, of which the data is provided in Appendix A, Table A-2 and Figure A-6. The results of the second set of tests yielded similar results, for both the reference concrete and slag based concrete. Hence, the notion of errors in sampling and mixing procedures (such as weighing off) can be stated to be invalid. Moreover, the strength results of mixes used to determine other parameters, such as shrinkage, also show similar results (Table A-4). Nonetheless, the results of the GGCS based mixes are still sufficient and comparable to that of the reference concrete.

4. 9. 3. The Effect of GGBS on Concrete Strength Development

The use of GGBS is associated with low early age strengths and improvement with age. The GGBS samples also performed relatively well compared to the reference. Similar to the GGCS based concrete mixes, increasing the amount of cement with slag does increase lead to a decrease in concrete strength; this is due to the dilution effect that GGBS has on concrete. The 25 % GGBS samples performed better compared to the 50 and 75% replacement levels. Between the 56 and 91 day a significant increase in strength was reported compared to the other substitution. The jump is suggested to be as a result of the pozzolanic reactions creating more hydration products during this time. However, in terms of the differences in strength development, the strength gain difference between the 25 and 75 % replacement levels seem to be significantly large; the difference is approximately 14.8 MPa between each age of testing. This highlights the reduced hydraulic capacity of GGBS in concrete with large replacement levels. However, the strengths obtained at 75 % cement replacement is still significant and can be implemented in construction projects.

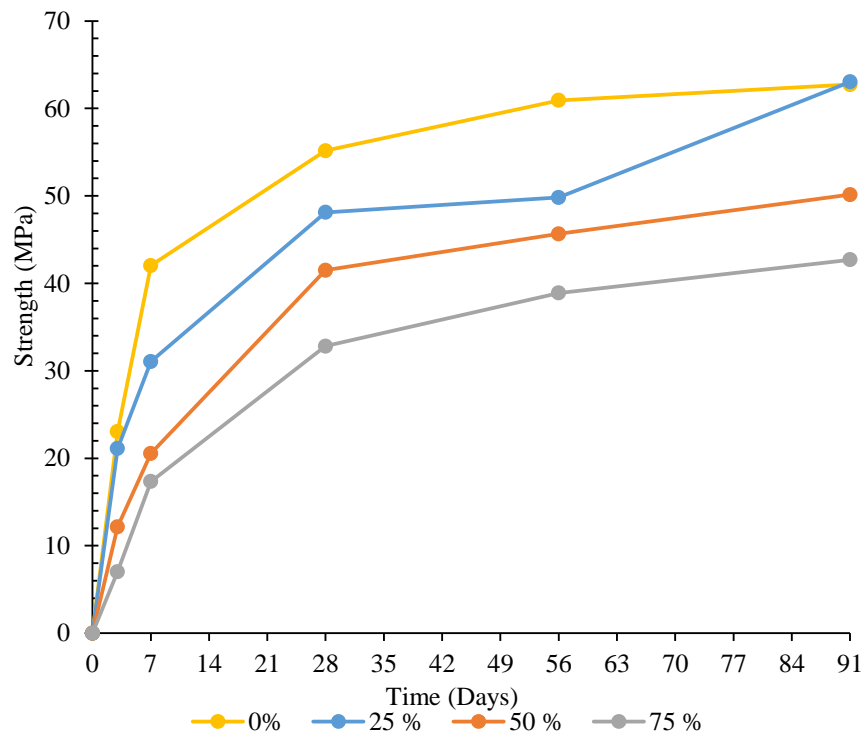


Figure 4-19. Strength development profile of GGBS at different partial cement percentages.

The effect of chemical composition is also important to evaluate when considering the strength development of GGBS-based concrete. The gradients for CaO, MgO, Al₂O₃ and SiO₂ are -26.48, 6.33, 8.75 and 15.81 %, respectively (Figure 4-20). Hence, the increase in compounds reducing reactivity are relatively high, as is the reduction of CaO, which enhances reactivity. Therefore, the influence of the composition provides a suggestion to the reason for reduced strength development with increasing substitution.

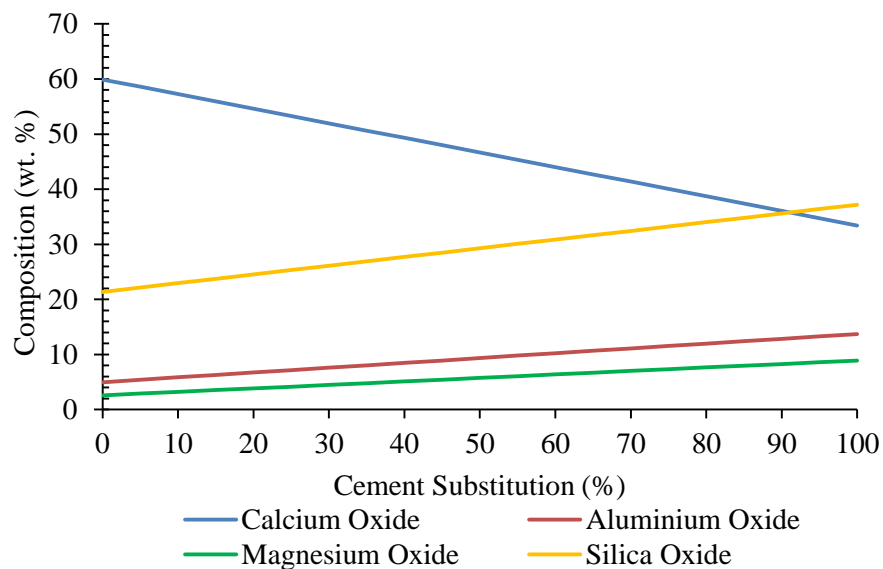


Figure 4-20. The representation of the changes in the chemical compounds present with continual substitution with GGBS.

4. 9. 4. The Relation between the SAI and Concrete Strength

The SAI (as previously discussed) gives an indication of the likely performance and use of slag within concrete. Moreover, research into the activation of slag, alkali-activated slags to be specific, can also be considered as a way to utilise slags of low reactivity. For this study, a relatively good correlation is established by investigating the relationship between the SAI (see Section 4.3) and the strength obtained at selected ages with 50 % replacement.

For example, looking at the GGCS samples, the SAI at 7 days is calculated to be 79.5 % for mortars and the strength index is 78.1 % for concrete samples at the same age of testing. At 28 days, the correlation is reduced; SAI and the strength index of concrete is 92.9 and 77.0 %, respectively. The concrete strength index is still higher than 75 % and could potentially be affected by the inclusion of coarse aggregates (stones). Nonetheless, for GGCS a relatively good correlation exists.

Based on the prediction of GGBS reactivity, a good correlation is established. The SAI at 7 and 28 days is 44.8 and 69.4 %, whereas the concrete strength index is 48.8 and 75.2 %. From the previous sections, the GGBS mortars were regarded to fail the standard requirements; even though the mortars did not meet the minimum requirement, it was established to be by a marginal percentage (less than 1 % in both instances). The GGBS samples do however exceed the minimum in terms of the percentages in concrete samples. Hence, the use of the GGBS still provides significant strength development and is suited for use in concrete.

4. 9. 5. The Comparison between GGBS and GGCS with Regard to Strength Development

Both the use of GGCS and GGBS, in terms of use in concrete, provide satisfying outcomes. Despite the GGCS not yielding expected results, the outcome is nonetheless sufficient for it to be used in concrete. In terms of general strength at respected ages, and the rate of development, the GGCS out performs the GGBS. This could be expected when considering the data obtained from the sections on reactivity and the properties. In all instances of measuring the potential performance of the two materials, the GGCS displayed favourable results.

The chemical composition (Table 4.2), and the associated indicators of reactivity that can be calculated from it (Table 4.4), the GGCS displayed higher levels of reactivity; hence, the use of GGCS in concrete is expected to have superior performance levels compared to GGBS. Even the reactivity determined from by the SAI showed a good correlation with the result from the concrete specimens.

In terms of the substitution level, is observed that at the same replacement level, the difference in strengths start to diminish. The demising effect can be explained by the pozzolanic reactions also contributing to the hydration, hence creating more structurally stable products. In other words, there is a gradual transformation of *weaker* CH into more stable and *stronger* C-S-H. However, at 75 % replacement, the GGCS sample has strengths significantly higher than the GGBS sample. The data of

25 and 75 % replacement is found in Appendix A, Figure A-5 and Figure A-6, respectively. Figure 4-21 provides to serve as an example of the strength differences at 50 % replacement.

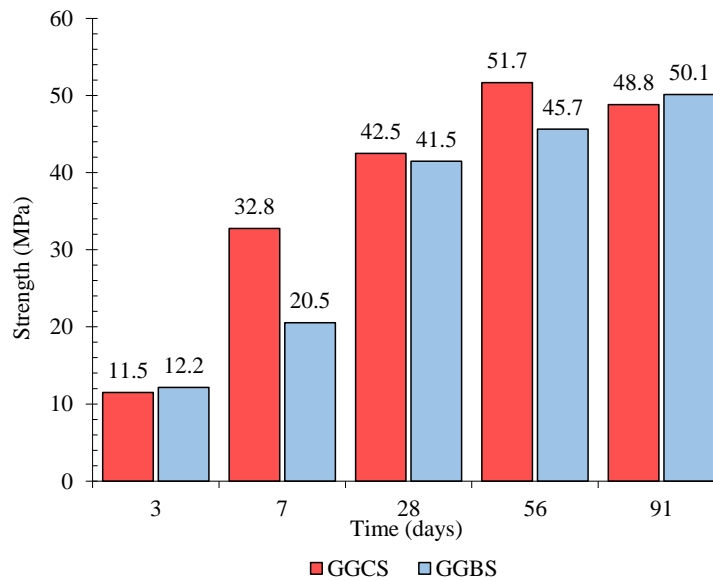


Figure 4-21. Strength development profile of GGBS and GGCS of 50 % cement replacement.

At three days, the GGBS samples exhibit higher strengths compared with the GGCS. The improved early age strength is suggested to be a result of the filler effect. The GGBS has a particle span of 3.3 which is related to a greater particle range i.e. improved packing capacity. The GGCS has a span of 2.6 and the PC 2.2. Moreover, at 75 % the GGCS exceeds the GGBS strength at 3 days. This could be explained by the possibility of the particle packing being disturbed by the increased amount of fines present. From the literature study, there is a hypothesis that slag particles less than 3 μm improve the early age strength. For the two samples used in this study, the percentage of particles less than 3 μm is found to be 10.7 and 11.0 % for GGCS and GGBS, respectively. Hence, the effect of the smaller particles can be suggested not to have an influence on the early age strength in this study due to the marginal difference.

4. 9. 6. Concluding Remarks

The results of the use of slag exhibited properties known and expected, to a certain degree, of SCM-based concrete, namely, a reduction of the early age strength, increasing in effect with the increase in cement substitution. However, the effect of the reduced strength diminished with the increase of curing periods. The GGCS-based concrete also displayed a relatively better strength development profile compared to the GGBS-based samples. The differences in slag composition, and inadvertently the difference in reactivity, are suggested reason for the noted differences. In addition, the dilution effect was noted to be a governing factor for the reduced strength development. Nonetheless, both types of slag depicted good strength development when used in concrete, hereby proving slag can be used as a sufficient means to reduce the cement content in construction projects, given that the concrete is designed properly and efficiently.

4. 10. Indirect Tensile Strength

The tensile strength of concrete is generally not considered in the design of structural elements, which is an area for improvement. Studies are typically done on the effects of the environment or method of testing, with a small area of focus on the effect of slag on the tensile strength. The indirect tensile strength was determined at three ages of testing and three slag substitution levels. The results obtained from the study is visually depicted in Figure 4-22. From the figure, it can be seen that the tensile strength increases with time, yet decreases with cement substitution.

4. 10. 1. The Effect of a Neat Concrete (0 % SCMs) on the Indirect Tensile Strength

As with compressive strength, the tensile strength of concrete also increases with time. The reference concrete mix exhibited an increasing trend in tensile strength; the tensile strengths were recorded to be 3.89, 4.60 and 4.83 MPa at ages of 7, 28 and 56 days of water curing. The increase in tensile strength was the greatest between the 7 and 28 day measurements (0.71 MPa increase). The increments were slower compared to the compressive strength development. However, the tensile strength of concrete is known to be substantially lower compared to that of the compressive strength; the tensile strength is approximated to be 10 % of the compressive strength. The slower development can be explained by the interactions occurring at the ITZ. At the ITZ there exists a higher water-to-binder ratio as well a more porous system due to the wall effect. Hence, the strength of at the interface is not as developed and creates a region of significant weakness.

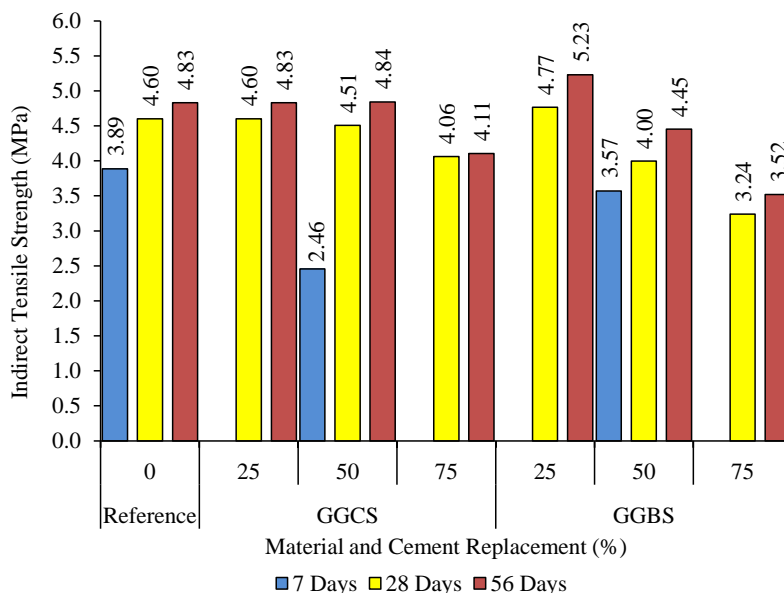


Figure 4-22. Indirect tensile strength of concrete mixes incorporating GGCS and GGBS.

Figure 4-23, gives the ratio between the indirect tensile and compressive strength. It is observed that the gradual drop in ratio is evident, suggesting that even though the compressive strength is increasing, the rate of strength gain in terms of tensile capacity is not as apparent.

4. 10. 2. The Effect of GGCS on the Indirect Tensile Strength

The use of GGCS reduced the indirect tensile strength of concrete with the increase in percentage of GGCS, except for the 25% that yield the same tensile capacity as the reference. The most significant reduction in tensile strength was noted to occur at 7 days of testing; a reduction in the tensile strength of 1.43 MPa was recorded at a 50% replacement. This approximates to almost three times higher reduction compared to any other age. At later ages and all replacements, the recorded reduction is not more than 0.54 MPa.

The low strength at early ages can be explained by the lack of hydration products formed during the initial 7 days. For that reason, the ITZ cannot develop the required, or rather increased, resistance to achieve the same strength as the reference. The improvement in tensile strength with age, for all replacement levels, however denote the improvement in both the ITZ and the increasing amount of hydration products formed by the secondary reactions. This is in line with the findings of Hooton (2000). Likewise, the fact that the 25% replacement level yielded similar results as the reference is indicative of the PC having a more pronounced impact compared to the GGCS.

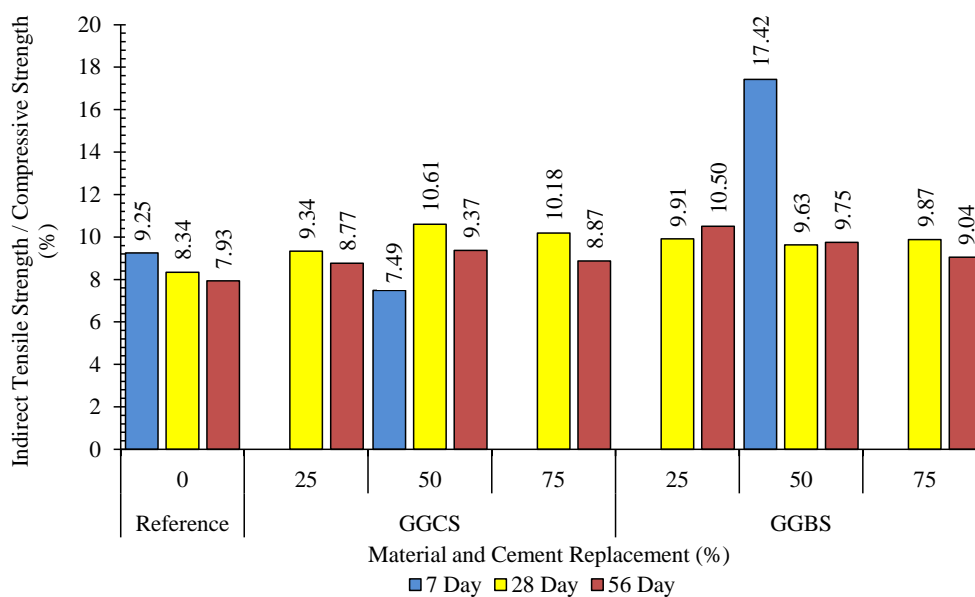


Figure 4-23. The ratio of the indirect tensile strength and the compressive strength for the different slags used at different replacement percentages.

Comparing the ratio of tensile-to-compressive strength, it can be seen from Figure 4-23, that the mentioned ratio exceeds that of the reference. This is noted at all ages of testing as well as for all replacement levels; an exception is the 50% replacement level at 7 days of testing, which recorded a lower ratio. Hence, it is evident that the addition of GGCS provides an improvement in tensile strength when compared to the actual strength of the specimen. Also, the mixture with a 50% GGCS content showed the optimal ratio at both 28 and 56 days of testing (10.61 and 9.37%, respectively). The optimum ratio at 50% cement replacement corroborates the findings of Aldea et al. (2000), Berndt (2009) and Nazari and Riahi (2011), who also reported 50% to yield optimum slag replacement levels

in terms of tensile strength. This is suggestive to be a result of the improved particle packing and significant improvement in the ITZ.

4. 10. 3. The Effect of GGBS on the Indirect Tensile Strength

The addition of GGBS displayed a similar trend as that of GGCS. Firstly, the tensile capacity at 7 days testing for 50 % was lower compared to the reference. This is most likely due to dilution being a governing factor at this early age. Moreover, the increase in replacement of PC with GGBS does display a reduction in tensile strength at all ages, which was also reported by Li et al. (2011). In addition, at constant replacement levels, the tensile strength does increase with increasing curing times. The reason being that the hydration process continues and therefore improves the IT.

When investigating the tensile-to-compressive strength ratios (Figure 4-23), the addition of GGBS proves beneficial. This is again related to a high tensile strength obtained relative to the compressive capacity. The largest ratio was achieved for 50 % replacement at 7 days testing. Interestingly, this sample however yielded the lowest tensile capacity. Yet, if one looks at the proportion of the tensile strength relative to the compressive capacity, it is significantly better. The reduced reactivity of the GGBS, compared to the reactivity of GGCS, provides an explanation for the results obtained.

For the GGBS samples, the optimum, for both the tensile strength and proportion of it relative to the compressive strength, the 25 % substitution yielded the optimum. This is most likely as a result of the greater span of the particles present in the GGBS, hence improving the particle packing. Similarly, Arivalagan (2014) reported that 25 % slag yielded the optimum. However, researchers such as Aldea et al. (2000), Berndt (2009) and Nazari and Riahi (2011) found the optimum to be at 50 % cement replacement. The differences in particle size distribution and chemical differences are reasoned to explain the observed differences.

4. 10. 4. The Comparison of GGBS and GGCS on the Indirect Tensile Strength

As mentioned, both types of slag displayed a similar trend in terms of the effect of substitution and curing on the tensile strength. Firstly, both samples displayed a similar trend in the decrease of the 7 day tensile strength; the GGCS yielding a greater reduction in comparison to the GGBS sample. From a particle packing perspective, the GGBS has a greater span and therefore arguably has a better particle packing. Therefore, the filler effect may be significant at early ages for improvement of the tensile strength.

For 25 % cement replacement, both samples resulted in similar, in the case of GGCS, or higher, for GGBS, tensile strengths in comparison to the reference. The reason for this may be the higher levels of cementing particles, providing a substantial amount of hydration products (C-S-H), and pozzolanic reactions, in conjunction with the improvement in particle packing; thereby, leading to the refinement of the ITZ. However, the increase in slag percentage did cause a reduction in tensile strength with increasing replacement percentages for both slags. Taking the latter into account, it is seen that the

GGCS yields higher tensile strengths for all replacement levels and curing ages; exceptions are the 25 % replacement level and the 7 day testing. The greater tensile capacity is suggested to be due to the higher reactivity of GGCS compared to that of the GGBS.

Likewise, increasing the curing period for both slags and at all replacement levels proved beneficial in terms of tensile strength, as stated by Aldea et al. (2000). The increase in indirect tensile strength is due to the hydration process being promoted, in addition to the consumption of CH and replacing it with C-S-H.

4. 10. 5. Concluding Remarks

The addition of slag causes a subsequent decrease in the tensile strength of concrete due to dilution and the delay of the pozzolanic reaction. When investigating the ratio of the tensile strength to the compressive strength, it can be noted that the inclusion of slag, either GGBS or GGCS, proves to improve the tensile strength gained per unit of compressive strength. Hence, the use of slag is quite beneficial in the use of concrete to increase the tensile strength. Moreover, in terms of construction purposes, designing a slag-based concrete mix on a strength basis is likely to yield an overall improvement in the tensile strength, and can most likely exceed that of an equivalent reference mixture.

4. 11. Flexural Strength

The 28 day modulus of rupture results are given in Table 4.11 and are the same as the previous section's results: the incorporation of slag improves tensile strength and therefore also the ITZ. Moreover, the results obtained from the flexural data is also higher than the indirect tensile splitting strength and it is advised to take this into account when including SCMs in the design process. This is in conjunction with the research undertaken by Oluokan (1991) and Oluokan et al. (1991), which found the flexural strength to overestimate the tensile strength. Hence, the flexural strength may overestimate the capacity of concrete containing SCMs, yet it does however display the improvement on the ITZ as a result of the inclusion of slag. Nonetheless, caution is advised when using the flexural strength as an indicator and more research into the observed differences may be beneficial.

Table 4.11. The flexural strength of slag samples.

Material	Slag (%)	Flexural Strength (MPa)	Flexural Strength / Indirect Tensile Strength	Compressive Strength (MPa)	Flexural Strength / Compressive Strength
PC	0	5.3	1.15	55.7	0.095
GGBS	25	5.5	1.15	43.5	0.126
GGCS	50	5.9	1.31	46.3	0.127

4. 12. Secant Modulus

The secant modulus of three mixes was determined and is given in Table 4.12. The secant modulus of the reference was similar in terms of numerical values as the cylinder strength, only the magnitude is different, i.e the secant modulus is approximately a thousand times greater than the compressive

strength. The use of 50 % GGCS displays a higher elastic modulus compared to the reference. In addition, there is a considerable difference between the cylinder strength and the elastic modulus unlike the reference. The GGBS mix only had 25 % replacement and had a similar numerical value for the elastic modulus and the cylinder strength with only the magnitude differing: 36.7 GPa and 34.2 MPa, respectively.

Table 4.12. Secant modulus for concrete containing different types of slag.

	Reference	GGCS	GGBS
Replacement (%)	0	50	25
Cube Strength (MPa)	51.9	43.2	47.3
Cylinder Strength (MPa)	37.4	31.4	34.2
Cylinder:Cube Strength	0.72	0.73	0.72
Secant Modulus (GPa)	37.5	40.0	36.7

Based on the prediction models discussed in the literature survey, the models given as per BS EN 1992 (2004) and the CEB-FIP (1993) respectively, were found to give the lowest percentage error when used to assess the secant modulus of the concrete samples i.e. Equation 2.21 and Table 2.8, respectively. Furthermore, these models are used to predict the elasticity of the concrete at other substitutions not given in Table 4.12. The results are given in Table 4.13. The calculation can be found for reference in Appendix A.

Table 4.13. The predicted elastic modulus for slag based concrete.

% Replacement	PC	GGCS			GGBS		
	0	25	50	75	25	50	75
Cube Strength (MPa)	55.2	48.1	41.5	32.8	49.3	42.5	39.9
CEB-FIP (GPa)	39.8	38.3	36.7	34.4	38.6	37.0	36.3
BS EN 1992 (GPa)	38.3	36.9	35.5	33.5	37.1	35.8	35.2

In all instances, an increase in slag causes a consequent decrease in the stiffness of the material based on the two prediction models. However, there is cause to suggest that these models do not account for the material properties on a micro-level. The establishments of these models are somewhat associated with the coarse aggregate having the greatest influence on the elastic properties. In addition, as these models only directly require cube strength, it stands to reason that a decrease in strength would result in a subsequent reduction in the elastic modulus.

4. 13. Drying Shrinkage

The drying shrinkage gives an indication of the strain induced on a specimen as a result of moisture loss. This section discusses the effect that the different types of slag have on the overall mass loss and associated strain. This is compared with a reference to distinguish what the possible influences can be of using slag in a concrete mix as well as identifying any potential benefits and pitfalls. In the literature study, it was shown that the drying shrinkage of concrete containing slag, produced varied results. There are studies that found that slag had no influence (Alexander et al.,2003), increased the drying

shrinkage (Prusinski (2006), Siddique and Kahn (2011)), or decreased the drying shrinkage (Dellinghausen et al. (2012)).

4. 13. 1. The Typical Drying Shrinkage of SCMs-free Concrete

For this study the reference mix (0 % slag) has an ultimate shrinkage strain of 362 μm at 137 days after curing. At this age, the mass cumulative mass loss was recorded to be 1.88 %. The drying shrinkage of the 0 % SCM based concrete mixture has a steep volume reduction in ages up to 14 days. This is reflected by both the cumulative mass loss and drying shrinkage. For instance, the strain after one day is approximately 61.67 $\mu\text{m}/\text{m}$ and increases by a factor of approximately 2 and 3 at ages of 4 and 7 days, respectively. From this point onwards, the shrinkage reduces to a gradual slope. The maximum strain was determined at 56 days with a strain of 423 $\mu\text{m}/\text{m}$. After this point the shrinkage was observed to reduce, indicative of swelling occurring; in addition, the mass loss also increased until 91 day and a drop is indicated at the final age reading of 137 days. The environmental factors were not recorded throughout the experiment and it is suggested that these parameters may have had a potential contribution on the readings. For instance, an increase in the relative humidity may have caused the specimens to absorb water at the noted age. In addition, the mass loss has stabilised after 91 days, yet the drying shrinkage displayed signs of stabilisation at an early age of 28 days.

4. 13. 2. The Effect of GGCS on Drying Shrinkage

Concrete containing GGCS has a similar profile, in terms of mass loss and drying shrinkage, as the reference (see Figure 4-24 and 4-27). From Figure 4-24, it can be seen that the increase in slag content causes a consequent reduction in mass loss. The 25 % replacement had a similar ultimate mass loss compared with the reference, 1.73 and 1.88 % respectively, however, the mass loss at 50 % cement substitution was 1.30 %; this is 0.50 % less than the reference. In addition, the mass loss of the GGCS and reference are approximately similar up to 7 days after wet curing, at which point the 50 % GGCS sample has a lower rate of mass loss compared to the reference.

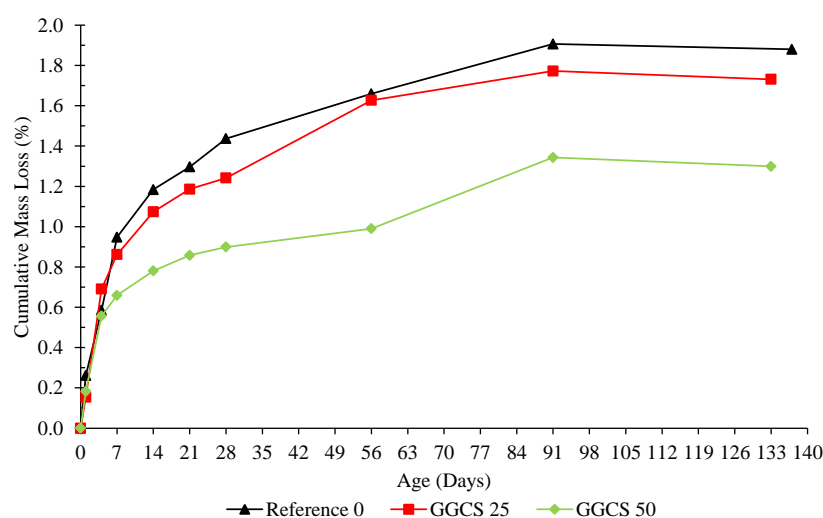


Figure 4-24. The cumulative mass loss of GGCS specimens at 0, 25 and 50 % cement replacement.

The increased substitution of cement with GGCS has the effect of increasing the ultimate drying shrinkage, which can be seen in Figure 4-25 and is recorded for all ages of shrinkages. Notably, the drying shrinkage of GGCS-based concrete initially had a steeper slope up to 14 days of testing and smoothens to reach a plateau from 28 days of testing onward.

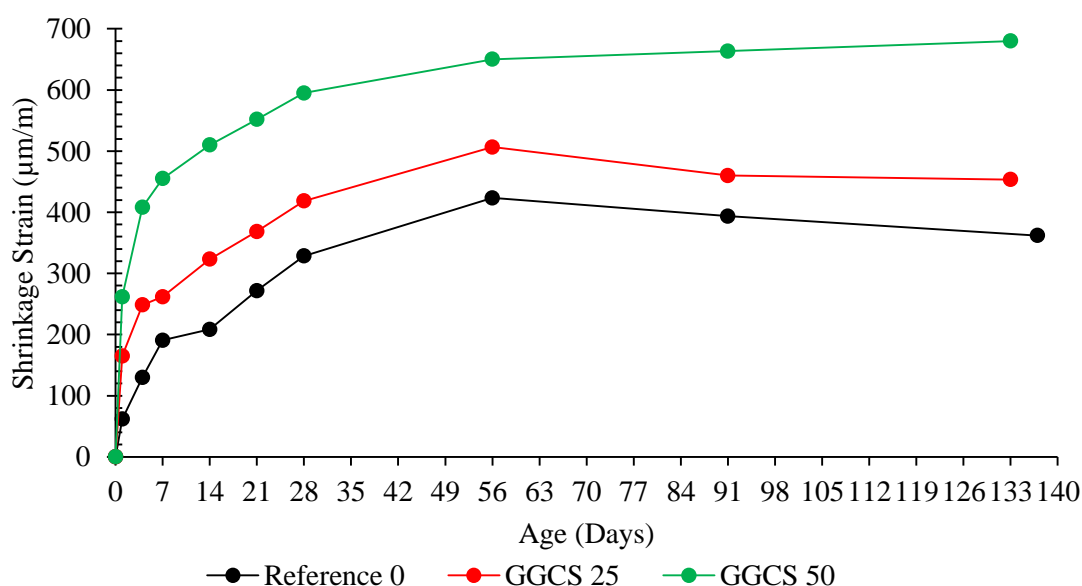


Figure 4-25. The drying shrinkage of GGCS specimens at 0, 25 and 50 % cement replacement.

Therefore, even though the total moisture evaporating from the system is relatively low, the associated shrinkage is relatively large, as shown in Figure 4-26. From Figure 4-26 it is apparent that the gradient of slag based concretes are relatively steeper than the reference's slope and increases with increasing slag replacement. For instance, at the same percentage mass loss, the samples with slag would exhibit a greater degree of shrinkage.

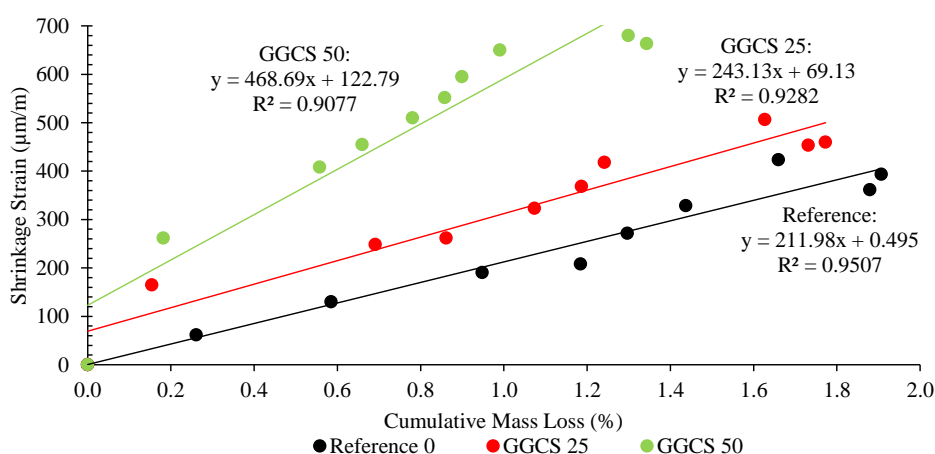


Figure 4-26. The plot of the mass loss vs shrinkage for concrete containing GGCS.

Aly and Sanjayan (2008) conducted research on the early age shrinkage of concrete, cured for 1 and 7 days. In general, the consensus is that increased water losses may induce the subsequent reduction in volume. However, the findings of the current research and the former mentioned research are in agreement that a lower moisture loss is not indicative of a lower degree of drying shrinkage. However,

the results (Figure 4-26) suggests that the increase in paste volume and pore refinement plays a subsequent role in the drying shrinkage.

The two factors, namely pore refinement and increased paste volume, work in tandem. Due the improved pore structure, there is arguably a net increase in the amount of critical pores in a system containing the GGCS. As shown in Figure 4-15, the inclusion of slag resulted in the increase in pores finer and equal to 1 mm, whereas the reference had a smaller count of pores less than 1 mm in size. Therefore, with a higher number of critical pores present, the loss in moisture could inevitable cause the increased degree of shrinkage. Similarly, Dellinghausen et al. (2012) found that the drying shrinkage is influenced by the mesopores (0.001 – 0.025 μm), which further supports the notion of microstructure refinement increasing the drying shrinkage.

However, with reference to the earlier mentioned increase in paste content, Hooton et al. (2004) state that unhydrated binder particles provide a means of internal restraint in a paste constituency. Hence, an increase in paste volume does not fully relate to an increase in C-S-H gel, which is the main component that instigates the drying shrinkage mechanism. The average 28 day compressive strength (Table A.9), of the 0, 25 and 50 % GGCS concrete mixes were 50.5, 47.8 and 50.2 MPa, respectively. The variation in strength can potentially relate to the notion of the 50 % GGCS-based mix to have an increase volume of paste as well as a higher degree of hydration. Therefore, more water can escape the gel and increase the shrinkage. In addition, with the associated finer pores, the effect of capillary tension potentially causes the magnification of the effect in shrinkage.

4. 13. 3. The Effect of GGBS on Drying Shrinkage

The concrete containing GGBS behaved similar to the reference (see Figure 4-27 and Figure 4-28). The mass loss was similar to that of the 25 % GGBS sample, which had the same cumulative mass loss at 133 days (1.88 %); the 50 % GGBS sample had a slightly higher mass loss of 1.93 %. The GGBS samples have an initial higher drying shrinkage compared to the reference, yet the samples stabilised at 28 days and have a profile in line with that of the reference. The ultimate shrinkage of the GGBS samples are 378 and 355 $\mu\text{m}/\text{m}$ for the respective replacements of 25 and 50 %. In addition, higher shrinkage values were observed at other ages compared to the final age. This can be seen in Figure 4-28. The highest recorded value was 455 $\mu\text{m}/\text{m}$ for the 25 % GGBS at 91 days and 440 $\mu\text{m}/\text{m}$ for the 50 % replacement and occurred at the same age.

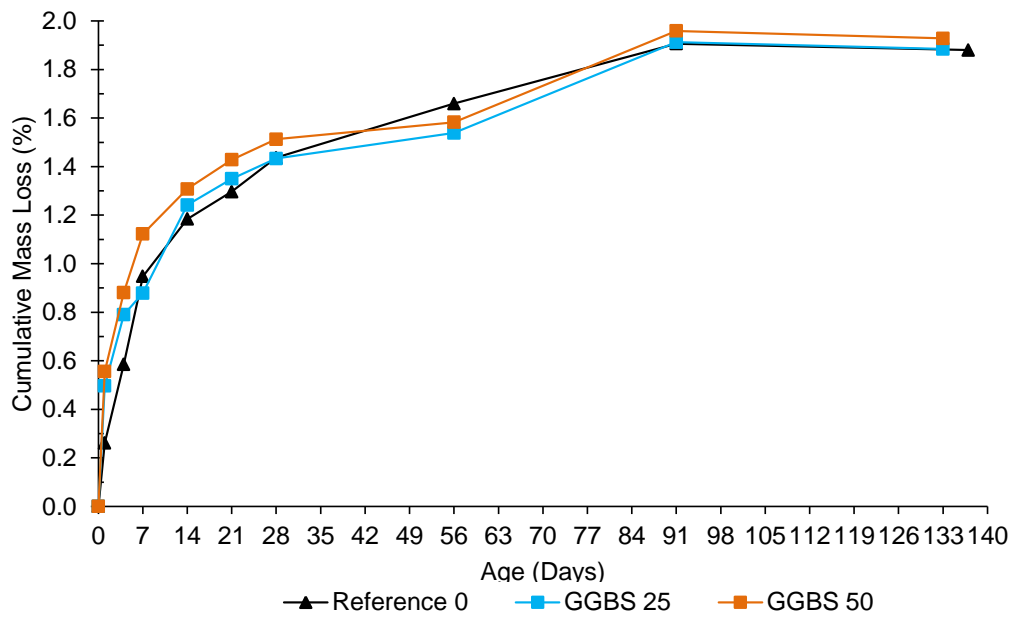


Figure 4-27. The cumulative mass loss of GGBS specimens at 0, 25 and 50 % cement replacement.

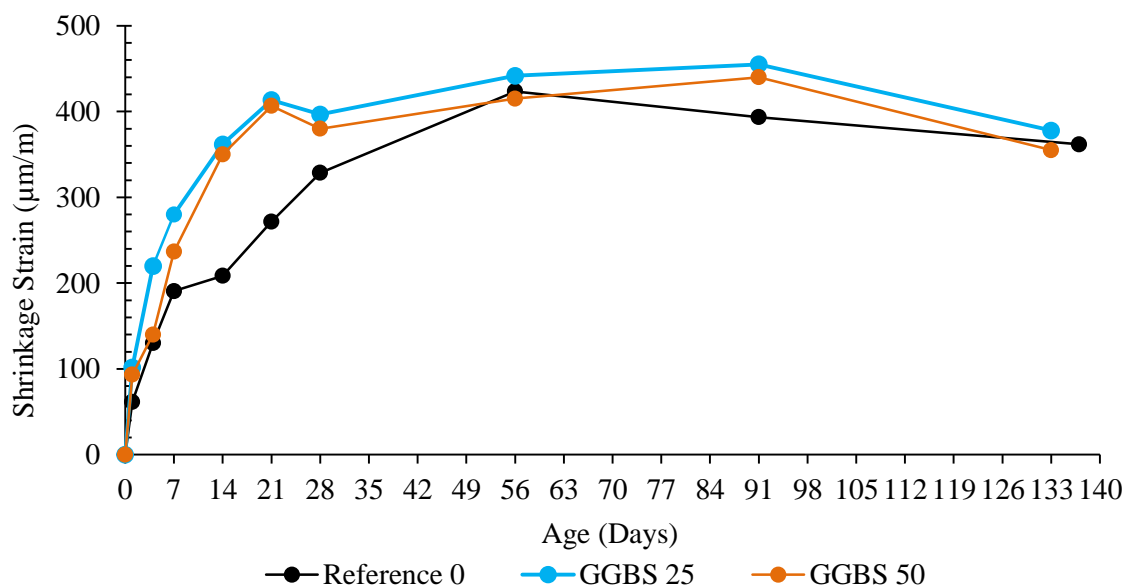


Figure 4-28. The drying shrinkage of GGBS specimens at 0, 25 and 50 % cement replacement.

The gradient of the shrinkage per mass loss of the three mixes are very similar when imposing a simple trend line on the data. This further supports the observed notion of the concrete mixtures yielding similar results: as the same mass loss yields near similar shrinkage. The trend between the mass loss and shrinkage can be seen in Figure 4-29.

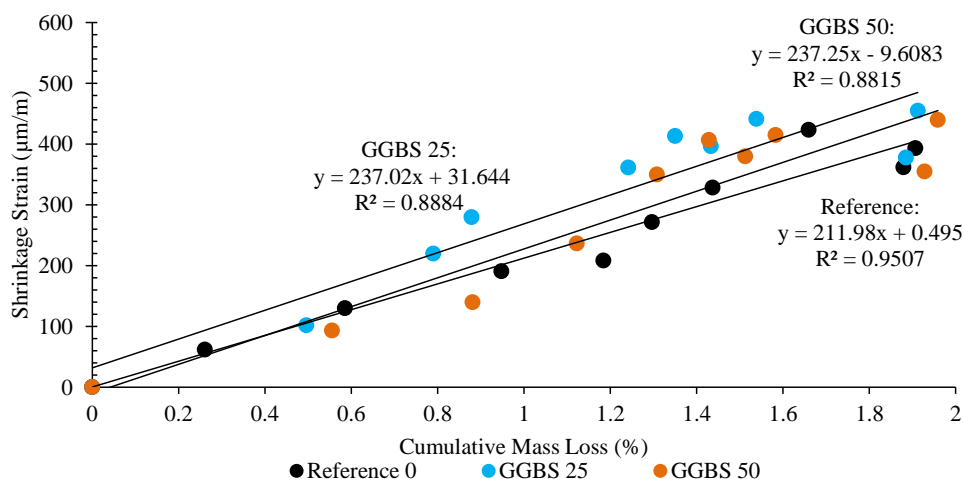


Figure 4-29. The plot of the mass loss vs shrinkage for concrete containing GGBS.

Even though the GGBS-based concrete had higher shrinkage values, these values are still comparatively the same as that of the reference. This is in agreement with the research undertaken by Bouzoubaa and Foo (2004) and Hooton et al. (2004). The similarity in shrinkage for both the 25 and 50 % cement replacements can be explained by the similarity in the pore structure (Figure 4-15). However, the fact that the GGBS-based concrete, with a higher degree of pore refinement, is approximately equivalent to the reference, is in contradiction with the previously discussed theory of capillary tension, as found by Aly and Sanjayan (2008).

The shrinkage of the GGBS-based concrete is higher than that of the reference up to 28 days of testing. This could be due to the increased porosity at early ages, therefore resulting in a higher percentage of critical pores. However, the drying shrinkage of concrete is affected by paste volume and the associated elasticity. Hence, the addition of GGBS causes a subsequent increase in paste volume, which arguably has a lower elasticity at early ages. Therefore, the higher porosity, in conjunction with the increased paste and lower elasticity causes the GGBS based mixes to exhibit higher early age shrinkage compared to the reference. At 28 days, the elastic modulus of the GGBS-based mix is equivalent to that of the control. From this point onward, the two materials (GGBS-based and control) have similar elasticity which leads to the noted convergence of ultimate shrinkage values.

4.13.4. Comparing the Drying Shrinkage Performance of GGBS and GGCS

The addition of slag, regardless of type, exhibited trends of decreased mass loss and increased shrinkage. The current study shows how the use of low levels of slag do not affect the shrinkage largely. The inclusion of GGBS did not exhibit any noticeable change in shrinkage compared to the reference, whereas the use of GGCS increased the shrinkage with an increase in the cement replacement; a significant increase in the shrinkage is noted at 50 % substitution with GGCS (Figure 4-25 and Figure 4-31). The graphical comparison of mixes of 25 % GGBS and GGCS, at same replacement levels, can be found in Appendix A.

It is evident that the mechanisms causing the slight increase in drying shrinkage of the slag-based mixes include: microstructure refinement, increased volume of paste, unhydrated cement present and the slight reduction in the elastic modulus. The effect of the coarse aggregate can be regarded as negligible when comparing the mixes relative to each other. The proportion of stones (35.6 %) remained at a constant volume percentage, therefore the influence of the restraint provided by the coarse aggregate remains the same for all mixes. In addition, the early age shrinkage of the slag based concrete is higher than that of the reference and is suggested to be due to the high early age porosity and lower strength, which can also result in lower paste elasticity. Hence, the slag based concrete has a lower elasticity at early ages.

The concrete mixture containing 50 % GGCS did show the largest drying shrinkage and as well as the lowest mass loss. The deviations can clearly be seen in Figure 4-24 to 4-27 when comparing the effect of slag percentage and Figure 4-31 to 4-33 when the type of slag is compared. The results found do not corroborate with pattern associated with the rest of the slag-based mixes. Even more so, the effect of the mechanisms influencing the shrinkage, such as pore refinement and the increase in paste volume, do not hold for the 50 % GGCS sample. Moreover, the secant modulus of the 50 % GGCS-based mix was higher than the reference (40.0 GPa and 37.5 GPa, respectively), despite prediction models estimating it to be lower (35.5 GPa). On closer inspection of the early age shrinkage of the mixes (Figure 4-31), the shrinkage of this mixture already exceeds that of the reference by a substantial degree. Within the first week, the shrinkage of the 50 % GGCS sample is approximately double that of the reference. It is therefore suggested that at early age the effect of the lowered porosity and decreased strength, in conjunction with the lower modulus of elasticity, has the biggest influence on the shrinkage behaviour.

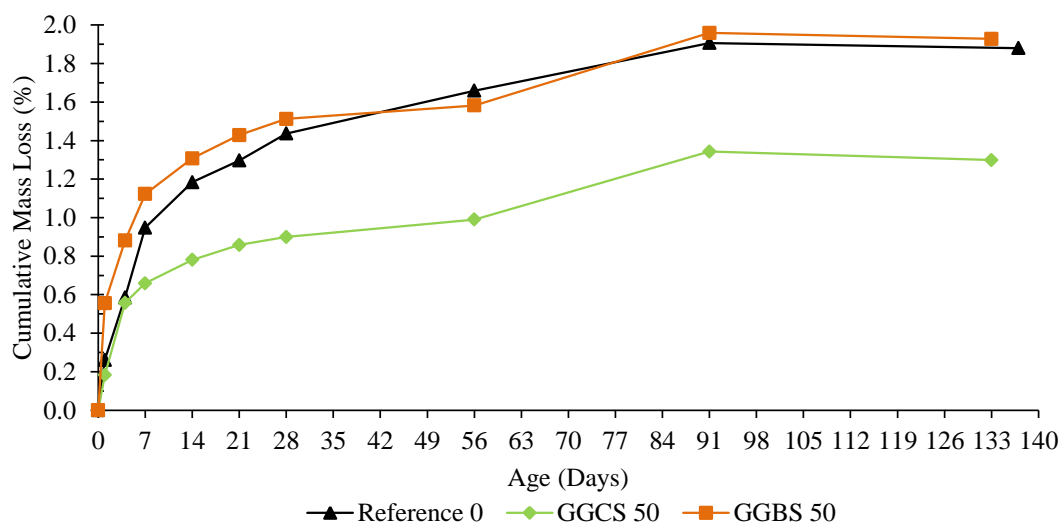


Figure 4-30. The cumulative mass loss of slag samples at 50 % cements replacement.

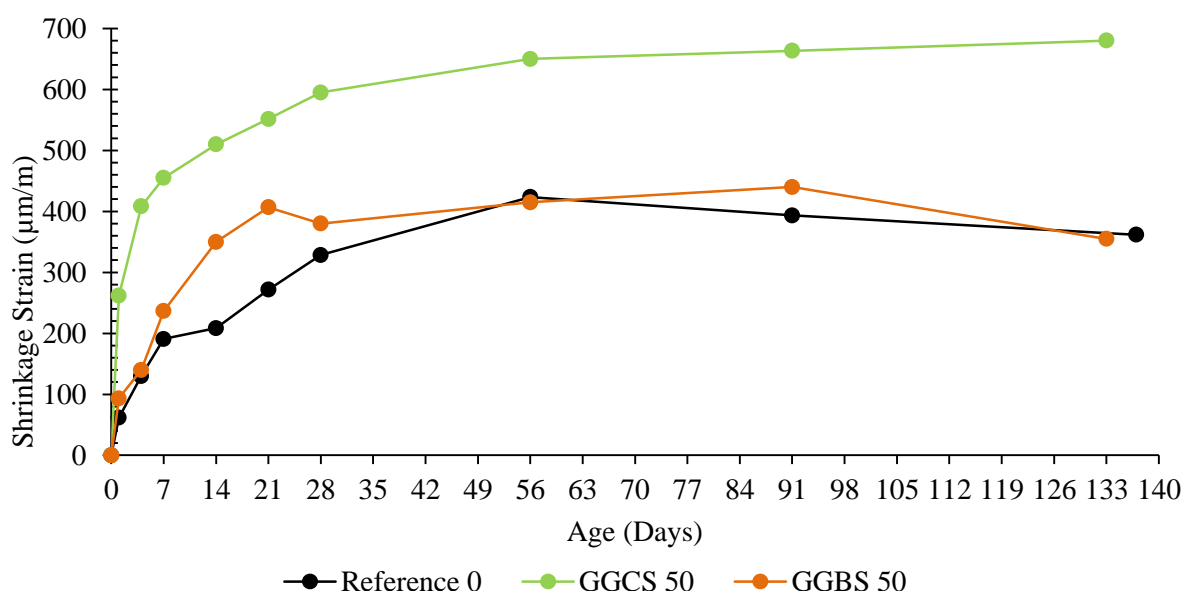


Figure 4-31. The drying shrinkage of slag samples at 50 % cement replacement.

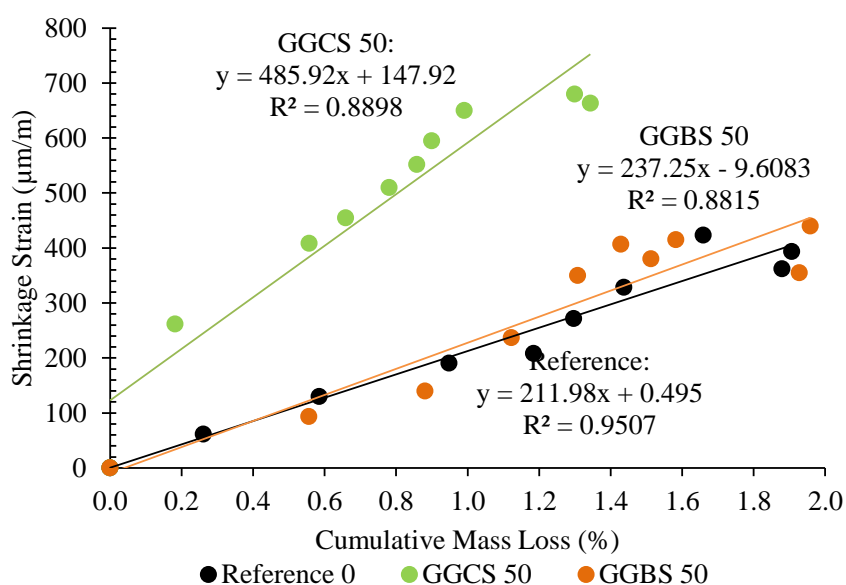


Figure 4-32. Mass loss vs shrinkage strain as a function of replacement level of 50 %.

4. 13. 5. Concluding Remarks

The shrinkage of concrete due to drying can be an issue of concern, especially in elements with relatively large surface areas exposed to the environment, such as slabs. Large values of shrinkage can lead to durability issues in the presence of cracking. For example, where restraints are present, increased levels of shrinkage can potentially lead to cracking and thereby provide pathways for deleterious substances to enter concrete. In general, the use of the different slag types had a minimal impact on the shrinkage. Hence, the use of slag in concrete yields similar drying shrinkage properties. This comes to reason that if the concrete containing slag does not hamper the concrete mixture's shrinkage behaviour negatively, the use of slag would have a beneficial outcome in the attempt to reduce cement usage.

4. 14. Durability

Durability is essential for concrete structures and is a key focus of modern research. In general, the use of SCMs, such as slag, is noted to have positive effects (in terms of durability) when incorporated in concrete mixtures. The South African durability tests were used to assess how the two types of slag perform in terms of durability, namely the oxygen permeability, sorptivity and chloride conductivity. The results of the tests are given in Table 4.14 to 4-19.

4. 14. 1. The Permeability of Slag-Based Concrete

From the results obtained, the OPI index for the reference i.e. 0 % slag replacement, has the most desirable performance with the highest index value of 10.22. This is followed by both slags at 25 % replacement (OPI = 10.11) and then followed the GGBS and GGCS of 50 % replacement. The increase in slag content, irrespective of type, caused a general increase in the permeability. Dellinghausen et al. (2012) recorded similar findings in their research.

Table 4.14. Permeability of slag based concrete.

		PC	GGCS		GGBS	
		0	25	50	25	50
k	(x 10 ⁻¹¹ m/s)	5.80	7.79	23.17	7.83	14.11
OPI	(Log Scale)	10.25	10.11	9.64	10.11	9.85
CoV	(%)	24.6	26.8	18.4	25.1	17.9

The high index of the reference is suggested to be due to the relatively high cement content as well as the higher degree of hydration. The increase in permeability with an increase in slag content is suggested to be due to dilution. However, it is suggested that with increased curing time, the permeability of the slag-based mixes will decrease. Hooton (1986) conducted research with slag and tested the permeability up to ages of 182 days. They found that the initial permeability was higher (for slag-based pastes compared to the control), yet decreased with testing ages. The results even yielded a permeability that was lower than the reference from 91 days onward. This is mainly due to the secondary hydration products formed that can block the capillary pathways. Initially, the pore structure is coarse for the slag-based concrete. However, with increased curing, the liberated CH is converted into C-S-H, which blocks pores and increases the refinement. In addition, the increased pore refinement and the inadvertent increase in tortuosity is expected to occur as well. The increase in pore refinement and tortuosity as a favourable outcome with regard to ingress of deleterious substances, as well as the blocking of the pores. These deleterious substances, such as chlorides and carbon dioxide, cannot penetrate the concrete as easily as a result of the mentioned effects.

The GGBS-based samples did prove to have more favourable permeability coefficients in comparison to those of the GGCS-based samples. Nonetheless, based on the classification of Table 3.7, all the concrete mixes can be deemed as either good (both 50 % slag-based concretes) or excellent (the reference and the 25 % slag based concrete).

4. 14. 2. The Sorptivity of Slag-Based Concrete

In terms of the sorptivity, 25 % GGCS based slag had the lowest average ($5.7 \text{ mm/hr}^{0.5}$) and the 25 % GGBS based had the highest sorptivity ($8.3 \text{ mm/hr}^{0.5}$). The reference on the other hand would be in the middle of the classification system ($7.4 \text{ mm/hr}^{0.5}$). In this regard, it is noted that with the increase in GGBS content, there is an overall decrease in sorptivity. The increase in GGCS content in contrast resulted in an overall increase in sorptivity.

Table 4.15. Sorptivity and porosity of slag-based concrete.

	PC	GGCS		GGBS	
	0	25	50	25	50
Sorptivity ($\text{mm/hr}^{1/2}$)	7.4	5.7	8.3	8.3	6.6
CoV (%)	4.8	17.5	23.5	21.6	7.0
Porosity (%)	10.0	9.3	8.5	8.2	10.7
CoV (%)	2.5	1.1	33.8	12.7	4.6

With regard to porosity, the 25 % GGBS and 50 % GGCS samples have similar values of 8.5 and 8.2 %, respectively. This correlates to the sorptivity being of the same magnitude as well for these two samples. The increase in GGBS to 50 % does increase the porosity of the sample. The GGCS samples however result in an opposite effect; the porosity is decreased with increasing substitution of cement. Considering the former in conjunction with the previous mentioned trend of sorptivity, it is noted that increasing porosity has an impact of reducing the sorptivity as shown in Figure 4-33.

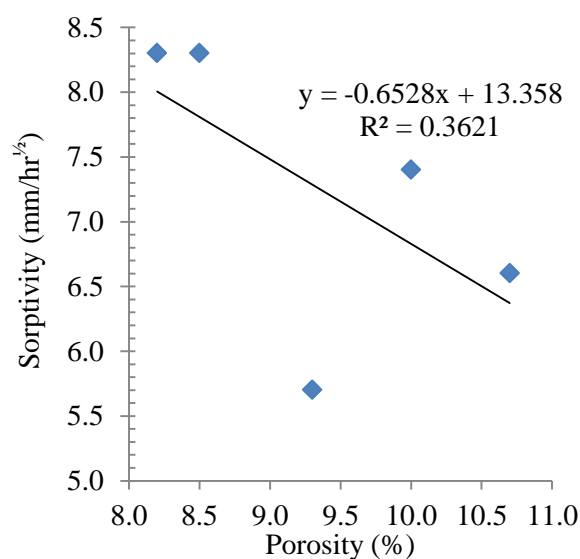


Figure 4-33. The relationship between porosity and sorptivity.

The negative relationship between porosity and sorptivity is best explained by the investigating capillary geometry and suction. For example, the higher porosity may result in larger pores being present in a sample and vice versa. Hence, with a larger pore diameter, the capillary suction is lower compared to a narrower capillary, this is due to the differences in capillary tensions forces. This is suggested to be due to the improved microstructure (Section 4.8).

In terms of Durability Index classification, only the 25 % GGCS mix is classified as excellent. Nevertheless, the rest of the mixes attain a classification of *good* in terms of the classification in Table 3.7. The differences between the slag-based concrete and the control do not differ by a substantial amount, still, with increased curing and associated pore refinement, the concrete containing slag is expected to be better compared to the control.

4. 14. 3. The Chloride Conductivity of Slag-Based Concrete

The chloride conductivity of the concrete containing slag was significantly better compared to the reference (Table 4.16). In terms of Durability Index classification (Table 3.7), the slag samples classify as *excellent*, while the reference is classified as *good*. All slag replacement, except the 25 % GGBS mix, had a conductivity coefficient of approximately 0.4 mS/cm. This is 3.25 times less than that of the reference. The 25 % GGBS still has a significantly lower conductivity coefficient compared with the reference, 0.7 and 1.3 mS/cm, respectively.

Table 4.16. Chloride conductivity of slag-based concrete.

	PC 0	GGCS 25	50	GGBS 25	50
Chloride Conductivity (mS/cm)	1.34	0.35	0.33	0.67	0.36
CoV (%)	17.3	6.5	2.3	4.5	5.0

The reduction in the chloride conductivity can firstly be explained to occur as a result of the pore refinement (Figure 4-15). This is in agreement with research undertaken by Aponte et al. (2012), Boa and Topu (2012), Shie et al. (2012) and Otieno et al. (2012). The finer pores, increase tortuosity and the blocking mechanism, impede the movement of chlorides ions through the concrete system.

The GGBS sample displays that an indirect correlation exists between slag content and chloride conductivity. The increase in GGCS shows a similar trend, albeit, not to the same extent. The increase is thought to occur as a result of the chloride binding phenomenon. The increase in the formation of Friedel's salt and chloride binding capacity of slag is suggested to be underlying reason for the improvement. Even though the current study did not investigate this phenomenon, studies undertaken by Aryan and Xu (1993), Luping and Nilsson (1993) and Leng et al. (2000) have proven this phenomenon. Since chloride-binding capacity is known to occur in slag-based concrete, it stands to reason that the phenomenon occurs for the slag used in the current study as well; the same is true for GGCS. The negative correlation between slag content and chloride conductivity is in agreement with results of other studies (Aponte et al., 2012; Boa & Topu, 2012; Zhang & Zhang, 2014).

The improved chloride conductivity results of the GGCS samples can also be correlated to its increased reactivity. Hence, with a more reactive nature, the GGCS is likely to produce secondary C-S-H gel at early age and is therefore able to increase the chloride binding capability.

To conclude, the improved resistance to chloride ions is signified by the immobilisation of the chloride ions, namely by the effect of blocking pores (via secondary hydration products or physical means),

chloride binding and the formation of Freidel's salt, and the pore refinement. In addition, the study thus shows that the addition of slag, regardless of type, is most beneficial to the reduction of chloride ion migration in comparison to the reference.

4. 14. 4. Durability Indices for South African Slags

In the preceding sections, reference is made to classify the concrete performance. This is based on an index system referenced in Section 3.12.5 where a concrete either has an *excellent*, *good*, *poor* or *very poor* classification based on the relative performance in terms of the three South African durability tests. Using this classification, a simple table (Table 4.17) is established to determine which of the mixes would exhibit substantially good performance in term of durability. A point system is chosen where an excellent concrete would receive two points for a category; the point system decreases systematically by one point as the performance decreases; poor performance achieves no points. The points are summed up and the concrete with the highest number of "points" is deemed the most durable.

Table 4.17. The DI classification for the investigated slags.

Material	% Slag	Permeability	Sorptivity	Chloride Conductivity	Total
PC	0	++	+	+	4
GGCS	25	++	++	++	6
	50	+	+	++	4
GGBS	25	++	+	++	5
	50	+	+	++	4
Key: (++) <i>Excellent</i> ; (+) <i>Good</i> ; (-) <i>Poor</i> ; (--) <i>Very Poor</i>					

As seen in Table 4.17, the 25 % GGCS had the highest points and can be classified the most durable mix for the study. The 25 % GGBS mix is second, followed by the 50 % slag based concretes and reference. The results show that the use of slag, irrespective of type, still exhibits properties equal to, or superior to that of the control. Hence, it can be concluded that the use of slag in concrete does not have a negative impact on concrete and can ultimately provide an economical, environmentally friendly and durable concrete.

4. 15. Concluding Summary

The objective of the study was to assess the use of South African slags in concrete. The aim was to establish how the use of the different slag-based concretes compare to each other and with a reference. This would in turn signify the beneficial use of slag in concrete in an attempt to reduce the Carbon footprint imposed by the cement production industry.

Firstly, the reactivity of the slags were investigated and found to be sufficient for use in terms of standards. The GGBS did show a slightly lower SAI then what is required, by less than 1 %, but did still perform adequately once incorporated in concrete. In addition, GGCS showed to be more reactive compared with the GGBS. This was expected and supported by the literature. The difference in

reactivity is suggested to occur as a result of the differences in production processes and slight differences in chemical composition.

The two slags had a varying impact on the fresh state properties. Both types of slag improved the workability, yet in different degrees; GGBS improved the workability more. In terms of setting time, both slags exhibited retardation with a subsequent increase in slag content. However, the GGCS samples show to have lower setting times compared to the reference. The bleeding of the slag based concrete were also comparable to that of the control. The GGBS exhibited better bleeding characteristics compared to the GGCS sample, and is suggested to be influenced by the particle packing.

With regard to the early age properties, the increase in slag, regardless of the type, showed an increase in plastic settlement. This is due to the increased volume of paste as well as the associated changes in workability. The addition of slag increased the overall workability, hence changing the concrete rheology to a degree at which the settlement increases. Hence, for construction purposes, adequate measures should be taken to ensure that the plastic settlement cracking is mitigated when incorporating slag, especially at higher levels of cement substitution. The incorporation of slag also reduced the capillary pressure build up and gradient. At low substitution levels, the plastic shrinkage is shown to be the highest, for both slag samples, and decreases with increasing cement substitution. At 50 % GGBS incorporation, the plastic shrinkage was found to be even less than that of the reference.

The microstructure of the slag-based concrete was also significantly improved. The pore distribution at both levels and for both types of slag was less than that of the reference. This is a clear indication of the secondary hydration products forming by utilising the liberated CH.

The compressive strength development of slag-based concrete was similar to that of the reference, yet at lower strengths. The strength did decrease with increased slag substitution, due to the dilution process. The GGCS showed results of lower capacity compared to that typically found in the literature. Further investigations concluded the likelihood of a bad batch being used or a potential incompatibility between the GGCS and PC used. Nonetheless, the results attained are still good and were even higher compared to that of the GGBS sample. The difference between the reference and the slag-based concrete decreased with increased curing, due to the pozzolanic reaction.

The tensile strength of slag-based concrete was lower compared to the reference. On average, the capacity of tensile strength per unit of compressive strength for slag-based concrete exceeded that of the control. This is indicative of the improvement of the ITZ. The GGBS showed better result at 25 % and GGCS at 50 % levels of cement substitution and the GGCS had higher ratios compared to the GGBS-based concrete samples.

The incorporation of slag resulted in similar drying shrinkage values compared to that of the reference. However, the mass loss associated with slag is less compared to that of the control. Also, the 50 %

GGCS sample had the greatest deviation of shrinkage from the reference. It is suggested that the high early age porosity may cause an increase in capillary tension, thereby affecting the shrinkage negatively.

The durability properties of slag-based concrete was equal to or better than that of the reference. The most significant impact is seen in the chloride conductivity; the incorporation of slag significantly reduces the ultimate conductivity due to pore refinement and chloride binding.

From the result obtained, it is clear that the use of slag has benefits and drawbacks. In the early ages, the slag-based concrete performs less than the control. However, in terms of long term properties, the use of slag shows to be most beneficial. In construction practices, the turn over, de-moulding and continued construction is preferred to be at a fast rate due to financial considerations and limitation by time issues. Hence, the use of slag can be seen as a drawback. With the correct mix design and proper studies, these short-term drawback may be limited and mitigated. Concrete structures are designed to withstand the environment and remain functional for long periods. The use of slag ultimately leads to concretes of similar properties compared to that of the reference. Taking into account the long term and short term impacts, it is evident that slag-based concrete appears more lucrative. This is enhanced by the fact that slag is a waste product and can potentially lead to the reduction of cement production. This provides benefits of a more sustainable production of concrete and at a potentially lower cost. The South African slags exhibit different properties when used in concrete, with near similar effects. To state which one is superior, various factors should be considered, such as intent of the project, estimated service life and design requirements, to name a few. Nonetheless, the use of either slag type will still yield positive results in the long run.

Chapter 5

Results and Discussion

Fly Ash

South Africa generates electricity from the combustion of coal as its major sources of energy. The combustion process generates waste, one of which is as fly ash. The coal that is used in the combustion process results in the production of Class F fly ash. The current study obtained four samples of fly ash and investigated the relative impacts these fly ashes have when used in concrete. The samples included Durapozz (DP), Pozzfill (PF) Ulula Ash (UA) and Sephaku Ash (SA). The fly ash samples are generated at different power stations and variation amongst the material is expected. The power stations from which the materials are obtained include: Lethabo (DP), Kendal (PF and SA) and Kriel (UA). This chapter discusses the results obtained from the experimental programme.

5. 1. Physical Properties

From the PSD results obtained (Figure 5-1) it can be seen that the fly ash samples span a wider range compared to the cement particles. It can also be seen that the particles of the fly ash samples are mostly larger than the cement particles. There is an exception noticed for the DP sample, which crosses the PC curve at about 20 μm . In addition, the volume frequency of all materials are noted to have a negative skewness as shown in Figure 5-1. Moreover, the peaks for the volume frequency are lower compared to that of the PC and only that of the SA sample is to the right of the PC's curve.

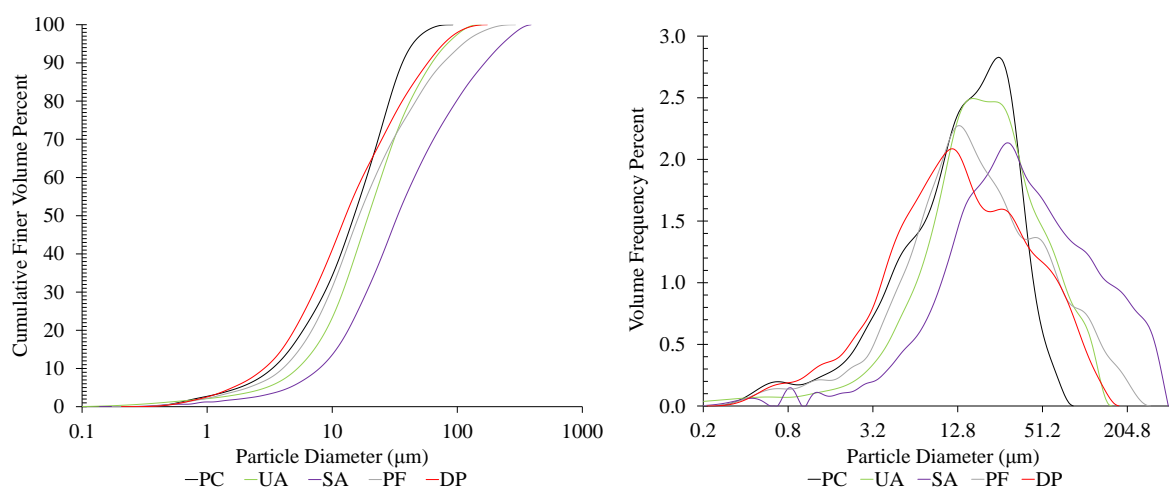


Figure 5-1. The PSD results (left) and the volume distribution (right) of the cement and fly ashes.

The relevant particle sizes are provide in Table 5.1, in addition to the spans and fineness. UA had the smallest maximum particle size (146 μm), yet this is almost double the size compared to the largest PC particle. PF, DP and SA followed in order of increasing maximum particle sizes. SA had the largest particle size of 367 μm , which is approximately 4 times larger than the cement particles. By comparing the spans, it is evident that all samples of fly ash, excluding the UA sample, had spans exceeding that of the PC by a factor of 2. The SA sample also has the largest span of particles. The UA sample had a span larger than that of the PC, yet not as significantly and comparably large as that of the PC.

Table 5.1. The physical properties of the cement and fly ash.

Material	Particle Sizes				Span $(d_{90} - d_{10})$ d_{50}
	Maximum μm	Median (d_{50}) μm	90% (d_{90}) μm	10% (d_{10}) μm	
PC	87	14.5	35.1	3.2	2.2
FA-UA	146	19.4	62.6	5.3	2.9
FA-SA	367	33.3	165.8	7.9	4.5
FA-DP	291	12.8	58.0	2.9	4.3
FA-PF	173	16.4	76.9	4.0	4.4

The SEM images provided in Figures 5-3 displays the morphology of the various samples. The fly ash samples all have the typical spherical shape; as opposed to cement particles which are angular (Figure 4-2). The images also provide a visual representation of the PSD. For instance, from the four images given, the large particles present in the SA sample (Figure 5-3 b) is clearly visible and appears more frequent compared to the displays in the remaining images (Figure 5-3 a, c and d). The SEM images also provide a visual data on any defect that may be present.

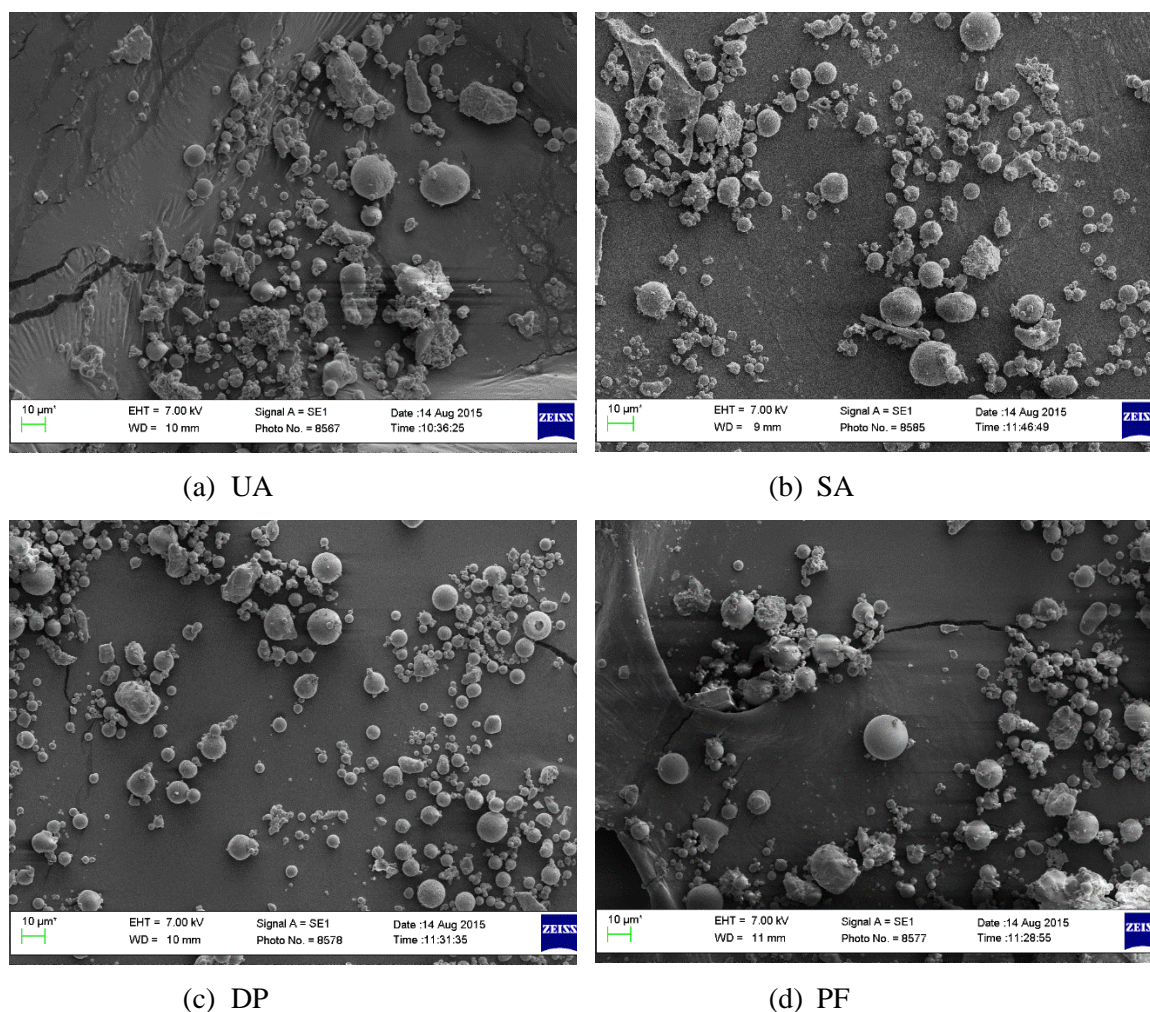


Figure 5-2. SEM image of the fly ash particle distribution and morphology.

The surface defects occur in different samples and in different frequencies. Figure 5-3 gives a visual example of a few defects that were observed. Etching (Figure 5-3 a) was seen on a few samples which hamper the surface area; this may influence the surface and fineness determination. Cenospheres housing more, smaller particles were also noted. The incomplete combustion of samples were also observed; this is seen with two adjoined spherical particles; the UA and SA samples had a significant number of this defect. All samples exhibited the effect of conglomeration. Irregular particles, that had a sphericity of 0, were also noticed. The SA sample had a substantial amount of the irregular particle, hence, this could explain the larger span it has as well as the reported larger particles present in it. Lastly, unburnt material, speculated to be coal, are also seen in the images; the unburnt material were especially noted in the SA and UA samples.

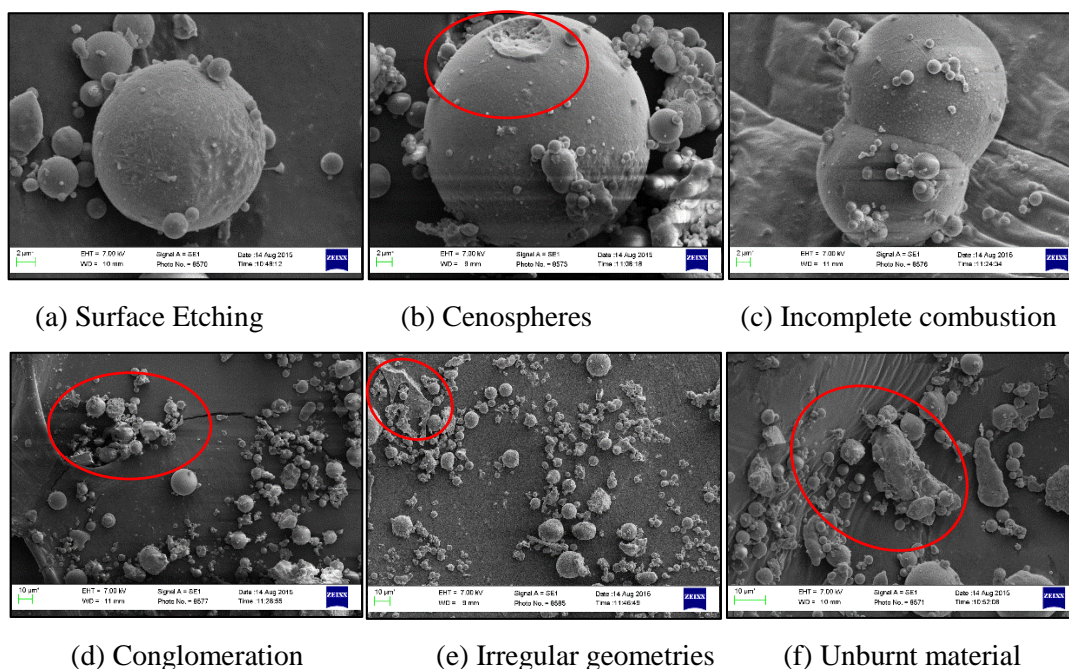


Figure 5-3. SEM image of the defects found.

5. 2. Chemical Properties

The chemical composition of the fly ashes are reported in Table 5.2. It can be seen that the deviation in composition of the four samples are negligible. All samples had a high mass percentage of silica present, in the range of 53 – 56 %. The alumina is also relatively high in terms of percentages (nearly 30 %). Using the classification provided by the Table 2.2, all the listed fly ash samples are similar when compared to typical South African fly ash. Based on the ASTM C618 classification, all fly ash samples can be regarded as Class F. In terms of the EN 450-1 specifications, all fly ash samples conform to the required mass percentage of silica exceeding 25 % (by more than double). The sum of reactive components (silica, alumina and iron oxide) are all above 86 %, which is significantly higher than the minimum requirement of 70 %.

Table 5.2. The chemical composition of the cementitious binders: cement and fly ashes.

Composition (%)	<i>PC</i>	<i>UA</i>	<i>SA</i>	<i>DP</i>	<i>PF</i>
SiO ₂	21.37	53.9	53.3	55.7	55.9
CaO	59.90	5.6	5.0	4.5	4.8
Fe ₂ O ₃	3.07	2.6	3.7	3.4	3.4
Al ₂ O ₃	4.98	29.8	29.8	30.1	29.2
MgO	2.58	1.2	1.3	1.0	1.1
K ₂ O	0.24	1.0	0.9	0.8	0.8
MnO	0.46	0.0	0.0	0.0	0.0
Cr ₂ O ₃	0.01	0.0	0.0	0.0	0.0
Na ₂ O	0.14	0.2	0.2	0.2	0.2
P ₂ O ₅	0.07	0.5	0.5	0.5	0.6
TiO ₂	0.43	2.1	2.2	0.7	0.7
L.O.I.	3.02	2.1	2.2	0.7	0.7
Sum Of Conc.	96.27	98.4	98.6	98.6	98.4
SiO ₂ + Al ₂ O ₃ + Fe ₂ O ₃		86.3	86.8	89.2	88.5
EN 450-1 Requirements: (i) SiO ₂ ≥ 25 %; (ii) SiO ₂ + Al ₂ O ₃ + Fe ₂ O ₃ ≥ 70 %					

In terms of the LOI categories, UA and SA are regarded as Category A (LOI < 5%) and or Category B (LOI 2 – 7 %). DP and PF however are strictly category A. In addition, the lower LOI of DP and PF were also noticed when the SEM Images were investigated. In contrast there were more unburnt coal particles observed for the samples of SA and UA.

5. 3. Reactivity

The reactivity of the fly ash samples vary as a result of the differences in the chemical composition, fineness and morphology. All the samples are classified as Class F fly ash (low calcium) and have a high proportion of silica, alumina and iron oxide (approximately 86 %). Evaluating the cementing efficiency (CaO/SiO₂) the samples yield a value of 0.10, 0.09, 0.08 and 0.09 for UA, SA, DP and PF, respectively. Thus, the materials have a low cementing efficiency and the former list is given in order of increasing reactivity (potentially) i.e. UA, SA, DP and PF. Table 5.3 and Figure 5-4 provide the data of the SAI for the fly ash samples.

Table 5.3. The SAI of fly ash samples.

Age (days)		Reference	UA	SA	DP	PF	EN 450-1
7	Flexural Strength (MPa)	3.7	2.5	2.6	2.9	2.6	
	Compressive Strength (MPa)	34.5	17.3	20.9	19.2	24.7	
	SAI (%)	-	50.0	60.5	55.7	71.6	-
28	Flexural Strength (MPa)	4.9	4.4	3.3	4.5	4.1	
	Compressive Strength (MPa)	52.0	32.3	39.8	41.0	49.6	
	SAI (%)	-	62.1	76.5	78.8	95.4	75.0
90	Flexural Strength (MPa)	5.7	6.3	5.0	5.7	5.5	
	Compressive Strength (MPa)	62.5	54.5	53.0	52.9	52.5	
	SAI (%)	-	87.3	84.7	84.6	84.0	85.0

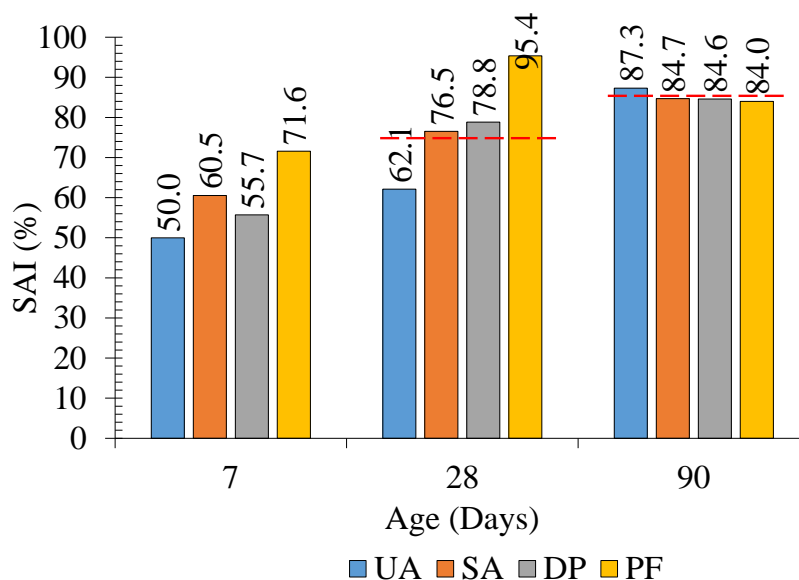


Figure 5-4. The SAI for the fly ash samples.

UA did not meet the 28 day SAI requirement of 75 %; the sample underperformed by 12.9 %. The PF sample displayed the opposite at both ages as it passed the 28 day requirement, yet not the 90 day

requirement. The results are indicative of the reactivity of UA only becoming significant after 28 days. The PF sample shows to be more reactive at earlier ages.

5. 4. Workability

The addition of fly ash to concrete improves the workability; of increasing the workability as the fly ash content is increased. The trend for the mixes is shown in Figure 4-5. In order of increasing effect on the slump recordings, the types of fly ashes performed in the following order: UA, SA, DP and PF.

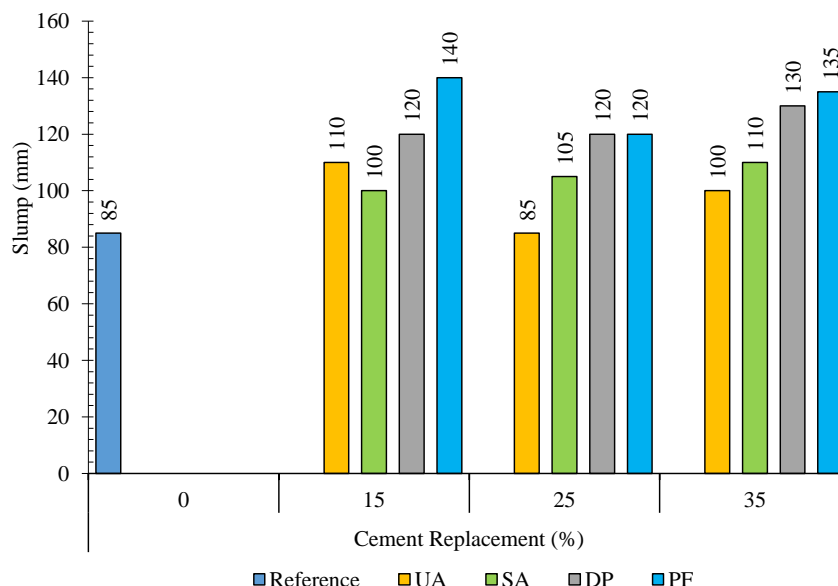


Figure 5-5. The workability of mixes containing different types of fly ash.

The increase in recorded slumps are as a result of:

- The spherical shape of fly ash adds a lubricant mechanism between the particles by behaving as ball bearings. The addition of these spherical particles causes a reduction in contact area between particles and as a result reduces the frictional forces.
- The incorporation of fly ash increases the total amount of paste and increases consistency and viscosity by improving particle distribution. These factors contribute to improving workability.
- The fly ash's spherical shape relates to a reduction in surface area compared to an irregular shaped particle: less water is therefore required to encapsulate each particle.

In terms of comparing the samples relative to each other, it is evident that the PF samples had the best performance compared to the other samples. UA samples recorded the lowest slumps, albeit still higher than the reference. The difference can be explained by the following:

- LOI content: The DP and PF sample recorded the lowest mass percentage of unburnt material at 0.7 %. The UA and SA samples had similar LOI values of 2.1 and 2.2, respectively. The unburnt coal is also visible (Figure 5-3 f) and more pronounced in the UA and SA samples. The unburnt material is more porous, has a higher surface area and absorbs more water. This is in agreement with the work of Xu (1996) and Siddique (2008).

- Irregular morphology (Figure 5-3 c and e): the DP and PF samples have more particles with a high sphericity, while the UA and SA samples did have a significant number of irregular particles present. The increase in irregular particles, likely due to the combustion process, counter acts the ball bearing effect and the reduced surface area phenomenon. Yet, these irregularities do not have a dominating effect, nonetheless, it does affect workability slightly.

From this study it is evident that the fly ash samples do improve the workability of concrete, as expected. The degree of improving workability is however affected by the type of fly ash. This is due to the differences in morphology and chemical composition, especially in terms of LOI content. Hence, the increase in spherical particles and reduction in LOI can have a significant impact on the slump. These parameters are also related to the combustion process. Higher temperatures and longer combustion times reduces the LOI and increases the sphericity.

5. 5. Setting Times

Class F fly ash is typically associated with the retardation of setting time due to the dilution and reduced reactivity. Figure 5-6 shows the effect of different fly ash samples on the setting time relative to the reference. It can be seen that there is a different effect on the setting time depending on the type of fly ash used and replacement level. The UA, SA and PF samples accelerated the initial set by 91, 16 and 45 minutes at 15 % replacement, respectively. PF also caused an acceleration of 17 minutes at 25 % cement replacement. DP had an effect of retarding the setting time, yet the effect reduced with increased substitution. In contrast, the effect of increasing fly ash content, excluding the DP mixes, caused an overall retardation of the concrete.

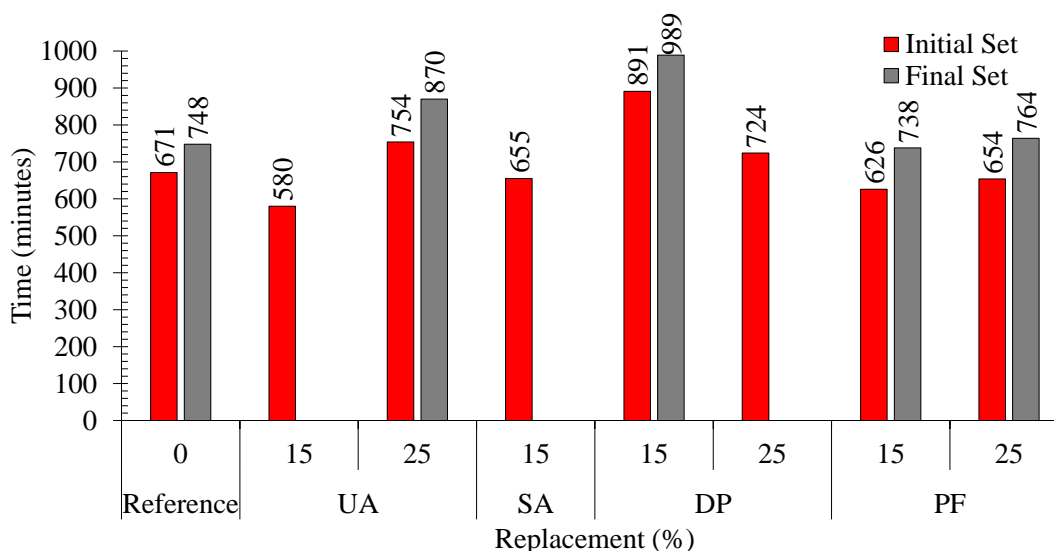


Figure 5-6. The setting times of fly ash based concretes.

Due to the dilution of hydration products, increasing the fly ash content causes retardation of the setting. Therefore, achieving similar degrees of hydration is prolonged. In addition, fly ash is reported

to act as a calcium ion sink, thus retarding the formation of CH and C-S-H (Langan et al., 2002) and could explain the increasing retardation with increasing fly ash concentration.

The inclusion of fly ash at low levels (15 %) can therefore actually accelerate the setting time. This can be explained by the finer fly ash particles providing nucleation sites for the formation of hydration products. The PF-based mix also accelerated the setting time at 25 % replacement; the rest of the samples causes a retardation at 25 % replacement. Based on the reactivity results, it is possible that the PF sample also part takes in the initial stages of hydration. However, the most likely reason is still suggested to be due to the particle packing being improved, plus the provision of additional nucleation sites.

5. 6. Bleeding

The effect of the fly ash samples on bleeding varied according to the type and the replacement level. The reasons for the differences are suggested to be that of differences observed in particle characteristics and fineness. The bleeding water curves for the fly ash samples are displayed in Figures 5.7, 5.8 to Figure B-2. The bleeding rate, capacity and duration are given in Table 5.4.

Table 5.4. The bleeding rate, capacity and time for the fly ash based concrete.

Material	SCM (%)	Bleeding Rate		Bleeding Capacity (%)	Bleed Duration (minutes)
		(g/m ² /s)	(kg/m ² /hr)		
PC	0	0.134	0.483	2.33	450
UA	15	0.093	0.336	2.09	580
	25	0.121	0.435	1.96	580
SA	15	0.077	0.277	2.56	600
	25	0.092	0.330	3.40	800
DP	25	0.070	0.253	2.41	700
PF	25	0.083	0.298	2.90	580

5. 6. 1. The Effect of Fly Ash Type on Bleeding

The bleeding rate for the fly ash-based concrete was less than that of the reference. At a 25 % cement replacement, the UA specimen had the steepest bleeding rate (0.121 g/m²/s), whereas the DP sample the lowest (0.083 g/m²/s). It is suggested that the bleeding rate decrease due to the viscosity of the mix being improved with the addition of fly ash sample. The fly ash samples are finer and also increase the powder-to-volume ratio of the mixture, which inadvertently leads to the reduced bleeding. As the density of the fly ash is lower compared to the reference, it can be arguably stated that the rate of settling is lower. Thus, the addition of fly ash, irrespective of type, lowers the bleeding rate of concrete and is visible on the figures displaying the bleeding profile.

If the particle size distribution is taken into account, it can be reasonable to state that the larger the span of the particles, the slower the bleeding rate is expected to be. For example, the UA sample had the steepest bleeding rate and also the smallest particle span (2.2) and these values were similar to the

reference compared to the other ashes. The lowest bleeding rate was recorded by the DP concrete mix and it had a span that is double that of the UA sample.

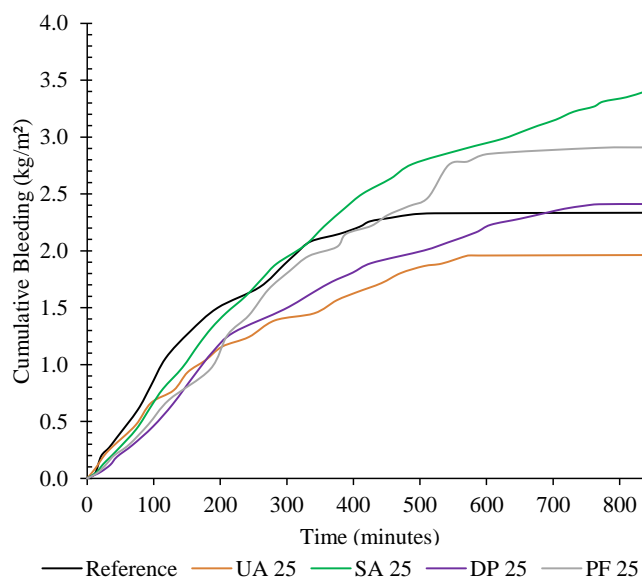


Figure 5-7. The effect of fly ash samples on bleeding at 25 % cement replacement.

The addition of fly ash prolonged the duration of bleeding. Comparing the results for 25 % cement replacement, the SA concrete mix attained the longest bleeding duration and mixture also took the longest to set. The PF and UA samples in contrast had the shortest bleeding time, and either had an accelerating effect (PF) or caused retardation to a lesser extent (UA). Dilution reduces the capillary pathways present through which water can travel in the case lower reactivity and vice versa.

The type of fly ash also affects the bleeding. Ranking the 25 % cement replacement mixes in terms of ascending order of bleed capacity yields: UA, DP, PF and SA. The bleeding capacity can be related to the PSD of the fly ash samples. The spans of these materials follow the same trend in terms of increasing spans (Table 5.1). This is in agreement with the suggestion by Olorungsogo (1998), namely, that the lower packing capacity of a mix would decrease the bleeding capacity as water fills the internal voids and does not migrate to the surface. As the UA sample had the lowest span, it yielded the lowest bleed capacity.

5. 6. 2. The Effect of Fly Ash Substitution on Bleeding

As seen from Figure 5-8 the increase in UA from 15 to 25 % resulted in an improvement in terms of bleeding characteristics. However, from Figure 5-8, the subsequent increase in SA results in an increase of bleeding severity. Hence, the effect of substitution is dictated by the material characteristics for substitution levels as well, which could be as a result of the relative particle packing effect. For example, the increase in UA samples potentially reduces the particle packing of a concrete mixture. Hence, as shown, the increase in UA reduces the bleed capacity as more voids are present due to the distorted particle packing. In contrast, the increase in SA particles improves the particle packing by

increasing the span. Therefore, fewer voids are present in the mixture and water can migrate to the top via capillary pathways.

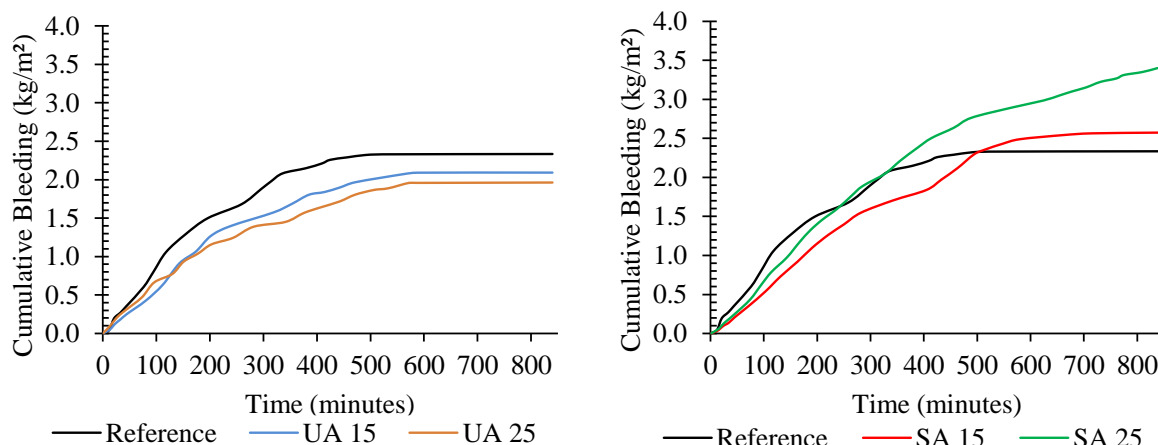


Figure 5-8. The bleeding of UA (left) and SA (right) specimens at 0, 15 and 25 % cement replacement.

5. 6. 3. Concluding Remarks

The impact of fly ash on concrete did vary according to the type and the replacement level. Hence, depending on the mentioned factors, adequate measures are to be taken in construction practice to ensure bleeding does not become an issue of concern. Three conclusions can be drawn from the conducted research: (i) the bleeding ends because of hydration, (ii) the reactivity also indirectly influences the bleeding duration and (iii) a narrower particle packing reduces bleeding characteristics.

5. 7. Early Age Deformation

Early age deformation can have a detrimental impact on the service life of concrete structures. The current discussion focuses on the early age deformation of fly ash-based concrete subjected to conditions associated with extreme conditions, such as high wind speed and temperatures with a low relative humidity, which is commonly referred to as *hot weather concreting*. Table 5.5 provides a short summary of the setting times and bleeding data of concrete containing the investigated fly ashes at elevated temperatures of 40 °C. The associated curves of the bleeding phenomena can be found in Appendix B, Figures B-3 to B-6.

Table 5.5. Setting times and bleeding data for fly ash –based concrete at elevated temperatures.

	Fly Ash (%)	Setting Times		Bleeding Characteristics		
		Initial (Minutes)	Final (Minutes)	Rate (g/m ² /s)	Duration (Minutes)	Capacity (%)
Reference	0	373	463	0.12	390	2.30
UA	15	400	497	0.10	420	2.12
	25	437	533	0.13	> 425	2.57
SA	15	-	430	0.07	> 550	3.07
	25	615	680	0.14	> 650	3.69
DP	15	561	637	-	-	-
	25	447	534	0.10	> 500	2.71
PF	15	440	-	-	-	-
	25	410	484	0.11	> 500	3.44

The setting time of all the concrete is lower than what is reported in Figure 5-6, which is to be expected. As mentioned in the Section 4.7, the higher temperature catalysis the exothermic hydration reaction. Hence, the rate of hydration is faster. Notably, all concrete with fly ash caused a slight retardation, except for the 25 % SA sample that had an accelerated final setting time. Overall, the bleeding rates were less than the in Section 5.6 (Table 5.4). In contrast, there is an observed increase in bleeding capacity at the elevated temperatures, which is likely due to a more porous system developing at higher temperatures, therefore creating more pathways for water to percolate to the surface.

5. 7. 1. Plastic Settlement

The plastic settlement for all concrete mixes with fly ash showed a settlement higher than that of the reference (Figure 5-9). The 25 % SA concrete mix did however exhibit a plastic settlement value similar to that of the reference. The 25 % PF mixture exhibited the largest settlement with a final shrinkage of double that of the reference. The increase in settlement from 15 to 25 % PF content displayed the greatest increase in settlement compared to the other fly ash based mixes, this equates to approximately 1 mm increase in settlement.

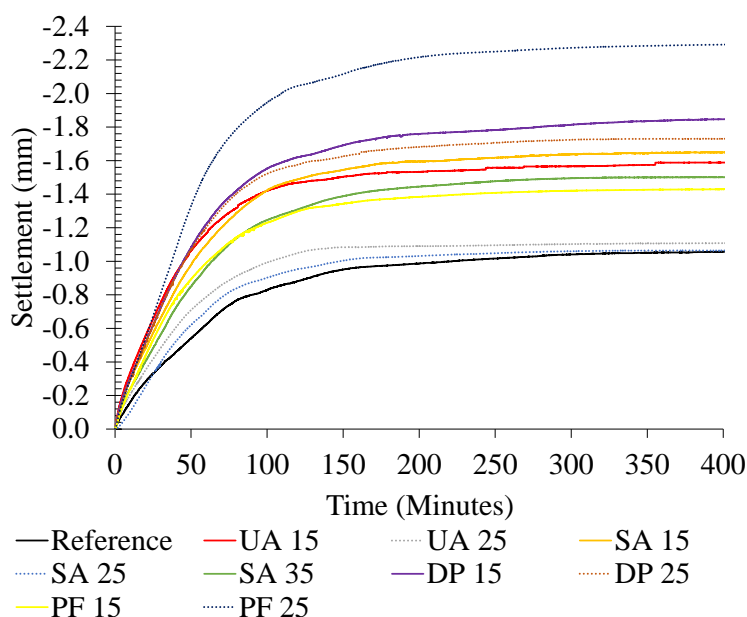


Figure 5-9. Consolidation of the concrete containing different cement substitution with fly ash.

As seen in Figure 5-9, adding fly ash causes an overall increase in settlement, initially i.e. from 0 % to 15 % cement substitution. The increase in settlement can be described by the reduction in viscosity with the addition of fly ash, making it easier for the paste to settle. Park et al. (2005) did research on the effect of fly ash on yield stress and viscosity and found an increase in both parameters with an increase in fly ash content. Albeit, that the yield stress and viscosity were less than that of the reference for the mentioned study. Although the current study did not investigate rheological properties, these former mentioned findings can still be used to explain the reported findings of the current study. This also highlights a possible area for future research. The addition of fly ash did increase the overall workability, which results in a subsequent change in rheology, i.e. potentially increasing the yield stress

and viscosity. Hence, these parameters are likely to increase with the increase of fly ash content, yet are still lower than that of the reference.

With an increase in fly ash content (25 to 50 % increase), there is a subsequent decrease in settlement; however this does not occur for the PF-based concrete. This can most likely be due to the increase in viscosity and yield stress with the increase in fly ash particles, as found by Park et al. (2005). The addition of finer spherical particles potentially create higher inter-particle forces, thereby increasing the overall viscosity. However, the result of the current study are not in agreement with the findings of Sonebi and Bartos (2002), who concluded that the increase in surface settlement is observed with an increase in slump and water-to-powder ratio. Increasing the amount of fly ash most certainly increases the volume of paste, due to the differences in relative densities of fly ash (2.3) and cement (3.14). However, looking at the slump data (Figure 4-5), it can be seen that the increase in UA causes a decrease in slump, hence explaining the observed decrease in settlement. The same accounts for SA, which does not cause a significant increase in slump. Yet, the high LOI of these two former fly ashes were relatively high, which explains the relative changes in viscosity and slump. Unburnt particles absorb more water due to their increased porosity (Xu, 1996; Park et al., 2005). The DP sample however does not have a substantial change in slump, hence explaining the relatively small change in settlement.

The result of the PF-based fly ash system was the only mixes which agrees with the findings of Sonebi and Bartos (2002). They state that an increase in fluidity can be achieved by decreasing the viscosity, which can lead to unstable dispersion of particles and segregation. Likely, this is the mechanism that is occurring with the addition of PF-based concrete.

5. 7. 2. Capillary Pressure Build-up

The capillary pressure of the concrete containing fly ash were lower than the reference mixture (Figure 5-10) and at lower level of fly ash addition, the slopes were steeper, and decreased with the increase in cement substitution.

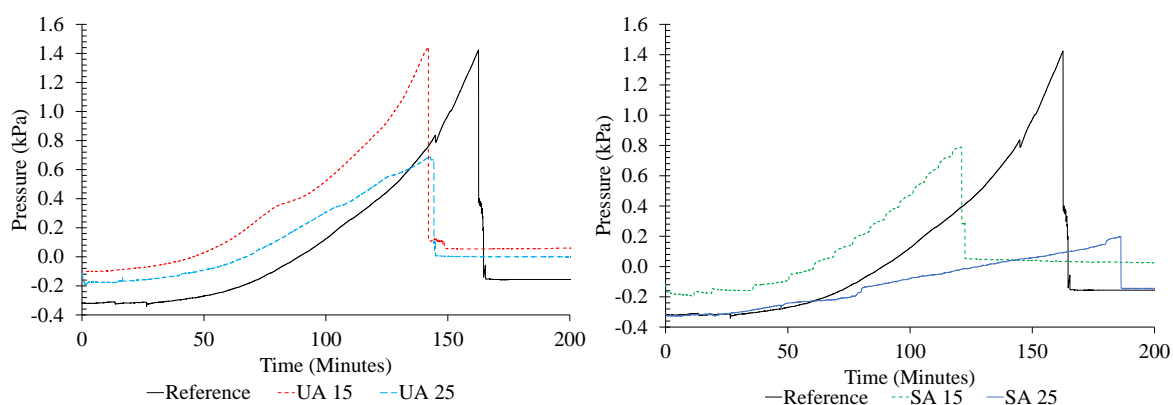


Figure 5-10. Capillary pressure build up for concrete containing UA (left) and SA (right) at different replacement levels.

The higher bleeding capacities of the concrete containing fly ash aids in the relative decrease in pressure build up. For example, the 25 % SA concrete, which had the highest bleeding rate and capacity, correspondingly yielded the lowest capillary pressure drop. From the bleeding data (Table 5.5), it can be seen that an increase in fly ash content increases the bleeding rate. This mix also yielded the longest bleed duration, which aids in explaining the gradual slope of the capillary pressure build up. Slowik et al. (2008) found that the capillary pressure is a function of the pore structure and rate of water loss. With an increase in the bleeding rate, a decrease in the difference between the evaporation rate and the mentioned bleeding rate, ergo, the rate of water lost from the surface decreases could be expected. This in turn leads to the decrease in the capillary pressure build up.

The steeper curve of the reference can also be explained by the degree of hydration. The reference arguably hydrates at a faster rate, hence establishing a capillary network. In other words, the capillary pressure is inclined to build up faster with the faster creation of the pore network.

Slowik and Ju (2011) suggest that the particle size of the materials also affect the capillary pressure build of the system, especially the smallest particles. With a smaller minimum particle size, there are subsequently smaller surface pores. The capillary pressure is defined by the Laplace equation (Equation 2.14), and is inversely proportional to the pore diameter. Hence, the menisci at the surface will be subjected to higher negative forces. By referring back to the data in Table 5-1, it is noted that d_{10} values for the UA and SA samples are larger than that of the reference, i.e. 5.3, 7.9 and 3.2 μm , respectively. The d_{10} is used, as it is difficult to justify what the smallest particle present would be. This theory can be used to explain the reduced capillary pressure in the fly ash based samples.

5. 7. 3. Plastic Shrinkage

The plastic shrinkage of the fly ash mixes (all types and associated replacement levels) exhibited an increase in unrestrained shrinkage (Figure 5-11 and Figure 5-12). When observing the different stages, it is noted that for all substitutions of cement with fly ash, a similar trend in the stages exist. Stage 1 is noted with a relatively higher initial shrinkage compared to the reference and ends after approximately 50 minutes, regardless of material type or cement substitution. Stage 2, shows variation in duration as the addition of fly ash prolongs it. The dilution of hydration products results in prolonging Stage 2. The capability of fly ash to reduce the impact of capillary shrinkage is related to the reduced reactivity of fly ash. As fly ash requires activation to start the pozzolanic reaction, the ability to form a skeleton that is rigid enough, is delayed.

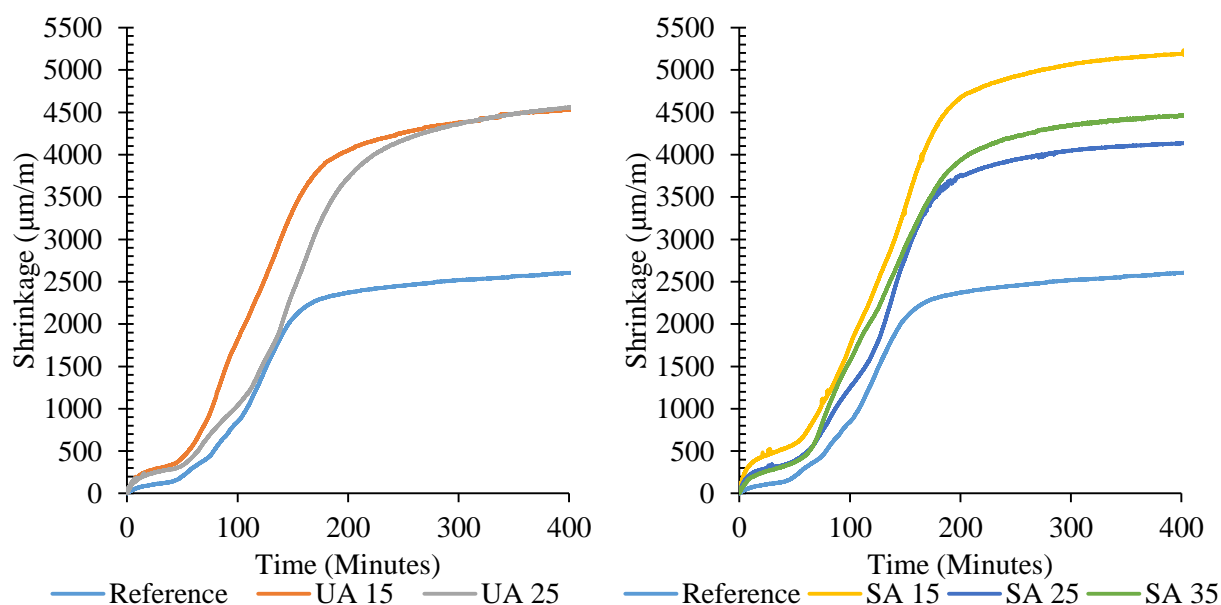


Figure 5-11. Plastic shrinkage for concrete containing UA (left) and SA (right) at different replacement levels.

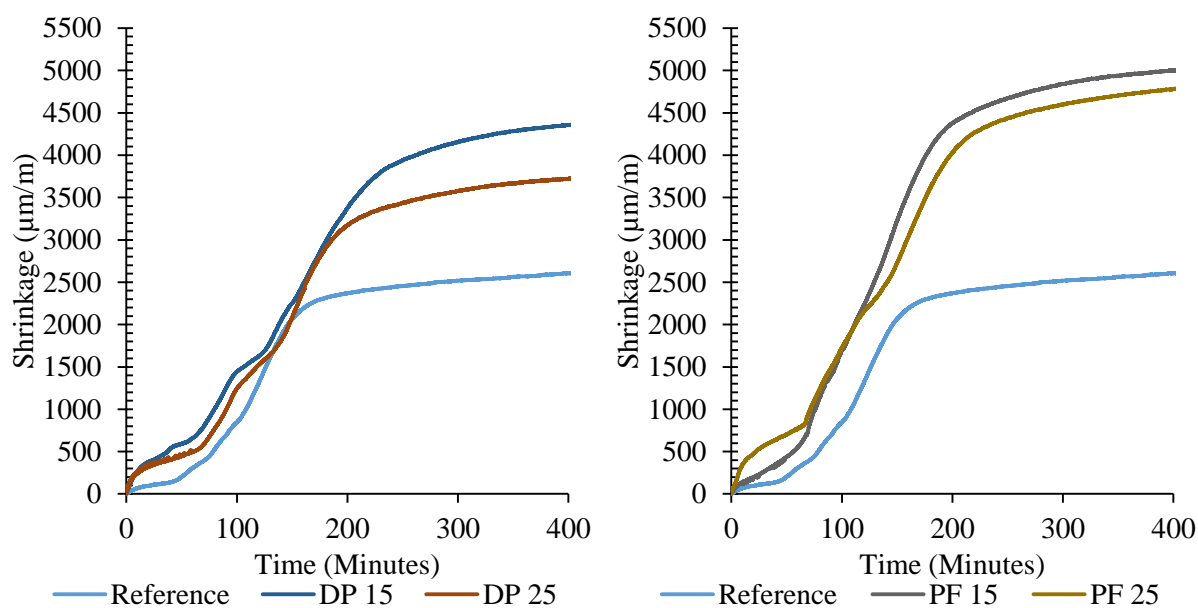


Figure 5-12. Plastic shrinkage for concrete containing DP (left) and PF (right) at different replacement levels.

Figure 5-12 shows that even with reduced capillary pressure and increased bleeding capacity, the overall plastic shrinkage is still relatively higher for fly ash samples. This is in agreement with the research of Krönlof et al. (1995), who found that a low capillary pressure does not relate to a low degree of plastic shrinkage. An explanation to the finding is likely due to the aforementioned lack in rigidity and potential increase in porosity at earlier ages resulting in hydrates forming, i.e. the impact of dilution.

Firstly, as discussed in Section 2. 6. 1, the increase in the degree of hydration can be correlated to an increase in rigidity as the material transgresses from a semi-solid to a solid state. The increase in

rigidity can therefore be related to an increase in the resistance to deformation as a result of the relatively large strains. Fly ash, especially Class F, has a low reactivity and requires an activator, such as CH, to initiate the pozzolanic reaction. From this, it can be concluded that the incorporation of fly ash results in a delay, if not lessening effect, of the overall stiffness. Therefore, the solid skeleton of hydrates forming is not as effective as that of the reference to reduce the shrinkage.

Secondly, due to the dilution effect and increasing number of fines present when incorporating fly ash, the porosity of the concrete at early ages can be relatively high. The increase in pores, in addition to the refinement, causes an increase in the overall applied pressure on the system, hereby, increasing the overall shrinkage.

In terms of product performance, the DP fly ash sources seem to exhibit better shrinkage performance, albeit still higher than the reference, compared to the other fly ash products. As aforementioned, the increase in UA had no noticeable effect on the shrinkage at all substitution levels. The increase in PF showed a slight reduction in shrinkage. Finally, 25 % SA based mixes exhibit the highest plastic shrinkage.

5. 7. 4. Concluding Remarks

From the results, it is clear that the incorporation of fly ash increases the plastic shrinkage, even though the bleeding rate and capacity is relatively higher than that of the reference. It is suggested that the delay in setting has a crucial role in this increase. In addition, the study found that the DP sample exhibited the lowest shrinkage compared to the rest of the samples.

5. 8. Microstructure

SCMs are known to enhance the refinement of pores present in concrete. The refinement occurs due to the secondary pozzolanic reactions creating additional C-S-H gel, by using the liberated CH from cement hydration. Figure 5-13, Figure 5-14 and Table 5.6 provide the data for the samples containing 25 % fly ash, when compared to the reference. It can be seen that all fly ash samples did cause a subsequent reduction in pore diameters (Figure 5-13). The volume of all pores, for all fly ash samples, are estimated to be equal to or less than 1 mm³. Figure 5-14 shows that, on average, approximately more than 90 % of the pores for fly ash based concrete are less than 1.5 mm³.

Table 5.6. The cumulative percentage of pore diameters for concrete with 25 % fly ash.

Cumulative %	Fly Ash				
	Reference	UA	SA	DP	PF
10	2.1	0.93	0.91	0.88	0.75
50	3.2	2.22	2.00	1.87	1.95
90	6.7	4.85	4.48	3.82	4.71

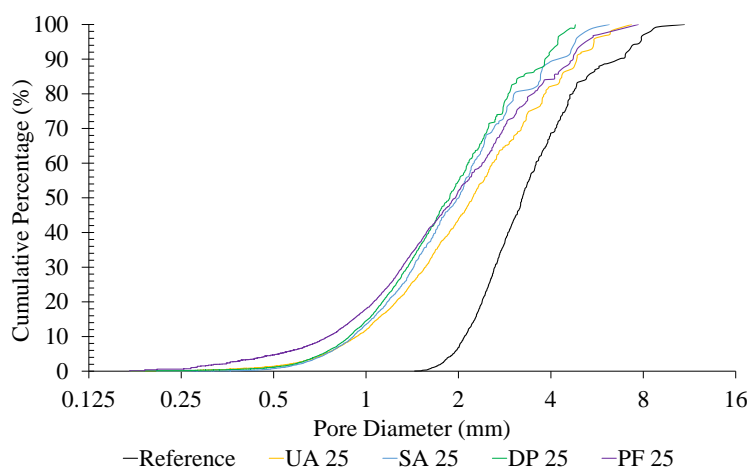


Figure 5-13. Cumulative percentage of the pore diameters of the concrete microstructure incorporating 25 % fly ash.

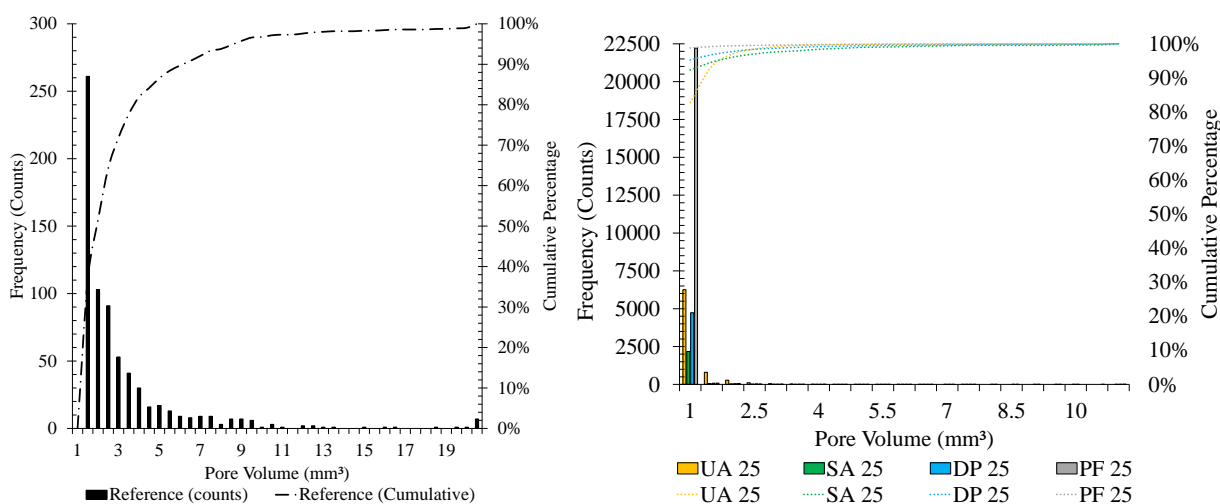


Figure 5-14. Differences between the pore volume for concrete containing no fly ash (left) and 25 % cement replacement (right), with the frequency and cumulative percentage presented by the histogram and dashed curves, respectively.

The findings, that fly ash refines the pore structure of concrete, are in agreement with those of other studies (Pandey & Sharma, 2000; Chindapasirt et al., 2005; Chindapasirt et al., 2007). Pandey and Sharman (2000) and Chindapasirt et al. (2005), found a subsequent decrease in the average pore size with the inclusion of fly ash. The current study also noted similar findings for all fly ash samples (Table 5-6). In addition, the span of the pore distribution also increased with the subsequent addition of fly ash (Figure 5-14). Similarly, Pandey and Sharman (2000) also reported an increase in the cumulative pore distribution in their study.

The pore refinement can be explained by the following: hydration, pozzolanic reaction, nucleation and packing (Chindapasirt et al., 2007). The hydration of cement creates C-S-H gel that progressively reduces the porosity of the paste. However, with the addition of fly ash, the liberated CH is utilised to form more C-S-H gel, which can be more voluminous. Hence, the porosity decreases. The reactivity of the fly ash used in the current study did show relatively good results, thereby correlating to the fact that

the pozzolanic reaction is certainly responsible for the increased refinement. In addition, the fly ash is also finer and is therefore suggested to partake in the nucleation and forming a denser paste. The PSD span of the fly ash samples also aids the particle packing (Zhang & Zhang, 2014), forming a denser structure with fewer voids. The fewer voids in turn can be filled with hydration products from the pozzolanic reaction. Taking an example, UA had the smallest particle span of 2.9. From Table 5-6, the UA sample has the largest cumulative pores for the fly ash samples; still, it is less than that of the reference. The PSD span of the UA also had the narrowest range amongst the fly ash samples. Hence, a narrower span of particles hampers the particle packing and therefore reduces the pore refinement. Nonetheless, the difference is not substantial when comparing the results amongst fly ash samples.

The study has shown that the use of fly ash is most beneficial with regard to the improvement in the concrete microstructure. This has a positive outcome when looking at the implications a finer pore structure could have. The latter is typically associated with the increased durability of concrete, as deleterious substances cannot permeate into the structure as easily. The performance of South African based concrete, in terms of microstructure, is therefore acceptable. The use of fly ash therefore yields positive impacts and can be used as a means to reduce average use of cement in concrete.

5. 9. Compressive Strength

The compressive strength results are presented in Figure 5-15 to Figure 5-18 for UA, PF, SA and DP. The data on the strength, in terms of replacement, is given in Table 5.7 as a percentage of the fly ash based concrete strength to that of the reference. All fly ash samples had a typical strength development profile with reduced early age strength and a gradual reduction in strength difference (relative to the reference).

Table 5.7. The strength of the fly ashes as a percentage of the control at different ages and cement replacement percentages.

	Cement Replacement (%)	Ratio (%)				
		Age (Days)				
		3	7	28	56	91
UA	15	106.5	63.8	89.7	96.9	101.0
	25	81.0	51.9	83.0	94.1	92.0
	35	68.4	38.6	70.1	83.3	89.0
SA	15	86.6	77.4	85.7	90.5	100.3
	25	81.8	65.7	80.1	83.1	87.7
	35	74.0	54.0	63.9	72.1	83.3
DP	15	105.6	75.7	83.9	82.8	86.9
	25	80.1	59.8	69.0	79.6	79.1
	35	66.7	50.7	63.4	72.4	80.2
PF	15	88.7	78.1	85.9	88.3	86.3
	25	81.0	64.0	73.7	84.6	91.7
	35	70.6	49.3	54.5	70.1	75.9

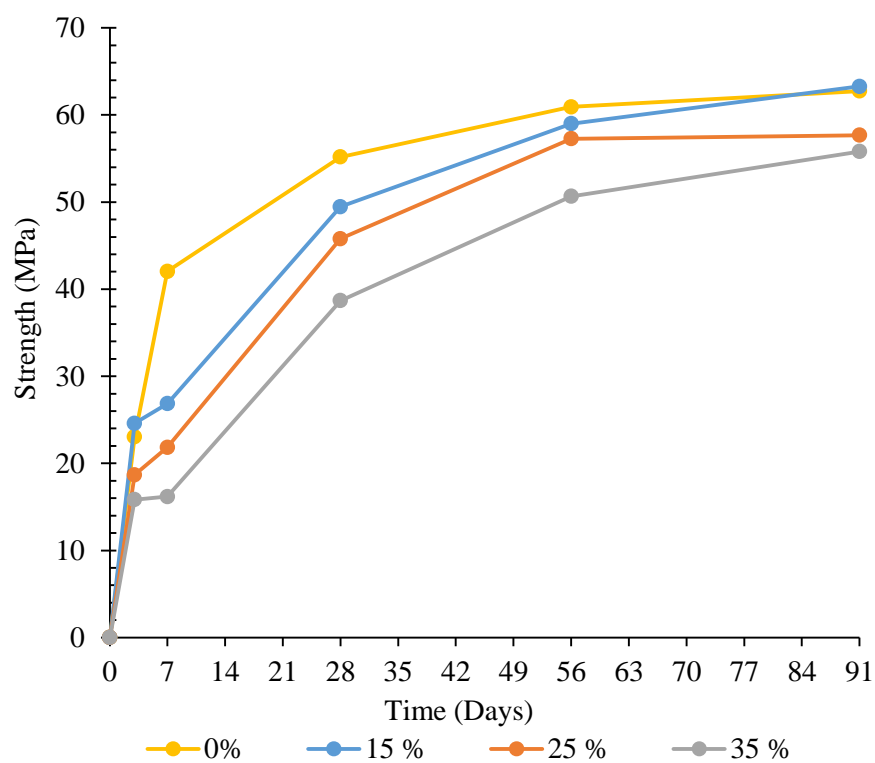


Figure 5-15. The strength development of the UA concrete mixes.

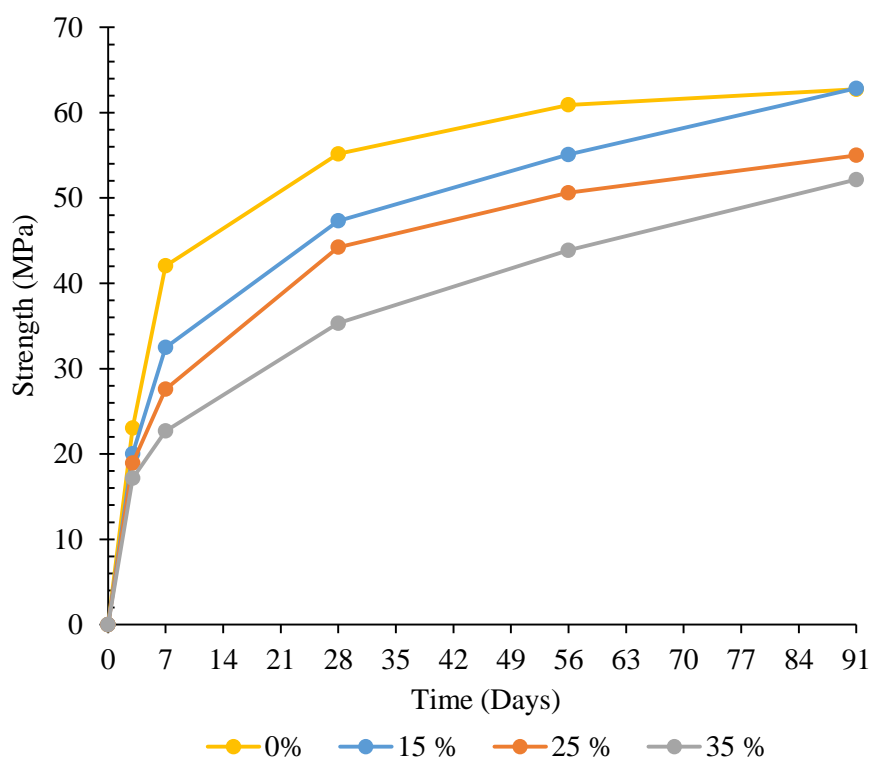


Figure 5-16. The strength development of the SA concrete mixes.

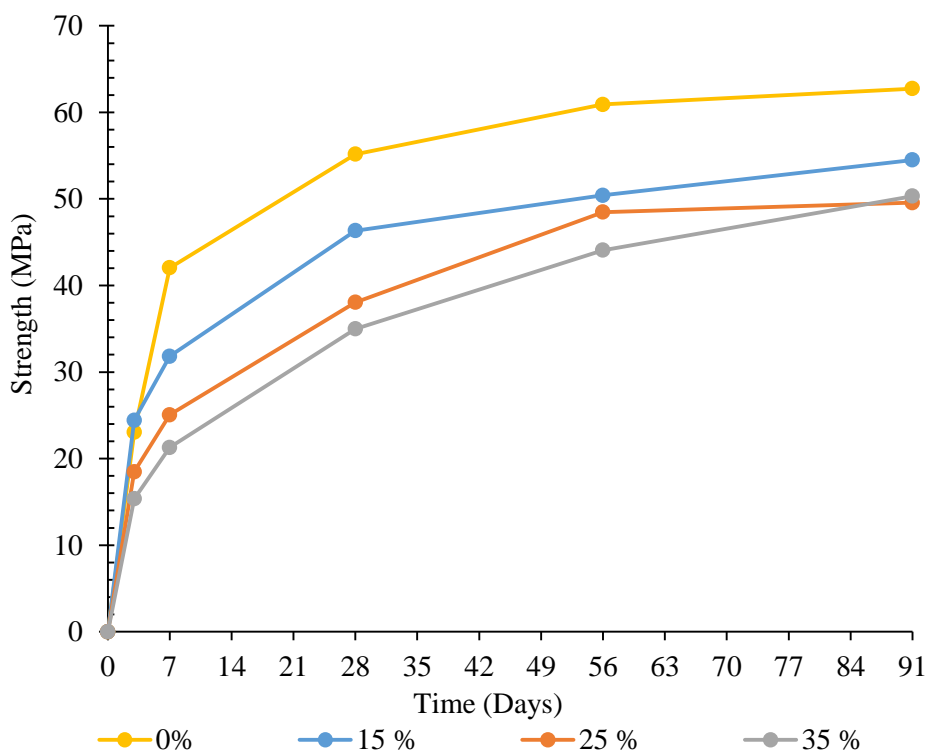


Figure 5-17. The strength development of the DP concrete mixes.

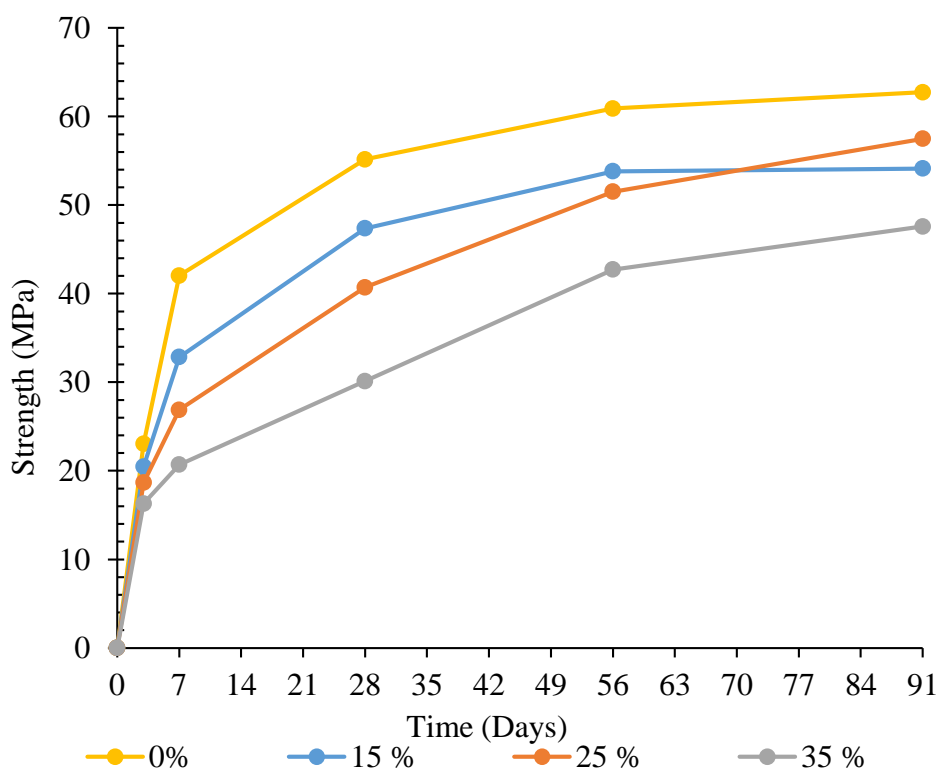


Figure 5-18. The strength development of the PF concrete mixes.

5. 9. 1. The Effect of Increasing Fly Ash Content

For each fly ash type, an increase in fly ash content results in the increase in difference of strength; the difference is relative to the reference and the replacement levels. The difference occurs at all ages of

testing and is particularly evident at earlier ages, yet diminishes with increased curing time as was also found in other studies (Papadakis et al., 2002; Berndt, 2009). Figure 5-15 and Figure 5-16 show the trend for UA and PF, samples respectively.

Firstly, at early ages of testing the difference in strength between the fly ash based concrete the reference is low as a result of (i) dilution, (ii) reduced reactivity, (iii) delayed pozzolanic reactivity, (iv) chemical interference on the development of compounds forming and (v) the establishment of an environment of high alkalinity. In a sense, all these factors are dependent on each other and it cannot be stated that one of the parameters is the main influencer. Increasing the amount of fly ash on a mass basis reduces the amount of initial reactants of hydration, i.e. the cement particles. Hence, there is a reduction in hydration products, which slows the strength gain with increasing cement reduction. The reduction in products consequently results in the delay of establishing the required environment of sufficient alkalinity ($\text{pH} > 12.5$). Langan et al. (2012) state that the aluminium present in fly ash suppresses the concentration of calcium ions in the pore solution. The reduction of calcium ion concentration therefore reduces the capability of C-S-H and CH to form. This furthermore delays the strength development and prolongs the time of achieving the required alkaline environment. Due to the reduced CH formed, the pozzolanic reaction is also retarded, which is furthermore enhanced by the lower reactivity of fly ash.

Concrete containing fly ash can achieve strengths similar to that of the reference, and even exceed it. At 3 days of water curing the 15 % UA and DP concrete yielded a strength greater than that of the reference (23.1 MPa), 24.6 and 24.4 MPa, respectively. All the other ashes and replacements were lower than the reference. The higher strength is explained by the mechanism of the filler effect having a dominant impact on the strength at early ages. Thus, the use of fly ash can provide stronger early age strengths. At 7 days of water curing, the strength of these two mixes were lower than the reference (42.0 MPa), as the reference now had a higher degree of saturation.

It can be seen, in Figure 5-15 and Figure 5-16, that the strength of the concrete containing fly ash reaches strengths similar to or higher than the reference. Oner et al. (2005) and Berndt (2009) had similar findings in the research undertaken by them. This is indicative of the better particle packing that is obtained by adding fly ash. The pozzolanic reaction generates C-S-H which adds to the strength whilst consuming the *weaker* CH present in concrete. Thus, the use of the fly ash in concrete is without a doubt beneficial for use in concrete, especially since similar age strengths compared with a reference can be achieved.

5. 9. 2. The Effect of Fly Ash Type

The substitution of fly ash has an effect on the concrete strength by causing an initial reduction in strength and subsequent gradual strength development. However, due to the differences found in fly ashes, such as fineness and reactivity, the relative effect on concrete strength varies with the type of fly

ash used. Figure 5-19 and Figure 5-20 displays the trends of the fly ash substituted at 15 % and 35 % respectively.

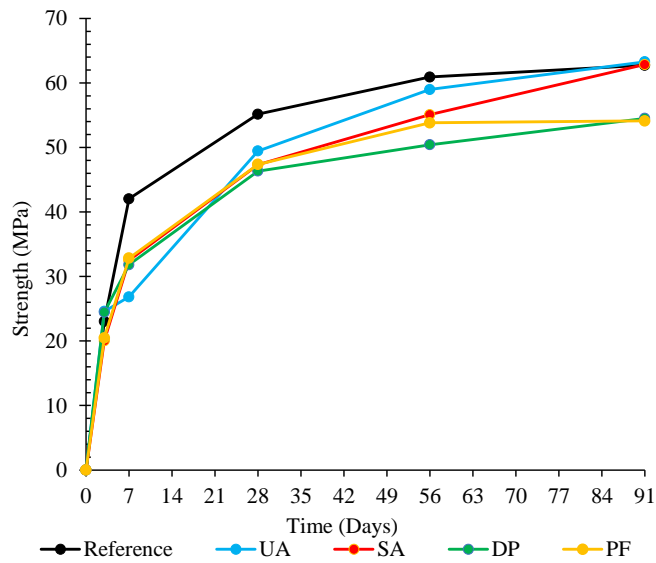


Figure 5-19. The compressive strength at 15 % cement replacement.

It is evident that the fly ash samples have different rates of achieving strength. For example, the UA fly ash sample in both cases display a low early age strengths at both substitutions, yet at 28 days the concrete containing UA yields the highest strength capacity and attains the superior performance for the remaining ages of testing. The SA sample followed and the PF sample yielded the lowest strength. Therefore, the type of fly ash is a factor in terms of strength development.

When comparing the workability of the different mixes, the samples yielding lower strengths (DP and PF) had higher slumps. Therefore, the strength of the concrete containing DP and PF can be increased by lowering the water-binder ratio to achieve the same slump. This is based on the assumption that the binder content remains the same.

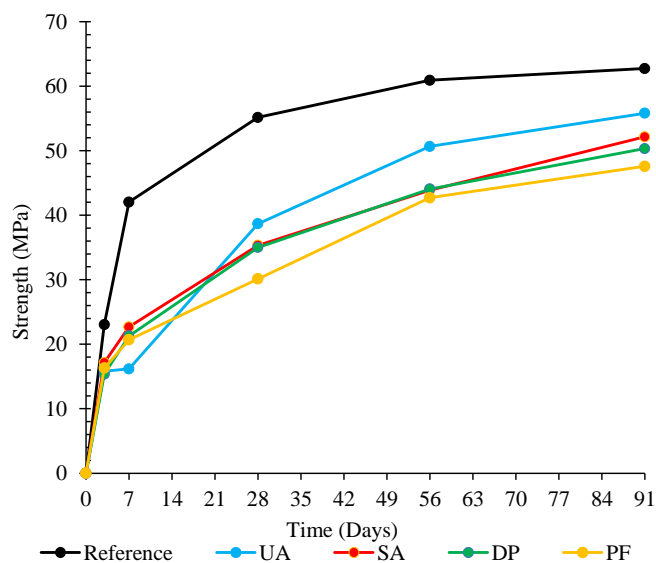


Figure 5-20. The compressive strength at 35 % cement replacement.

The comparison results of the SAI index seems to not be a good representative of the pozzolanic activity of the materials. For instance, the UA sample did not meet the 28 day requirement, yet yielded the highest compressive strengths at all replacement levels at 28 days. Even more so, looking at the results at 25 % replacement (Figure B-8), ensuring that the same level of substitution and water-to-binder ratio is applicable, the SAI for mortar was 62.1 % and the AI for concrete was 83.0 %. In addition, the SAI results would classify the PF sample to have the highest level of reactivity at 95.4 % for 28 days. Here the correlation with the concrete performance is better as the AI for concrete at the same substitution and age of testing is 85.9 %. This highlights one pitfall of the SAI based test that requires further investigation. The 90 day SAI results seem to be more reliable in indicating which material is more reactive when used in concrete. However, the fineness of the UA sample is suggested to be the reason for the improved performance. The finer particles enhance the packing, provide nucleation sites and increase the reactivity at later ages of the sample.

5. 9. 3. Concluding Remarks

From the results, it is evident that similar, if not higher, compressive strengths can be achieved with the incorporation of fly ash in concrete. However, the early age strength of the concrete is adversely affected; the strength is lower as a result of dilution and the slower pozzolanic reaction. This can be seen as a problem with regard to the construction process. Nevertheless, the low early age strength properties can be mitigated by improved mix design procedures. The current study only aimed to compare the materials at a constant binder mass and water-to-binder ratio. Hence, investigating the concrete on a same strength basis would most likely yield results that favour the use of fly ash. Therefore, the use of fly ash is therefore a good substitute to implement in the concrete production process.

5. 10. Indirect Tensile Strength

The addition of fly ash has been found to decrease the tensile strength of concrete (Berndt, 2009; Jalal et al., 2013; Li & Li, 2015). The indirect tensile strength was conducted at replacement levels of 0, 15, 25 and 35 % and tested at ages of 7, 28 and 56 days. The data is provided in Figure 5-21 and Figure 5-22, with the statistical data provided in Appendix B, Table B-5.

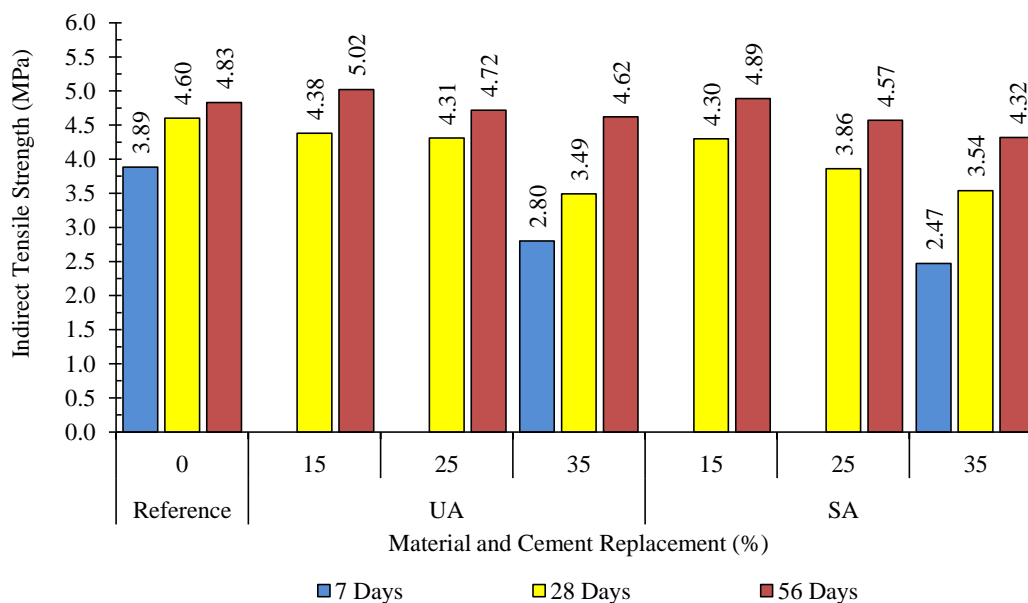


Figure 5-21. Indirect tensile strength of concrete mixes incorporating UA and SA.

At similar ages of testing, the fly ash samples display results comparable to that of the reference. There is a noted trend of the tensile strength decreasing with the increase in cement substitution, which was also found by Jalal et al. (2013). The trend is most likely due to dilution of hydration products. In addition, the variation in tensile strength between samples at the same level of substitution is also negligible, suggesting that the influence of the type of fly ash does not have an impact of great significance. The concrete incorporating the UA samples does however have slightly greater tensile strengths, which is most likely as a result of the fineness. The UA material is finer than the SA sample, and is suggested to improve the ITZ to a slightly better degree than the SA concrete.

The tensile capacity does also improve with increased curing as the hydration process continues and the pozzolanic reactions contribute to the strength gaining properties. This is likely due to the improvement in the ITZ. Berndt (2009) found that the use of SCMs (slag and fly ash), improve the ITZ of concrete.

Investigating the ratio between tensile and compressive strength (Figure 5-22) suggests that the tensile strength develops at a similar, but slightly slower rate to that of the compressive strength. The decreased rate of strength development can be explained by the slower pozzolanic reaction. At an early age of 3 days of water curing, the ratio between the tensile strength and compressive strength is relatively high. Therefore, relative to the early age compressive strength, the concrete containing fly ash performs better. A further indication of the improved ITZ is visible for the UA concrete mix containing 15 % fly ash. At 56 day of testing, the compressive strength of both it and the reference is roughly the same (with a difference of 1.9 MPa), yet the tensile strength of the UA mixture is higher.

To summarise, the tensile strength of the concrete is not affected by the type of fly ash used, but rather by the level of cement substitution. An increase in fly ash content caused a decrease in tensile strength. The reduction results from the lower reactivity and dilution. However, the results show that the use of

fly ash improves the ITZ, thereby increasing the tensile capacity of the concrete. It can be seen that the tensile strength gained per unit compressive strength, for fly ash based concrete, is always higher than the reference, regardless of age of testing and/or level of substitution. In terms of structural implementation, it will be more beneficial to use fly ash in concrete, especially elements which depend on adequate tensile capacities, such as industrial slabs.

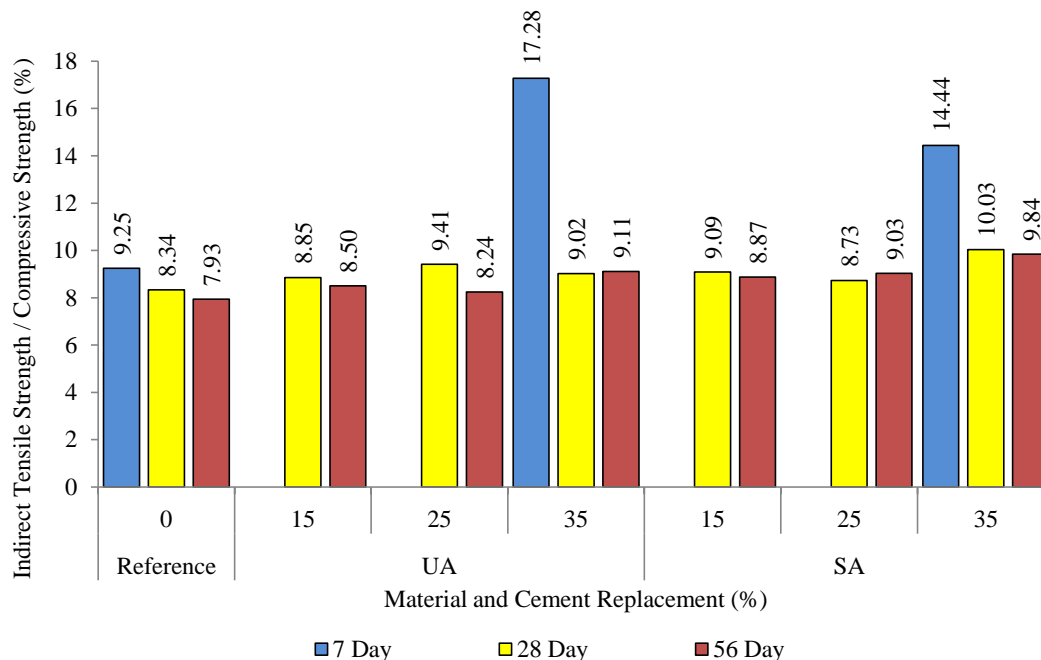


Figure 5-22. The ratio of the indirect tensile and the compressive strength.

5. 11. Flexural Strength

The flexural strength was also recorded for three concrete mixes (Table 5.8) and shows that the use of using the flexural capacity, as a means of assessing the tensile capacity of concrete, yields lower results when compared to the results from indirect tensile strength tests. The addition of fly ash to concrete proves to yield a higher tensile strength per unit of compressive strength. The increase in volumetric paste and improved ITZ are reasons for the increased strength. The data obtained from the flexural strength is similar to that of the indirect tensile strength, in that the ratio of tensile strength to compressive strength is always higher when fly ash is included.

Table 5.8. The flexural strength of fly ash samples.

Material	Fly Ash (%)	Flexural Strength (MPa)	Flexural Indirect Strength	Strength: Tensile	Compressive Strength (MPa)	Flexural : Compressive Strength
PC	0	5.3	1.15	55.7	0.095	
UA	15	4.3	0.98	38.4	0.112	
SA	25	3.7	0.86	36.2	0.102	
DP	35	3.5	-	28.1	0.125	

5. 12. Secant Modulus

The Secant Modulus is provided in Table 5.9. The addition of fly ash is seen to decrease the overall elastic modulus. The reference shows a good correlation between the cylinder strength and the modulus; the value of the cylinder strength and elastic modulus are similar in numeric value and differs in magnitude of a thousand i.e. 37.4 MPa cylinder strength and 37.5 GPa for the secant modulus. Yet for the fly ash based concrete the correlation is not as apparent. Table B.7 (Appendix B) provides the values obtained when assessing the elasticity using prediction models, and shows that the CEB-FIP model best describes the modulus when compared to the obtained data (average percentage error of 1.2 %).

Table 5.9. Secant modulus for concrete containing different types of fly ash.

	Reference	UA	SA	DP	PF
Replacement (%)	0	15	25	35	15
Cube Strength (MPa)	51.9	45.8	38.9	26.8	38.6
Cylinder Strength (MPa)	37.4	30.8	23.9	25.9	28.5
Cylinder:Cube Strength	0.72	0.67	0.61	0.97	0.74
Secant Modulus (GPa)	37.5	33.5	29.2	32.7	30.8

5. 13. Drying Shrinkage

Volumetric deformation related to the drying shrinkage of concrete can have adverse effects in terms of structural elements that are limited in terms of movement by restraints. The restriction of movement can induce strains, which in turn can lead to durability issues via the generation of cracks. The results of concrete containing the four samples of fly ash investigated study are given in Appendix B (Figures B-9 to B-17). The concrete samples all have a profile mimicking an inverse exponential curve. There is a subsequent increase in the early age shrinkage due to rapid moisture loss (to achieve equilibrium with the environmental humidity) where after the shrinkage starts to stabilise. The fly ash used in the study yielded variable trends depending on the fly ash properties.

All the concrete mixes containing fly ash had cumulative masses greater than the reference at most of the ages. The cumulative mass loss for the samples containing 25 % fly ash is shown in Figure 5-23. The samples with PF had the highest mass loss (3.08 %) and those containing UA had the lowest average mass loss (2.82 %), although this is still higher than the reference's mass loss (1.88 %).

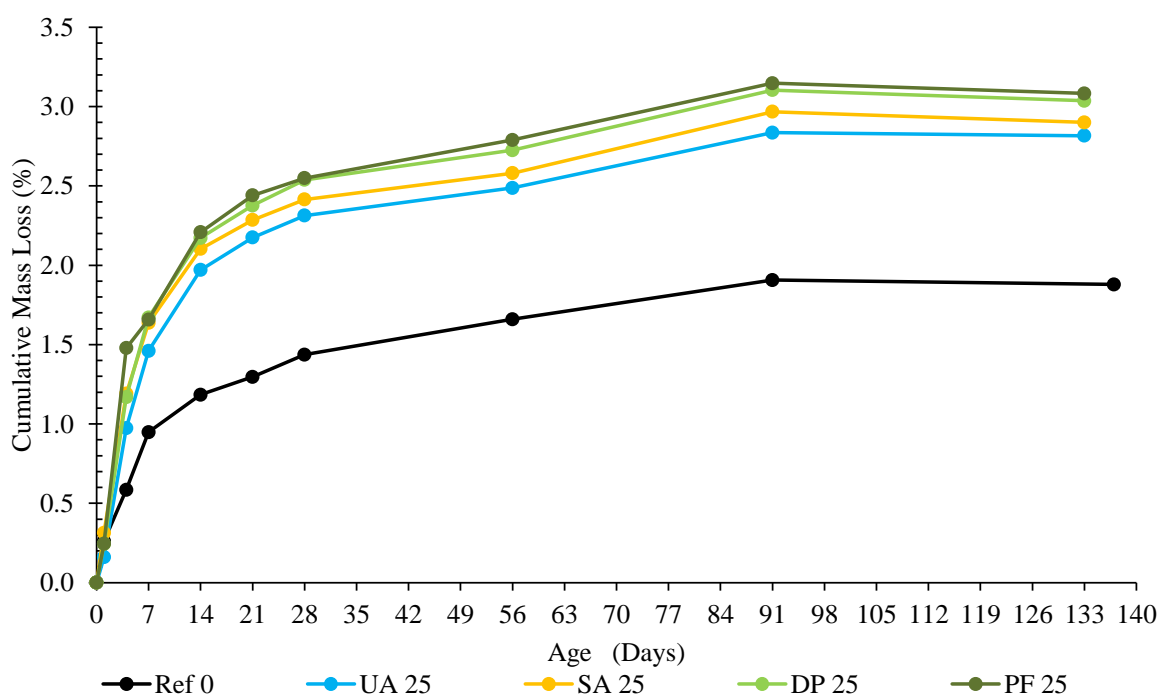


Figure 5-23. The cumulative mass loss of the fly ash samples (25 %).

The increase in mass loss may be explained by the relative amount of free water that is in the concrete system. As seen from the workability results, the fly ash samples had a higher slump values, related to the capability of fly ash to reduce the water content of mixes. The 15 % fly ash mixes had a similar trend and the graphical presentation can be found in Appendix B (Figure B-9).

In terms of drying shrinkage, all fly ash samples recorded a higher ultimate shrinkage compared to the reference. The SA and UA had the highest shrinkage (555.0 and 480.0 $\mu\text{m}/\text{m}$) relative to the reference (361.8 $\mu\text{m}/\text{m}$). The DP and PF samples had strains of 323.8 and 420.0 $\mu\text{m}/\text{m}$, correspondingly. The subsequent addition of fly ash therefore increases the drying shrinkage, except for the DP sample, which recorded a reduction of the drying shrinkage relative to the reference.

The first suggestion of the increased shrinkage is related to the subsequent increase in paste volume when fly ash is incorporated. In addition, the paste consists of critical pores, and with the onset of water removal from the mentioned pores, the drying shrinkage is initiated. Secondly, as fly ash concretes are said to refine the microstructure, it stands to argue that fly ash concrete potentially has a higher proportion of finer capillaries, hence, higher capillary forces are generated in these pores when water evaporates.

From Figure 5-24 it can be seen that the fly ash samples tend to stabilise at an earlier age compared to the reference. All the 25 % fly ash based concretes seem to have a relatively stabilised plateau from the 28 days on, as was also found by Khatib (2008). In addition, the initial linear portion of the fly ash based mixes are steeper compared to the reference. It is suggested that the early age porosity of the fly ash samples are relatively higher. Due to the increase in pore refinement with fly ash concrete, it stands to reason that the increased paste volume at this early age is porous, yet contains a high degree of

narrow pores. Narrower pores are likely to be subjected to a higher capillary pressure and therefore a higher internal tensile force. The breach of an early age plateau in drying shrinkage could be the result of the capillaries being blocked once the pozzolanic reaction starts to accelerate. It may be a coincidence that the plateau is reached at 28 day, as this also coincides with the age at which fly ash is said to contribute hydration products.

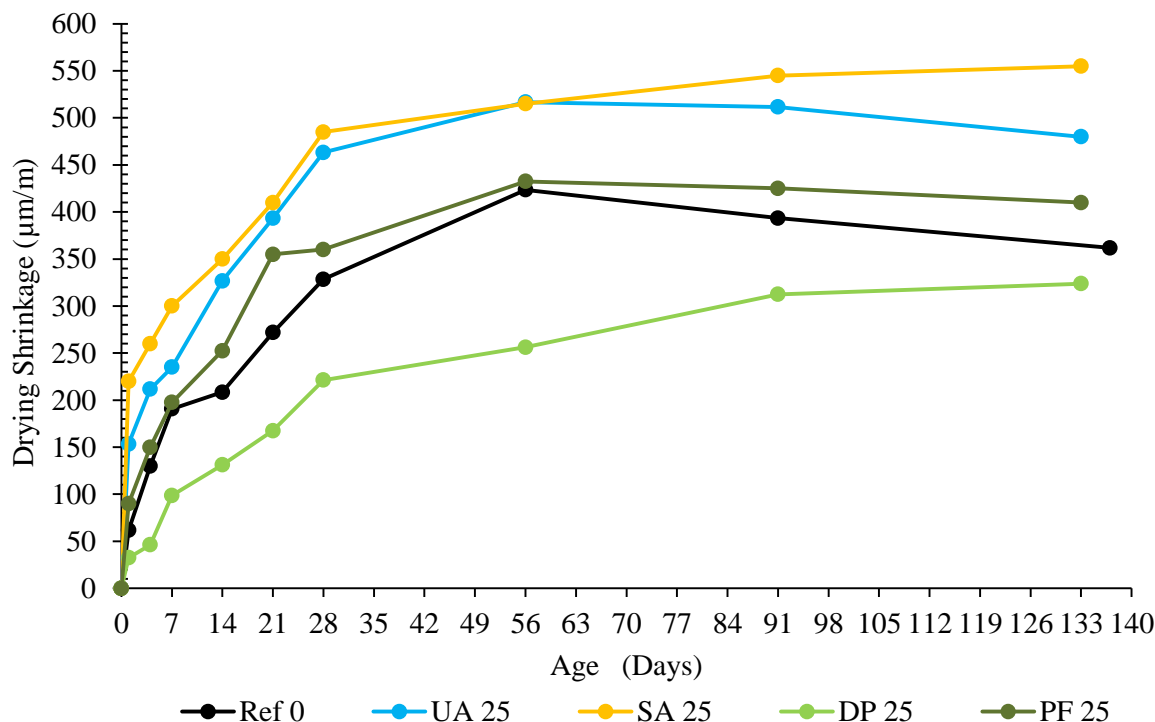


Figure 5-24. The drying shrinkage of fly ash concrete (25 %).

Chindaprasirt et al. (2004) conducted research on the effect of fineness of fly ash on drying shrinkage and discovered that finer fly ash reduces the drying shrinkage. A similar trend is found in the current study, albeit in terms of the PSD (Figure 5-1). The DP sample had a range that was greater than the reference and overlapped it; the 25 % DP based mix also exhibited the lowest shrinkage (even less than the reference). The SA cumulative particles curve is shifted to the right the most, and reported the highest shrinkage. Hence, it becomes evident that if the PSD curve of the fly ash is closer, or even incorporating more finer particles, compared to the cement, the greater the capability to reduce the drying shrinkage. In other words, the dryings shrinkage is reduced with fly ash containing more fine particles or having a curve similar to that of the cement it replaces.

Plotting cumulative mass loss against the drying shrinkage yields a linear relationship which is expected as the increase in water loss is associated with a subsequent increase in strain. Yet, for the same amount of moisture loss, the fly ash based mixes perform better compared to the reference. Hence, it can be reasoned that fly ash based concrete will have lower shrinkage capacities in regions where relatively high levels of moisture loss can be expected.

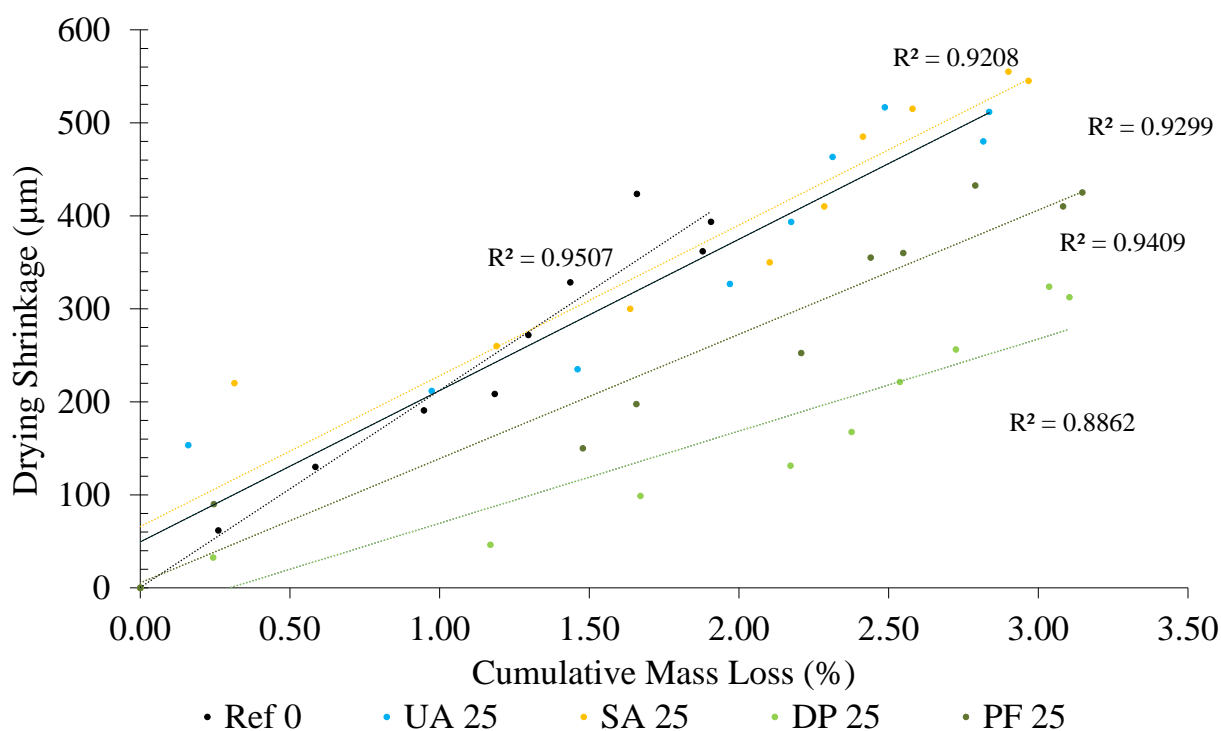


Figure 5-25. The cumulative mass loss vs drying shrinkage of the fly ash samples (25 %).

Increasing the fly ash content from 15 to 25 % resulted in an overall decrease in drying shrinkage. The shrinkage curves, and corresponding cumulative mass loss curves, can be found in Appendix B (Figure B-9 to Figure B-17). Figure 5-26 serves as a typical example of the results. Chindaprasirt et al. (2004) and Khatib (2008) also reported that the increase in fly ash content caused by a decrease in the shrinkage values. The slope of the early age shrinkage curves are steeper than the reference, and occurs likely due to the increased porosity. The lower shrinkage of the higher fly ash based mixes may be due to the unhydrated fly ash acting as an internal restraint at the early ages, hereby reducing the shrinkage. After 28 days, the stiffness increases as a result of the pozzolanic activity, thereby reducing the overall shrinkage and reaching a stabilised state.

In conclusion, the incorporation of fly ash resulted in a subsequent increase in the shrinkage of the concrete and the cumulative mass loss. The former occurs likely due to the increased paste volume and pore refinement, hereby increasing the capillary tension. The latter occurring as a result of the relatively greater amount of free water in the concrete. The effect of the PSD is suggested to be an influencing factor in the shrinkage of the concrete. A wider PSD, yet containing equal or finer material, than the reference causes a subsequent decrease in drying shrinkage. An increase in fly ash content resulted in a decrease in drying shrinkage. The reduction is suggested to occur as a result of the increased quantity of fly ash particles providing internal restraint at early ages. Hence, sufficient restraint is provided until the pozzolanic reaction also creates additional C-S-H, thereby increasing the capacity of the rigid skeleton.

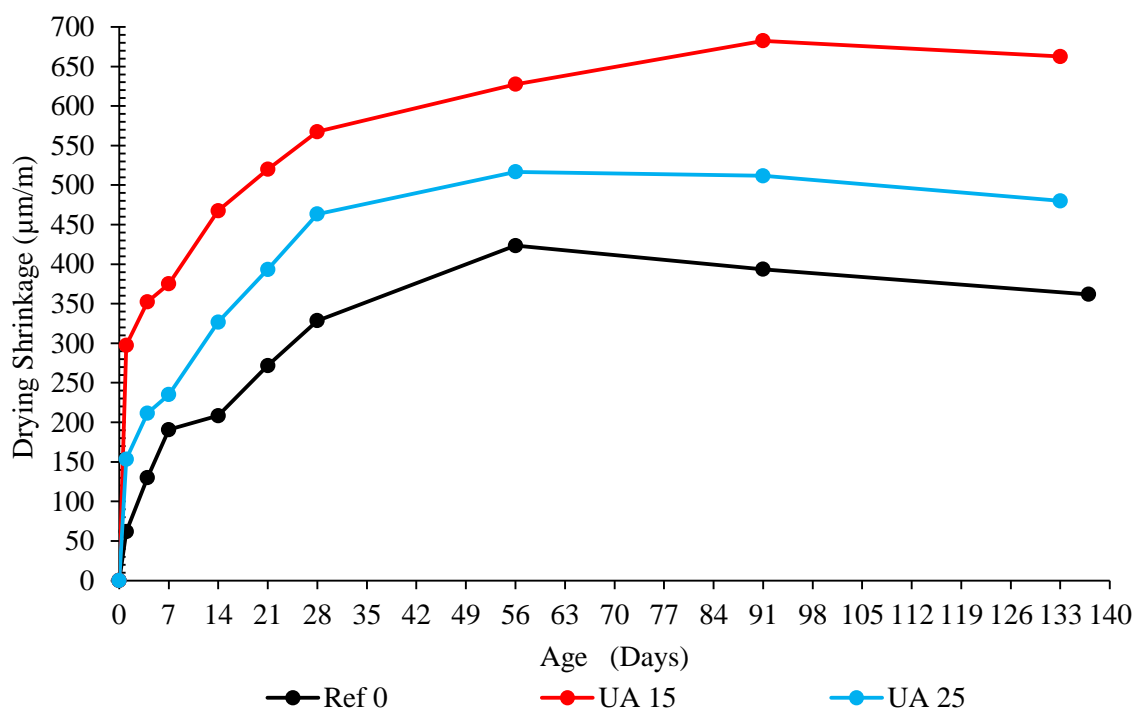


Figure 5-26. The effect on drying shrinkage with the increase of UA from 15 to 25 %.

5. 14. Durability

SCMs reap the benefit of increasing the durability properties of concrete. This is mainly achieved by pore refinement and the conversion of CH to C-S-H. The current study investigated three durability properties of fly ash based concrete and discusses the results in this section.

5. 14. 1. The Permeability of Fly Ash Based Concrete

Research conducted by Thomas and Matthews (1992), Dhir et al. (1997), Khan and Lynsdale (2002) and Salvoldi et al. (2015) all found that the incorporation of fly ash reduces the permeability of concrete compared to a control. However, based on the data of the current study, displayed in Table 5.10, it is evident that the trend varies. Some of the concrete mixes are in agreement with the former mentioned studies, such as the UA-based mixes and the 15 % SA based mix. However, the remaining mixes did not improve the permeability. In addition, the increase in fly ash content caused an increase in permeability for all mixes, excluding the PF-based mixes.

Table 5.10. Permeability of fly ash based concrete.

		PC	UA	SA	DP	PF				
		0	15	25	15	25	15	25	15	25
k	($\times 10^{-11}$ m/s)	5.94	4.65	4.73	5.65	5.03	6.97	8.58	16.04	13.00
OPI	(Log Scale)	10.22	10.33	10.33	10.25	10.30	10.17	10.07	9.79	9.88
CoV	(%)	21.7	21.67	29.11	13.61	15.31	27.78	57.8	58.7	53.6

It is suggested that the preparation of the samples for testing could have influenced the results. The samples were prepared at 21 days and tested at 28 days after casting. The effect of dilution may therefore result in the increase in permeability as a more porous structure is developed. Due to the

slower pozzolanic reaction, insufficient secondary hydration products may have formed to be able to initiate the pore blocking and increase in tortuosity.

The UA samples showed superior performance compared to all fly ash samples and the reference as well. The fineness of the samples may cause an enhancing effect on the microstructure refinement. In addition, the UA sample recorded the highest 28 strength, at both replacement levels, and compared to the other concrete mixes. This provides two possible explanations for the improved permeability. Firstly, the strength property alludes that there are more hydration products in these sample which could block the capillaries. Secondly, the increased tensile strength is an indication of an improved ITZ. The ITZ is typically more porous and can act as an eased pathway for gas permeation. Therefore, it is suggested that the UA mixes refine the ITZ and as a result reduce the permeation, resulting in a lower permeability.

The increase of the permeability can also be as a result of the increased amount of free water. The workability of fly ash based mixes increase with increasing fly ash substitution. Thomas and Matthews (1992) found that permeability decreases with water content. Also, the current study performed investigations based on a constant water-to-binder ratio and binder content; therefore, free water is higher for fly ash based mixes. The evidently higher water content therefore provides an explanation into the higher recorded permeability.

In terms of the DI, all samples are regarded as exhibiting excellent permeability properties, excluding the PF based concrete mixes, which are regarded as having good permeability properties. Even so, the use of fly ash is expected to improve with curing time as the pozzolanic reaction also continues.

5. 14. 2. The Sorptivity of Fly Ash Based Concrete

The sorptivity of the fly ash samples shows lower values compared to the reference, as seen in Table 5.11, and there is no notable trend with regard to the effect that the increase in fly ash on the sorptivity. UA samples reported an increase in sorptivity with an increase in cement substitution, whereas SA showed the opposite trend. The decreased sorptivity is most likely due to the improved microstructure associated with fly ash based concrete. The increase in porosity can be justified by the effect of cement dilution: not a sufficient level of hydration products have been created to fill all the pores and capillaries present in the mixture. In terms of the DI classification, all samples pass as *good*.

Table 5.11. Sorptivity and porosity of fly ash based concrete.

		PC		UA		SA		DP		PF	
		0	15	25	15	25	15	25	15	25	
Sorptivity	(mm/hr ^{1/2})	7.4	6.9	7.2	7.3	6.2	5.9	6.6	8.8	7.7	
CoV	(%)	4.8	1.6	4.2	1.7	9.7	4.7	7.0	19.4	14.0	
Porosity	(%)	10.0	11.2	11.7	11.7	12.0	11.1	10.9	10.6	10.3	
CoV	(%)	2.5	5.2	3.3	4.8	3.3	1.1	4.1	1.8	1.55	

5. 14. 3. The Chloride Resistance of Fly Ash Based Concrete

Studies by Thomas (1996), Leng et al. (2000) and Chindaprasirt et al. (2007) show that the inclusion of fly ash improves the chloride resistance of. For the current study, the fly ash samples had similar chloride conductivity values as that of the reference (Table 5.12). In terms of increasing fly ash content, the UA and SA showed a decrease in conductivity, DP had a relatively constant conductivity and PF showed an increase in conductivity.

Table 5.12. Chloride conductivity of fly ash based concrete.

		PC	UA		SA		DP		PF	
		0	15	25	15	25	15	25	15	25
Chloride										
Conductivity	(mS/cm)	1.34	1.43	1.37	1.54	1.46	1.37	1.38	1.46	1.77
CoV	(%)	17.3	4.01	2.33	14.82	1.71	15.39	2.08	6.69	5.88

The subsequent decrease in chloride conductivity, with increasing fly ash content, can be explained by the increase in chloride binding of fly ash based systems. In addition, the pore refinement also causes a subsequent decrease in the mobility of the chloride ions, thereby reducing the conductivity. The fact that the samples did not perform significantly better than the control is likely due to the impact of age of testing. The pozzolanic reaction may not have had reached a significant degree of hydration to produce products of significance. In other words, the chloride binding capacity, pore blocking and pore refinement had not achieved its true capacity. However, with the increased time, the chloride resistance capacity of the fly ash based concrete is certainly to be superior to that of the reference.

In terms of the DI, the fly ash systems and the reference can all be classified as good in terms of chloride resistance. However, the 25 % PF system is classified as performing poorly.

5. 14. 4. Durability Indices for South African Fly Ash

Similar to the section on slag based concrete, a point system is established to evaluate the performance of the fly ash samples relative to each other and the reference. The results are given in Table 5-15.

Table 5.13. The DI classification for the investigated fly ash.

Material	% Slag	Permeability	Sorptivity	Chloride Conductivity	Total
PC	0	++	+	+	4
UA	15	++	+	+	4
	25	++	+	+	4
SA	15	++	+	-	3
	25	++	+	+	4
DP	15	++	+	+	4
	25	++	+	+	4
PF	15	+	++	+	4
	25	+	+	-	2

Key: (++) *Excellent*; (+) *Good*; (-) *Poor*; (--) *Very Poor*

From the table, it is evident that the performance of the concrete containing fly ash has the same level of performance as the reference. The performance of the concrete is based on a 28 day basis and it can

be reasoned that the performance of the fly ash base concrete systems are to increase, and even likely surpass, the performance of the control. This is due to the increase in pozzolanic reactions that furthermore improve the concrete pores distribution and increase the pore blocking effect. In addition, the chloride binding will also increase. Hence, the incorporation of fly ash can be used as a cement replacement to improve concrete durability. The higher replacement levels of cement yielded good results, excluding the 25 % PF system. Nonetheless, the use of fly ash, regardless of type, can be a useful way to reduce the carbon footprint of the cement production industry.

5. 15. Concluding Summary

South Africa has a heavy reliance on coal for its energy production. The EIA (2015) reported South Africa to be the 7th largest coal mining country in the world, producing 282502 thousand short tons in 2013. In addition, the EIA (2015) reports that in 2012, South Africa ranked 16th in terms of electricity generation, producing 239 billion kilowatt-hours. The statistics prove cumbersome when considering the likely impact on GHG emissions. The cement industry also contributes to the GHG emissions and solutions are required to reduce the impact. Fly ash is a waste product of the coal combustion and can be efficiently used in concrete. Incorporating the waste of the energy sector can cause, albeit small, a reduction in the total GHG emissions of South Africa. Hence, the aim of the investigation was to show how the use of fly ash in concrete is most beneficial.

The use of fly ash did improve workability of concrete. The impact the difference samples had was influenced by the LOI and physical defects of the fly ash samples. The DP and PF had lower LOI values and fewer physical defects compared to the UA and SA sample. Hence, the former yielded higher workability, which also increased with increased fly ash content. Low replacement level of cement with fly ash (15 %) resulted in an acceleration of setting times. A subsequent increase in fly ash to 25 % did however result in the retardation of concrete. The impact of fly ash on the bleeding of concrete varied according to the sample used. Overall, the PSD was a leading factor in affecting the bleeding characteristics. Hence, the use of fly has positive and negative effect, in terms of fresh state properties, and depending on the concrete requirements and specifications, adequate consideration and measures are to be taken when using fly ash.

The impact of fly ash usage in concrete, in terms of hot weather concreting, was also investigated. The study found that the plastic settlement increased with the use of fly ash. However, increasing the fly ash content resulted in a reduction in settlement. Hence, precautionary measures are to be implemented to avoid plastic settlement cracking. The increase in fly ash content also reduced the slope and the total capillary pressure drop. The unrestrained plastic shrinkage of fly ash based concrete was also recorded to be higher than that of the control. The shrinkage did decrease with a subsequent increase in fly ash from 15 to 25 %. However, the reduction did not cause shrinkage lower than that of the reference. From this, it is evident the early age properties of the fly ash based concrete requires attention to ensure that any plastic shrinkage cracking can be mitigated.

SCMs are reported to improve concrete microstructure by means of the pozzolanic reactions and the pore refinement, as well as pore blocking. The current study found similar results. The pore distribution increased, yet more skewed towards the finer pores, as did the pore volume of all fly ash based concrete. The inclusion of fly ash provides an economical solution to the production of durable concrete.

Concrete performance is generally based on its compressive strength, as greater compressive strengths make it a lucrative product. The addition of fly ash was found to however reduce the early age strength. For 15 % fly ash mixes, UA and DP, showed higher 3 day strengths than the reference; due to the increase in particle packing. The difference between sample strength did diminish with age, and at 91 days of testing, some mixes (15 % SA and UA) had compressive strengths greater than the reference. The increase in fly ash content also resulted in a decrease in strength, as expected.

The fly ash type did not affect the indirect tensile strength in, yet the level of cement substitution did. Increasing the fly ash content caused a reduction in tensile strength. However, the fly ash based concrete did show superior performance when investigating the ratio of tensile strength to compressive strength.

The use of fly ash increased the mass loss and drying shrinkage of concrete. The particle packing is suggested to influence the shrinkage: a wider particle range decreases the drying shrinkage. Increasing the fly ash content did cause a subsequent decrease in drying shrinkage with the 25 % DP mixture even recorded an ultimate shrinkage lower than the control.

The durability indices of concrete containing fly ash was in most instances equal to that of the control. UA samples showed improved intrinsic permeability whereas the PF samples had the worst results, yet were still acceptable. Similar results were found in the water sorptivity. The chloride resistance of the fly ash samples were less than that of the reference. However, the age of testing is suggested to have influenced the results. The conductivity is expected to improve with age.

To conclude, the use of fly ash has some drawbacks in terms of the early age properties of concrete. With efficient measures taken, these drawbacks can be circumvented. The later age properties of fly ash based concrete showed to be equivalent, if not superior, to that of the control. Hence, regardless of the type, the use of fly ash is shown to be a sure means of reducing the impact of cement production on the environment.

Chapter 6

Discussion: A Comparison between Slag and Fly Ash

The previous two chapters of this report discuss the effect that South African manufactured slag and fly ash when incorporated in concrete. Firstly, it consisted of comparing two types of slag, namely, a ground granulated Corex slag (GGCS) and a ground granulated blastfurnace slag (GGBS), relative to each other and a reference. Secondly, four types of fly ash were compared with each other plus a reference. The performance of these materials were measured when incorporated in a concrete mixture. The study assessed the fresh state, early age, hardened state and durability properties. This chapter compares these two materials relative to one another.

6.1. Reactivity

Reactivity is a means to evaluate the potential of a material to be used as a SCM in concrete and the SAI is one of the methods that can be used. For this study, the SAI of the GGCS had a higher SAI than GGBS at both test ages; establishing that GGCS is more reactive. A study conducted by Alexander et al. (2003) reported similar findings. The SAI of the fly ash samples reported that PF sample had the highest degree of reactivity at 28 days, yet the lowest at 90 days. UA had the opposite trend, having the lowest SAI at 28 days and the highest at 90 days.

Establishing a comparison based on the reactivity of these two types of materials proved difficult based on two conditions: the differences in age of testing and replacement level. Slag has self-cementing capabilities, hence, justifying the use of higher replacement levels and earlier ages of testing. Table 6.1 provides the SAI of the materials at 28 days of testing.

Table 6.1. The SAI of the cementitious binders at 28 days.

	Slags (50 %)		Fly Ash (25 %)			
	GGBS	GGCS	UA	SA	DP	PF
SAI (%)	69.4	92.9	62.1	76.5	78.8	95.4

Based on the results given in Table 6.1, the PF system shows to have the highest reactivity overall. The GGCS is second, in terms of reactivity according to the SAI followed by DP, SA and GGCS and UA. Typically, the reactivity of GGCS is reported to be higher than the reference; and GGCS has

reported to have a 28 day SAI exceeding 100 % (Alexander et al., 2003; Beushausen et al., 2012). The low reactivity in this study is possibility due to a bad batch being used. Even so, the reactivity is still relatively high and, the reactivity exceeds that of 4 out of the 6 samples used. The materials also show favourable properties for use in concrete. The UA sample did have a lower SAI than required by the BS EN 450-1 (2012), yet at 90 days, the SAI was significantly higher at 87.3 %.

6. 2. Fresh State Properties

The current study investigated the effect of slag and fly ash on the fresh state properties, namely: workability, setting time and bleeding. These properties are important in order to ensure that the concrete performs better at an early age. The early age properties is the time where concrete is handled the most and in its weakest state.

6. 2. 1. Workability

Both the use of slag and fly ash improved the workability, measured as a function of the slump, of concrete. Figure 6-1 presents graphically the slump data at 25 % cement replacement and shows that all materials, excluding the UA, had an effect of increasing the workability.

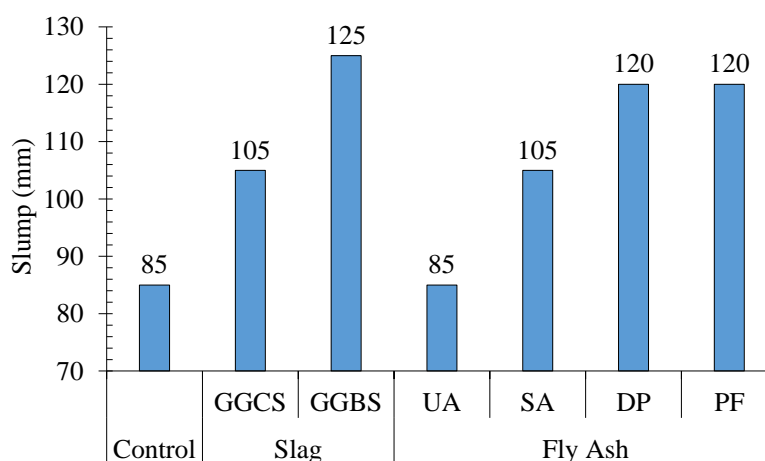


Figure 6-1. The workability of the control and 25 % cement SCM-based concrete.

From the results, it can be seen that the water can be reduced for SCM-based concrete in general, since the slumps are relatively higher than that of the control. This means that the amount of binder can be reduced, with the corresponding reduction in water, to produce concrete mixes of the same strength. Alternatively, by decreasing the water content and keeping the binder content constant, a change in water-to-binder ratio is achievable that may result in concrete of higher compressive strength. The former is favoured, as the reduction in binder content can ultimately reduce the amount of cement used for a given construction project. Moreover, the latter has potential for the incorporation of fly ash and slag in the study of high performance concrete (HPC), which requires a low water-to-binder ratio. Due to the capability to increase the workability, and the high fines present, the use of SCMs may have a beneficial use in self-compacting concrete (SCC).

In conclusion, the inclusion of these materials show good improvement in concrete workability. In addition, the increase in these materials did show a trend of increasing the workability. Finally, the GGBS and PF samples showed the greatest improvement when considering slag and fly ash respectively. Irrespective of the SCM used, whether it is fly ash or slag, have the potential to reduce the binder required to achieve a certain state of workability.

6. 2. 2. Setting Time

The impact of SCMs on the setting time varied due to the material used as well as the level of substitution. There was a general trend of increasing retardation with the increase in cement replacement with the respective SCMs. This was discussed to occur as a result of dilution. Some SCMs caused an acceleration of the setting time due to the increased reactivity (GGCS) and the filler effect (15 % UA). At lower cement replacement levels, the physical effects of the system causes accelerated hydration. Therefore, incorporating SCMs in concrete at low levels does not result in extremely severe effects; it is only at relatively high substitutions that the retardation has a significant impact. Still considering the former, it is necessary to mention that the reactivity of the sample can counter the delay experienced as was seen with GGCS. With an increase in studies on the alkali-activation of binders, the early on activation of SCMs can potentially reduce the retardation. In terms of the investigated material, the GGCS showed superior performance of all the materials. The worst retardation was detected with DP at 15 % cement replacement (with an approximate retardation of 4 hours).

6. 2. 3. Bleeding

The particle distribution of SCMs had a greater influence on the bleeding capacity as a result of the improved particle packing. Figure 6-2 provides the bleeding rate and capacity of concrete containing fly ash and slag.

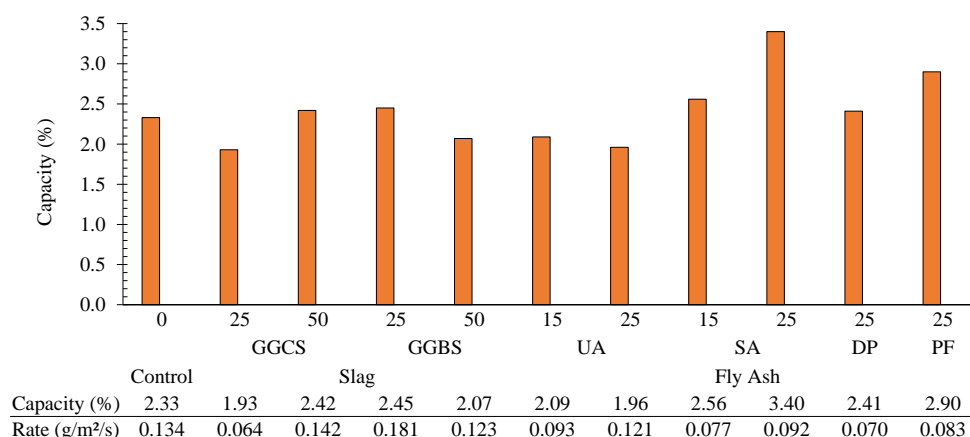


Figure 6-2. The bleeding information of the investigated SCMs.

Fly ash in concrete is seen to reduce the bleeding rate, yet subsequently increases the bleeding capacity, due to the longer duration of plasticity. The effect of slag on these properties varied amongst the two slag types. Increasing the GGCS content increased both the rate and capacity,

whereas GGBS had the converse effect with increasing substitution. When comparing the SCMs at 25 % level, it can be seen that the fly ash samples exhibit better bleeding characteristics. The lower bleeding rates may be due to the higher paste content and differences in material relative densities. The increased capacities in turn are related to the higher water content and longer duration in a plastic state.

6. 3. Early Age Deformation: Plastic Settlement and Shrinkage

Figure 6-3 provides the ultimate plastic settlement of the different concrete mixes. The concrete mixtures containing the lowest percentage difference, or even reduced settlement are the 25 % GGCS, SA and UA, with percentages of -30.3, 0.2 and 6.3, respectively. The reduction in the shrinkage of these specimens were noted to have good consistency. In general, the slag based concrete showing lower degree of settlement compared to the fly ash samples. The observed differences can be explained by the differences in workability as slags have lower workability. The increase in workability is suggested to decrease the overall viscosity as a greater amount of free water is present. This is in agreement with a study on rheology by Park et al. (2005). Their research found an increase with continual increase in fly ash, yet a decrease with slag. Hence, the slags seem to have a better performance in terms of the settlement, with the 25 % GGCS slag performing the best of all the mixes; it reduced the settlement by up to 30 %. Increasing the slag content seems to yield an increase in settlement, whereas the increase in fly ash has the opposite effect of reducing the settlement. It is suggested that the increase in fines causes an increase in particle dispersion and increase in colloidal forces, which increases the cohesiveness and results in the improved settling condition.

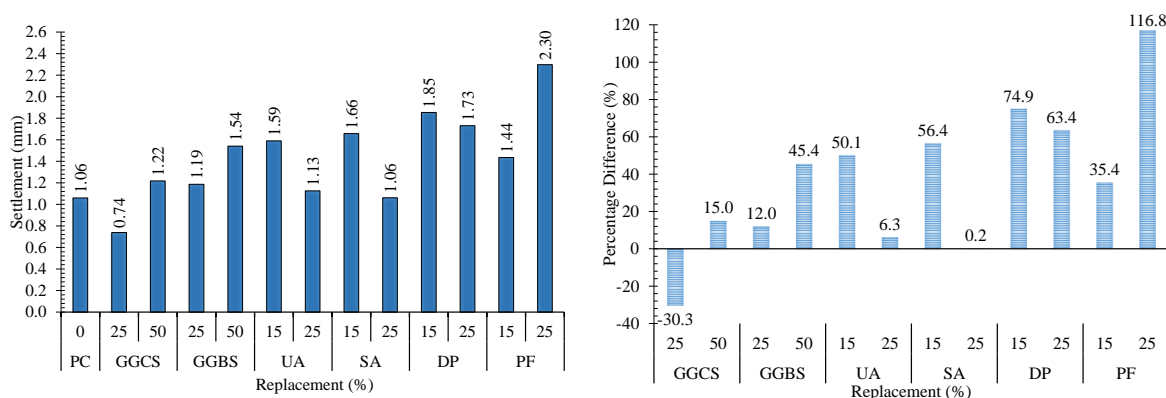


Figure 6-3. The ultimate plastic settlement (left) of the SCM-based concrete and associated percentage difference (right).

SCMs are noted to increase the plastic shrinkage of concrete mixtures, yet the subsequent increase in the amount of cement replacement causes a subsequent decrease in the amount of shrinkage experienced, as shown in Figure 6-3. It is observed that the percentage increase in shrinkage is relatively lower on average for mixes with slags compared to those with fly ash. This is most likely

due to the higher level of workability of the fly ash based concretes. In addition, this trend of slag having lower shrinkage than fly ash mixes was not expected as the bleeding characteristics of the slags mixes had lower capacities, rates and durations. When comparing the concrete mixtures on the percentage increase relative to that of the reference, it can be seen that the slag mixes have lower averages relative to that of the fly ash based concrete, 49.02 and 78.75 %, respectively. From the results obtained by the current study it is concluded that the effect of rigidity as a result of hydration also contributed to the difference in shrinkage values. It can therefore be concluded that the slag samples perform better compared to the fly ash samples in terms of plastic shrinkage.

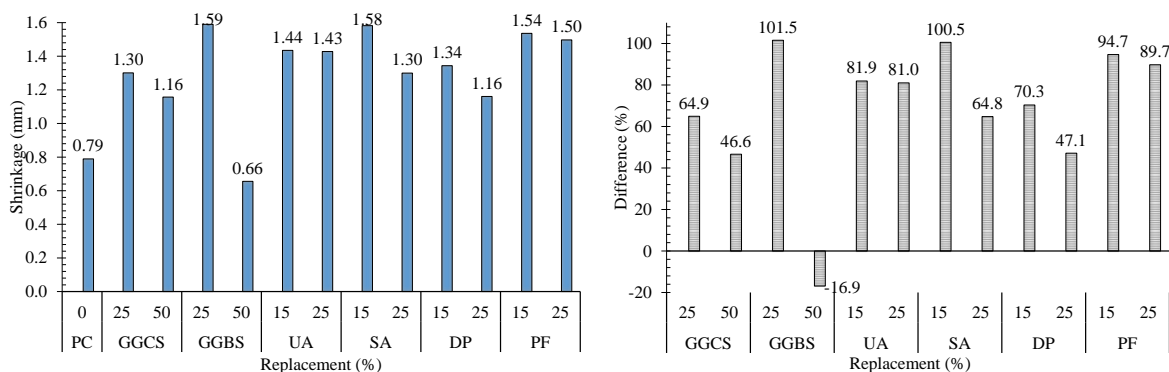


Figure 6-4. The ultimate plastic shrinkage (per 300 mm) (left) of the SCM-based concrete and associated percentage difference (right).

Holt and Leivo (2004) suggested a maximum strain threshold of 1000 $\mu\text{m}/\text{m}$ as the limit at which the risk of plastic cracking of concrete is relatively high. Based on this imposed limit and the data of Figure 6-5, it can be seen that the risk of plastic shrinkage cracking occurring is relatively high and measures should be taken to limit, if not mitigate, the cracking of concrete. Preventive measures include the incorporation of microfibres and efficient curing to prevent the evaporation from inducing drying cracking.

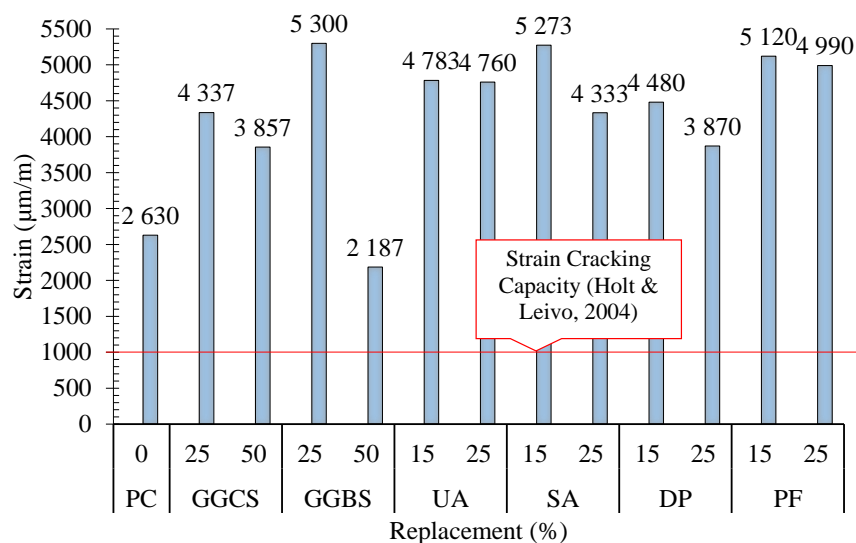


Figure 6-5. The ultimate plastic shrinkage strain induced in the concrete.

6. 4. Concrete Microstructure

SCMs improve concrete microstructure due to the pozzolanic reactions and the pore-blocking phenomenon. The current study found that the addition of either slag or fly ash showed significant improvement of the pore distribution as shown in Figure 6-6. The benefits of the pore refinement include the inhibiting of deleterious substances, such as chloride ions, into concrete. Hence, using SCMs, regardless of the type, provides a significant level of improvement in the durability of the concrete, which has benefits with regard to increasing the design life.

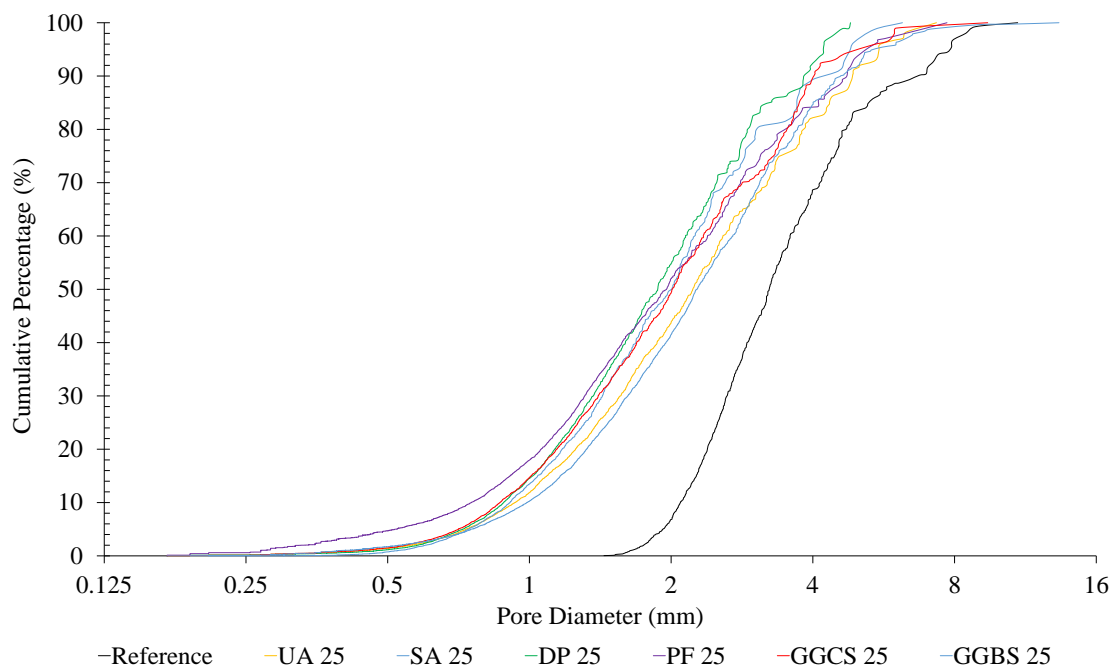


Figure 6-6. The cumulative pore distribution of concrete containing 25 % fly ash or slag compared to the reference.

6. 5. Hardened State Properties of Concrete

6. 5. 1. Compressive Strength

The compressive strength of concrete containing SCMs did exhibit a trend of low early age strengths, due to dilution and lower reactivity. The results of 25 % cement replacement are summarised in Figure 6-7. Two fly ash (15 % UA and PF) mixes did have compressive strengths that were equal to or greater than that of the reference, as a result of the filler effect. In addition, the trend of decreasing strength with increasing SCM content was also noted.

From Figure 6-7 it is seen, that for all ages, the strength of the slag-based concrete exceeds those of the fly ash samples. This correlates to the differences observed in the reactivity. Slag has self-cementing properties and reacts at ages as early as 7 days. The fly ash samples require the silica chain to be broken before the pozzolanic reaction can commence; the pozzolanic reaction is believed to only be significant from 28 days. The strength gain of the reference starts to reduce with increased curing time, which is due to the hydration being limited by limited space for the products and

moisture. The SCMs still have appreciable strength gain due to the secondary reaction and the replacement of CH with C-S-H.

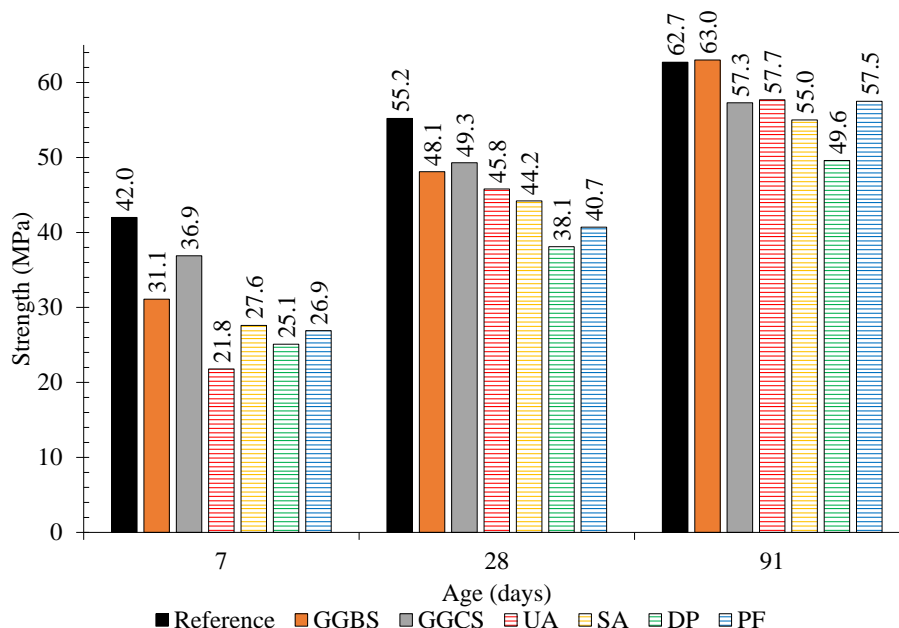


Figure 6-7. The compressive strength development of 25 % cement replacement with SCMs.

Nonetheless, the strength of concrete is predominately affected, or more correctly chosen on the basis of a 28 day strength requirement. Therefore, considering this, it is clear that the effect of choosing the *best* SCMs-based concrete should be assessed on the relative strength required at a specified age. The effect of continual strength increase should also still be taken into account, as this is an area often ignored. Table 6.2 displays the maximum strength of the slag and fly ash samples at different ages of testing.

Table 6.2. The slag and fly ash with the highest strength at specified ages.

		Age (Days)				
		3	7	28	56	91
Reference	MPa	23.1	42.0	55.2	60.9	62.7
Slag	MPa	21.1	36.9	49.3	55.1	63.0
	Type:	GGBS	GGCS	GGCS	GGCS	GGBS
	(%)	25	25	25	25	25
Fly Ash	MPa	24.6	32.8	49.5	59.0	63.3
	Type:	UA	PF	UA	UA	UA
	(%)	15	15	15	15	15

From Table 6.2 it can be seen that the GGCS sample performs relatively better compared to the GGBS sample (this was concluded in the previous chapters), due to the higher reactivity. The UA sample also performed better than the fly ash samples. In addition, the sample recorded higher strengths compared to that of the slag. It is suggested that the fly ash sample has a better filler effect which explains the strength differences. Even at 28 days the strength difference between the 15 %

UA sample and reference was only 5.7 MPa. This is indicative that similar strengths can be achieved with SCMs.

The replacement level also differs for slag and fly ash, with the replacement for slag exceeding that of fly ash. Reason being that slag is more reactive. In addition, the strength results do show that higher substitutions of slag can achieve strengths equal to or higher than that of a low level fly ash based concrete. For example, at 28 days, the 75 % GGCS had an average compressive strength of 39.9 MPa, which is higher than all 35 % fly ash based mixes (UA = 38.9 MPa, SA = 35.3 MPa, DP 35.0 MPa and PF = 30.1 MPa). Hence, the potential of cement replacement of slag is greater than that of fly ash. In other words, using slag at larger quantities will have fewer detrimental effects compared to fly ash in terms of compressive strength.

6. 5. 2. Indirect Tensile Strength

Using the data from Figure 4-22 and Figure 5-21, and isolating the 25 % SCM based concrete results, it is apparent that slag based concrete yields higher tensile strengths compared to the concrete incorporating fly ash. The GGCS- and GGBS-based mixes have strengths of 4.60, 4.77 MPa, respectively and the UA and SA had 4.31 and 3.86 MPa, respectively. Both of these materials are suspected to improve the ITZ of the concrete due to the filler effect. It is probable that the addition of the slag has both a filler effect at the ITZ and due to the higher reactivity, starts to produce hydration products at the specified zone earlier.

6. 6. Drying Shrinkage

The shrinkage and cumulative mass loss of fly ash based concrete increased from 0 to 15 % content. However, the shrinkage decreased as more fly ash was included in the concrete. For slag-based concrete the trend varied. GGBS had a minimal impact on the drying shrinkage, even with an increase in GGBS content. A similar trend was noted with respect to the cumulative mass loss. GGCS mixes in contrast showed a trend of decreasing mass loss with added slag. The cumulative mass loss was less than that of the control. However, the increase in GGCS did cause an increase in drying shrinkage.

6. 7. Durability

The use of both fly ash and slag is known to result in the production of more durable concrete. This is due to the refined and dense microstructure as well as the conversion of CH into C-S-H as part of the pozzolanic reaction. The study investigated three durability parameters namely: permeability, sorptivity and chloride conductivity.

6. 7. 1. Permeability

The permeability of the majority of mixes increased with the increase in SCM content. A few concrete mixes did have permeability constants (k) less than the reference (15 and 25 % UA and

15 % SA). The increase in permeability is suggested to be a result of the dilution effect. It is suspected that the permeability of the SCM based concrete will improve with increasing curing age, as this is commonly found in the literature. The permeability values of most of the fly ash samples were relatively lower (ranging between 4.6 and 8.6×10^{-11} m/s) compared to that of the slag ($7.83 - 9.85 \times 10^{-11}$ m/s); the mixes containing the PF fly ash is an exception with higher values of 16 and 13×10^{-11} m/s. The improvement by the use of fly ash is likely due to the fly ash having a wider PSD span, which improves the particle packing and smaller particles can therefore block the capillaries. This results in an estimated increase in the tortuosity of the concrete.

6. 7. 2. Sorptivity

The sorptivity is approximately the same for both fly ash and slag samples, and does not differ as much compared to that of the reference. The high cement content, and its relative fineness, is suggested to be the reason for this. It is suggested that the data from the study is not sufficient to establish a good correlation between the sorptivity and the different materials. It would be worthwhile to investigate the impact of South African products on a larger scale, such as varying the water-to-binder ratio and SCM content. Nevertheless, the study has found that the sorptivity results are still good in terms of durability indices.

6. 7. 3. Chloride Conductivity

The difference in chloride conductivity between slag and fly ash samples were quite significant. The conductivity values for the fly ash samples exceeded those of the reference and values of the slag-based mixes were almost 4 times greater than that of the fly ash concrete. The reference had a conductivity of 1.3 mS/cm, whereas the fly ash based concrete had values exceeding 1.4 mS/cm. In contrast, three of the four slag mixtures had conductivity values of 0.4 mS/cm: the 50 % GGCS sample had a higher value of 0.7 mS/cm. This implies that the use of slag is favourable for concrete exposed to environments high in chloride content, such as coastal regions. One mechanism of chloride conductivity is the formation of Friedel's salt, a compound formed by the aluminate phases of concrete incorporating chloride ions in the concrete crystal system, thereby immobilising the ions. Plain concrete also form this salt, yet as can be seen, not as effectively as when compared to slag based concrete. Moreover, the ITZ of concrete with slag is thought to be improved largely compared to that of the reference. The improvement can be justified by the fact of the indirect tensile strength of slag based concrete being greater than that of the reference and the fly ash based concretes. Greater tensile strengths are typically associated with improved ITZ. Hence, the pathways for chloride ions are limited to a certain degree.

6. 7. 4. Concluding Remarks

In conclusion, the durability of concrete containing SCMs are comparatively good. It is suggested, that with increased curing times, properties will improve even more. The choice of incorporating a

certain SCM will depend on the specification of the project. Considering this, it is clear that there is a need to start migrating towards the design specification that incorporate, or at least consider, the durability requirements of concrete as well.

6. 8. Concluding Summary

The results discussed, lean toward the notion that the incorporation of slag or fly ash provide adequate concrete properties in relation to the control used. Using SCMs provides a suitable means of relieving the strain that cement production has on the environment. It is noted that the early age properties of concrete is somewhat adversely affected, such as the early age strength and the early age deformation. With adequate design procedures and the implementation of new technology, these problems can be mitigated. To establish which material, fly ash or slag, is more effective for use in concrete, additional factors would have to be considered. For example, slag would be most suited for use in high chloride environments, such as coastal structures. However, fly ash would also be well suited. For large floorplans, fly ash would be best suited due to the lower drying shrinkage. It is worth mentioning that slag would also be sufficient. Ultimately, the type of material that is available is an influencing factor. The final outcome is that the use of SCMs provide a good substitution for cement replacement, which could potentially reduce the impact of cement production on the environment.

Chapter 7

Conclusion and Recommendations

There is a great negative impact of cement production on global climate issues and energy and natural resource consumption. Cement production forms a key element for social and economic development and therefore solutions to reduce the impact, without adversely affecting development need to be found. The objective of the study was to investigate the use of supplementary cementitious materials (SCMs), viz. fly ash and slag that are available in South Africa, to reduce the dependency on cement as a standalone binder. This was achieved by conducting physical experiments on concrete mixtures, evaluating the performance of the materials that were incorporated and comparing them to a control mixture. Experiments included: the evaluation of the reactivity, fresh state properties, early age deformation, mechanical properties and durability.

7.1. Conclusions

Two types of slag (GGBS and GGCS) and four fly ash samples (all Class F) were used in the study. The four fly ash samples included samples from four suppliers in South Africa. These samples included Ulula Ash (UA), Sphaku Ash (SA), Durapozz (DP) and Pozzfill (PF). Concrete mixes were designed at a constant binder content and water-to-binder ratio and a control (0 % cement replacement) was used as a reference. Cement substitution was done on three levels for both slag (25, 50 and 75 %) and fly ash (15, 25 and 35 %) based concrete. The following conclusions were made:

Reactivity:

- GGCS was reported to be more reactive than GGBS, which is commonly found in literature.
- UA showed poor levels of reactivity at 28 days, but were most reactive at 90 days of testing.
- The SAI is better at predicting the performance of slags than for fly ash samples.

Fresh State Properties

- Workability was significantly improved by the incorporation of either slag or fly ash, as increasing the SCM content increased the recorded slump. High LOI percentages has an adverse effect on workability due to the increased porosity and surface area.

- More reactive materials (GGCS) and low cement replacement levels with fly ash (15 %) accelerated the setting times. This is suggested to be due to nucleation and surface chemical effects.
- Bleeding was affected by the PSD of the SCM sample. Higher bleeding capacity occurred with wider particle spans.

Early Age Deformation

- Both slag and fly ash increased the settling of concrete, therefore increasing the risk of settlement cracking. The increase in fly ash content from 15 to 25 % however reduced the settlement. In contrast, increasing slag content resulted in the increase of settlement.
- Plastic shrinkage increases with the addition of fly ash and slag. The subsequent increase in SCMs did however reduce the plastic shrinkage.
- The study found that lower capillary pressure drops do not necessarily relate to higher lower plastic shrinkage values. The pressure drops of the SCM-based concrete were lower compared to the reference, yet these mixes did have higher plastic shrinkage values.

Hardened State Properties

- Both slag and fly ash improved the microstructure. The pores are refined, as is the pore volume. More than 95 % of pores were equal or less than 1 mm³ in volume when SCMs were incorporated.
- The early age compressive strength decreases with the addition, and increase, of SCMs. Slag achieved higher strengths and can be used to substitute larger proportions of cement, when compared to the fly ash mixes. Nevertheless, both these materials showed to be able to achieve strengths equal to the reference with prolonged ages of curing.
- Three notable trends were observed with inclusion of SCMs in concrete with regard to the tensile capacity. Firstly, indirect tensile strength increased with curing ages. Secondly, there is a subsequent decrease in the indirect tensile strength with a corresponding increase in the cement replacement. Thirdly, the ratio of the indirect tensile strength to compressive strength for SCM based concrete is higher than that of a SCM-free mix.
- Slag based concrete yielded higher indirect tensile strength than fly ash mixes.
- The drying shrinkage was higher or equal to the control for SCM based mixes. A higher incorporation of fly ash improved the drying shrinkage behaviour of the mixes.

Durability

- Slag based concrete had potentially better durability performances compared to fly ash mixes.
- The use of SCMs did show to potentially reduce the permeability of concrete, as UA based concrete is a good example of this. Nevertheless, the permeability is believed to eventually

improve with increased curing, despite the higher permeability constants (k) that were reported for some of the SCM-based concrete, such as the PF based mixes.

- The porosity of fly ash based mixes were slightly higher than that of the control. The largest increase was by 2 % for a 25 % SA mix. The increase is suggested to occur because of the lower reactivity of fly ash at the age of testing. Slag mixes showed a decrease in porosity, which is related to the higher reactivity at early ages compared to fly ash.
- The use of slag exhibited the greatest reduction in chloride conductivity and this improved with increased slag content. Slag based mixes reported conductivity coefficients that were up to four times less than that of the control, and fly ash based mixes.

7.2. Recommendations

From the knowledge gained of the current study, the following can be identified as potential areas for future research:

- An LCA for South African materials is required to establish to what extent the reduction, in terms of SCMs use, relates too. In addition, an economic study would can also accommodate the study.
- The study focussed on *normal* concrete, i.e. typical strength and without any admixtures. Hence, a the study on the incorporation of these materials in mixes such as SCC and HPC may provide more ways of reducing the carbon footprint.
- From the study, it is apparent that the PSD of the SCMs has an impact on the properties, especially in the fresh state, of concrete, such as bleeding and shrinkage. Investigating the effect could provide means of reducing the adverse impacts on shrinkage.
- Additional durability studies can be undertaken to further the knowledge of SCMs being used to mitigate concrete deterioration.

7.3. Concluding Statement

The study investigated the potential of SCMs to reduce the dependency on cement utilisation. It is evident that the total replacement of cement as a construction material is still a not n evident outcome for the next 50 years at least, yet may be inevitable. The results showed that the incorporation of slag or fly ash performed as well or even better than the control. This substantiates the potential to reduce the cement dependency, which can lead to a reduction in GHG outputs. It is concluded that of South African slag and fly ash can be used as partial replacement of concrete with beneficial results.

References

- ACI, 2003. *Slag Cement in Concrete and Mortar Reported by ACI Committee 233*, Farmington Hills, Michigan: American Concrete Institute.
- ACI, 1986. *Use of fly ash in concrete Reported by ACI Committee 232*, Farmington Hills, Michigan: American Concrete Institute.
- ACI Committee 302.1 R-96, 1997. *Guide for Concrete Floor and Slab Construction*, Farmington Hills, Michigan.
- ACI Committee 318, 2008. *Building Code Requirements for Structural Concrete (ACI 318-08)*, West Conshohocken, PA: ACI.
- Addis, B. and Goodman, J., 2009. Concrete Mix Design. In G. Owens, ed. *Fulton's Concrete Technology*. Midrand, South Africa: Cement & Concrete Institute.
- Aldea, C.M., Young, F., Wang, K., and Shah, S.P., 2000. Effects of curing conditions on properties of concrete using slag replacement. *Cement and Concrete Research*, 30, pp.465–472.
- Alexander, M.G., Ballim, Y., and Mackechnie, J.R., 2009. Durability Index Testing Procedure Manual. , 2009.
- Alexander, M.G., Jaufeerally, H., and Mackechnie, J.R., 2003. Structural and durability properties of concrete made with Corex slag. *Research monograph*, (6).
- Alexander, M.G., Santhanam, M., and Ballim, Y., 2010. Durability design and specification for concrete structures—the way forward. *International Journal of Advances in Engineering Sciences and Applied Mathematics*, 2(3), pp.95–105.
- Almusallam, A., Maslehuddin, M., Abdul-Waris, M., and Khan, M., 1998. Effect of mix proportions on plastic shrinkage cracking of concrete in hot environments. *Construction and Building Materials*, 12(6-7), pp.353–358.
- Aly, T. and Sanjayan, J.G., 2008. Mechanism of early age shrinkage of concretes. *Materials and Structures*, 42(4), pp.461–468.
- Ampadu, K.O., Torii, K., and Kawamura, M., 1999. Beneficial effect of fly ash on chloride diffusivity of hardened cement paste. *Cement and Concrete Research*, 29(4), pp.585–590.
- Aponte, D.F., Barra, M., and Vázquez, E., 2012. Durability and cementing efficiency of fly ash in concretes. *Construction and Building Materials*, 30, pp.537–546.
- Arioglu, N., Canan Girgin, Z., and Arioglu, E., 2006. Evaluation of ratio between splitting tensile strength and compressive strength for concretes up to 120 MPa and its application in strength criterion. *ACI Materials Journal*, 103(1), pp.18–24.
- Arivalagan, S., 2014. Sustainable Studies on Concrete with GGBS As a Replacement Material in Cement. *Jordan Journal of Civil Engineering*, 8(3), pp.263–270.
- Arya, C., Buenfeld, N.R., and Newman, J.B., 1990. Factors influencing chloride-binding in concrete. *Cement and Concrete Research*, 20(2), pp.291–300.
- Arya, C. and Xu, Y., 1995. Effect of cement type on chloride binding and corrosion of steel in concrete. *Cement and Concrete Research*, 25(4), pp.893–902.
- ASTM Standards C125, 2011. *Standard Terminology Relating to Concrete and Concrete Aggregates*, West Conshohocken, PA: ASTM International.

- ASTM Standards C1202, 2013. *Standard Method of Test for Electrical Indication of Concrete's Ability to Resist Chloride Ion Penetration*, West Conshohocken, PA: ASTM International.
- ASTM Standards C232/C232M-09, 2010. *ASTM C232 / C232M-09. Standard Test Methods for Bleeding of Concrete*, West Conshohocken, PA: ASTM International.
- ASTM Standards C618, 2010. *Standard Specification for Coal Fly Ash and Raw or Calcined Natural Pozzolan for Use in Concrete*, West Conshohocken, PA: ASTM International.
- ASTM Standards C989, 2013. *Standard Specification for Slag Cement for Use in Concrete and Mortars*, West Conshohocken, PA: ASTM International.
- Ballim, Y., Alexander, M., and Beushausen, H., 2009. Durability of concrete. In G. Owen, ed. *Fulton's Concrete Technology*. Midrand, South Africa: Cement & Concrete Institute, pp. 155–188.
- Basheer, L., Kropp, J., and Cleland, D.J., 2001. Assessment of the durability of concrete from its permeation properties: A review. *Construction and Building Materials*, 15(2-3), pp.93–103.
- Basheer, P.A.M. and Barbhuiya, S., 2009. Pore structure and transport processes. In M. Soutsos, ed. *Concrete durability: a practical guide to the design of durable concrete structures*. London: Thomas Telford, pp. 14–33.
- Basheer, P.A.M. and Barbhuiya, S., 2010. Pore structure and transport processes. In M. Soutsos, ed. *Concrete durability: a practical guide to the design of durable concrete structures*. London: Thomas Telford, pp. 14–33.
- Bentur, A. and Alexander, M.G., 2000. A review of the work of the RILEM TC 159-ETC: Engineering of the interfacial transition zone in cementitious composites. *Materials and Structures*, 33(March), pp.82–87.
- Bentz, D.P., Garboczi, E.J., Haecker, C.J., and Jensen, O.M., 1999. Effects of cement particle size distribution on performance properties of Portland cement-based materials. *Cement and Concrete Research*, 29(10), pp.1663–1671.
- Bentz, D.P., Hansen, A.S., and Guynn, J.M., 2011. Optimization of cement and fly ash particle sizes to produce sustainable concretes. *Cement and Concrete Composites*, 33(8), pp.824–831.
- Berndt, M.L., 2009. Properties of sustainable concrete containing fly ash, slag and recycled concrete aggregate. *Construction and Building Materials*, 23(7), pp.2606–2613.
- Beushausen, H., Alexander, M., and Ballim, Y., 2012. Early-age properties, strength development and heat of hydration of concrete containing various South African slags at different replacement ratios. *Construction and Building Materials*, 29, pp.533–540.
- Beushausen, H. and Alexander, M.G., 2008. The South African durability index tests in an international comparison. *Journal of the South African Institution of Civil Engineering*, 50(1), pp.25–31.
- Bijen, J., 2003. Concrete. In *Durability of Engineering Structures - Design, Repair and Maintenance*. Elsevier, pp. 54–138.
- Bissonnette, B., Pierre, P., and Pigeon, M., 1999. Influence of key parameters on drying shrinkage of cementitious materials. *Cement and Concrete Research*, 29(10), pp.1655–1662.
- Boa, A.R. and Topu, L.B., 2012. Influence of fly ash on corrosion resistance and chloride ion permeability of concrete. *Construction and Building Materials*, 31, pp.258–264.
- Boshoff, W.P., 2012. *Report number : ISI2012-17 Plastic Shrinkage Cracking of Concrete*, University of Stellenbosch.
- Boshoff, W.P. and Combrinck, R., 2013. Modelling the severity of plastic shrinkage cracking in concrete. *Cement and Concrete Research*, 48, pp.34–39.
- Bouikni, A., Swamy, R.N., and Bali, A., 2009. Durability properties of concrete containing 50% and 65% slag. *Construction and Building Materials*, 23(8), pp.2836–2845.
- Bouzoubaa, N. and Foo, S., 2004. *Use of fly ash and slag in concrete: A Best Practice Guide*, Canada: MTL.
- BRITISH STANDARDS INSTITUTE, 2009a. *BS EN 12350-2. Testing Fresh Concrete. Slump Test.*

- London: British Standards Institute.
- BRITISH STANDARDS INSTITUTE, 2013. *BS EN 12390-13. Determination of the Secant Modulus of Elasticity in Compression.*, London: British Standards Institute.
- BRITISH STANDARDS INSTITUTE, 2002. *BS EN 12390-3. Testing Hardened Concrete. Compressive Strength of Test Specimens*, London: British Standards Institute.
- BRITISH STANDARDS INSTITUTE, 2009b. *BS EN 12390-5. Testing Hardened Concrete. Flexural Strength of Test Specimens.*, London: British Standards Institute.
- BRITISH STANDARDS INSTITUTE, 2003. *BS EN 12390-6. Testing Hardened Concrete. Tensile Splitting Strength of Test Specimens.*, London: British Standards Institute.
- BRITISH STANDARDS INSTITUTE, 2006. *BS EN 15167-1: Ground granulated blast furnace slag for use in concrete, mortar and grout. Definitions, specifications and conformity criteria*, London: British Standards Institute.
- BRITISH STANDARDS INSTITUTE, 2011. *BS EN 196-5: Methods of testing cement. Pozzolanicity test for pozzolanic cement*, London: British Standards Institute.
- BRITISH STANDARDS INSTITUTE, 2012. *BS EN 450-1: Fly ash for concrete. Definition, specifications and conformity criteria*, London: British Standards Institute.
- BRITISH STANDARDS INSTITUTE, 2009c. *BS ISO 1920-8. Testing of Concrete. Determination of Drying Shrinkage of Concrete for Samples Prepared in the Field or in the Laboratory.*, London: British Standards Institute.
- BRITISH STANDARDS INSTITUTE, 2005a. *EN 196-1 - Methods of Testing Cement. Determination of Strength.*, London: British Standards Institute.
- BRITISH STANDARDS INSTITUTE, 2005b. *EN 196-3. Methods of Testing Cement. Determination of Setting Times and Soundness.*, London: British Standards Institute.
- BRITISH STANDARDS INSTITUTE, 2004. *Eurocode 2: Design of concrete structures. General rules and rules for buildings*, London: British Standards Institute.
- Brooks, J., 2003. Elasticity , shrinkage , creep and thermal movement. In J. Newman & B. S. Choo, eds. *Advanced Concrete Technology*. Elsevier, pp. 1–18.
- Bullard, J.W., Jennings, H.M., Livingston, R. a., Nonat, A., Scherer, G.W., Schweitzer, J.S., Scrivener, K.L., and Thomas, J.J., 2011. Mechanisms of cement hydration. *Cement and Concrete Research*, 41(12), pp.1208–1223.
- Bulletin d'Information, 1993. *CEB-FIP Model Code 1990*, London: Thomas Telford.
- Celik, I.B., 2009. The effects of particle size distribution and surface area upon cement strength development. *Powder Technology*, 188(3), pp.272–276.
- Chindapasirt, P., Chotithanorn, C., Cao, H.T., and Sirivivatnanon, V., 2007. Influence of fly ash fineness on the chloride penetration of concrete. *Construction and Building Materials*, 21(2), pp.356–361.
- Chindapasirt, P., Homwuttiwong, S., and Sirivivatnanon, V., 2004. Influence of fly ash fineness on strength, drying shrinkage and sulfate resistance of blended cement mortar. *Cement and Concrete Research*, 34(7), pp.1087–1092.
- Chindapasirt, P., Jaturapitakkul, C., and Sinsiri, T., 2005. Effect of fly ash fineness on compressive strength and pore size of blended cement paste. *Cement and Concrete Composites*, 27(4), pp.425–428.
- Chindapasirt, P., Jaturapitakkul, C., and Sinsiri, T., 2007. Effect of fly ash fineness on microstructure of blended cement paste. *Construction and Building Materials*, 21(7), pp.1534–1541.
- Combrinck, R., 2012. *Plastic shrinkage cracking in conventional and low volume fibre reinforced concrete*. University of Stellenbosch.
- Combrinck, R. and Boshoff, W.P., 2012. *Report number : ISI2012-17 Plastic Shrinkage Cracking of Concrete*. University of Stellenbosch.

- Czernin, W., 1980. *Cement Chemistry and Physics for Civil Engineers* 2nd English., Wiebaden and Berlin: Bauverlag.
- Darquennes, A., Khokhar, M.I.A., Rozière, E., Loukili, A., Grondin, F., and Staquet, S., 2011. Early age deformations of concrete with high content of mineral additions. *Construction and Building Materials*, 25(4), pp.1836–1847.
- Dellinghausen, L.M., Gastaldini, A.L.G., Vanzin, F.J., and Veiga, K.K., 2012. Total shrinkage, oxygen permeability, and chloride ion penetration in concrete made with white Portland cement and blast-furnace slag. *Construction and Building Materials*, 37, pp.652–659.
- Dhir, R.K., El-Mohr, M. a K., and Dyer, T.D., 1996. Chloride binding in GGBS concrete. *Cement and Concrete Research*, 26(12), pp.1767–1773.
- Dhir, R.K., El-Mohr, M.A.K., and Dyer, T.D., 1997. Developing Chloride Resisting Concrete Using PFA. *Cement and Concrete Research*, 27(11), pp.1633–1639.
- Domone, P. and Illston, J. eds., 2010. *Construction Materials, their Nature and Behaviour* Fourth Edi., London: Spon Press.
- Donatello, S., Tyrer, M., and Cheeseman, C.R., 2010. Comparison of test methods to assess pozzolanic activity. *Cement and Concrete Composites*, 32(2), pp.121–127.
- du Plessis, A., Olawuyi, B.J., Boshoff, W.P., and le Roux, S.G., 2014. Simple and fast porosity analysis of concrete using X-ray computed tomography. *Materials and Structures*, pp.1–10.
- Eguchi, K. and Teranishi, K., 2005. Prediction equation of drying shrinkage of concrete based on composite model. *Cement and Concrete Research*, 35(3), pp.483–493.
- EIA, 2015. International Energy Data and Analysis. Available at: <http://www.eia.gov/beta/international/?src=home-f1> [Accessed November 11, 2015].
- Flower, D.J.M. and Sanjayan, J.G., 2007. Green house gas emissions due to concrete manufacture. *The International Journal of Life Cycle Assessment*, 12(5), pp.282–288.
- Gao, T., Shen, L., Shen, M., Chen, F., Liu, L., and Gao, L., 2015. Analysis on differences of carbon dioxide emission from cement production and their major determinants. *Journal of Cleaner Production*, 103, pp.160–170.
- Glasser, F.P., Marchand, J., and Samson, E., 2008. Durability of concrete - Degradation phenomena involving detrimental chemical reactions. *Cement and Concrete Research*, 38(2), pp.226–246.
- Grieve, G., 2009. Cementitious Materials. In G. Owens, ed. *Fulton's Concrete Technology*. Midrand, South Africa: Cement & Concrete Institute, pp. 1–16.
- Holt, E. and Leivo, M., 2004. Cracking risks associated with early age shrinkage. *Cement and Concrete Composites*, 26(5), pp.521–530.
- Hooton, R.D., 2000. Canadian use of ground granulated blast-furnace slag as a supplementary cementing material for enhanced performance of concrete. *Canadian Journal of Civil Engineering*, 27(4), pp.754–760.
- Hooton, R.D., 1986. Permeability and Pore Structure of Cement Pastes Containing Fly Ash, Slag and Silica Fume. In G. Frohnsdorff, ed. *Blended Cements: A Symposium*. Philadelphia: ASTM International, pp. 128–143.
- Hooton, R.D., Stanish, K., Angel, J.P., and Prusinski, J., 2004. The Effect of Ground Granulated Blast Furnace Slag (Slag Cement) on the Drying Shrinkage of Concrete — A Critical Review of the Literature. In *ACI Eighth CANMET: International Confererence on Fly Ash, Silica Fume, Slag and Natural Pozzolans in Concrete*. West Conshohocken, PA: American Concrete Institute, pp. 79–94.
- Ishak, S.A. and Hashim, H., 2014. Low carbon measures for cement plant – a review. *Journal of Cleaner Production*, 103, pp.260–274.
- Jalal, M., Ramezani-pour, Ali, A., and Pool, M.K., 2013. Split tensile strength of binary blended self compacting concrete containing low volume fly ash and TiO₂ nanoparticles. *Composites Part B: Engineering*, 55, pp.324–337.
- Jin, F., Gu, K., and Al-Tabbaa, A., 2015. Strength and hydration properties of reactive MgO-activated

- ground granulated blastfurnace slag paste. *Cement and Concrete Composites*, 57, pp.8–16.
- Juenger, M.C.G. and Siddique, R., 2015. Recent advances in understanding the role of supplementary cementitious materials in concrete. *Cement and Concrete Research*.
- Khan, M.I. and Lynsdale, C.J., 2002. Strength, permeability, and carbonation of high-performance concrete. *Cement and Concrete Research*, 32(1), pp.123–131.
- Khan, S.U., Nuruddin, M.F., Ayub, T., and Shafiq, N., 2014. Effects of different mineral admixtures on the properties of fresh concrete. *The Scientific World Journal*, 2014, pp.1–11.
- Khatib, J.M., 2008. Performance of self-compacting concrete containing fly ash. *Construction and Building Materials*, 22(9), pp.1963–1971.
- Khatib, J.M. and Hibbert, J.J., 2005. Selected engineering properties of concrete incorporating slag and metakaolin. *Construction and Building Materials*, 19(6), pp.460–472.
- Kosmatka, S.H., Kerkhoff, B., and Panarese, W.C., 2003. *Design and Control Design and Control of Concrete Mixtures*. Illinois: Portland Cement Association (PCA).
- Kronlöf, A., Leivo, M., and Sipari, P., 1995. Experimental study on the basic phenomena of shrinkage and cracking of fresh mortar. *Cement and Concrete Research*, 25(8), pp.1747–1754.
- Kropp, J., 1999. RILEM TC 116-PCD Permeability of Concrete as a Criterion of its Durability.pdf. *RILEM Materials and Structures*, 32(April), pp.174–179.
- Kurdowski, W., 2014. *Cement and Concrete Chemistry* 2nd ed., Dordrecht: Springer Netherlands.
- Langan, B.W., Weng, K., and Ward, M. a., 2002. Effect of silica fume and fly ash on heat of hydration of Portland cement. *Cement and Concrete Research*, 32(7), pp.1045–1051.
- Lea, F.M. and Hewlett, P.C., 1998. *Lea's chemistry of cement and concrete.*, London; New York: Arnold ; Copublished in North, Central, and South America by J. Wiley.
- Leng, F., Feng, N., and Lu, X., 2000. Experimental study on the properties of resistance to diffusion of chloride ions of fly ash and blast furnace slag concrete. *Cement and Concrete Research*, 30(6), pp.989–992.
- Lewis, R., Sear, L., Wainwright, P., and Ryle, R., 2003. Cementitious additions. In J. Newman & B. S. Choo, eds. *Advanced Concrete Technology*. Elsevier, pp. 3–66.
- Li, Y., Bao, J.L., Sui, C.E., and Du, X.L., 2011. The Relationship between the Strength and the Pore Structures of Cement Paste with Mineral Admixtures. *Advanced Materials Research*, 250-253, pp.104–108.
- Li, Y. and Li, J., 2015. Relationship between fracture area and tensile strength of cement paste with supplementary cementitious materials. *Construction and Building Materials*, 79, pp.223–228.
- Lin, S.-T., Huang, R., and Weng, T.-L., 2011. Effect of mineral admixtures and viscosity modifying admixtures on plastic shrinkage cracking of cementitious composites. *Journal of the Chinese Institute of Engineers*, 34(2), pp.287–297.
- Lohtia, P.R. and Joshi, R.C., 1995. Mineral Admixtures. *Concrete Admixtures Handbook: Properties, Science and Technology*, pp.657–739.
- Lothenbach, B., Scrivener, K., and Hooton, R.D., 2011. Supplementary cementitious materials. *Cement and Concrete Research*, 41(12), pp.1244–1256.
- Luo, R., Cai, Y., Wang, C., and Huang, X., 2003. Study of chloride binding and diffusion in GGBS concrete. *Cement and Concrete Research*, 33(1), pp.1–7.
- Luping, T. and Nilsson, L.-O., 1993. Chloride binding capacity and binding isotherms of OPC pastes and mortars. *Cement and Concrete Research*, 23(2), pp.247–253.
- Metha, P.K. and Monteiro, P.J.M., 2006. *Concrete: Microstructure, Properties, and Materials*. Third Edition. New York: McGraw-Hill.
- Meyer, C., 2009. The greening of the concrete industry. *Cement and Concrete Composites*, 31(8), pp.601–605.
- Moosberg-Bustnes, H., Lagerblad, B., and Forssberg, E., 2004. The function of fillers in concrete.

- Materials and Structures*, 37(266), pp.74–81.
- Nazari, A. and Riahi, S., 2011. Splitting tensile strength of concrete using ground granulated blast furnace slag and SiO₂ nanoparticles as binder. *Energy and Buildings*, 43(4), pp.864–872.
- Neville, A.M., 2011. *Properties of Concrete* Fourth., New York: John Wiley & Sons, Inc.
- Neville, A.M. and Brooks, J.J., 2010. *Concrete Technology* Second Edition. , p.460.
- NT BUILD 433, 1995. *Nord Test Method: Concrete , Hardened : Accelerated Chloride Penetration*, Espoo: NORDTEST.
- Olorunsogo, F.T., 1998. Particle Size Distribution of GGBS and Bleeding Characteristics of Slag Cement Mortars. *Cement and Concrete Research*, 28(6), pp.907–919.
- Oluokun, F., 1991. Prediction of Concrete Tensile Strength from its Compressive Strength: an Evaluation of Existing Relations for Normal Weight Concrete. *ACI Materials Journal*, 88(3).
- Oluokun, F.A., Burdette, E.G., and Deatherage, J.H., 1991. Splitting tensile strength and compressive strength relationship at early ages. *ACI Materials Journal*, 88(2), pp.115–121.
- Oner, A. and Akyuz, S., 2007. An experimental study on optimum usage of GGBS for the compressive strength of concrete. *Cement and Concrete Composites*, 29(6), pp.505–514.
- Oner, A., Akyuz, S., and Yildiz, R., 2005. An experimental study on strength development of concrete containing fly ash and optimum usage of fly ash in concrete. *Cement and Concrete Research*, 35(6), pp.1165–1171.
- Otieno, M., Beushausen, H., and Alexander, M., 2014. Effect of chemical composition of slag on chloride penetration resistance of concrete. *Cement and Concrete Composites*, 46, pp.56–64.
- Pal, S.C., Mukherjee, a., and Pathak, S.R., 2003. Investigation of hydraulic activity of ground granulated blast furnace slag in concrete. *Cement and Concrete Research*, 33(9), pp.1481–1486.
- Pandey, S.P. and Sharma, R.L., 2000. Influence of mineral additives on the strength and porosity of OPC mortar. *Cement and Concrete Research*, 30(1), pp.19–23.
- Papadakis, V.G., Antiohos, S., and Tsimas, S., 2002. Supplementary cementing materials in concrete. Part II: A fundamental estimation of the efficiency factor. *Cement and Concrete Research*, 32(10), pp.1533–1538.
- Park, C.K., Noh, M.H., and Park, T.H., 2005. Rheological properties of cementitious materials containing mineral admixtures. *Cement and Concrete Research*, 35, pp.842–849.
- Perrie, B., 2009. Strength of hardened concrete. In G. Owens, ed. *Fulton's Concrete Technology*. Midrand, South Africa: Portland Cement Institute, pp. 97–110.
- Pourkhorshidi, A.R., 2013. Tests to evaluate pozzolanic activity in eco-efficient concrete. In *Eco-Efficient Concrete*. Cambridge: Woodhead Publishing, pp. 123–137.
- Pourkhorshidi, A.R., Hillemeier, B., Najimi, M., Herr, R., and Parhizkar, T., 2010. A comparative study of the evaluation methods for pozzolans. *Advances in Cement Research*, 22(3), pp.157–164.
- Pourkhorshidi, A.R., Najimi, M., Parhizkar, T., Jafarpour, F., and Hillemeier, B., 2010. Applicability of the standard specifications of ASTM C618 for evaluation of natural pozzolans. *Cement and Concrete Composites*, 32(10), pp.794–800.
- Prusinski, J., 2006. Slag as a cementitious material. In J. F. Lamond & J. H. Pielert, eds. *Significance of Tests and Properties of Concrete and Concrete-Making Materials: (STP 169D)*. ASTM International, pp. 512–531.
- Ramachandran, V.S., Paroli, R.M., Beaudoin, J.J., and Delgado, A.H., 2002. Supplementary Cementing Materials and Other Additions. In *Handbook of Thermal Analysis of Construction Materials*. Elsevier, pp. 293–353.
- Ramezaniapour, A.A. and Malhotra, V.M., 1995. Effect of curing on the compressive strength, resistance to chloride-ion penetration and porosity of concretes incorporating slag, fly ash or silica fume. *Cement and Concrete Composites*, 17(2), pp.125–133.
- Ramezaniapour, A.A., Pilvar, A., Mahdikhani, M., and Moodi, F., 2011. Practical evaluation of

- relationship between concrete resistivity, water penetration, rapid chloride penetration and compressive strength. *Construction and Building Materials*, 25(5), pp.2472–2479.
- SABS SM 829, 2002. *Sieve Analysis, Fines Content and Dust Content of Aggregates* 2.1 ed., Pretoria: South African Bureau of Standards.
- Salvoldi, B.G., Beushausen, H., and Alexander, M.G., 2015. Oxygen permeability of concrete and its relation to carbonation. *Construction and Building Materials*, 85, pp.30–37.
- SANS 5844, 2006. *Particle and Relative Densities of Aggregates*, Pretoria: South African Bureau of Standards.
- Shi, X., Xie, N., Fortune, K., and Gong, J., 2012. Durability of steel reinforced concrete in chloride environments: An overview. *Construction and Building Materials*, 30, pp.125–138.
- Siddique, R., 2008. *Waste materials and by-products in concrete*, Berlin: Springer.
- Siddique, R. and Khan, M.I., 2011. *Supplementary Cementing Materials*, Berlin: Springer.
- Slowik, V. and Ju, J.W., 2011. Discrete modeling of plastic cement paste subjected to drying. *Cement and Concrete Composites*, 33, pp.925–935.
- Slowik, V., Schmidt, M., and Fritzsche, R., 2008. Capillary pressure in fresh cement-based materials and identification of the air entry value. *Cement and Concrete Composites*, 30(7), pp.557–565.
- Snellings, R., Mertens, G., and Elsen, J., 2012. Supplementary Cementitious Materials. *Reviews in Mineralogy and Geochemistry*, 74(1), pp.211–278.
- Sonebi, M. and Bartos, P.J.M., 2002. Filling ability and plastic settlement of self-compacting concrete. *Materials and Structures/Matériaux et Constructions*, 35(October), pp.462–469.
- Soutsos, M., 2010. Deterioration mechanisms - chemical. In *Concrete Durability - A Practical Guide to the Design of Durable Concrete Structures*. ICE Publishing.
- Stanish, K., Alexander, M.G., and Ballim, Y., 2006. Assessing the repeatability and reproducibility values of South African. *Journal of the South African Institution of Civil Engineering*, 48(2), pp.10–17.
- Swamy, R.N., 1990. Properties of Fresh Concrete: Proceedings of the International RILEM Colloquium. In H. J. Wierig, ed. *Properties of Fresh Concrete: Proceedings of the International RILEM Colloquium*. Rilem Proceedings. London: Chapman and Hall, pp. 125–133.
- Talling, B. and Krivenko, P., 1996. Blast furnace slag - the ultimate binder. In S. Chandra, ed. *Waste Materials Used in Concrete Manufacturing*. Elsevier, pp. 235–289.
- Taylor-Lange, S.C., Lamon, E.L., Riding, K.A., and Juenger, M.C.G., 2015. Calcined kaolinite–bentonite clay blends as supplementary cementitious materials. *Applied Clay Science*, 108, pp.84–93.
- Thomas, M., 1996. Chloride thresholds in marine concrete. *Cement and Concrete Research*, 26(4), pp.513–519.
- Thomas, M.D.A. and Matthews, J.D., 1992. The permeability of fly ash concrete. *Materials and Structures*, 25(7), pp.388–396.
- Torrent, R.J., 1992. A two-chamber vacuum cell for measuring the coefficient of permeability to air of the concrete cover on site. *RILEM Materials and Structures*, 25(6), pp.358–365.
- Uno, P.J., 1998. Plastic shrinkage cracking and evaporation formulas. *ACI Materials Journal*, 95(95), pp.365–375.
- Uwasu, M., Hara, K., and Yabar, H., 2014. World cement production and environmental implications. *Environmental Development*, 10(1), pp.36–47.
- von Berg, W. and Kukko, H., 2004. Fresh mortar and concrete with fly ash. In K. Wesche, ed. *Fly Ash in Concrete: Properties and performance*. Rilem Report. Taylor & Francis, pp. 24–42.
- Wainwright, P. and Ait-Aider, H., 1995. The influence of cement source and slag additions on the bleeding of concrete. *Cement and Concrete Research*, 25(7), pp.1445–1456.
- Wainwright, P.J. and Rey, N., 2000. Influence of ground granulated blastfurnace slag (GGBS) additions and time delay on the bleeding of concrete. *Cement and Concrete Composites*, 22(4), pp.253–257.

- Wang, Q., Yan, P., Yang, J., and Zhang, B., 2013. Influence of steel slag on mechanical properties and durability of concrete. *Construction and Building Materials*, 47, pp.1414–1420.
- Xu, A., 1996. Fly Ash in Concrete. In S. Chandra, ed. *Waste Materials Used in Concrete Manufacturing*. Elsevier, pp. 142–183.
- Yang, K.H., Jung, Y.B., Cho, M.S., and Tae, S.H., 2014. Effect of supplementary cementitious materials on reduction of CO₂ emissions from concrete. *Journal of Cleaner Production*, 103, pp.774–783.
- Yim, H.J., Kim, J.H., Han, S.H., and Kwak, H.-G., 2015. Influence of Portland cement and ground-granulated blast-furnace slag on bleeding of fresh mix. *Construction and Building Materials*, 80, pp.132–140.
- Yuan, J., Lindquist, W., Darwin, D., and Browning, J., 2015. Effect of Slag Cement on Drying Shrinkage of Concrete. *ACI Materials Journal*, 112(2).
- Zhang, T., Gao, P., Gao, P., Wei, J., and Yu, Q., 2013. Effectiveness of novel and traditional methods to incorporate industrial wastes in cementitious materials - An overview. *Resources, Conservation and Recycling*, 74, pp.134–143.
- Zhang, T., Yu, Q., Wei, J., and Zhang, P., 2011. Effects of size fraction on composition and fundamental properties of Portland cement. *Construction and Building Materials*, 25(7), pp.3038–3043.
- Zhang, Y. and Zhang, M., 2014. Transport properties in unsaturated cement-based materials – A review. *Construction and Building Materials*, 72, pp.367–379.
- Zhang, Y.M. and Napier-Munn, T.J., 1995. Effects of particle size distribution, surface area and chemical composition on Portland cement strength. *Powder Technology*, 83(3), pp.245–252.

Appendix A

Results: Slags

A. 1. Strength Activity Index (SAI) Data

Tables A.1 to A.3 provide the raw data used to assess the SAI for the slags used in the study. All the values for the failure of a prism are given. However, an “X” is used to denote the calculation of a compressive strength that does not fall within a 90 % confidence interval. Hence, there is a difference in the statistical parameters given, most notably with the coefficient of variation (CoV).

Table A.1. The SAI data for slag at 7 days.

		Prism Halves						Statistics		
		1	2	3	4	5	6	Average	St. Dev	CoV
Reference	kN	45.5	56.3	38.7	51.6	59.7	53.4	50.9	7.6	15.0
	MPa	X	35.2	X	32.3	37.3	33.4	34.5	2.2	6.4
GGCS	kN	44.1	58.0	40.8	44.0	46.9	53.3	47.7	6.4	13.3
	MPa	27.6	X	25.5	27.5	29.3	X	27.5	1.6	5.7
GGBS	kN	24.1	31.6	24.0	24.7	26.1	22.6	25.5	3.2	12.5
	MPa	15.1	X	15.0	15.4	16.3	X	15.5	0.6	3.9

Table A.2. The SAI data for slag at 28 days.

		Prism Halves						Statistics		
		1	2	3	4	5	6	Average	St. Dev	CoV
Reference	kN	87.9	76.6	80.6	79.8	87.1	87.3	83.2	4.8	5.8
	MPa	54.9	47.9	50.4	49.9	54.4	54.6	52.0	3.0	5.8
GGCS	kN	83.2	74.1	77.4	66.1	76.9	74.9	75.4	5.6	7.4
	MPa	52.0	46.3	48.4	X	48.1	46.8	48.3	2.2	4.6
GGBS	kN	53.9	59.2	57.0	57.5	49.1	61.1	56.3	4.3	7.6
	MPa	33.7	37.0	35.6	35.9	X	38.2	36.1	1.7	4.6

Table A.3. The SAI data for the second batch of GGCS.

Age (days)		Prism Halves						Statistics		
		1	2	3	4	5	6	Average	St. Dev	CoV
7	kN	41.2	39.3	36.6	38.6	38.7	42.9	39.6	2.2	5.6
	MPa	25.8	24.6	22.9	24.1	24.2	26.8	24.7	1.4	5.6
28	kN	78.5	74.3	81.1	69.2	83.6	65.0	75.3	7.2	9.5
	MPa	49.1	46.4	50.7	X	52.3	X	49.6	2.5	5.0

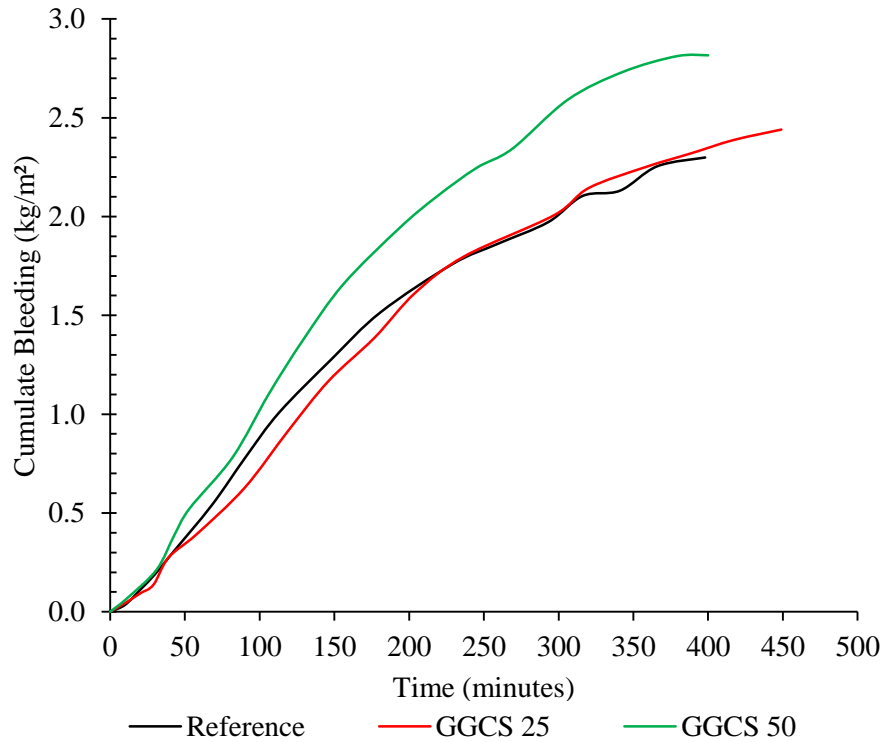
A. 2. The Bleeding Curves for Concrete at 40 °C:

Figure A-1. Bleeding curves for GGCS at different replacement levels (40 °C).

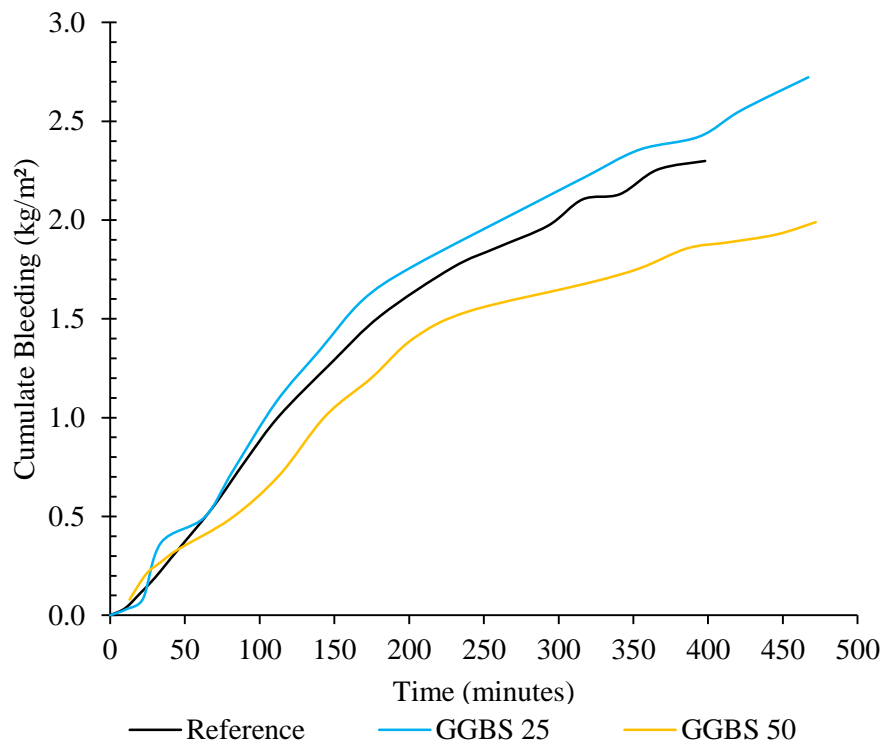


Figure A-2. Bleeding curves for GGBS at different replacement levels (40 °C).

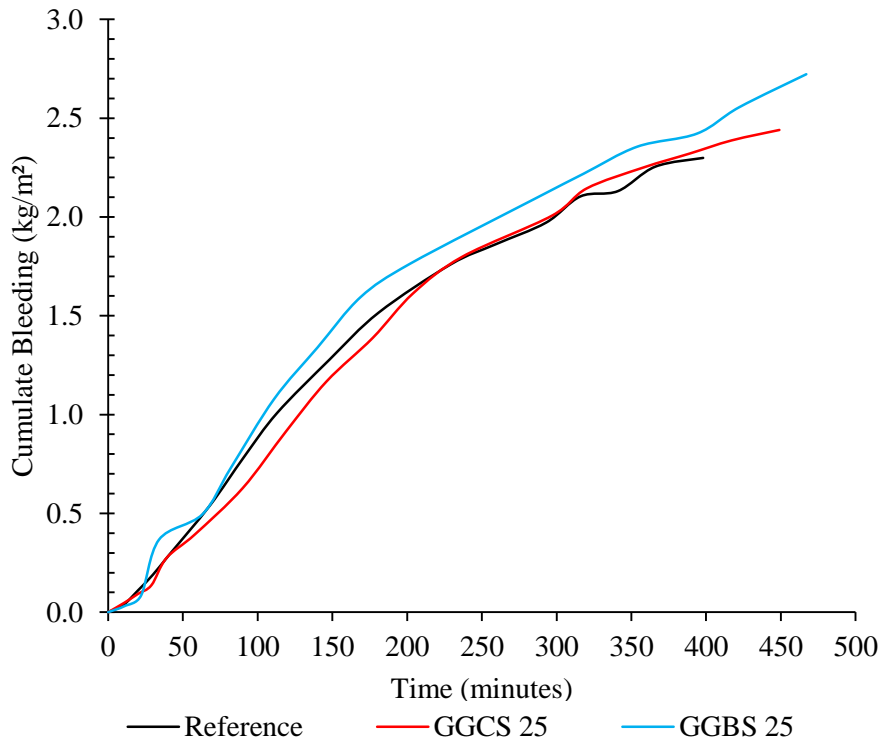


Figure A-3. Bleeding curves comparing GGBS and GGCS at 25 % cement replacement (40 °C).

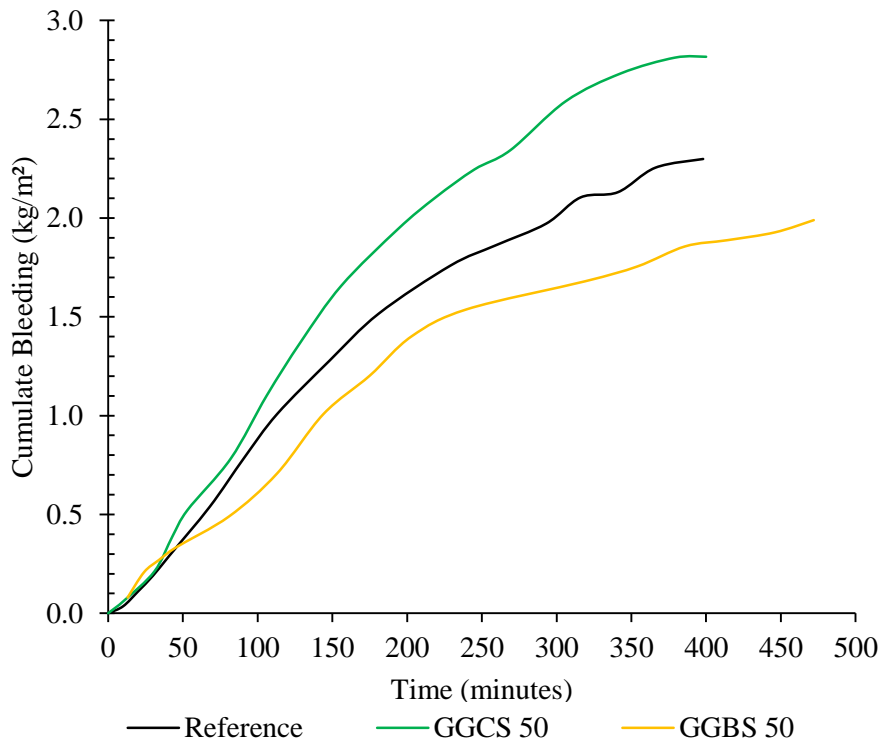


Figure A-4. Bleeding curves comparing GGBS and GGCS at 50 % cement replacement (40 °C).

A. 3. Compressive Strength

Table A.4. Summary of the Statistical data of the compressive strength development data for slag samples.

Age (days)		Reference	GGCS			GGBS		
			25	50	75	25	50	75
3	Std Dev (MPa)	1.13	0.39	0.66	0.29	0.41	0.43	0.11
	CoV (%)	4.90	2.16	5.71	2.63	1.92	3.57	1.57
7	Std Dev (MPa)	2.42	0.39	0.77	1.63	0.96	0.33	0.24
	CoV (%)	5.75	1.06	2.34	5.29	3.08	1.59	1.41
28	Std Dev (MPa)	3.04	0.46	1.31	0.91	0.22	0.36	1.46
	CoV (%)	5.52	0.93	3.09	2.28	0.45	0.87	4.45
56	Std Dev (MPa)	0.95	0.92	4.24	0.92	3.46	1.25	0.67
	CoV (%)	1.55	1.67	8.20	2.00	6.95	2.73	1.73
91	Std Dev (MPa)	2.56	1.64	0.95	2.3	1.30	0.71	3.18
	CoV (%)	4.08	2.87	1.95	5.04	2.06	1.42	7.45

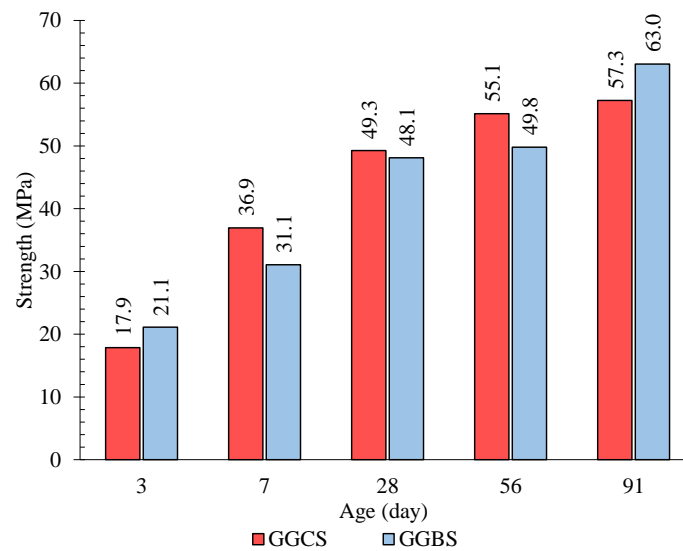


Figure A-5. The compressive strength development at 25 % cement replacement.

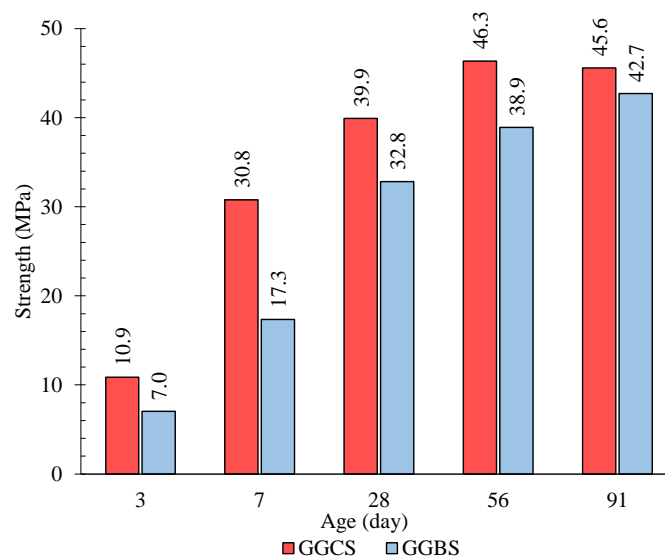


Figure A-6. The compressive strength development at 75 % cement replacement.

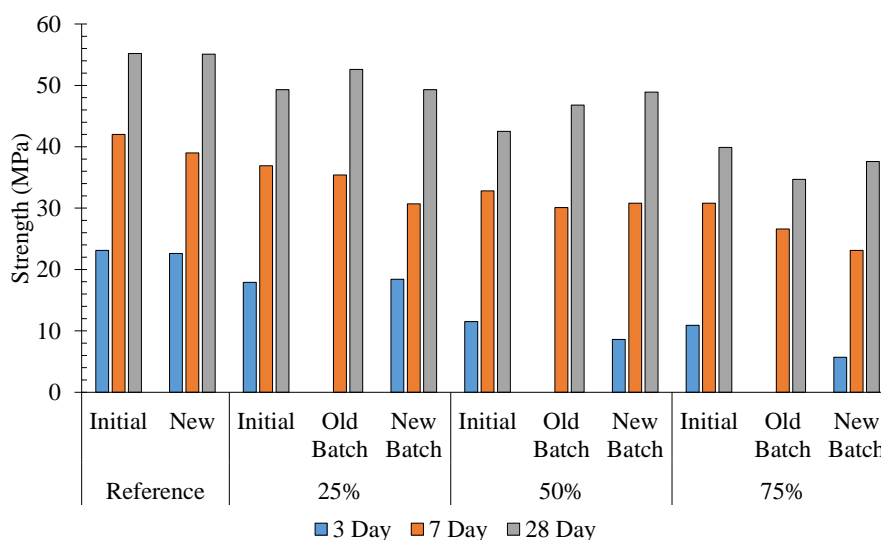


Figure A-7. The compressive strength development for the second batch of CCGS.

Table A.5. The compressive strength (MPa) data for the second batch of GGCS.

	Age:	3			7			28		
		Ave. (MPa)	Std. Dev (MPa)	CoV (%)	Ave. (MPa)	Std. Dev (MPa)	CoV (%)	Ave. (MPa)	Std. Dev (MPa)	CoV (%)
Reference	Initial	23.1	1.1	4.90	42.0	2.4	5.75	55.2	3.0	5.52
	New	22.6	0.6	2.48	39.0	1.9	4.90	55.1	1.1	1.95
GGCS 25	Initial	17.9	0.4	2.16	36.9	0.4	1.06	49.3	0.5	0.93
	Old	-	-	-	35.4	1.2	3.40	52.6	2.7	5.21
GGCS 50	New	18.4	0.4	2.43	30.7	1.5	4.99	49.3	1.8	3.66
	Initial	11.5	0.7	5.71	32.8	0.8	2.34	42.5	1.3	3.09
GGCS 50	Old	-	-	-	30.1	1.1	3.78	46.8	2.0	4.27
	New	8.6	0.3	3.28	30.8	1.0	3.16	48.9	2.4	4.94
GGCS 75	Initial	10.9	0.3	2.63	30.8	1.6	5.29	39.9	0.9	2.28
	Old	-	-	-	26.6	0.5	1.87	34.7	1.2	3.46
GGCS 75	New	5.7	0.1	0.89	23.1	0.5	2.18	37.6	1.2	3.12

Note:

Initial = Original data.

Old = The original batch of slag used.

New = A new batch of slag used.

Ave. = Average

A. 4. Indirect Tensile Strength

Table A.6. The indirect tensile strength data for slag samples at 0, 25 50 and 75 % cement replacement.

			Sample:	1	2	3	Average	STD	CoV	
Reference	0	7 Day	Force (kN)	66.10	64.40	52.60	61.03	7.35	12.05	
			Stress (MPa)	4.21	4.10	3.35	3.89	0.47	12.05	
		28 Day	Force (kN)	77.40	71.50	68.00	72.30	4.75	6.57	
			Stress (MPa)	4.93	4.55	4.33	4.60	0.30	6.57	
		56 Day	Force (kN)	72.7	77.8	77.2	75.90	2.79	3.67	
			Stress (MPa)	4.63	4.95	4.91	4.83	0.18	3.67	
GGCS	25	28 Day	Force (kN)	64.90	71.20	70.20	68.77	3.39	11.46	
			Stress (MPa)	4.13	4.53	4.47	4.38	0.22	0.05	
		56 Day	Force (kN)	77.30	80.10	75.00	77.47	2.55	6.52	
			Stress (MPa)	4.92	5.10	4.77	4.93	0.16	0.03	
	50	7 Day	Force (kN)	58.70	53.90	55.70	56.10	2.42	4.32	
			Stress (MPa)	3.74	3.43	3.55	3.57	0.15	0.02	
		28 Day	Force (kN)	66.00	79.90	66.50	70.80	7.88	62.17	
			Stress (MPa)	4.20	5.09	4.23	4.51	0.50	0.25	
		56 Day	Force (kN)	76	76.6	75.6	76.07	0.50	0.25	
			Stress (MPa)	4.84	4.88	4.81	4.84	0.03	0.00	
	75	28 Day	Force (kN)	61.00	65.20	65.30	63.83	2.45	6.02	
			Stress (MPa)	3.88	4.15	4.16	4.06	0.16	0.02	
		56 Day	Force (kN)	66.6	65.7	61.2	64.50	2.89	8.37	
			Stress (MPa)	4.24	4.18	3.90	4.11	0.18	0.03	
	GGBS	25	28 Day	Force (kN)	74.50	73.50	76.60	74.87	1.58	2.50
				Stress (MPa)	4.74	4.68	4.88	4.77	0.10	0.01
			56 Day	Force (kN)	81	80.1	85.4	82.17	2.84	8.04
				Stress (MPa)	5.16	5.10	5.44	5.23	0.18	0.03
50		7 Day	Force (kN)	37.40	39.20	39.10	38.57	1.01	2.62	
			Stress (MPa)	2.38	2.50	2.49	2.46	0.06	0.00	
		28 Day	Force (kN)	63.70	60.00	64.70	62.80	2.48	6.13	
			Stress (MPa)	4.06	3.82	4.12	4.00	0.16	0.02	
		56 Day	Force (kN)	69.2	73.5	67.2	69.97	3.22	10.36	
			Stress (MPa)	4.41	4.68	4.28	4.45	0.20	0.04	
75		28 Day	Force (kN)	50.80	52.50	49.30	50.87	1.60	2.56	
			Stress (MPa)	3.23	3.34	3.14	3.24	0.10	0.01	
		56 Day	Force (kN)	54.8	52.7	58.3	55.27	2.83	8.00	
			Stress (MPa)	3.49	3.35	3.71	3.52	0.18	0.03	

A. 5. Flexural Strength

Table A.7. The flexural strength data for selected slag samples at 0, 25 and 50 % cement replacement.

		1	2	3	4	Average	Std.Dev	CoV (%)	
<u>Reference:</u>									
Cubes:	Mass	g	2396.3	2382.8	2362.4	2382.8	2381.1	14.0	0.6
	Dimension	mm	102.0	101.0	101.0	100.0	101.0	0.8	0.8
	Density	kg/m ³	2349.3	2359.2	2339.0	2382.8	2357.6	18.7	0.8
	Force	kN	554.0	568.4	565.7	538.4	556.6	13.7	2.5
	Stress	MPa	55.4	56.8	56.6	53.8	55.7	1.4	2.5
Beam:	Load	kN	17.5	19.1	16.8		17.8	1.2	6.6
	Stress	MPa	5.3	5.7	5.0		5.3	0.4	6.6
<u>GGCS 50:</u>									
Cubes:	Mass	g	2341.8	2341.9	2324.9	2391.0	2349.9	28.5	1.2
	Dimension	mm	99.0	99.0	98.0	99.0	98.8	0.5	0.5
	Density	kg/m ³	2365.5	2365.6	2372.3	2415.2	2379.6	23.9	1.0
	Force	kN	449.3	489.3	465.7	423.8	457.0	27.6	6.0
	Stress	MPa	45.4	49.4	47.5	42.8	46.3	2.8	6.1
Beam:	Load	kN	18.6	20.8			19.7	1.6	7.9
	Stress	MPa	5.6	6.2			5.9	0.5	7.9
<u>GGBS 25:</u>									
Cubes:	Mass	g	2360.2	2388.0	2352.5	2378.0	2369.7	16.2	0.7
	Dimension	mm	98.0	102.0	101.0	100.0	100.3	1.7	1.7
	Density	kg/m ³	2408.4	2341.2	2329.2	2378.0	2364.2	36.0	1.5
	Force	kN	436.4	435.6	440.7	419.4	433.0	9.4	2.2
	Stress	MPa	44.5	43.6	44.1	41.9	43.5	1.1	2.6
Beam:	Load	kN	16.5	20.3	18.6		18.5	1.9	10.3
	Stress	MPa	5.0	6.1	5.6		5.5	0.6	10.3

A. 6. Secant Modulus

Table A.8. The use of prediction models to determine the elastic modulus of concrete.

		PC				GGBS				GGCS			
		0	2	3	Average	25	2	3	Average	50	2	3	Average
Cube Strength	MPa	41.6	42.7	42.6	42.3	33.9	41.4	41.7	39.0	47.9	50.4	35.4	44.6
Cylinder Strength	MPa	35.0	33.1	44.2	37.4	37.1	33.9	31.6	34.2	36.9	31.0	26.2	31.4
Cylinder/Cube Strength	-				0.88				0.88				0.70
Density	kg/m ³	2405.1	2393.9	2425.3	2408.1	2407.7	2410.4	2391.3	2403.1	2410.3	2417.8	2432.2	2420.1
Actual	GPa	35.9	39.7	36.8	37.5	37.1	34.9	38.2	36.7	44.5	33.5	41.9	40.0
BS EN 8110-2:1985	GPa	27.0	26.6	28.8	27.5	27.4	26.8	26.3	26.8	27.4	26.2	25.2	26.3
Error	%	24.8	32.9	21.6	26.6	26.1	23.3	31.1	26.9	38.5	21.8	39.8	34.3
CEB -FIB	GPa	35.0	34.5	37.4	35.7	35.6	34.7	34.1	34.8	35.5	33.9	32.5	34.0
Error	%	2.4	13.1	-1.6	4.8	4.1	0.5	10.8	5.2	20.1	-1.2	22.5	14.9
BS EN 1992:2004	GPa	35.6	35.8	35.8	35.7	33.8	35.5	35.6	35.0	36.9	37.4	34.2	36.2
Error	%	0.9	9.8	2.8	4.7	8.9	-1.8	6.8	4.7	17.2	-11.5	18.4	9.4
ACI 318-05	GPa	27.8	27.0	31.2	28.8	28.6	27.4	26.4	27.5	28.6	26.2	24.1	26.3
Error	%	22.5	31.9	15.1	23.2	22.8	21.6	30.8	25.2	35.8	21.9	42.6	34.1

A. 7. Drying Shrinkage Data

Table A.9. Strength of the concrete mixes used for the drying shrinkage.

Sample	1	2	3	4	Average	Std. Dev	Unit	CoV (%)
Reference (0 %)								
Mass	2354.2	2402.6	2412.5	2369.5	2384.7	27.4	g	1.15
Height	100.0	100.0	101.0	100.0	100.3	0.5	mm	0.50
Density	2354.2	2402.6	2388.6	2369.5	2378.7	21.2	kg/m ³	0.89
Cube	-	-	489.9	519.2	504.6	20.7	kN	4.11
Strength	-	-	49.0	51.9	50.5	2.1	MPa	4.11
25 % GGCS								
Mass	2363.3	2376.1	2387.3	2383.4	2377.5	10.6	g	0.44
Height	100.0	100.0	102.0	100.0	100.5	1	mm	1.00
Density	2363.3	2376.1	2340.5	2383.4	2365.7	18.8	kg/m ³	0.80
Cube	469.0	477.8	486.8	478.1	477.9	7.3	kN	1.52
Strength	46.9	47.8	48.7	47.8	47.8	0.7	MPa	1.52
50 % GGCS								
Mass	2363.6	2386.0	-	-	2374.8	15.8	g	0.67
Height	100.0	100.0	-	-	100.0	0	mm	0.00
Density	2363.6	2386.0	-	-	2374.8	15.8	kg/m ³	0.67
Cube	506.9	497.1	-	-	502.0	6.9	kN	1.38
Strength	50.7	49.7	-	-	50.2	0.7	MPa	1.38
25 % GGBS								
Mass	2401.3	2393.6	2402.9	-	2399.3	5.0	g	0.21
Height	100.0	99.0	101.0	-	100.0	1	mm	1.00
Density	2401.3	2417.8	2379.1	-	2399.4	19.4	kg/m ³	0.81
Cube	474.6	462.9	446.5	-	461.3	14.1	kN	3.06
Strength	47.5	46.3	44.7	-	46.1	1.4	MPa	3.06
50 % GGBS								
Mass	2393.6	2399.0	2378.0	2384.8	2388.9	9.3	g	0.39
Height	100.0	100.0	101.0	100.0	100.3	0.5	mm	0.50
Density	2393.6	2399.0	2354.5	2384.8	2383.0	19.9	kg/m ³	0.83
Cube	390.9	416.9	420.3	406.4	408.6	13.2	kN	3.23
Strength	39.1	41.7	42.0	40.6	40.9	1.3	MPa	3.23

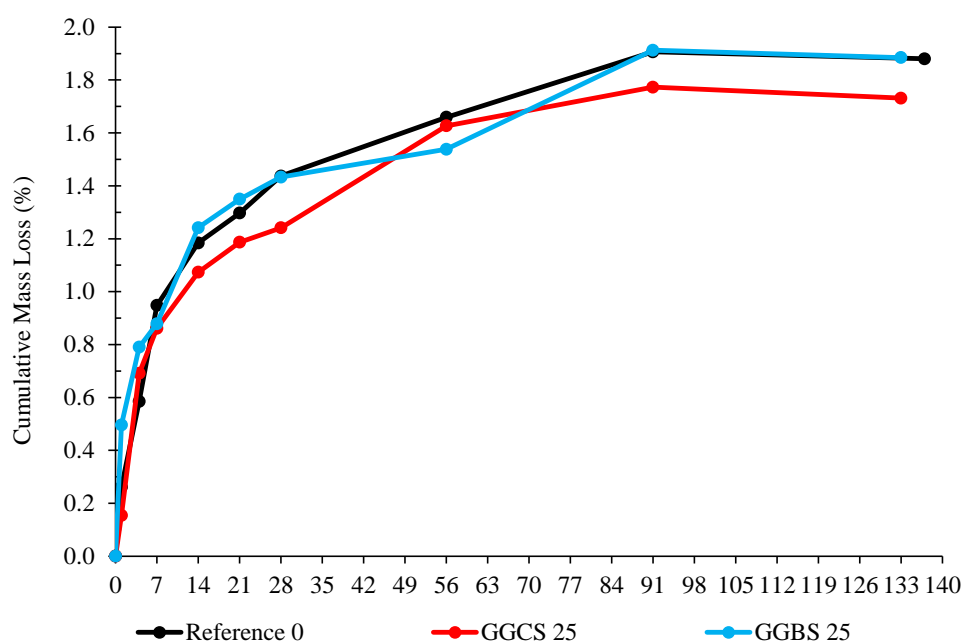


Figure A-8. The cumulative mass loss of slag samples at 25 % cements replacement.

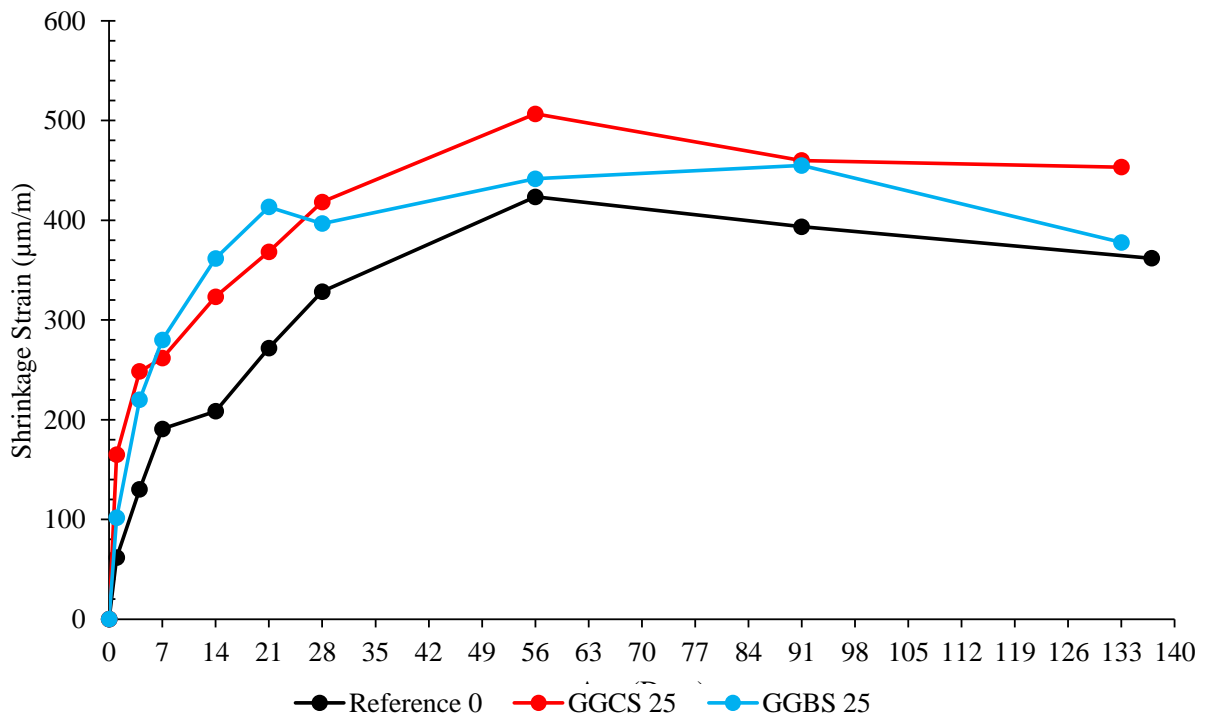


Figure A-9. The drying shrinkage of slag samples at 25 % cement replacement.

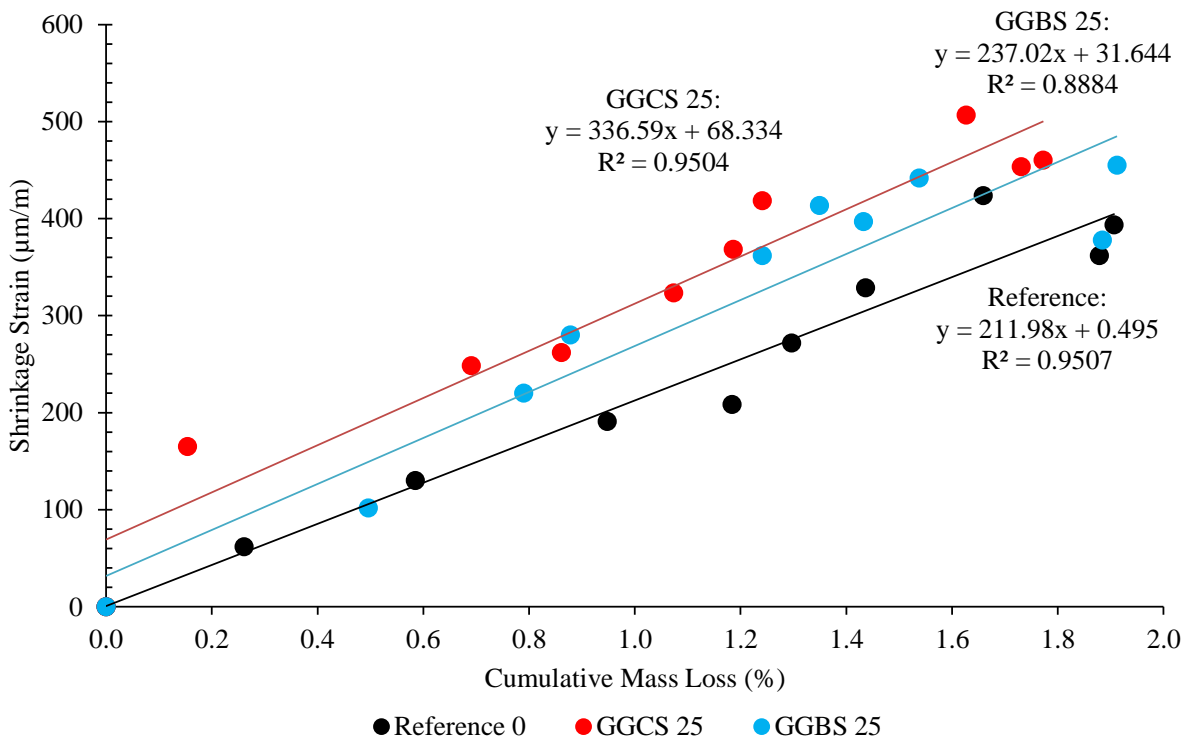


Figure A-10. Mass loss vs shrinkage strain as a function of replacement level of 50 %.

A. 8. Durability Data

Table A.10. OPI data for the PC samples.

		Samples							
		1	2	3	4				
PC	Diameter (mm):	1	69.38	69.39	69.52	69.35			
		2	70.06	69.83	69.53	69.94			
	Average		69.72	69.61	69.53	69.65			
	St. Dev (mm)		0.48	0.31	0.01	0.42			
	CoV (%)		0.69	0.45	0.01	0.60			
Thickness (mm):		1	32.11	30.39	30.74	30.77			
		2	31.47	31.62	30.77	30.75			
		3	30.12	31.62	30.62	31.48			
		4	31.99	31.68	30.99	30.66			
	Average		31.42	31.33	30.78	30.92			
St. Dev (mm)		0.91	0.63	0.15	0.38				
CoV (%)		2.90	2.00	0.50	1.23	Average	St.Dev	CoV	
k (m/s)	k (m/s)		6.793E-11	4.577E-11	4.577E-11	7.260E-11	5.802E-11	1E-11	24.59
r ²	r ²		0.9990	0.9980	0.9980	0.9994			
r ² Validity	r ² Validity		Valid	Valid	Valid	Valid			
OPI	OPI		10.17	10.34	10.34	10.14	10.25	0.108	1.05

Table A.11. OPI data for the GGCS and GGBS samples.

		Samples							
		1	2	3	4				
GGCS 25	Diameter (mm):	1	69.43	69.75	69.26	69.24			
		2	69.40	69.15	69.37	69.34			
	Average		69.42	69.45	69.32	69.29			
	St. Dev (mm)		0.02	0.42	0.08	0.07			
	CoV (%)		0.03	0.61	0.11	0.10			
Thickness (mm):		1	29.17	29.05	29.65	29.80			
		2	28.42	29.73	29.70	30.55			
		3	29.73	29.98	30.24	29.82			
		4	29.85	30.10	30.48	29.99			
	Average		29.29	29.72	30.02	30.04			
St. Dev (mm)		0.65	0.47	0.41	0.35				
CoV (%)		2.23	1.58	1.36	1.17	Average	St.Dc	CoV	
k (m/s)	k (m/s)		5.284E-11	6.934E-11	9.029E-11	9.931E-11	7.795E-11	0	26.84
r ²	r ²		0.9995	0.9991	0.9998	0.9995			
r ² Validity	r ² Validity		Valid	Valid	Valid	Valid			
OPI	OPI		10.28	10.16	10.04	10.00	10.12	0.1	1.25
GGCS 50	Diameter (mm):	1	69.21	69.61	69.12	69.14			
		2	69.31	69.46	69.18	69.80			
	Average		69.26	69.54	69.15	69.47			
	St. Dev (mm)		0.07	0.11	0.04	0.47			
	CoV (%)		0.10	0.15	0.06	0.67			
Thickness (mm):		1	30.44	28.89	30.14	29.44			
		2	30.47	29.28	29.45	29.38			
		3	30.82	28.82	29.07	29.33			
		4	30.92	29.48	30.40	29.95			
	Average		30.66	29.12	29.77	29.53			
St. Dev (mm)		0.24	0.32	0.61	0.29				
CoV (%)		0.79	1.08	2.06	0.97	Average	St.Dc	CoV	
k (m/s)	k (m/s)		1.889E-10	2.321E-10	2.741E-10	2.317E-10	0	18.38	
r ²	r ²		0.9997	0.9960	0.9985				
r ² Validity	r ² Validity		Valid	Valid	Valid				
OPI	OPI		9.72	9.63	9.56	9.64	0.1	0.84	
GGBS 25	Diameter (mm):	1	69.15	69.29	69.14	69.10			
		2	69.13	69.47	69.28	69.27			
	Average		69.14	69.38	69.21	69.19			
	St. Dev (mm)		0.01	0.13	0.10	0.12			
	CoV (%)		0.02	0.18	0.14	0.17			
Thickness (mm):		1	31.28	31.09	30.91	31.05			
		2	30.86	30.46	31.37	31.18			
		3	31.06	31.09	31.03	30.73			
		4	31.19	31.21	30.91	30.62			
	Average		31.10	30.96	31.06	30.90			
St. Dev (mm)		0.18	0.34	0.22	0.26				
CoV (%)		0.59	1.10	0.70	0.85	Average	St.Dc	CoV	
k (m/s)	k (m/s)		7.345E-11	7.448E-11	5.936E-11	1.058E-10	7.828E-11	0	25.06
r ²	r ²		0.9986	0.9998	0.9981	0.9990			
r ² Validity	r ² Validity		Valid	Valid	Valid	Valid			
OPI	OPI		10.13	10.13	10.23	9.98	10.12	0.1	1.03
GGBS 50	Diameter (mm):	1	69.26	69.41	69.48	69.33			
		2	69.55	69.29	69.3	69.32			
	Average		69.41	69.35	69.39	69.33			
	St. Dev (mm)		0.21	0.08	0.13	0.01			
	CoV (%)		0.30	0.12	0.18	0.01			
Thickness (mm):		1	28.53	30.92	30.69	31.42			
		2	29.38	31.8	30.86	30.65			
		3	28.94	31.56	31.07	30.63			
		4	28.78	31.13	31.05	31.16			
	Average		28.91	31.35	30.92	30.97			
St. Dev (mm)		0.36	0.40	0.18	0.39				
CoV (%)		1.24	1.28	0.58	1.26	Average	St.Dc	CoV	
k (m/s)	k (m/s)		1.677E-10	1.402E-10	1.075E-10	1.491E-10	1.411E-10	0	17.85
r ²	r ²		0.9974	0.9994	0.9997	0.9988			
r ² Validity	r ² Validity		Valid	Valid	Valid	Valid			
OPI	OPI		9.78	9.85	9.97	9.83	9.86	0.1	0.83

Table A.12. Sorptivity data for the PC samples.

Sample	1	2	3	4	Average	St. Dev	CoV
Diameter (mm)	69.72	69.61	69.53	69.65	69.63	0.08	0.12
Thickness (mm)	31.42	31.33	30.78	30.92	31.11	0.31	1.00
Time (min)	Mass (g)	Mass (g)	Mass (g)	Mass (g)			
0	273.89	268.18	269.81	268.42			
3	274.64	269.19	270.74	269.39			
5	274.95	269.42	270.94	269.57			
7	275.03	269.63	271.05	269.73			
9	275.13	269.72	271.20	269.83			
12	275.31	269.90	271.34	269.96			
16	275.49	270.17	271.58	270.23			
20	275.69	270.29	271.74	270.36			
25	275.81	270.53	271.89	270.57			
Saturated Mass (g)	285.53	280.44	281.48	280.37			
r2 (Must be >0.98)	0.9896	0.9962	0.9977	0.9967			
Sorptivity (mm/hr0.5)	7.29	7.97	7.30	7.20	7.44	0.36	4.77
Porosity (%)	9.70	10.28	9.99	10.15	10.03	0.25	2.49

Table A.13. Sorptivity data for the slag samples.

25 % GGCS:								25 % GGBS							
Sample	1	2	3	4	Average	St. Dev	CoV	Sample	1	2	3	4	Average	St. Dev	CoV
Diameter (mm)	69.42	69.45	69.32	69.29	69.37	0.08	0.11	Diameter (mm)	69.14	69.38	69.21	69.19	69.23	0.10	0.15
Thickness (mm)	29.29	29.72	30.02	30.04	29.77	0.35	1.17	Thickness (mm)	31.10	30.96	31.06	30.90	31.00	0.09	0.29
Time (min)	Mass (g)	Mass (g)	Mass (g)	Mass (g)				Time (min)	Mass (g)	Mass (g)	Mass (g)	Mass (g)			
0	254.70	260.78	262.09	258.65				0	268.70	267.33	269.61	272.37			
3	255.69	261.61	263.02	259.68				3	269.80	268.17	269.83	273.28			
5	255.87	261.78	263.16	259.81				5	270.01	268.36	270.02	273.38			
7	256.03	261.78	263.28	259.99				7	270.21	268.51	270.02	273.60			
9	256.11	261.88	263.39	260.02				9	270.33	268.60	270.14	273.62			
12	256.26	261.97	263.51	260.17				12	270.54	268.74	270.28	273.78			
16	256.45	262.12	263.69	260.38				16	270.72	268.89	270.39	273.88			
20	256.50	262.21	263.79	260.48				20	270.99	269.05	270.62	274.03			
25	256.68	262.28	263.96	260.64				25	271.11	269.26	270.85	274.24			
Saturated Mass (g)	281.58	271.17	272.66	269.33				Saturated Mass (g)	279.01	275.9	280.83	283.32			
r2 (Must be >0.98)	0.9909	0.9854	0.9990	0.9941				r2 (Must be >0.98)	0.9958	0.9969	Invalid	0.9868			
Sorptivity (mm/hr0.5)		4.57	6.32	6.44	5.78	1.05	18.10	Sorptivity (mm/hr0.5)	9.56	8.97	Invalid	6.22	8.25	1.78	21.63
Porosity (%)		9.23	9.33	9.43	9.33	0.10	1.06	Porosity (%)	8.83	7.32	Invalid	9.43	8.53	1.09	12.73
50 % GGCS								50 % GGBS							
Sample	1	2	3	4	Average	St. Dev	CoV	Sample	1	2	3	4	Average	St. Dev	CoV
Diameter (mm)	69.26	69.54	69.15	69.47	69.35	0.18	0.26	Diameter (mm)	69.41	69.35	69.39	69.33	69.37	0.04	0.05
Thickness (mm)	30.66	29.12	29.77	29.53	29.77	0.65	2.20	Thickness (mm)	28.91	31.35	30.92	30.97	30.54	1.10	3.61
Time (min)	Mass (g)	Mass (g)	Mass (g)	Mass (g)				Time (min)	Mass (g)	Mass (g)	Mass (g)	Mass (g)			
0	255.70	256.39	263.65	259.78				0	265.73	271.14	267.10	266.33			
3	256.60	257.52	264.50	260.86				3	266.71	272.02	268.04	267.27			
5	256.80	257.71	264.65	261.08				5	266.98	272.27	268.34	267.51			
7	256.99	257.94	264.84	261.20				7	267.13	272.40	268.49	267.61			
9	257.05	258.10	264.89	261.38				9	267.26	272.48	268.61	267.74			
12	257.19	258.23	264.97	261.48				12	267.44	272.66	268.78	267.88			
16	257.37	258.39	265.10	261.60				16	267.68	272.84	268.94	268.05			
20	257.46	258.50	265.25	261.81				20	267.86	272.98	269.09	268.16			
25	257.59	258.66	265.33	261.91				25	267.96	273.12	269.25	268.29			
Saturated Mass (g)	264.29	265.66	269.35	272.94				Saturated Mass (g)	278.18	283.25	279.51	278.69			
r2 (Must be >0.98)	0.9866	0.9809	0.9835	0.9881				r2 (Must be >0.98)	0.9918	0.9937	0.9874	0.9911			
Sorptivity (mm/hr0.5)	8.23	8.40	10.11	5.52	8.07	1.90	23.54	Sorptivity (mm/hr0.5)	6.97	6.62	6.85	5.95	6.60	0.46	6.95
Porosity (%)	7.44	8.38	5.10	11.76	8.17	2.76	33.82	Porosity (%)	11.38	10.23	10.61	10.57	10.70	0.49	4.56

Table A.14. Chloride conductivity data for the PC samples.

Sample	1	2	3	4
Thickness				
	30.58	30.56	31.44	31.29
	29.75	30.79	30.88	31.14
	30.00	30.90	31.10	31.22
	30.75	30.78	30.55	31.06
Average	30.27	30.76	30.99	31.18
St Dev	0.47	0.14	0.37	0.10
CoV	1.56	0.46	1.21	0.32
Diameter				
	70.06	69.51	69.73	68.90
	69.61	69.65	69.54	69.53
Average	69.84	69.58	69.64	69.22
St Dev	0.32	0.10	0.13	0.45
CoV	0.46	0.14	0.19	0.64
Porosity				
Mso (g)	271.98	269.34	265.98	272.80
Msv (g)	284.80	281.94	279.66	285.51
Porosity (%)	9.29	9.05	9.74	9.10
Average	9.30			
St Dev	0.31			
CoV	3.36			
Conductivity				
Voltage (V)	10.22	10.19	10.38	10.60
Current (mA)	181.5	180.5	187.7	126.6
Conductivity (mS/cm)	1.45	1.43	1.47	0.99
Average	1.34			
St Dev	0.23			
CoV	17.30			

Table A.15. Chloride conductivity data for the slag samples.

GGCS 25					GGBS 25				
Sample	1	2	3	4	Sample	1	2	3	4
Thickness					Thickness				
	30.58	31.05	30.04	29.06		31.47	29.79	30.56	31.36
	29.75	29.03	29.72	29.12		31.92	30.29	30.82	30.55
	30.00	28.82	29.56	28.89		30.51	31.54	31.53	30.62
	30.75	29.28	29.67	29.33		30.71	31.74	31.26	31.65
Average	30.27	29.55	29.75	29.10	Average	31.15	30.84	31.04	31.05
St Dev	0.47	1.02	0.21	0.18	St Dev	0.66	0.95	0.43	0.54
CoV	1.56	3.46	0.69	0.62	CoV	2.11	3.08	1.40	1.76
Diameter					Diameter				
	68.36	69.49	68.72	69.20		69.78	69.17	69.83	69.66
	68.16	69.79	68.93	69.12		69.89	69.58	69.64	69.33
Average	68.26	69.64	68.83	69.16	Average	69.84	69.38	69.74	69.50
St Dev	0.14	0.21	0.15	0.06	St Dev	0.08	0.29	0.13	0.23
CoV	0.21	0.30	0.22	0.08	CoV	0.11	0.42	0.19	0.34
Porosity					Porosity				
Mso (g)	248.58	262.90	255.32	256.75	Mso (g)	273.44	268.26	270.82	273.93
Msv (g)	258.71	272.93	265.73	267.11	Msv (g)	286.62	281.98	283.87	2876.52
Porosity (%)	7.68	7.49	7.90	7.96	Porosity (%)	9.28	9.89	9.25	1857.25
Average	7.76				Average	471.42			
St Dev	0.22				St Dev	923.89			
CoV	2.79				CoV	195.98			
Conductivity					Conductivity				
Voltage (V)	10.75	10.78	10.72	10.78	Voltage (V)	10.66	10.59	10.52	10.42
Current (mA)	48.1	51.1	48.3	44.6	Current (mA)	86.8	89.4	89.2	79.7
Conductivity (mS/cm)	0.37	0.37	0.36	0.32	Conductivity (mS/cm)	0.66	0.69	0.69	0.63
Average	0.35				Average	0.67			
St Dev	0.02				St Dev	0.03			
CoV	6.53				CoV	4.47			
GGCS 50					GGBS 50				
Sample	1	2	3	4	Sample	1	2	3	4
Thickness					Thickness				
	29.15	31.05	30.04	29.06		30.65	30.36	30.69	30.93
	30.19	29.03	29.72	29.12		30.22	30.09	30.52	30.75
	29.91	28.82	29.56	28.89		29.55	30.07	31.03	30.91
	28.71	29.28	29.67	29.33		29.94	31.31	30.73	31.03
Average	29.49	29.55	29.75	29.10	Average	30.09	30.46	30.74	30.91
St Dev	0.68	1.02	0.21	0.18	St Dev	0.46	0.58	0.21	0.12
CoV	2.31	3.46	0.69	0.62	CoV	1.54	1.92	0.69	0.38
Diameter					Diameter				
	68.36	69.49	68.72	69.20		69.40	69.50	69.87	69.38
	68.16	69.79	68.93	69.12		69.81	69.58	69.43	69.50
Average	68.26	69.64	68.83	69.16	Average	69.61	69.54	69.65	69.44
St Dev	0.14	0.21	0.15	0.06	St Dev	0.29	0.06	0.31	0.08
CoV	0.21	0.30	0.22	0.08	CoV	0.42	0.08	0.45	0.12
Porosity					Porosity				
Mso (g)	248.58	262.90	255.32	256.75	Mso (g)	260.00	263.23	269.06	270.28
Msv (g)	258.71	272.93	265.73	267.11	Msv (g)	272.72	275.99	281.88	282.79
Porosity (%)	7.89	7.49	7.90	7.96	Porosity (%)	9.34	9.27	9.20	8.98
Average	7.81				Average	9.20			
St Dev	0.22				St Dev	0.15			
CoV	2.78				CoV	1.67			
Conductivity					Conductivity				
Voltage (V)	10.43	10.32	10.53	10.56	Voltage (V)	10.75	10.78	10.72	10.78
Current (mA)	41.6	61.7	43.2	45.9	Current (mA)	48.1	51.1	48.3	44.6
Conductivity (mS/cm)	0.32	0.46	0.33	0.34	Conductivity (mS/cm)	0.35	0.38	0.36	0.34
Average	0.36				Average	0.36			
St Dev	0.07				St Dev	0.02			
CoV	18.71				CoV	4.96			

Appendix B

Results: Fly Ash

B. 1. Strength Activity Index (SAI) Data:

Tables B.1 to B.2 provide the raw data used to assess the SAI for the slags used in the study. All the values for the failure of a prism are given. However, an “X” is used to denote the calculation of a compressive strength that does not fall within a 90 % confidence interval. Hence, there is a difference in the statistical parameters given, most notably with the coefficient of variation (CoV).

Table B.1. The SAI data for fly ash and the reference at 28 days.

		Prism Halves						Statistics		
		1	2	3	4	5	6	Average	St. Dev	CoV
Reference	kN	87.9	76.6	80.6	79.8	87.1	87.3	83.2	4.8	5.8
	MPa	54.9	47.9	50.4	49.9	54.4	54.6	52.0	3.0	5.8
UA	kN	62.3	56.5	65.5	55.7	73.8	65.2	63.2	6.7	10.6
	MPa	38.9	35.3	40.9	34.8	X	40.8	38.2	2.9	.7.7
SA	kN	50.3	56.0	50.9	49.5	51.8	37.6	49.4	6.2	12.5
	MPa	31.4	35.0	31.8	30.9	32.4	X	32.3	1.6	4.9
DP	kN	60.1	67.2	50.0	62.0	72.5	65.5	62.9	7.6	12.2
	MPa	37.6	42.0	X	38.8	X	40.9	39.8	2.0	5.1
PF	kN	68.5	59.5	71.6	67.9	71.7	65.6	67.5	4.5	6.7
	MPa	42.8	X	44.8	42.4	44.8	41.0	43.2	1.6	3.8

Table B.2. The SAI data for fly ash and the reference at 90 days.

		Prism Halves						Statistics		
		1	2	3	4	5	6	Average	St. Dev	CoV
Reference	kN	101.0	91.1	101.3	103.0	85.2	103.0	98.9	7.0	7.1
	MPa	63.1	61.3	64.4	64.4	X	64.4	63.5	1.3	2.1
UA	kN	89.4	61.6	89.3	86.6	87.0	84.0	93.0	10.7	12.9
	MPa	55.9	X	55.8	54.1	54.4	52.5	54.5	1.4	2.6
SA	kN	82.1	83.1	82.9	82.2	89.0	98.2	84.7	3.4	4.0
	MPa	51.3	51.9	51.8	51.3	55.6	55.8	53.0	2.1	4.0
DP	kN	78.1	78.8	90.2	84.6	84.4	91.6	84.6	5.6	6.6
	MPa	48.8	49.3	56.4	52.9	52.8	57.3	52.9	3.5	6.6
PF	kN	73.9	78.4	85.3	87.5	85.4	83.4	82.3	5.2	6.3
	MPa	X	49.0	53.3	54.7	53.4	52.1	52.5	2.2	4.1

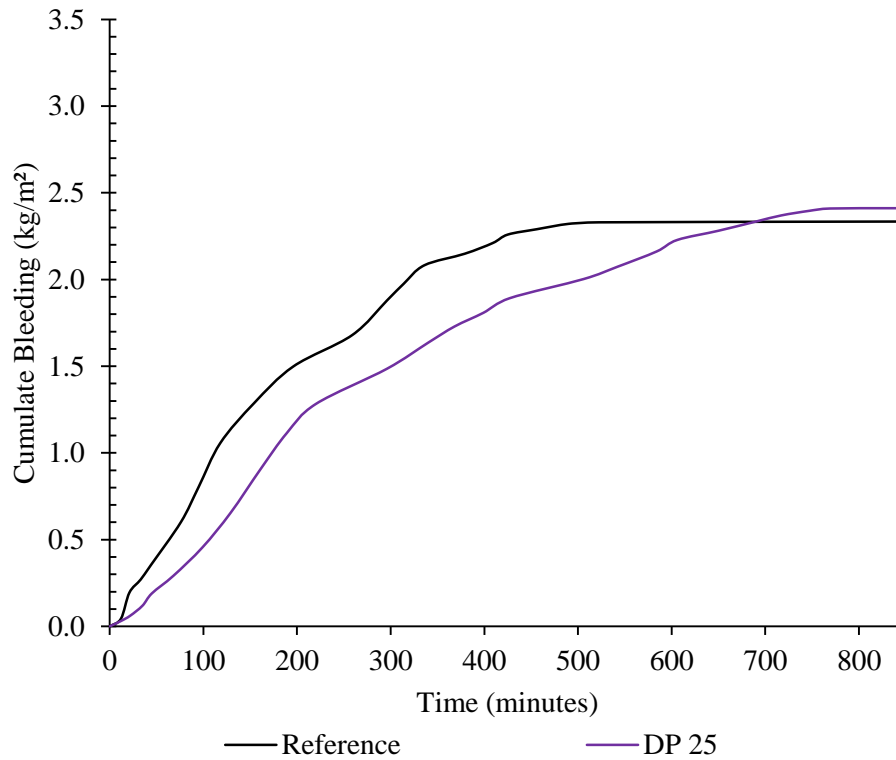
B. 2. The Bleeding Curves for Concrete at 23 °C:

Figure B-1. The bleeding of DP specimens at 0, and 25 % cement replacement.

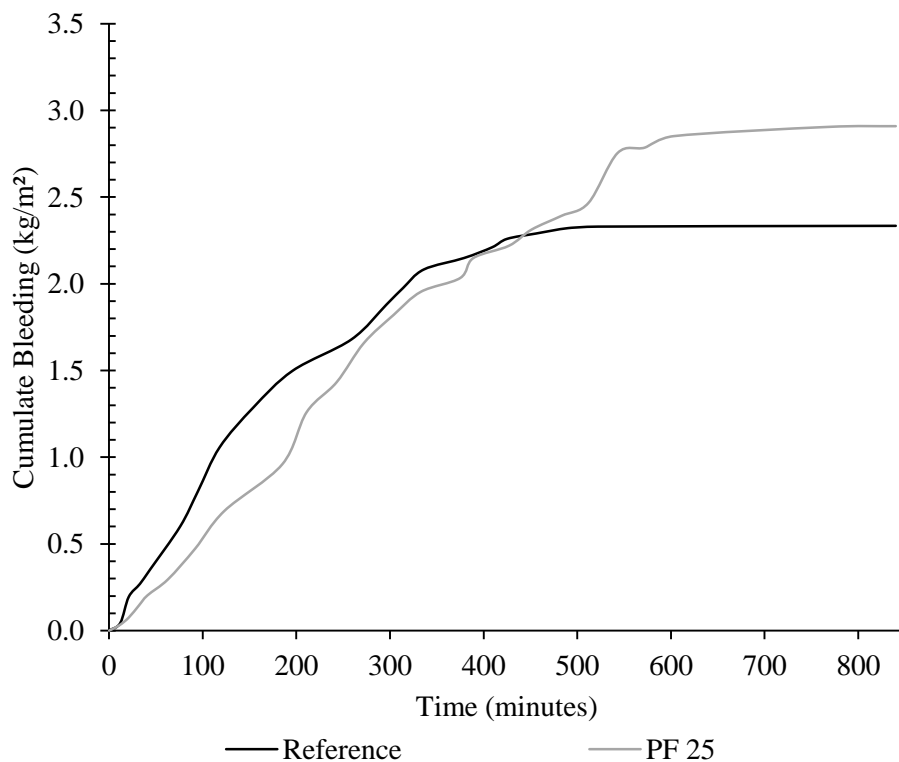


Figure B-2. The bleeding of PF specimens at 0, and 25 % cement replacement.

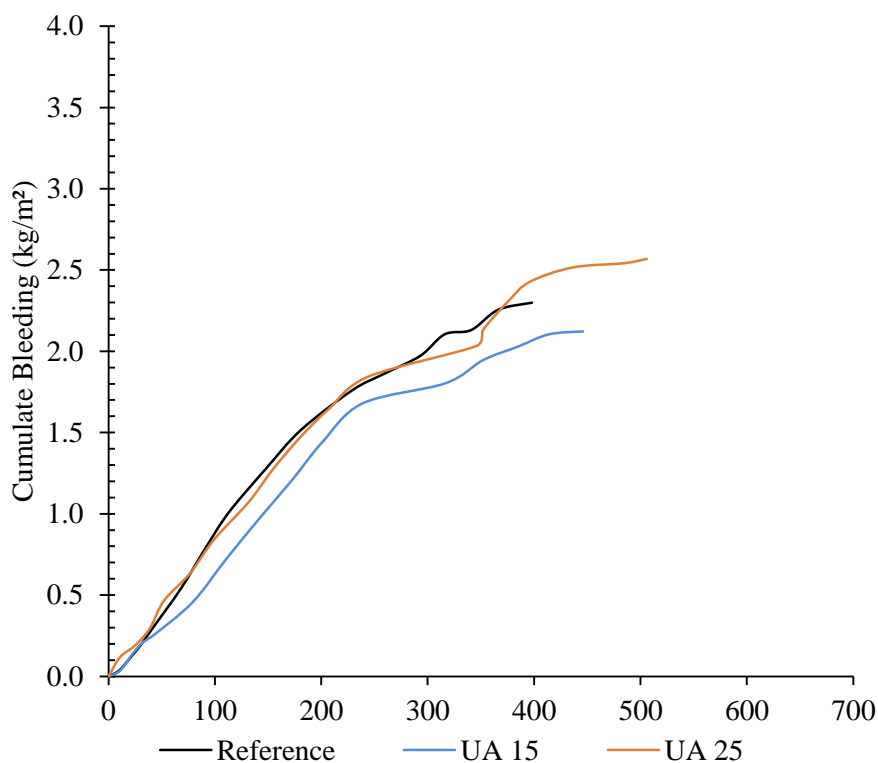
B. 3. The Bleeding Curves for Concrete at 40 °C

Figure B-3. Bleeding curves for UA at different replacement levels (40 °C).

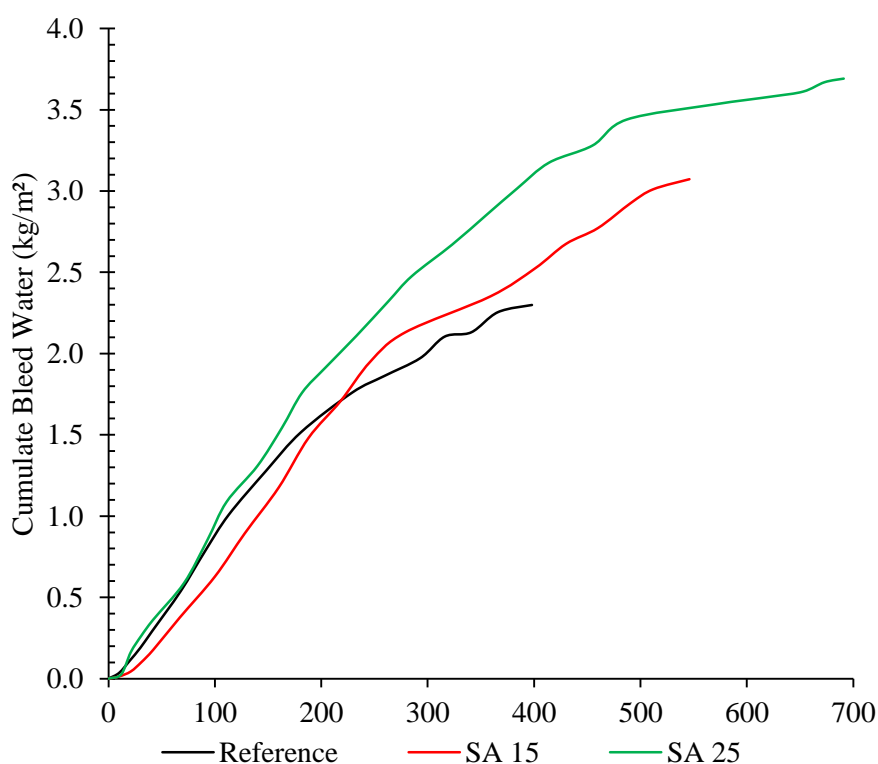


Figure B-4. Bleeding curves for SA at different replacement levels (40 °C).

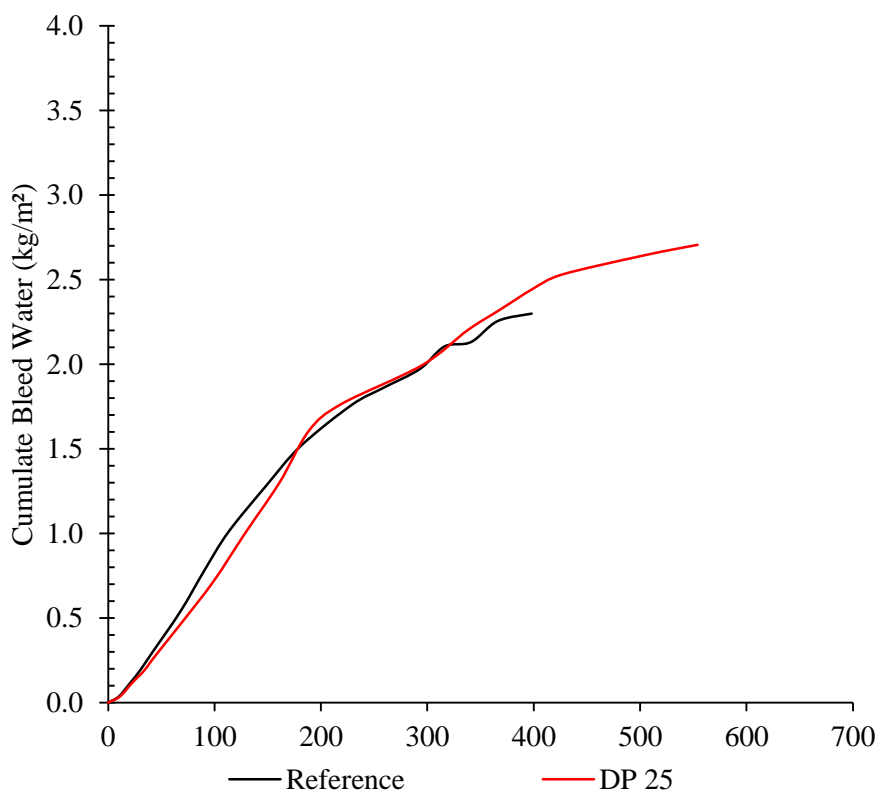


Figure B-5. Bleeding curves for DP (40 °C).

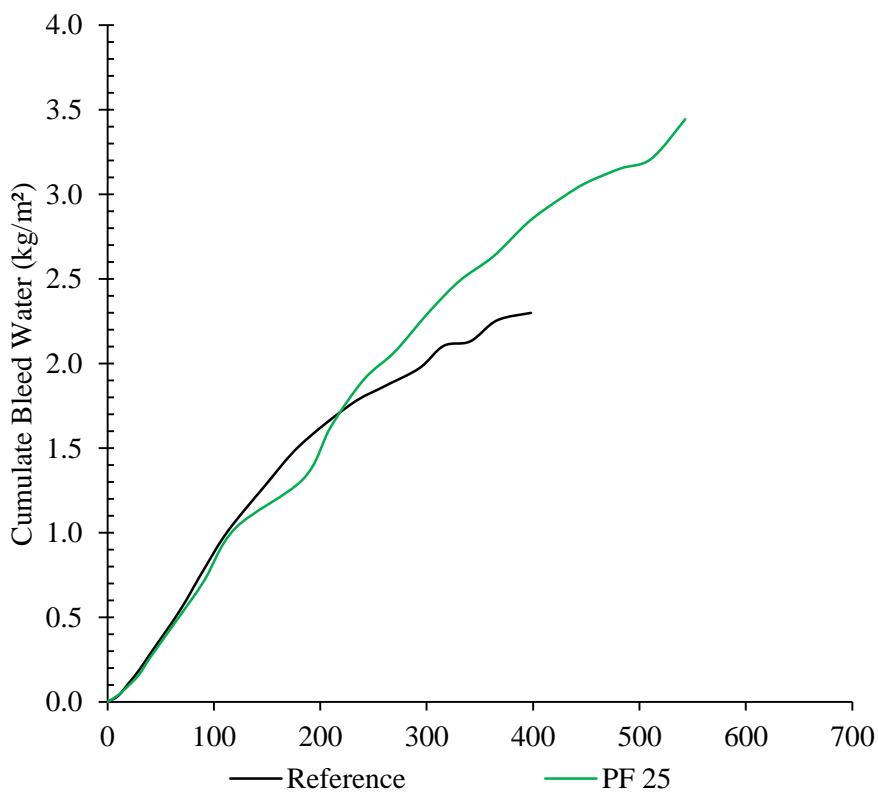


Figure B-6. Bleeding curves for PF (40 °C).

B. 4. Capillary Pressure Build-Up

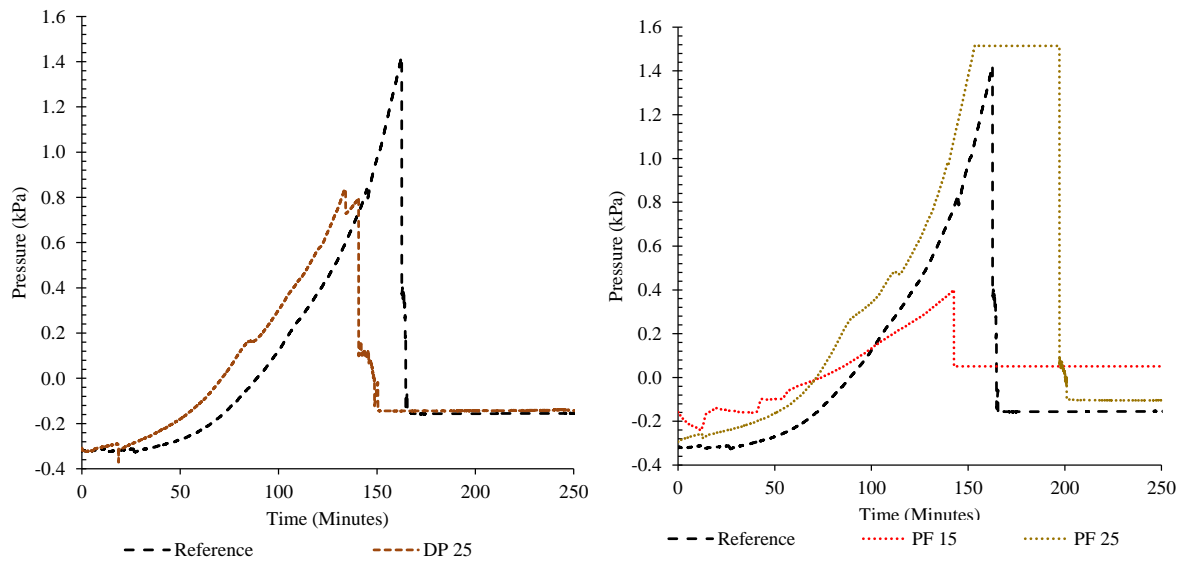


Figure B-7. Capillary pressure build up for concrete containing DP (left) and PF (right) at different replacement levels.

B. 5. Compressive Strength

Table B.3. The strength (MPa) of the fly ashes at different ages and cement replacement percentages.

	Cement Replacement (%)	Compressive Strength (MPa)				
		Age (Days)				
		3	7	28	56	91
Reference	0	23.1	42.0	55.2	60.9	62.7
UA	15	24.6	26.8	49.5	59.0	63.3
	25	18.7	21.8	45.8	57.3	57.7
	35	15.8	16.2	38.7	50.7	55.8
SA	15	20.0	32.5	47.3	55.1	62.9
	25	18.9	27.6	44.2	50.6	55.0
	35	17.1	22.7	35.3	43.9	52.2
DP	15	24.4	31.8	46.3	50.4	54.5
	25	18.5	25.1	38.1	48.5	49.6
	35	15.4	21.3	35.0	44.1	50.3
PF	15	20.5	32.8	47.4	53.8	54.1
	25	18.7	26.9	40.7	51.5	57.5
	35	16.3	20.7	30.1	42.7	47.6

Table B.4. Summary of the statistical data of the compressive strength development data for fly ash samples.

Age (days)		UA			SA		
		15	25	35	15	25	35
3	Std Dev (MPa)	0.20	0.40	0.20	1.10	0.40	0.20
	CoV (%)	1.00	2.35	1.53	5.46	2.10	1.02
7	Std Dev (MPa)	1.30	0.70	0.50	0.50	0.30	0.80
	CoV (%)	5.01	3.20	3.40	1.65	1.23	3.70
28	Std Dev (MPa)	1.30	0.80	0.70	0.90	1.60	0.40
	CoV (%)	2.56	1.67	1.85	1.95	3.58	1.24
56	Std Dev (MPa)	1.00	2.50	0.60	3.20	0.90	3.10
	CoV (%)	1.75	4.41	1.20	5.80	1.83	7.00
91	Std Dev (MPa)	0.80	3.70	1.70	1.20	3.10	1.20
	CoV (%)	1.19	6.36	3.12	1.91	5.63	2.24

Age (days)		DP			PF		
		15	25	35	15	25	35
3	Std Dev (MPa)	0.50	0.30	0.30	0.60	0.30	0.30
	CoV (%)	2.22	1.89	1.83	3.12	1.57	1.91
7	Std Dev (MPa)	0.30	0.80	0.30	1.20	0.90	0.40
	CoV (%)	0.80	3.25	1.31	3.72	3.38	2.09
28	Std Dev (MPa)	2.20	0.80	0.40	1.10	0.80	0.40
	CoV (%)	4.70	2.08	1.01	2.31	4.52	1.45
56	Std Dev (MPa)	2.20	2.70	1.40	2.30	1.50	1.20
	CoV (%)	4.34	5.66	3.29	4.27	2.84	2.83
91	Std Dev (MPa)	3.30	3.20	1.50	3.70	1.60	2.60
	CoV (%)	6.09	6.37	3.02	6.82	2.79	5.55

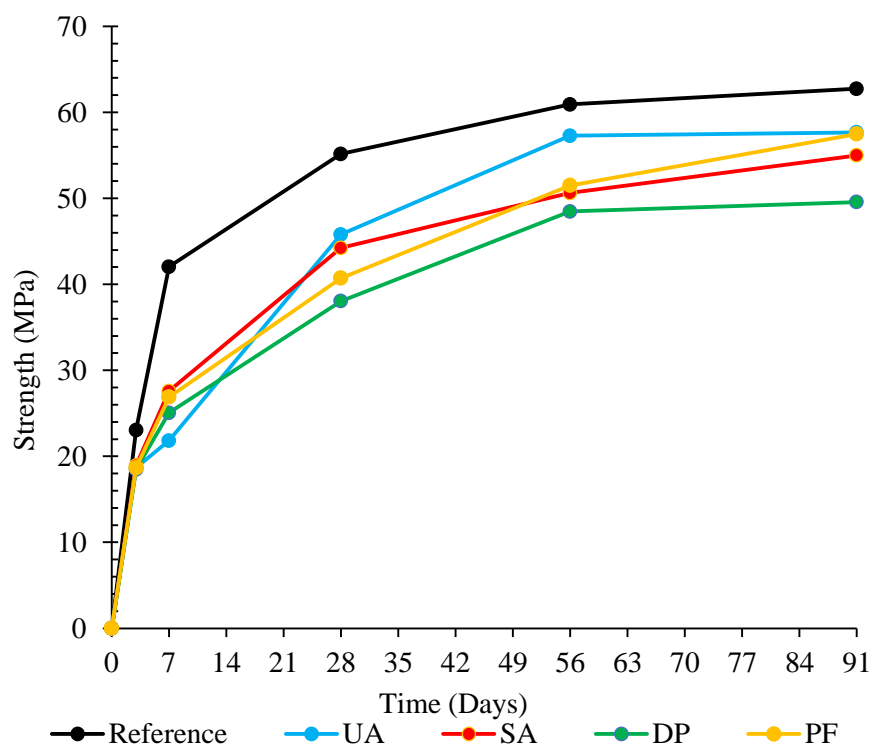


Figure B-8. The strength development of the fly ash concrete mixes at 25 % cement replacement.

B. 6. Indirect Tensile Strength

Table B.5. The indirect tensile strength data for fly as samples at 15, 25 and 35 % cement replacement.

Sample:			1	2	3	Average	STD	CoV	
UA	15	28 Day	Force (kN)	62.20	74.80	69.20	68.73	6.31	39.85
			Stress (MPa)	3.96	4.76	4.41	4.38	0.40	0.16
	25	28 Day	Force (kN)	70.00	65.10	67.80	67.63	2.45	6.02
			Stress (MPa)	4.46	4.14	4.32	4.31	0.16	0.02
	35	7 Day	Force (kN)	40.3	48	43.7	44.00	3.86	14.89
			Stress (MPa)	2.57	3.06	2.78	2.80	0.25	0.06
		28 Day	Force (kN)	57.60	53.20	53.80	54.87	2.39	5.69
			Stress (MPa)	3.67	3.39	3.43	3.49	0.15	0.02
SA	15	28 Day	Force (kN)	67.60	71.20	63.60	67.47	3.80	14.45
			Stress (MPa)	4.30	4.53	4.05	4.30	0.24	0.06
	25	28 Day	Force (kN)	57.80	63.40	60.90	60.70	2.81	7.87
			Stress (MPa)	3.68	4.04	3.88	3.86	0.18	0.03
	35	7 Day	Force (kN)	40.3	35.5	40.8	38.87	2.93	8.56
			Stress (MPa)	2.57	2.26	2.60	2.47	0.19	0.03
		28 Day	Force (kN)	57.70	54.70	54.50	55.63	1.79	3.21
			Stress (MPa)	3.67	3.48	3.47	3.54	0.11	0.01

B. 7. Flexural Strength

Table B.6. The flexural strength data for selected slag samples at 0, 25 and 50 % cement replacement.

			1	2	3	4	Average	Std.Dev	CoV (%)
<u>UA 15:</u>									
Cubes:	Mass	g	2383.2	2370.0	2375.5	2398.0	2381.7	12.2	0.5
	Dimension	mm	101.0	100.0	101.0	101.0	100.8	0.5	0.5
	Density	kg/m ³	2359.6	2370.0	2352.0	2374.3	2364.0	10.1	0.4
	Force	kN	399.7	385.1	378.7	373.4	384.2	11.4	3.0
	Stress	MPa	40.0	38.5	37.9	37.3	38.4	1.1	3.0
Beam:	Load	kN	13.9	14.0	15.1		14.3	0.7	4.6
	Stress	MPa	4.2	4.2	4.5		4.3	0.2	4.6
<u>SA 25:</u>									
Cubes:	Mass	g	101.0	100.0	100.0	99.0	100.0	0.8	0.8
	Dimension	mm	2333.8	2357.5	2351.1	2379.4	2355.4	18.9	0.8
	Density	kg/m ³	365.0	348.0	367.4	364.4	361.2	8.9	2.5
	Force	kN	36.5	34.8	36.7	36.8	36.2	1.0	2.6
	Stress	MPa	10.7	12.5	13.6		12.3	1.5	12.0
Beam:	Load	kN	3.2	3.8	4.1		3.7	0.4	12.0
	Stress	MPa		2370.8	2366.2	2355.6	2352.6	2361.3	8.6
<u>DP 35:</u>									
Cubes:	Mass	g	2324.3	2366.2	2355.6	2329.3	2343.9	20.3	0.9
	Dimension	mm	267.5	286.8	284.3	284.3	280.7	8.9	3.2
	Density	kg/m ³	26.8	28.7	28.4	28.4	28.1	0.9	3.2
	Force	kN	10.9	11.2	12.9		11.7	1.1	9.2
	Stress	MPa	3.3	3.4	3.9		3.5	0.3	9.2
Beam:	Load	kN	2383.2	2370.0	2375.5	2398.0	2381.7	12.2	0.5
	Stress	MPa	101.0	100.0	101.0	101.0	100.8	0.5	0.5

B. 8. Secant Modulus

Table B.7. The use of prediction models to determine the Secant modulus of concrete containing fly ash.

		UA 15				SA 25				DP 35				PF 15				
		1	2	3	Average	1	2	3	Average	1	2	3	Average	1	2	3	Average	
Cube Strength	MPa	45.4	46.6	45.5	45.8	41.5	37.2	38.1	38.9	32.5	24.0	24.0	26.8	38.6	38.9	38.4	38.6	38.6
Cylinder Strength	MPa	28.1	31.1	33.3	30.8	25.5	24.0	22.2	23.9	26.7	25.0	26.0	25.9	25.2	31.7	28.7	28.7	28.5
Cylinder/Cube Strength	-				0.67				0.61				0.97					0.74
Density	kg/m ³	2398.3	2390.5	2380.9	2389.9	2401.7	2360.4	2373.8	2378.6	2389.2	2376.5	2384.5	2383.4	2393.0	2401.9	2376.8	2390.6	2390.6
Actual	GPa	34.8	36.6	29.0	33.5	29.8	22.3	35.5	29.2	35.0	31.5	31.5	32.7	32.1	33.1	27.1	30.8	30.8
BS EN 8110-2:1985	GPa	25.6	26.2	26.7	26.2	25.1	24.8	24.4	24.8	25.3	25.0	25.2	25.2	25.0	26.3	25.7	25.7	25.7
Error	%	26.4	28.4	8.1	21.8	15.8	-11.2	31.2	15.1	27.6	20.6	20.0	22.9	22.0	20.4	5.0	16.4	16.4
CEB-FIB	GPa	33.0	33.9	34.6	33.9	32.2	31.7	31.1	31.7	32.6	32.1	32.4	32.4	32.1	34.1	33.2	33.2	33.2
Error	%	5.0	7.3	-19.2	-1.2	-8.2	-42.4	12.3	-8.6	6.8	-1.8	-2.8	0.9	-0.1	-3.1	-22.6	-7.8	-7.8
BS EN 1992:2004	GPa	36.4	36.6	36.4	36.5	35.5	34.6	34.8	35.0	33.5	31.2	31.2	32.0	34.9	35.0	34.9	34.9	34.9
Error	%	-4.5	0.0	-25.5	-8.9	-19.3	-55.1	2.0	-19.8	4.4	1.0	1.0	2.1	-8.8	-5.7	-28.6	-13.5	-13.5
ACI 318-05	GPa	24.9	26.2	27.1	26.1	23.7	23.0	22.1	23.0	24.3	23.5	24.0	23.9	23.6	26.5	25.2	25.1	25.1
Error	%	28.4	28.4	6.5	22.0	20.4	-3.3	37.6	21.3	30.6	25.4	23.9	26.8	26.5	20.1	7.1	18.4	18.4

B. 9. Drying Shrinkage

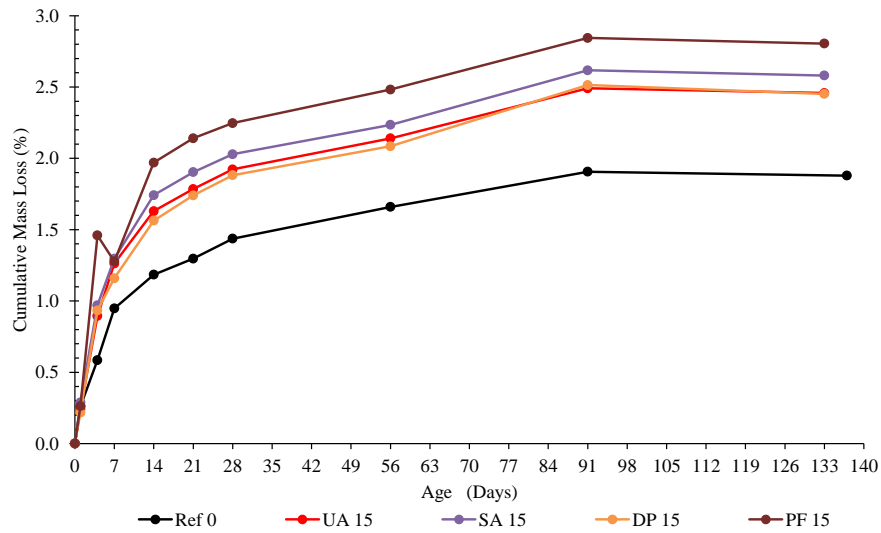


Figure B-9. The cumulative mass loss of the fly ash samples (15 %).

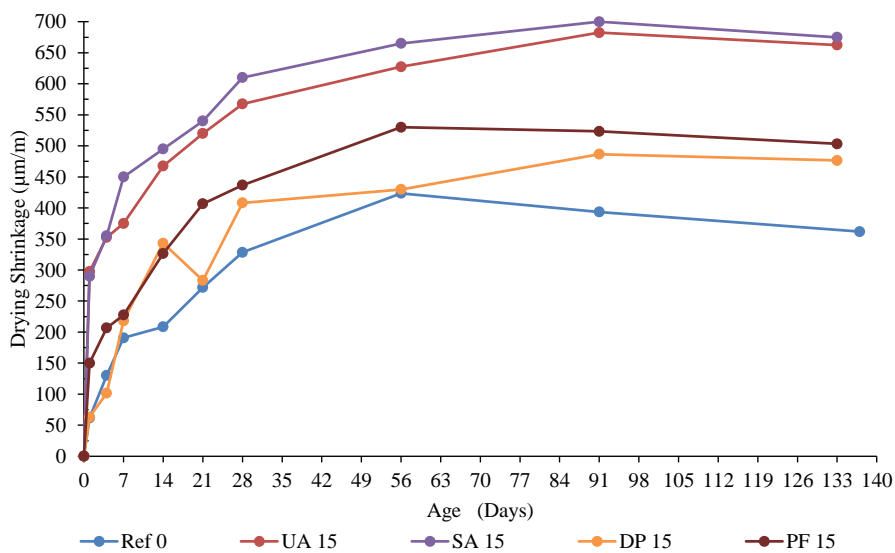


Figure B-10. The drying shrinkage of the fly ash concrete (15 %).

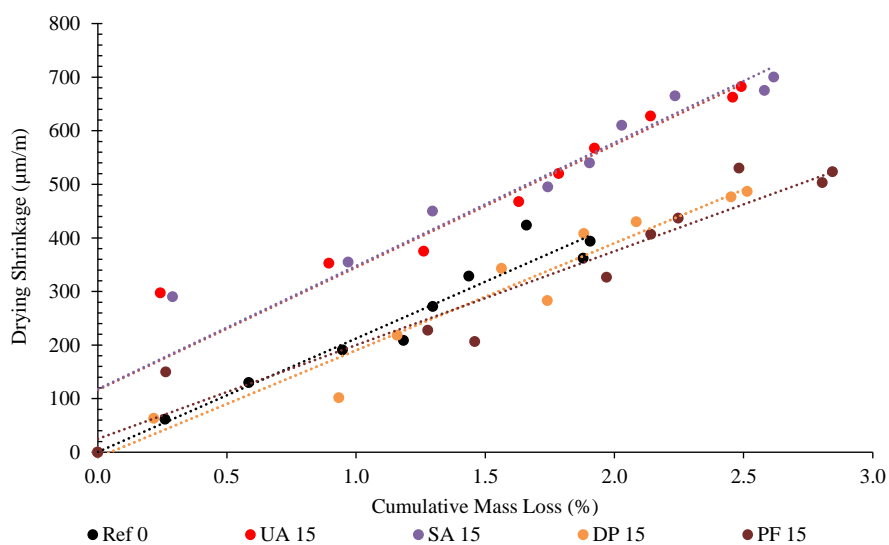


Figure B-11. The cumulative mass loss vs drying shrinkage of the fly ash samples (15 %).

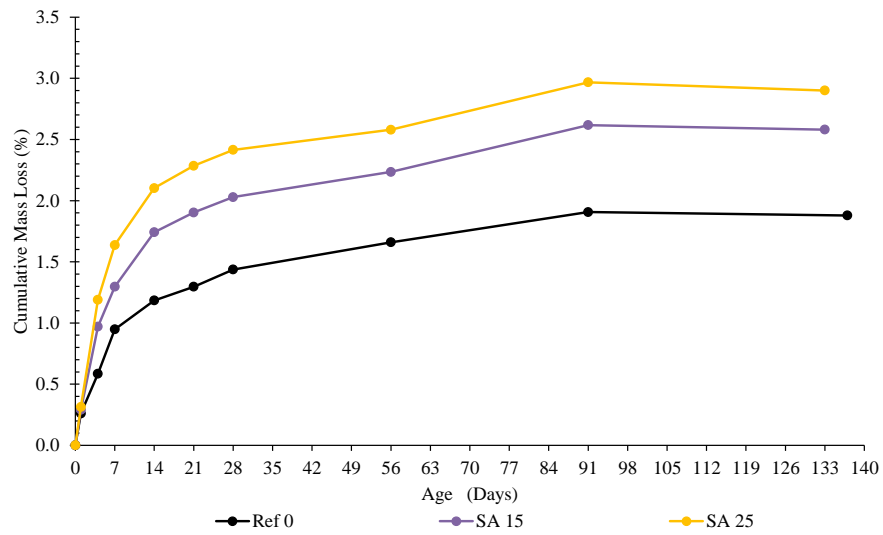


Figure B-12. The cumulative mass loss of the SA based mixes.

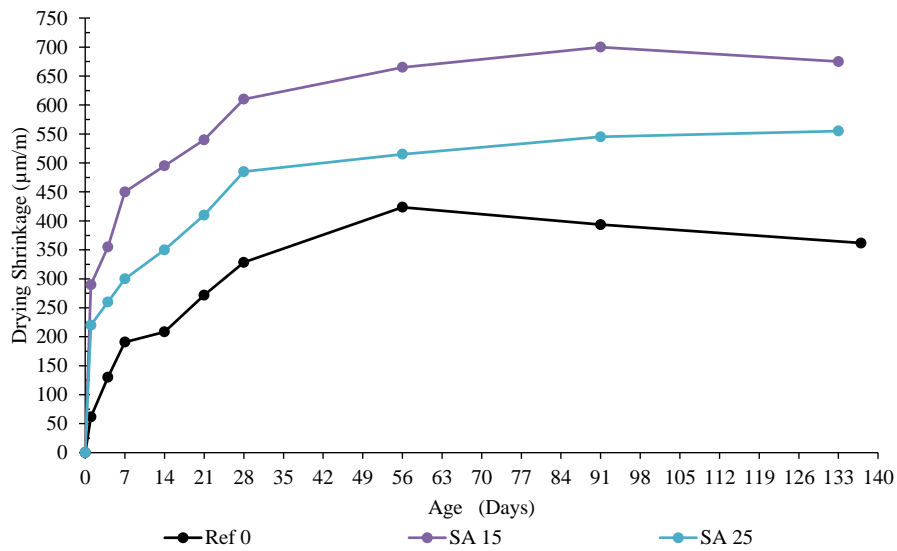


Figure B-13. The drying shrinkage of the SA based mixes.

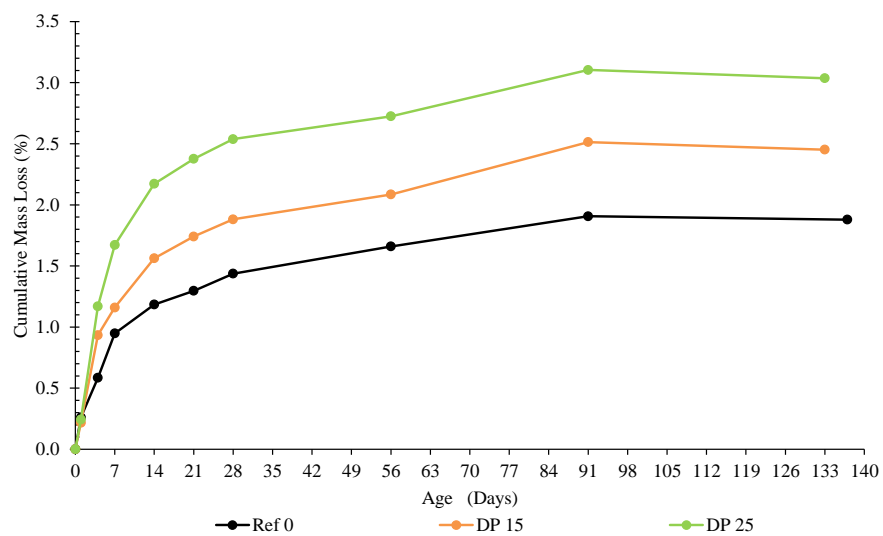


Figure B-14. The cumulative mass loss of the DP based mixes.

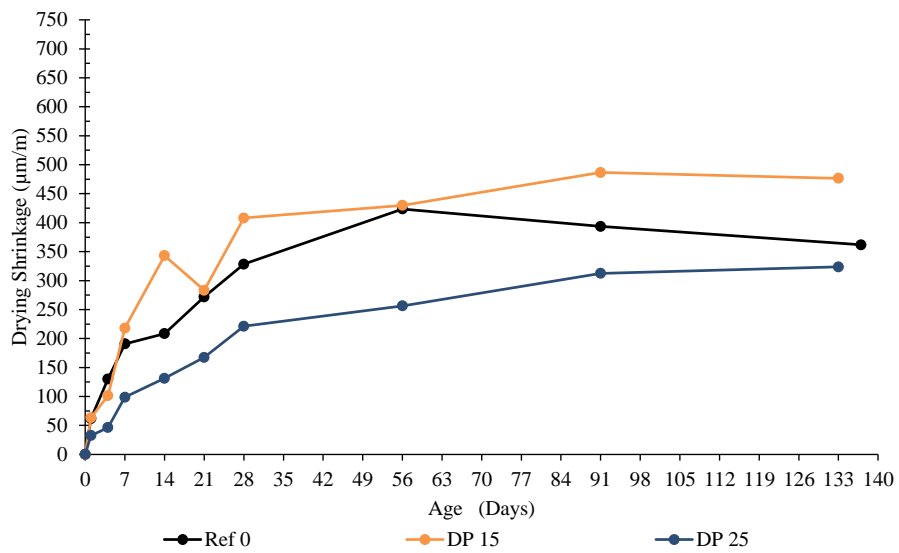


Figure B-15. The drying shrinkage of the DP based mixes

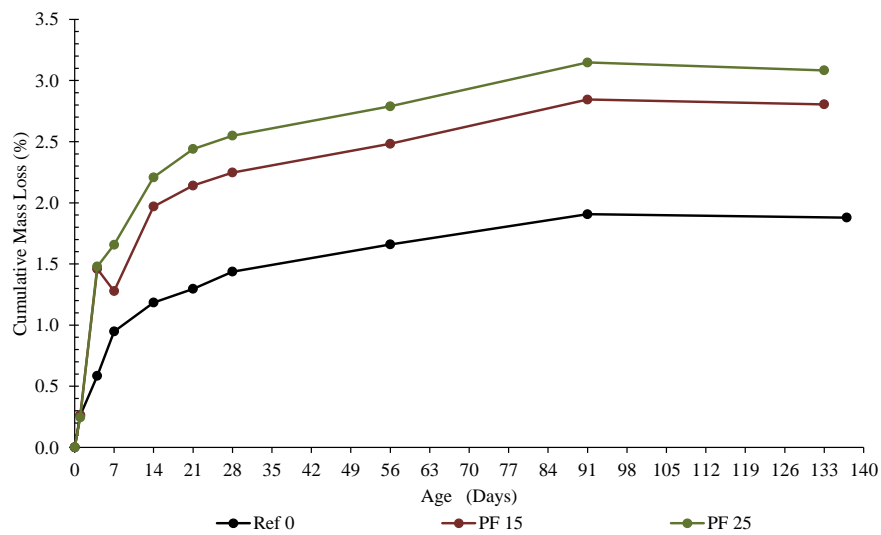


Figure B-16. The cumulative mass loss of the PF based mixes.

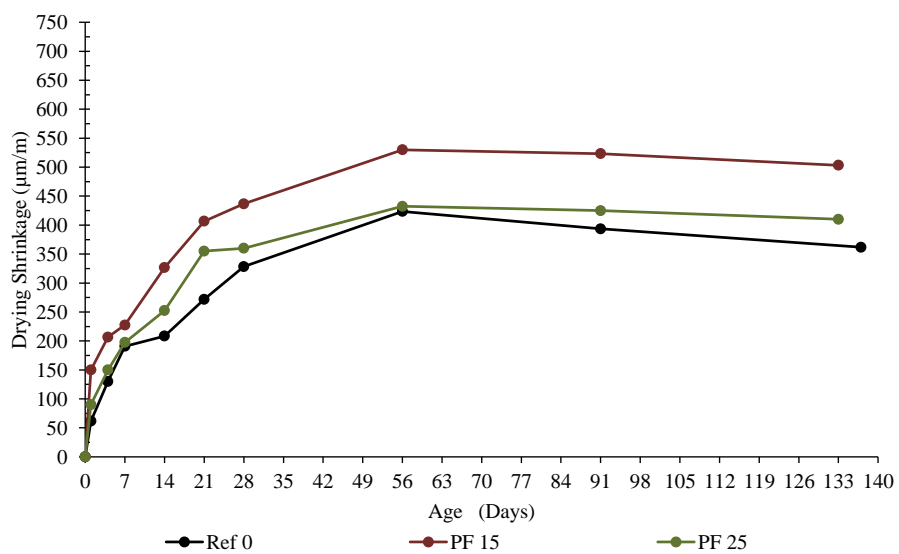


Figure B-17. The drying shrinkage of the PF based mixes.

B. 9. Drying Shrinkage

Table B.8. OPI data for the fly ash samples.

Samples												
		1	2	3	4							
UA 15 Diameter (mm):	1	69.13	69.52	69.19	69.41							
	2	69.31	69.88	69.19	69.44							
	Average	69.22	69.70	69.19	69.43							
	St. Dev (mm)	0.13	0.25	0.00	0.02							
	CoV (%)	0.18	0.37	0.00	0.03							
	Thickness (mm):	1	28.55	28.78	28.44	29.05						
	2	28.42	29.42	28.07	31.07							
	3	28.57	30.05	28.66	30.32							
	4	29.57	29.53	29.32	29.72							
	Average	28.78	29.45	28.62	30.04							
	St. Dev (mm)	0.53	0.52	0.52	0.86							
	CoV (%)	1.85	1.77	1.83	2.86	Average	St.Dev	CoV				
	k (m/s)	k (m/s)	4.919E-11	3.199E-11	4.955E-11	5.511E-11	4.646E-11	1.00201E-11	21.57			
	r ²	r ²	0.9987	0.9980	0.9980	0.9994						
	r ² Validity	r ² Validity	Valid	Valid	Valid	Valid						
	OPI	OPI	10.31	10.49	10.30	10.26	10.34	0.102306728	0.99			
UA 25 Diameter (mm):	1	69.06	69.10	69.29	69.11							
	2	69.21	69.26	69.18	69.24							
	Average	69.14	69.18	69.24	69.18							
	St. Dev (mm)	0.11	0.11	0.08	0.09							
	CoV (%)	0.15	0.16	0.11	0.13							
	Thickness (mm):	1	29.57	29.45	29.63	28.82						
	2	29.11	28.41	29.12	28.98							
	3	29.67	28.38	28.56	29.42							
	4	29.06	28.81	29.23	29.38							
	Average	29.35	28.76	29.14	29.15							
	St. Dev (mm)	0.31	0.50	0.44	0.30							
	CoV (%)	1.06	1.73	1.52	1.02	Average	St.Dev	CoV				
	k (m/s)	k (m/s)	3.316E-11	4.189E-11	4.845E-11	6.569E-11	4.730E-11	1.37686E-11	29.11			
	r ²	r ²	0.9990	0.9970	0.9991	0.9994						
	r ² Validity	r ² Validity	Valid	Valid	Valid	Valid						
	OPI	OPI	10.48	10.38	10.31	10.18	10.34	0.126062154	1.22			
SA 15 Diameter (mm):	1	69.19	69.10	69.25	69.17							
	2	69.12	69.81	69.28	69.80							
	Average	69.16	69.46	69.27	69.49							
	St. Dev (mm)	0.05	0.50	0.02	0.45							
	CoV (%)	0.07	0.72	0.03	0.64							
	Thickness (mm):	1	28.54	29.55	29.31	28.66						
	2	29.00	28.74	29.20	28.75							
	3	28.93	29.08	28.95	28.73							
	4	28.60	29.06	28.68	28.73							
	Average	28.77	29.11	29.04	28.72							
	St. Dev (mm)	0.23	0.33	0.28	0.04							
	CoV (%)	0.80	1.15	0.97	0.14	Average	St.Dev	CoV				
	k (m/s)	k (m/s)	6.716E-11	4.889E-11	5.524E-11	5.449E-11	5.645E-11	7.68469E-12	13.61			
	r ²	r ²	0.9998	0.9996	0.9993	0.9995						
	r ² Validity	r ² Validity	Valid	Valid	Valid	Valid						
	OPI	OPI	10.17	10.31	10.26	10.26	10.25	0.059261931	0.58			
SA 25 Diameter (mm):	1	69.13	69.12	69.94	69.17							
	2	69.12	69.19	69.82	69.17							
	Average	69.13	69.16	69.88	69.17							
	St. Dev (mm)	0.01	0.05	0.08	0.00							
	CoV (%)	0.01	0.07	0.12	0.00							
	Thickness (mm):	1	30.55	27.96	29.96	28.99						
	2	29.11	29.12	29.70	28.98							
	3	29.38	28.81	29.10	28.69							
	4	29.04	27.97	28.84	29.04							
	Average	29.52	28.47	29.40	28.93							
	St. Dev (mm)	0.70	0.59	0.52	0.16							
	CoV (%)	2.38	2.08	1.76	0.55	Average	St.Dev	CoV				
	k (m/s)	k (m/s)	4.624E-11	4.419E-11	4.938E-11	6.140E-11	5.030E-11	7.70004E-12	15.31			
	r ²	r ²	0.9986	0.9968	0.9991	0.9981						
	r ² Validity	r ² Validity	Valid	Valid	Valid	Valid						
	OPI	OPI	10.33	10.35	10.31	10.21	10.30	0.062182527	0.60			
DP 15 Diameter (mm):	1	69.35	69.39	69.19	69.82							
	2	69.21	69.25	69.14	69.43							
	Average	69.28	69.32	69.17	69.63							
	St. Dev (mm)	0.10	0.10	0.04	0.28							
	CoV (%)	0.14	0.14	0.05	0.40							
	Thickness (mm):	1	28.76	29.52	29.44	29.18						
	2	28.86	29.28	29.01	29.17							
	3	29.90	29.88	28.01	28.74							
	4	29.61	28.75	28.78	28.81							
	Average	29.28	29.36	28.81	28.98							
	St. Dev (mm)	0.56	0.47	0.60	0.23							
	CoV (%)	1.91	1.62	2.08	0.80	Average	St.Dev	CoV				
	k (m/s)	k (m/s)	4.606E-11	6.350E-11	7.810E-11	9.107E-11	6.968E-11	1.93608E-11	27.78			
	r ²	r ²	0.9994	0.9998	0.9993	0.9999						
	r ² Validity	r ² Validity	Valid	Valid	Valid	Valid						
	OPI	OPI	10.34	10.20	10.11	10.04	10.17	0.129453982	1.27			
DP 25 Diameter (mm):	1	69.12	69.3	69.2	69.14							
	2	69.07	69.2	69.08	69.41							
	Average	69.10	69.25	69.14	69.28							
	St. Dev (mm)	0.04	0.07	0.08	0.19							
	CoV (%)	0.05	0.10	0.12	0.28							
	Thickness (mm):	1	30.19	29.49	28.08	28.09						
	2	30.36	29.98	28.65	28.25							
	3	30.03	28.99	28.56	28.3							
	4	29.68	28.92	28.29	27.87							
	Average	30.07	29.35	28.40	28.13							
	St. Dev (mm)	0.29	0.49	0.26	0.19							
	CoV (%)	0.96	1.68	0.91	0.69	Average	St.Dev	CoV				
	k (m/s)	k (m/s)	3.887E-11	8.086E-11	1.376E-10	8.604E-10	2.794E-10	3.89419E-10	139.36			
	r ²	r ²	0.9990	0.9996	0.9997	0.9987						
	r ² Validity	r ² Validity	Valid	Valid	Valid	Valid						
	OPI	OPI	10.41	10.09	9.86	9.07	9.86	0.571394493	5.80			
PF 15 Diameter (mm):	1	69.28	69.31	69.64	69.21							
	2	69.40	69.59	70.08	69.28							
	Average	69.34	69.45	69.86	69.25							
	St. Dev (mm)	0.08	0.20	0.31	0.05							
	CoV (%)	0.12	0.29	0.45	0.07							
	Thickness (mm):	1	29.80	30.11	29.58	29.02						
	2	30.30	29.3	29.2	28.84							
	3	29.88	29.05	29.56	29.13							
	4	29.34	29.51	29.08	28.95							
	Average	29.83	29.49	29.36	28.99							
	St. Dev (mm)	0.39	0.45	0.25	0.12							
	CoV (%)	1.32	1.53	0.86	0.42	Average	St.Dev	CoV				
	k (m/s)	k (m/s)	8.849E-11	1.259E-10	-	2.669E-10	1.604E-10	9.40839E-11	58.64			
	r ²	r ²	0.9998	0.9986	-	0.9981						
	r ² Validity	r ² Validity	Valid	Valid	Invalid	Valid						
	OPI	OPI	10.05	9.90	-	9.57	9.84	0.245560583	2.50			
PF 25 Diameter (mm):	1	69.10	69.19	69.18	69.19							
	2	69.28	69.22	69.21	69.27							
	Average	69.19	69.21	69.20	69.23							
	St. Dev (mm)	0.13	0.02	0.02	0.06							
	CoV (%)	0.18	0.03	0.03	0.08							
	Thickness (mm):	1	28.94	29.02	29.41	29.12						
	2	28.75	28.88	30.03	30.01							
	3	29.29	29.2	29.01	28.69							
	4	29.43	29.7	29.12	28.13							
	Average	29.10	29.20	29.39	28.99							
	St. Dev (mm)	0.31	0.36	0.46	0.79							
	CoV (%)	1.07	1.23	1.56	2.74	Average	St.Dev	CoV				
	k (m/s)	k (m/s)	6.478E-11	1.615E-10	8.131E-11	2.139E-10	1.304E-10	6.98934E-11	53.61			
	r ²	r ²	0.9978	0.9999	0.9995	0.9985						
	r ² Validity	r ² Validity	Valid	Valid	Valid	Valid						
	OPI	OPI	10.19	9.79	10.09	9.67	9.94	0.245153013	2.47			

Table B.9. Sorptivity data for the fly ash samples.

15 % UA								15 % SA									
Sample	1	2	3	4	Average	St. Dev	CoV	Sample	1	2	3	4	Average	St. Dev	CoV		
Diameter (mm)	69.22	69.70	69.19	69.43	69.38	0.24	0.34	Diameter (mm)	69.16	69.46	69.27	69.49	69.34	0.16	0.23		
Thickness (mm)	28.70	29.45	28.62	30.04	29.20	0.67	2.29	Thickness (mm)	28.77	29.11	29.04	28.72	28.91	0.19	0.67		
Time (min)	Mass (g)	Mass (g)	Mass (g)	Mass (g)					Time (min)	Mass (g)	Mass (g)	Mass (g)	Mass (g)				
0	250.33	249.51		261.47					0	246.15	247.55	249.56	251.50				
3	251.21	250.39		262.49					3	247.01	248.57	250.59	252.32				
5	251.45	250.67		262.69					5	247.27	248.87	250.90	252.59				
7	251.61	250.80		262.83					7	247.48	249.04	251.03	252.71				
9	251.84	251.06		263.01					9	247.63	249.18	251.16	252.86				
12	251.94	251.16		263.14					12	247.84	249.42	251.40	253.07				
16	252.11	251.31		263.29					16	248.05	249.58	251.57	253.24				
20	252.31	251.51		263.48					20	248.25	249.82	251.79	253.43				
25	252.47	251.73		263.71					25	248.45	249.99	251.95	253.61				
Saturated Mass (g)	262.61	262.66		273.48					Saturated Mass (g)	259.12	260.90	262.26	263.33				
r2 (Must be >0.98)	0.9894	0.9866	Invalid	0.9962					r2 (Must be >0.98)	0.9970	0.9944	0.9939	0.9966				
Sorptivity (mm/hr0.5)	6.88	6.81	Invalid	7.02	6.91	0.11	1.56	Sorptivity (mm/hr0.5)	7.51	7.23	7.26	7.32	7.33	0.13	1.72		
Porosity (%)	11.37	11.70	Invalid	10.56	11.21	0.59	5.24	Porosity (%)	12.00	12.11	11.61	10.86	11.65	0.56	4.84		
25 % UA								25 % SA									
Sample	1	2	3	4	Average	St. Dev	CoV	Sample	1	2	3	4	Average	St. Dev	CoV		
Diameter (mm)	69.14	69.18	69.24	69.18	69.18	0.04	0.06	Diameter (mm)	69.16	69.16	69.73	69.17	69.30	0.28	0.41		
Thickness (mm)	29.35	28.76	29.14	29.15	29.10	0.25	0.84	Thickness (mm)	29.52	28.47	29.40	28.93	29.08	0.48	1.66		
Time (min)	Mass (g)	Mass (g)	Mass (g)	Mass (g)					Time (min)	Mass (g)	Mass (g)	Mass (g)	Mass (g)				
0	250.75	247.78	252.12	252.06					0		246.22	249.98	250.19				
3	251.62	248.76	252.97	252.99					3		247.13	251.10	251.31				
5	251.82	248.94	253.11	253.12					5		247.33	251.28	251.50				
7	252.03	249.22	253.32	253.40					7		247.44	251.38	251.69				
9	252.17	249.37	253.49	253.51					9		247.57	251.56	251.87				
12	252.38	249.53	253.61	253.72					12		247.77	251.75	252.07				
16	252.52	249.73	253.78	253.91					16		247.91	251.89	252.18				
20	252.77	249.98	253.99	254.11					20		248.00	252.01	252.46				
25	252.97	250.18	254.20	254.31					25		248.26	252.24	252.61				
Saturated Mass (g)	263.44	261.10	264.72	264.80					Saturated Mass (g)		258.55	263.77	263.35				
r2 (Must be >0.98)	0.9969	0.9948	0.9953	0.9950					r2 (Must be >0.98)	Invalid	0.9930	0.9945	0.9933				
Sorptivity (mm/hr0.5)	7.36	7.28	6.72	7.30	7.17	0.30	4.15	Sorptivity (mm/hr0.5)	Invalid	5.96	5.70	6.85	6.17	0.60	9.75		
Porosity (%)	11.52	12.32	11.49	11.63	11.74	0.39	3.35	Porosity (%)	Invalid	11.53	12.28	12.11	11.97	0.39	3.28		
15 % DP								15 % PF									
Sample	1	2	3	4	Average	St. Dev	CoV	Sample	1	2	3	4	Average	St. Dev	CoV		
Diameter (mm)	69.28	69.32	69.17	69.63	69.35	0.20	0.28	Diameter (mm)	69.34	69.45	69.86	69.25	69.47	0.27	0.39		
Thickness (mm)	29.28	29.36	28.81	28.98	29.11	0.26	0.89	Thickness (mm)	29.83	29.49	29.36	28.99	29.42	0.35	1.19		
Time (min)	Mass (g)	Mass (g)	Mass (g)	Mass (g)					Time (min)	Mass (g)	Mass (g)	Mass (g)	Mass (g)				
0	253.38	253.03	247.14	250.55					0	256.88	255.34	253.55	250.77				
3	254.22	253.84	248.15	251.56					3	257.76	256.31	254.69	251.81				
5	254.58	254.04	248.26	251.62					5	258.08	256.62	255.02	251.95				
7	254.77	254.25	248.39	251.82					7	258.23	256.80	255.25	252.23				
9	254.89	254.36	248.61	251.97					9	258.37	256.94	255.44	252.42				
12	254.99	254.47	248.73	252.11					12	258.59	257.17	255.71	252.64				
16	255.23	254.70	248.98	252.36					16	258.85	257.51	256.03	252.95				
20	255.50	254.88	249.19	252.48					20	259.04	257.76	256.23	253.20				
25	255.59	255.06	249.33	252.65					25	259.23	257.96	256.49	253.41				
Saturated Mass (g)	267.64	267.22	260.99	264.68					Saturated Mass (g)	271.08	269.39	267.60	264.64				
r2 (Must be >0.98)	Invalid	0.9958	0.9916	0.9910					r2 (Must be >0.98)	0.9960	0.9968	0.9974	0.9958				
Sorptivity (mm/hr0.5)	Invalid	5.90	6.18	5.63	5.90	0.27	4.65	Sorptivity (mm/hr0.5)	7.24	8.28	8.91	8.31	8.18	0.69	8.46		
Porosity (%)	Invalid	12.81	12.80	12.81	12.80	0.01	0.06	Porosity (%)	12.61	12.58	12.49	12.71	12.59	0.09	0.72		
25 % DP								25 % PF									
Sample	1	2	3	4	Average	St. Dev	CoV	Sample	1	2	3	4	Average	St. Dev	CoV		
Diameter (mm)	69.12	69.25	69.14	69.28	69.20	0.08	0.11	Diameter (mm)	69.19	69.21	69.20	69.23	69.21	0.02	0.03		
Thickness (mm)	30.07	29.35	28.40	28.13	28.98	0.89	3.07	Thickness (mm)	29.10	29.20	29.39	28.99	29.17	0.17	0.59		
Time (min)	Mass (g)	Mass (g)	Mass (g)	Mass (g)					Time (min)	Mass (g)	Mass (g)	Mass (g)	Mass (g)				
0	256.78	248.81	243.67	246.39					0	248.69	250.26	252.02	252.09				
3	258.02	249.98	245.00	247.54					3	249.84	251.31	253.30	253.15				
5	258.02	250.10	245.10	247.60					5	250.06	251.53	253.52	253.33				
7	258.25	250.20	245.25	247.76					7	250.25	251.64	253.76	253.46				
9	258.39	250.41	245.40	247.88					9	250.44	251.87	253.96	253.65				
12	258.52	250.52	245.56	247.99					12	250.73	251.99	254.22	253.88				
16	258.81	250.88	245.96	248.35					16	250.91	252.27	254.52	254.08				
20	259.00	251.10	246.14	248.60					20	251.16	252.42	254.75	254.24				
25	259.21	251.25	246.41	248.71					25	251.41	252.66	255.05	254.49				
Saturated Mass (g)	271.60	263.20	257.76	260.60					Saturated Mass (g)	262.10	263.80	265.60	265.70				
r2 (Must be >0.98)	0.9814	0.9821	0.9807	Invalid					r2 (Must be >0.98)	0.9977	0.9962	0.9993	0.9970				
Sorptivity (mm/hr0.5)	6.13	6.58	7.06	Invalid	6.59	0.46	6.99	Sorptivity (mm/hr0.5)	8.16	6.89	9.10	6.84	7.75	1.09	14.03		
Porosity (%)	13.14	13.02	13.22	Invalid	13.12	0.10	0.76	Porosity (%)	12.26	12.33	12.29	12.47	12.34	0.10	0.78		

Table B.10. Chloride conductivity data for the fly ash samples.

UA 15					SA 15				
Sample	1	2	3	4	Sample	1	2	3	4
Thickness					Thickness				
	28.53	28.22	28.75	29.91		29.38	29.65	29.71	28.73
	28.16	28.26	28.87	28.65		29.13	30.55	29.37	28.33
	29.15	28.99	29.27	28.66		28.58	29.44	29.05	28.63
	29.93	28.50	29.38	29.99		28.90	28.99	29.10	28.99
Average	28.94	28.49	29.07	29.30	Average	29.00	29.66	29.31	28.67
St Dev	0.77	0.35	0.30	0.75	St Dev	0.34	0.66	0.30	0.27
CoV	2.68	1.24	1.05	2.55	CoV	1.17	2.21	1.03	0.95
Diameter					Diameter				
	69.90	69.84	69.54	69.53		69.50	69.36	69.50	69.60
	69.49	69.43	69.43	69.45		69.47	69.40	69.41	69.59
Average	69.70	69.64	69.49	69.49	Average	69.49	69.38	69.46	69.60
St Dev	0.29	0.29	0.08	0.06	St Dev	0.02	0.03	0.06	0.01
CoV	0.42	0.42	0.11	0.08	CoV	0.03	0.04	0.09	0.01
Porosity					Porosity				
Mso (g)	249.15	242.97	249.73	250.56	Mso (g)	249.75	256.43	245.08	251.26
Msv (g)	262.63	256.94	263.63	264.55	Msv (g)	263.81	270.12	265.36	259.25
Porosity (%)	10.26	10.82	10.60	10.58	Porosity (%)	10.74	10.26	15.35	6.16
Average	10.56				Average	10.63			
St Dev	0.23				St Dev	3.76			
CoV	2.18				CoV	35.38			
Conductivity					Conductivity				
Voltage (V)	10.29	10.83	10.73	10.34	Voltage (V)	10.71	10.84	10.65	10.27
Current (mA)	194.2	195.2	208.1	192.2	Current (mA)	193.4	179.9	238.3	236.1
Conductivity (mS/cm)	1.43	1.35	1.49	1.44	Conductivity (mS/cm)	1.38	1.30	1.73	1.73
Average	1.43				Average	1.54			
St Dev	0.06				St Dev	0.23			
CoV	4.06				CoV	14.82			
UA 25					SA 25				
Sample	1	2	3	4	Sample	1	2	3	4
Thickness					Thickness				
	28.85	29.60	28.62	28.25		30.07	29.20	28.87	28.66
	28.92	30.08	28.49	28.48		29.36	29.32	28.95	28.23
	29.19	29.70	28.64	29.29		28.88	28.84	28.22	28.44
	29.28	29.12	28.98	29.37		29.14	28.82	28.97	28.92
Average	29.06	29.63	28.68	28.85	Average	29.36	29.05	28.75	28.56
St Dev	0.21	0.40	0.21	0.57	St Dev	0.51	0.25	0.36	0.30
CoV	0.71	1.33	0.73	1.96	CoV	1.74	0.87	1.24	1.04
Diameter					Diameter				
	69.93	69.50	69.87	69.55		69.63	69.87	69.62	69.60
	69.62	69.66	69.52	69.42		69.56	69.85	69.50	69.44
Average	69.78	69.58	69.70	69.49	Average	69.60	69.86	69.56	69.52
St Dev	0.22	0.11	0.25	0.09	St Dev	0.05	0.01	0.08	0.11
CoV	0.31	0.16	0.36	0.13	CoV	0.07	0.02	0.12	0.16
Porosity					Porosity				
Mso (g)	250.41	251.28	244.75	248.56	Mso (g)	247.91	249.26	247.03	244.53
Msv (g)	264.76	266.10	259.45	262.49	Msv (g)	263.01	263.65	262.08	258.82
Porosity (%)	10.85	11.06	11.29	10.70	Porosity (%)	11.36	10.86	11.57	11.08
Average	10.97				Average	11.22			
St Dev	0.26				St Dev	0.31			
CoV	2.33				CoV	2.79			
Conductivity					Conductivity				
Voltage (V)	10.36	10.45	10.41	10.51	Voltage (V)	10.47	10.35	10.30	10.35
Current (mA)	187.6	189.3	185.0	187.5	Current (mA)	195.3	199.6	204.1	200.5
Conductivity (mS/cm)	1.38	1.41	1.34	1.36	Conductivity (mS/cm)	1.44	1.46	1.50	1.46
Average	1.37				Average	1.47			
St Dev	0.03				St Dev	0.03			
CoV	2.18				CoV	1.72			

Table B. 10. (cont.) Chloride conductivity data for the fly ash samples.

DP 15					PF 15				
Sample	1	2	3	4	Sample	1	2	3	4
Thickness					Thickness				
	30.06	29.09	29.78	29.28		29.13	29.16	30.34	30.11
	29.16	29.03	29.08	29.43		28.76	29.31	30.20	29.74
	28.12	28.71	28.78	28.72		28.71	29.41	28.06	28.83
	29.12	29.40	29.21	29.10		28.71	30.18	29.14	28.89
Average	29.12	29.06	29.21	29.13	Average	28.83	29.52	29.44	29.39
St Dev	0.79	0.28	0.42	0.31	St Dev	0.20	0.46	1.06	0.63
CoV	2.72	0.97	1.43	1.05	CoV	0.70	1.54	3.61	2.16
Diameter					Diameter				
	69.50	69.33	69.33	69.59		69.56	69.21	69.43	69.47
	69.22	69.66	69.41	69.89		69.61	69.64	69.41	69.58
Average	69.36	69.50	69.37	69.74	Average	69.59	69.43	69.42	69.53
St Dev	0.20	0.23	0.06	0.21	St Dev	0.04	0.30	0.01	0.08
CoV	0.29	0.34	0.08	0.30	CoV	0.05	0.44	0.02	0.11
Porosity					Porosity				
Mso (g)	249.61	251.88	252.59	250.28	Mso (g)	253.78	256.48	254.59	252.92
Msv (g)	264.34	264.85	266.28	264.25	Msv (g)	267.42	270.41	268.81	267.32
Porosity (%)	11.25	9.89	10.42	10.55	Porosity (%)	10.46	10.48	10.73	10.84
Average	10.53				Average	10.63			
St Dev	0.56				St Dev	0.19			
CoV	5.33				CoV	1.79			
Conductivity					Conductivity				
Voltage (V)	10.63	10.68	10.81	10.73	Voltage (V)	10.73	10.51	10.65	10.68
Current (mA)	203.4	178.6	179.7	173.6	Current (mA)	195.6	215.7	193.8	197.5
Conductivity (mS/cm)	1.47	1.28	1.28	1.23	Conductivity (mS/cm)	1.38	1.60	1.42	1.43
Average	1.32				Average	1.46			
St Dev	0.11				St Dev	0.10			
CoV	8.06				CoV	6.68			
DP 25					PF 25				
Sample	1	2	3	4	Sample	1	2	3	4
Thickness					Thickness				
	29.03	29.58	27.49	27.12		29.13	30.78	30.53	30.81
	29.54	29.37	27.38	27.45		30.42	31.74	31.87	30.89
	30.15	29.22	27.75	27.68		30.88	30.38	32.42	31.68
	29.43	29.14	28.32	27.51		30.84	30.32	31.37	31.16
Average	29.54	29.33	27.74	27.44	Average	30.32	30.81	31.55	31.14
St Dev	0.46	0.19	0.42	0.23	St Dev	0.82	0.66	0.80	0.39
CoV	1.57	0.66	1.51	0.85	CoV	2.70	2.13	2.54	1.26
Diameter					Diameter				
	69.45	69.68	69.37	69.55		69.20	69.21	69.26	69.61
	69.51	69.77	69.40	69.44		69.18	69.46	69.45	69.52
Average	69.48	69.73	69.39	69.50	Average	69.19	69.34	69.36	69.57
St Dev	0.04	0.06	0.02	0.08	St Dev	0.01	0.18	0.13	0.06
CoV	0.06	0.09	0.03	0.11	CoV	0.02	0.25	0.19	0.09
Porosity					Porosity				
Mso (g)	252.59	250.91	236.22	237.03	Mso (g)	255.74	262.73	266.24	270.97
Msv (g)	267.28	265.79	250.27	249.75	Msv (g)	269.61	277.06	280.97	285.10
Porosity (%)	11.02	11.17	11.26	10.27	Porosity (%)	10.22	10.35	10.39	10.03
Average	10.93				Average	10.25			
St Dev	0.45				St Dev	0.16			
CoV	4.12				CoV	1.56			
Conductivity					Conductivity				
Voltage (V)	10.69	10.80	10.62	10.14	Voltage (V)	10.56	10.56	10.53	10.50
Current (mA)	193.5	188.7	198.3	194.3	Current (mA)	220.3	221.3	222.9	245.5
Conductivity (mS/cm)	1.41	1.34	1.37	1.39	Conductivity (mS/cm)	1.68	1.71	1.77	1.92
Average	1.38				Average	1.77			
St Dev	0.03				St Dev	0.11			
CoV	2.17				CoV	6.03			